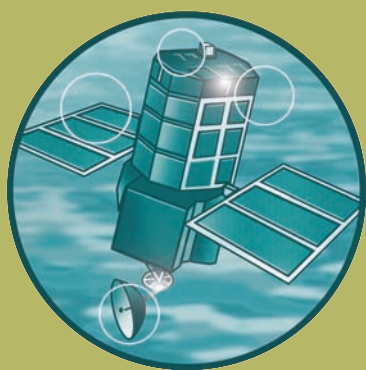


Extreme Events Recognition Phase 2

Spatio-temporal rainfall datasets and their use
in evaluating the extreme event performance
of hydrological models

R&D Project Report FD2208/PR



Joint Defra/EA Flood and Coastal Erosion Risk
Management R&D Programme

Spatio-temporal rainfall datasets and their use in evaluating the extreme event performance of hydrological models

R&D Project Report FD2208/PR

Authors: R. J. Moore, V. A. Bell, S. J. Cole
and D. A. Jones

Produced: August 2006

Statement of Use

This report documents the outcome of Work Package 4 of Project FD2208 “Extreme Event Recognition Phase 2” concerned with spatio-temporal rainfall datasets and their use in evaluating the extreme event performance of hydrological models. The Work Package aims to provide an extremes dataset and methodology of use to the Environment Agency in flood management.

Dissemination status

Internal: Released Internally
External: Released to Public Domain.

Keywords: artificial storm, dataset, destruction testing, extreme rainfall, flood, forecasting, hydrological model, warning

Research Contractor:

CEH Wallingford
Maclean Building, Crowmarsh Gifford, Wallingford, Oxon, OX10 8BB
Project manager: Bob Moore Email: rm@ceh.ac.uk

Consortium leader:

Brian Golding, Met Office Email: brian.golding@metoffice.gov.uk

Defra project officer: Linda Aucott Email: linda.aucott@defra.gsi.gov.uk

This document is also available on the Defra website
www.defra.gov.uk/environ/fcd/research

Department for Environment, Food and Rural Affairs,
Flood Management Division
Ergon House, Horseferry Road,
London SW1P 2AL.

Tel: 0207 238 3000 Fax: 0207 238 6187
www.defra.gov.uk/environ/fcd

© Crown copyright (Defra); August 2006

Copyright in the typographical arrangement and design rests with the Crown. This publication (excluding the logo) may be reproduced free of charge in any format or medium provided that it is reproduced accurately and not used in a misleading context. The material must be acknowledged as Crown copyright with the title and source of the publication specified. The views expressed in this document are not necessarily those of Defra or the Environment Agency. Its officers, servants or agents accept no liability whatsoever for any loss or damage arising from the interpretation or use of the information, or reliance on views contained herein.

Acknowledgements

Particular thanks are due to the following members of the Project Board:

Linda Aucott, Defra (Defra Project Officer)
Brian Golding, Met Office (Consortium Leader)
Ian Pearse, Environment Agency
Helen Stanley, Environment Agency
Tim Wood, Environment Agency

The Environment Agency and Met Office are thanked for helping with case study selection and for supplying supporting data and information.

Alice Robson and Kevin Black (Centre for Ecology & Hydrology) are thanked for their help in preparing the Extremes Dataset.

Executive Summary

This study aims to develop a spatio-temporal rainfall dataset of extreme storms for use in evaluating the extreme event performance of hydrological models. The Extremes Dataset contains a selection of extreme storms, recent enough to have weather radar coverage, along with artificially-enhanced forms of them. Some of the historical storms - embracing rainfall of convective, orographic and frontal type – are chosen for hydrological model case studies. One lumped and one distributed hydrological model, representative of other models of these types, are used to evaluate model performance. The lumped model, the PDM, is used operationally for flood forecasting by the Environment Agency whilst the distributed Grid-to-Grid model was specifically developed for use with radar data. Shortcomings in model performance for a lowland case study serve as a catalyst for model development and improvement of the Grid-to-Grid model.

A methodology for transforming a historical extreme radar rainfall dataset to create a more extreme one is developed in detail. The rainfall transformation tool can change the position, movement, orientation, size and shape of a chosen storm. It is used in flood response experiments involving the hydrological models - allowing a storm to be transposed over a catchment and modified in speed and direction, as well as shape and magnitude – to understand the genesis of flood response as a function of storm characteristics, catchment form and soil wetness. This proves of value in identifying locations that may be particularly vulnerable to flooding, and under what conditions, providing support to extreme flood recognition in advance of one occurring.

Associating a frequency of occurrence to the amplified storms is not straightforward and two approaches are considered. One approach uses a framework within which, for a flood peak of given return period and for a chosen hydrological model, a rainfall dataset is derived that just matches the peak value when input to the model. The result is a collection of storms, with different characteristics, each of which is sufficient for the modelled flow to reach the critical level for the given return period. The effect of soil wetness can also be introduced through the initial condition of the model. This approach is used with simple artificial storms as an illustration of model destruction testing. A second approach generates spatio-temporal datasets that - for a given catchment, duration and return period – attain rainfall amounts derived by the Flood Estimation Handbook methodology. The second approach is independent of the hydrological model used and is adopted for the case study flood response investigations and experiments.

The importance of areal rainfall estimation on rainfall-runoff model performance is recognised. New methods for deriving linear weights for combining raingauge values for catchments and gridded areas are developed based on an integrated multiquadric surface. These are extended to obtain estimators that combine raingauge and radar measurements that are recommended for operational use. Further recommendations, along with a summary and final conclusions of the study, are given. The collated dataset of storms and floods is available as a DVD along with supporting documentation and software for use within Hyrad.

CONTENTS

| | |
|---|------------|
| Executive Summary | v |
| List of Figures | xi |
| List of Tables | xvi |
| 1 Introduction | 1 |
| 1.1 Objectives and approach | 1 |
| 1.2 Methodological framework | 2 |
| 1.3 Report overview | 3 |
| 2 Case study selection | 5 |
| 2.1 Introduction | 5 |
| 2.2 Menu of storm events | 5 |
| 2.3 Identification of case studies | 7 |
| 3 Hydrological model selection | 10 |
| 3.1 Introduction | 10 |
| 3.2 The PDM (Probability Distributed Model)..... | 11 |
| 3.3 The Grid-to-Grid Model | 12 |
| 4 Methodologies for constructing and using extreme spatio-temporal rainfall datasets | 19 |
| 4.1 Introduction | 19 |
| 4.2 Rainfall estimators | 20 |
| 4.3 Rainfall amplification | 21 |
| 4.4 Rainfall datasets and frequency of occurrence | 24 |
| 4.5 River flows and frequency of occurrence | 28 |
| 4.6 Generation and application of extreme spatio-temporal rainfall datasets for flood response experiments..... | 29 |

| | | |
|----------|--|------------|
| 4.7 | Destruction testing of rainfall-runoff models using extreme rainfall datasets..... | 31 |
| 5 | The case study storms and catchments | 36 |
| 5.1 | Orographic events | 36 |
| 5.2 | Frontal events..... | 45 |
| 5.3 | Convective events | 55 |
| 6 | Rainfall estimators for the case studies..... | 79 |
| 6.1 | Spatial rainfall estimators and performance assessment | 79 |
| 6.2 | The River Darwen case study | 85 |
| 6.3 | The River Kent case study | 93 |
| 6.4 | The Upper Thames case study | 99 |
| 6.5 | Conclusions..... | 103 |
| 7 | Flood response modelling using case study storms | 105 |
| 7.1 | Introduction..... | 105 |
| 7.2 | Model calibration and performance assessment methodology | 105 |
| 7.3 | Hydrological case study 1: River Kent (Orographic)..... | 110 |
| 7.4 | Hydrological case study 2: Upper Thames and Stour (Frontal)..... | 121 |
| 7.5 | Hydrological case study 3: River Darwen (Convective)..... | 133 |
| 7.6 | Prototype model development incorporating soil/geology information.. | 139 |
| 7.7 | Conclusions..... | 150 |
| 8 | Flood response experiments using amplified storms..... | 154 |
| 8.1 | Introduction..... | 154 |
| 8.2 | Historical storm characteristics | 154 |
| 8.3 | Guidelines for applying storm modification and transposition..... | 156 |
| 8.4 | The amplified extreme storms | 158 |
| 8.5 | Flood response experiments | 159 |

| | | |
|----------|--|------------|
| 8.6 | Conclusions | 184 |
| 9 | Summary, conclusions and recommendations..... | 187 |
| 9.1 | Summary..... | 187 |
| 9.2 | Conclusions | 189 |
| 9.3 | Recommendations | 192 |
| | References | 194 |
| | Appendix A Amplification of extreme spatio-temporal rainfall datasets | 197 |
| A.1 | Context..... | 197 |
| A.2 | Specification of storm characteristics | 197 |
| A.3 | Summary..... | 202 |
| | Appendix B Formulae for rainfall modification | 203 |
| B.1 | Introduction | 203 |
| B.2 | Removal of initial velocity..... | 203 |
| B.3 | Expansion and scaling | 203 |
| B.4 | Turning..... | 205 |
| B.5 | Addition of target velocity | 205 |
| B.6 | Construction of values: extended form..... | 206 |
| B.7 | Construction of values: reduced form | 207 |
| | Appendix C Multiquadric surface fitting and areal rainfall estimation.. | 208 |
| C.1 | Introduction | 208 |
| C.2 | Multiquadric surface fitting techniques | 208 |
| C.3 | Estimation of areal average rainfall totals | 211 |
| C.4 | Outline of method for calculating the volume vector \underline{V} | 214 |
| | Appendix D Destruction testing of rainfall-runoff models | 218 |

| | | |
|---|---|------------|
| D.1 | Introduction..... | 218 |
| D.2 | Destruction testing..... | 218 |
| D.3 | Overview of the special models..... | 219 |
| D.4 | Results of model destruction testing..... | 223 |
| Appendix E Deriving flow path directions and drainage areas for the Grid-to-Grid model | | 227 |
| Appendix F Calibrated model parameters | | 230 |
| F.1 | PDM models..... | 230 |
| F.2 | Grid-to-Grid models..... | 235 |
| Appendix G R^2 model performance statistics for case studies..... | | 236 |
| Appendix H Catalogue of amplified storms | | 241 |
| H.1 | River Kent case study..... | 241 |
| H.2 | River Darwen case study..... | 246 |
| H.3 | Upper Thames and Stour case study | 252 |

List of Figures

| | |
|--|----|
| Figure 1.1 Methodological framework for the study | 2 |
| Figure 3.1 The PDM rainfall-runoff model | 11 |
| Figure 3.2 Schematic of the distributed model structure | 12 |
| Figure 3.3 A typical grid-box storage illustrating the components of the water balance | 14 |
| Figure 4.1 Rotation and compression of a radar rainfall field using the Rainfall Transformation Tool | 23 |
| Figure 4.2 Rainfall amount (mm) versus duration (hours) (on a logarithmic scale) for the 50 most extreme rainfall events of the 20 th Century using data from the Phase 1 Report. See key for event category. The solid line indicates the extreme rainfall threshold used in the Phase 1 Report and the dashed line shows the 100 year return period derived from the FSR. Raingauge totals relating to the case studies are also shown. | 26 |
| Figure 4.3 Critical Rainfall (mm) as a function of Duration (hrs), for different Starting Flows: River Rhondda at Trehafod | 32 |
| Figure 4.4 Critical Rainfall (mm) as a function of Starting Flow (m^3s^{-1}) for a given Duration: River Rhondda at Tehafod | 32 |
| Figure 4.5 Critical Rainfall (mm) as a function of Duration (hrs), for different Starting Flows: River Lavant at Graylingwell | 33 |
| Figure 4.6 Critical Rainfall (mm) as a function of Starting Flow (m^3s^{-1}) for a given Duration: River Lavant at Graylingwell | 33 |
| Figure 5.1 Rainfall accumulation (in mm), using Nimrod composite analysis, for Event 1: 96 hours to 12:00 GMT 3 February 2004. Image (a) shows the orographic enhancement over Snowdonia and Cumbria. Image (b) shows the River Kent catchments. Raingauge locations are marked with solid circles. | 37 |
| Figure 5.2 Cumulative hyetographs for a selection of raingauges in and around the Kent and Upper Ure catchments, and the flow response of the River Kent at Sedgwick, for the period 29 January to 8 February 2004. | 38 |
| Figure 5.3 Maps of relief and SAAR (1km grid) for the River Kent catchment and surrounding area. | 40 |
| Figure 5.4 Rainfall accumulation (in mm), using 2 and 5km Nimrod single site radar data from Chenies for Event 2: 18 hours to 18:00 GMT 9 April 1998. Image (a) shows the heavy rainfall affecting Central England. The square region in (a) is enlarged in image (b) to show the Stour, Sor and Cherwell catchments and the raingauge locations (marked with solid circles). | 46 |
| Figure 5.5 Relief map of the Stour, Sor and Cherwell catchments showing the river network, catchment boundaries and the hydrometric network. | 48 |
| Figure 5.6 Map of SAAR (1km grid) for the Stour, Sor and Cherwell catchments. Heavy lines show the catchment boundaries. | 48 |
| Figure 5.7 Cumulative hyetographs for raingauges in and around the Upper Thames and the flow response of the River Cherwell at Banbury, for the period 09:00 8 April to 09:00 11 April 1998. | 50 |
| Figure 5.8 Cumulative hyetographs for the relevant raingauges in and around the Shipston catchment, and the flow response of the River Stour at Shipston, for the period 09:00 8 April to 09:00 11 April 1998. | 54 |

- Figure 5.9 Rainfall accumulation (in mm), using 1km raw radar data from Hameldon Hill for Event 3: 4 hours to 18:30 GMT, 14 June 2002. The River Darwen catchments are also shown. 56
- Figure 5.10 A sequence of 1km raw radar images, at time intervals of 15 minutes, from 15:20 GMT to 16:55 GMT on 14 June 2002. The River Darwen catchments are also shown. The first image indicates the storm direction of travel. 57
- Figure 5.11 Relief map of the Darwen catchment showing the river network, catchment boundaries and the hydrometric network. 59
- Figure 5.12 Map of SAAR (1km grid) for the Darwen catchment. Heavy lines show the reservoir drainage areas (1-5) and naturally draining areas (others). 59
- Figure 5.13 Flow hydrographs from the River Darwen at Blue Bridge comparing ultrasonic flow estimates and rating equation inferred estimates: (a) shows February 2002 data and (b) shows August 2002 data. 62
- Figure 5.14 (a) Cumulative hyetograph of raingauges in and around the River Darwen catchment and catchment average rainfall derived from 2km raw and 2km QC radar data. (b) The flow response of the River Darwen at Blue Bridge as measured by an ultrasonic flow gauge and inferred from a rating equation. Both plots relate to the 24 hours starting at 09:00 14 June 2002. 63
- Figure 5.15 A sequence of 2km Nimrod QC radar images, at time intervals of 15 minutes, from 09:00 GMT to 09:45 GMT on 10 August 2003. The Wiske catchment and the local raingauge network are also shown. 65
- Figure 5.16 Cumulative hyetographs for the telemetry raingauge network in and around the River Wiske catchment and the flow response of the River Wiske at Kirby Wiske for the period 00:00 10 August to 00:00 13 August 2003. 67
- Figure 5.17 Relief map of the Wiske catchment showing the river network, catchment boundary and the hydrometric network. 68
- Figure 5.18 Rainfall accumulation (in mm), using 2km raw radar data from Hameldon Hill for Event 5: 5 hours up to 19:00 GMT, 19 May 1989 70
- Figure 5.19 A sequence of 2km raw radar images, at time intervals of 45 minutes, from 14:00 GMT to 17:45 GMT on 19 May 1989. The location of the Walshaw Dean raingauge is also shown. 71
- Figure 5.20 Rainfall accumulation, using 2km Nimrod QC data from the Cobbacombe Cross radar, for Event 6: 5 hours up to 17:00 GMT, 16 Aug 2004. Figures give actual radar grid square values. The Boscastle and Crackington Haven catchments are highlighted and solid circles mark the location of the daily and telemetry raingauges in the vicinity. 74
- Figure 5.21 A sequence of 2km Nimrod QC images from the Cobbacombe Cross radar, at time intervals of 45 minutes, from 12:00 GMT to 15:45 GMT on 16 Aug 2004. The Boscastle catchment is also shown. 75
- Figure 5.22 Cumulative hyetographs for selected tipping-bucket raingauges in and around the Boscastle catchment for the period 09:00 16 August to 00:00 17 August 2004. 76
- Figure 6.1 Flowchart for deriving raingauge weights for a given grid-square 82
- Figure 6.2 15 minute rainfall accumulations derived using different rainfall estimators for the convective storm affecting the River Darwen on 14 June 2002. Left column: raw 1km radar. Middle column: raingauge-only

estimator using the Euclidean distance measure with a zero offset parameter ($K=0$ km) and no rainfall rate transformation. Right column: optimised raingauge-only estimator using the Euclidean distance measure with an offset parameter of $K=18$ km and a rainfall rate transformation with $R_0=7.5$ mm hr⁻¹. Circles denote raingauges and triangles denote gauging stations. Note that the right hand column uses a significantly smaller intensity scale. 87

Figure 6.3 15 minute rainfall accumulations derived using different rainfall estimators for the convective storm affecting the River Darwen on 14 June 2002. Left column: raw 1km radar. Middle column: dynamically gauge-adjusted 1km radar using the optimised Euclidean distance. Right column: zero parameter raingauge-only estimator. Circles denote raingauges and triangles denote gauging stations. 92

Figure 6.4 15 minute rainfall accumulations derived using different rainfall estimators for the orographic storm affecting the River Kent on 3 February 2004. Left column: raw Nimrod 2km QC radar. Middle column: raingauge-only estimator using the Euclidean distance measure with a zero offset parameter ($K=0$ km) and no rainfall rate transformation. Right column: optimised raingauge-only estimator using the Euclidean distance measure with an offset parameter of $K=10$ km and a rainfall rate transformation with $R_0=7.5$ mm hr⁻¹. Circles denote raingauges and triangles denote gauging stations 95

Figure 6.5 15 minute rainfall accumulations derived using different rainfall estimators for the orographic storm affecting the River Kent on 3 February 2004. Left column: Nimrod 2km QC radar. Middle column: dynamically gauge-adjusted 2km QC radar using the optimised Euclidean distance. Right column: zero parameter raingauge-only estimator using the Euclidean distance measure with an offset parameter of $K=0$ km and no rainfall rate transformation. Circles denote raingauges and triangles denote gauging stations. The scales used for each time period are given. 98

Figure 7.1 River Kent catchments: R^2 statistics for PDM and Grid-to-Grid models using different rainfall estimators. 111

Figure 7.2 River Kent at Sedgwick: Hydrographs for the PDM and Grid-to-Grid models over the calibration event: 25 October to 30 December 2003. The rainfall estimator used is the raingauge rainfall surface. The figure below the axis is the maximum 15 minute catchment average rainfall for that event. 112

Figure 7.3 River Kent catchments: Hydrographs for the PDM models over the case study extreme event: 29 January to 8 February 2004. The rainfall estimator used is the raingauge surface. The figure below the axis is the maximum 15 minute catchment average rainfall for that catchment. The dashed line above the axis indicates the flow associated with the maximum stage used to derive the rating equation for that catchment. 116

Figure 7.4 River Kent catchments: Hydrographs for the Grid-to-Grid model over the case study extreme event: 29 January to 8 February 2004. The rainfall estimator used is the raingauge surface. The figure below the axis is the maximum 15 minute catchment average rainfall for that catchment. The dashed line above the axis indicates the flow associated with the maximum stage used to derive the rating equation for that catchment. 117

- Figure 7.5 River Kent at Sedgwick: Hydrographs for the PDM model over the case study extreme event 29 January to 8 February 2004 for different rainfall estimators. The figure below the axis is the maximum 15 minute catchment average rainfall for that catchment. The dashed line above the axis indicates the flow associated with the maximum stage used to derive the rating equation. 119
- Figure 7.6 River Kent at Sedgwick: Hydrographs for the Grid-to-Grid model over the case study extreme event 29 January to 8 February 2004 for different rainfall estimators. The figure below the axis is the maximum 15 minute catchment average rainfall for that catchment. The dashed line above the axis indicates the flow associated with the maximum stage used to derive the rating equation. 120
- Figure 7.7 Digital datasets for the Upper Thames and Stour catchments. The 1 km river network and associated catchment boundaries are also shown. 122
- Figure 7.8 Cherwell at Banbury hydrographs for the PDM and Grid-to-Grid models over the calibration event 1 September 2000 to 1 June 2001. The rainfall estimator used is the raingauge rainfall surface. The figure below the axis is the maximum 15 minute catchment average rainfall for that event. 123
- Figure 7.9 Upper Thames catchments: R^2 statistics for PDM and Grid-to-Grid models using different rainfall estimators. 124
- Figure 7.10 Sor at Bodicote hydrographs for the PDM and Grid-to-Grid models over the calibration event 1 September 2000 to 1 June 2001. The rainfall estimator used is the raingauge rainfall surface. The figure below the axis is the maximum 15 minute catchment average rainfall for that event. 125
- Figure 7.11 Stour at Shipston: R^2 statistics for PDM and Grid-to-Grid (G2G) models using different rainfall estimators. 126
- Figure 7.12 Stour at Shipston hydrographs for the PDM and Grid-to-Grid models over the calibration event 8 January to 8 April 1990. The rainfall estimator used is the raingauge rainfall surface. The figure below the axis is the maximum 15 minute catchment average rainfall for that event. 127
- Figure 7.13 Upper Thames and Stour catchment hydrographs for the PDM and Grid-to-Grid models over the case study extreme event: 6 to 19 April 1998. The rainfall estimator used is the raingauge rainfall surface. The figure below the axis is the maximum 15 minute catchment average rainfall for that catchment. The dashed line above the axis indicates the flow associated with the maximum stage used to derive the rating equation for that catchment. 130
- Figure 7.14 River Cherwell at Banbury hydrographs for the PDM and Grid-to-Grid models over the case study extreme event: 6 to 19 April 1998 for different rainfall estimators. The figure below the axis is the maximum 15 minute catchment average rainfall for that catchment. The dashed line above the axis indicates the flow associated with the maximum stage used to derive the rating equation. 132
- Figure 7.15 River Darwen catchments: R^2 statistics for PDM and Grid-to-Grid models using different rainfall estimators. 134
- Figure 7.16 River Darwen catchment hydrographs for the PDM and Grid-to-Grid models over the calibration event 17 February to 9 March 2002. The rainfall estimator used is the raingauge rainfall surface. The figure below the axis is the maximum 15 minute catchment average rainfall for that event. 135

- Figure 7.17 River Darwen catchment hydrographs for the PDM and Grid-to-Grid models over the case study extreme event: 13 to 16 June 2002. The rainfall estimator used is the raingauge rainfall surface. The figure below the axis is the maximum 15 minute catchment average rainfall for that catchment. The dashed line above the axis indicates the flow associated with the maximum stage used to derive the rating equation for that catchment. 137
- Figure 7.18 River Darwen at Blue Bridge hydrographs for the PDM and Grid-to-Grid models over the case study extreme event: 13 to 16 June 2002 for different rainfall estimators. The figure below the axis is the maximum 15 minute catchment average rainfall for that catchment. The dashed line above the axis indicates the flow associated with the maximum stage used to derive the rating equation. 138
- Figure 7.19 Conceptual diagram showing runoff production and lateral drainage in a sloping soil column. 142
- Figure 7.20 Key features of the coupled runoff-production and routing scheme. 145
- Figure 7.21 Upper Thames and Stour hydrographs for the prototype distributed model over the calibration event (1 September 2000 to 1 June 2000 for the Upper Thames, 1 November 1991 to 1 May 1992 for the Stour at Shipston) and evaluation event (6 to 19 April 1998). The rainfall estimator used is the raingauge rainfall surface. 149
- Figure 8.1 Amplified storms and hydrological model flood response for the River Kent at Victoria Bridge catchment. Experiment 1 using the River Kent orographic storm. 161
- Figure 8.2 Amplified storm accumulations over the River Kent. Arrow indicates storm direction of travel. Experiment 2 using the Carlton-in-Cleveland convective storm. 163
- Figure 8.3 Amplified storms and hydrological model flood response for the River Kent at Victoria Bridge catchment (left hand column) and the River Kent at Bowston catchment (right hand column). Experiment 2 using the Carlton-in-Cleveland convective storm. 164
- Figure 8.4 Amplified storms and hydrological model flood response for the River Darwen at Blue Bridge catchment. Left column: Experiment 3 on effect of storm direction and orientation. Right column: Experiment 4 on effect of soil moisture initial condition. The River Darwen convective storm is used. 166
- Figure 8.5 Amplified storms and hydrological model flood response for the River Darwen at Blue Bridge catchment. Left hand column: Experiment 5 using Upper Thames frontal storm. Right column: Experiment 6 using Boscastle convective storm. 168
- Figure 8.6 Amplified storm accumulations (left hand column) and maximum simulated river flow from the Grid-to-Grid model (right hand column) over the River Darwen catchment. Experiment 6 using the Boscastle convective storm. 170
- Figure 8.7 Grid-to-Grid model simulations at a sequence of grid squares between the modelling point for the River Darwen at Ewood (point A) to the modelling point for the River Darwen at Blue Bridge (point G). The points are marked in Figure 8.6. Experiment 6 using the Boscastle convective storm. 171

| | |
|---|-----|
| Figure 8.8 Amplified storms and hydrological model flood response for the Stour at Shipston catchment. Experiment 7 using the Upper Thames and Stour frontal storm. | 173 |
| Figure 8.9 Amplified storms and hydrological model flood response for the Stour at Shipston catchment. Left column: Experiment 8 using the Boscastle convective storm. Right column: Experiment 9 using a variety of convective storms. | 174 |
| Figure 8.10 Amplified storms and hydrological model flood response for the Sor at Bodicote catchment. Experiment 10 using the Upper Thames frontal storm. | 179 |
| Figure 8.11 Amplified storms and hydrological model flood response for the Sor at Bodicote catchment. Left column: Experiment 11 using Darwen convective storm. Right column: Experiment 12 using a variety of convective storms. | 182 |
| Figure A.1 Definition of “orientation” of rainfall bands | 198 |
| Figure A.2 Illustration of turning (turning through a negative angle) | 200 |
| Figure A.3 Illustration of the squeezing/relaxation and contraction/expansion transformations for the time-dimension | 202 |
| Figure C.1 Configuration of a simple catchment region R within a polygon boundary with vertices \underline{x}_1 to \underline{x}_4 and with a raingauge located at \underline{x}_0 | 215 |
| Figure C.2 Construction of triangle T_1 | 215 |
| Figure C.3 Evaluation of rotation factor r_1 | 216 |
| Figure C.4 Illustration of method for calculating the volume vector \underline{V} | 217 |
| Figure D.1 Structure of the simple rainfall-runoff model | 220 |
| Figure D.2 Destruction testing of Version 1 implementation. Flow response at fixed times to different rainfalls in 12 hours. | 224 |
| Figure D.3 Destruction testing of Version 2 implementation. Flow response at fixed times to different rainfalls in 12 hours. | 225 |
| Figure D.4 Destruction testing of Version 2 implementation. Flow response at fixed times to different rainfalls in 12 hours. Lower range of rainfall. | 226 |
| Figure E.1 Fekete derived 1km and IHDTM 50m resolution flow directions and catchment boundaries: River Kent catchment. | 229 |
| Figure E.2 Hand corrected 1km and IHDTM 50m resolution flow directions and catchment boundaries: River Kent catchment. | 229 |

List of Tables

| | |
|---|----|
| Table 2.1 Menu of storm events | 6 |
| Table 2.2 Summary of case studies | 9 |
| Table 4.1 M100, M1000 and M10000 rainfall amounts, growth factors (that are applied to M5 rainfall) and estimated M5 rainfall for the AAR range 2000-2800 mm. These are derived from FSR Vol. II. | 24 |
| Table 4.2 FEH estimated return periods for the historical extreme storms, based on raingauge records | 27 |
| Table 5.1 River gauging stations: River Kent | 42 |
| Table 5.2 Rating equations: River Kent | 43 |
| Table 5.3 FEH-estimated flows (m^3s^{-1}) for given return periods (years) for gauging stations: River Kent | 44 |

| | |
|--|-----|
| Table 5.4 Telemetry raingauges: River Kent | 44 |
| Table 5.5 River gauging stations: Upper Thames | 49 |
| Table 5.6 Rating equation details: Upper Thames | 49 |
| Table 5.7 FEH-estimated flows (m^3s^{-1}) for given return periods (years) for gauging stations: Upper Thames | 51 |
| Table 5.8 Telemetry raingauges: Upper Thames | 52 |
| Table 5.9 River gauging station: River Stour at Shipston | 53 |
| Table 5.10 Rating equation: River Stour at Shipston | 53 |
| Table 5.11 FEH-estimated flows (m^3s^{-1}) for given return periods (years) for the gauging station at Shipston | 53 |
| Table 5.12 River Stour catchment: Raingauges | 55 |
| Table 5.13 Catchment, reservoir and natural drainage areas: River Darwen | 58 |
| Table 5.14 River gauging stations: River Darwen | 60 |
| Table 5.15 Rating equations: River Darwen | 60 |
| Table 5.16 FEH-estimated flows (m^3s^{-1}) for given return periods (years) for gauging stations: River Darwen | 61 |
| Table 5.17 Telemetry raingauges: River Darwen | 64 |
| Table 5.18 Raingauges: River Wiske | 69 |
| Table 5.19 Rolling peak maximum rainfall accumulations for the Lesnewth raingauge and FEH estimated return periods. | 76 |
| Table 5.20 Raingauges: Boscastle area | 78 |
| Table 6.1 Optimal parameter sets and rainfall estimation performance for raingauge-only rainfall estimation: River Darwen case study. The performance of the 1km raw radar and the zero parameter surface are given for comparison. | 86 |
| Table 6.2 Long-term bias statistics for each raingauge location (final column, second table): River Darwen case study. Bias statistics for individual months are also given. | 89 |
| Table 6.3 Optimal parameter sets and rainfall estimation performance for gauge-adjusted radar rainfall estimation: River Darwen case study. The performance of the 1km raw radar is given for comparison. | 91 |
| Table 6.4 Optimal parameter sets and rainfall estimation performance for raingauge-only rainfall estimation: River Kent case study. The performance of the radar estimates and the zero parameter raingauge-only surface are given for comparison. | 93 |
| Table 6.5 Long-term bias statistics of 2km raw and 2km Nimrod QC radar data for each raingauge location: River Kent case study. Raingauge elevations are also listed. | 96 |
| Table 6.6 Optimal parameter sets and rainfall estimation performance for gauge-adjusted 2km raw radar rainfall estimation: River Kent case study. The performance of the unadjusted 2km raw radar is given for comparison. | 96 |
| Table 6.7 Optimal parameter sets and rainfall estimation performance for gauge-adjusted 2km Nimrod QC radar rainfall estimation: River Kent case study. The performance of the unadjusted 2km Nimrod QC radar is given for comparison. | 97 |
| Table 6.8 Optimal parameter sets and rainfall estimation performance for raingauge-only rainfall estimation: Upper Thames and Stour case study. The performance of the radar estimates is given for comparison. | 100 |

| | |
|---|-----|
| Table 6.9 Long-term bias statistics of 2km and 5km raw radar data for each raingauge location for the Upper Thames and Stour case study. Raingauge elevations are also listed. | 101 |
| Table 6.10 Optimal parameter sets and rainfall estimation performance for gauge-adjusted 2km raw radar rainfall estimation: Upper Thames and Stour case study. The performance of the unadjusted 2km raw radar is given for comparison. | 102 |
| Table 6.11 Optimal parameter sets and rainfall estimation performance for gauge-adjusted 5km raw radar rainfall estimation: Upper Thames and Stour case study. The performance of the unadjusted 5km raw radar is given for comparison. | 103 |
| Table 7.1 Definition of modelled quantities for the PDM and Grid-to-Grid models | 109 |
| Table 7.2 Periods used for model calibration and periods encompassing the extreme storms | 110 |
| Table 7.3 Soil properties associated with each HOST class | 141 |
| Table 7.4 Catchment average values of soil properties for the Upper Thames and Stour catchments | 146 |
| Table 7.5 Parameter values for the prototype distributed model | 147 |
| Table 7.6 Summary of model performance for the prototype distributed model using 15 minute raingauge rainfall surface data | 148 |
| Table 8.1 Summary of the methodology used in identifying historical storm characteristics | 155 |
| Table 8.2 Historical storm characteristics: (O) denotes orographic, (C) denotes convective and (F) denotes frontal. | 156 |
| Table 8.3 Guidelines for applying storm modification and transposition options by storm type | 157 |
| Table 8.4 Summary of spatial rainfall data used as the basis for the modified storms | 159 |
| Table 8.5 Water balance information for Experiment 8 for the Stour at Shipston catchment using storms 3030, 3041 and 3047 | 176 |
| Table 8.6 Water balance information for Experiment 10 for the Sor at Bodicote using storms 3000, 3004 and 3013 | 180 |
| Table D.1 Versions of numerical scheme for the special cubic model | 222 |
| Table E.1 Comparison of observed and DTM-derived catchment areas | 228 |
| Table F.1 River Kent catchments. Calibrated PDM model parameters. The different rainfall factors used for each rainfall estimator are given (other parameters remain the same). | 230 |
| Table F.2 River Kent catchments. Sets of linear weights derived using Thiessen and multiquadric surface fitting methods and revised final sets used within the PDM | 231 |
| Table F.3 Upper Thames and Stour catchments. Calibrated PDM model parameters. The different rainfall factors used for each rainfall estimator are given (other parameters remain the same). | 232 |
| Table F.4 Upper Thames catchments. Sets of linear weights derived using Thiessen and multiquadric surface fitting methods and revised final sets used within the PDM (only Thames Region raingauges are considered). | 233 |
| Table F.5 Stour catchment. Sets of linear weights derived using Thiessen and multiquadric surface fitting methods and revised final sets used within the PDM (only Midlands Region raingauges are considered). | 233 |

| | |
|---|-----|
| Table F.6 River Darwen catchments. Calibrated PDM model parameters. The different rainfall factors used for each rainfall estimator are given (other parameters remain the same). | 234 |
| Table F.7 River Darwen catchments. Sets of linear weights derived using Thiessen and multiquadric surface fitting methods and revised final sets used within the PDM | 235 |
| Table F.8 All case studies: Calibrated Grid-to-Grid model parameters | 235 |
| Table G.1 River Kent catchments. R^2 performance statistics for the PDM (Grid-to-Grid results are in brackets) over calibration events listed by type of rainfall estimator used | 237 |
| Table G.2 River Kent catchments. R^2 performance statistics for the PDM over the case study extreme event 09:00 29 January to 09:00 8 February 2004, listed by type of rainfall estimator used (Grid-to-Grid model results are in brackets). | 238 |
| Table G.3 Upper Thames and Stour catchments. R^2 performance statistics for the PDM (Grid-to-Grid results are in brackets) over calibration events, listed by type of rainfall estimator used | 239 |
| Table G.4 Upper Thames and Stour catchments. R^2 performance statistics for the PDM over the case study extreme event 09:00 6 April to 09:00 19 April 1998, listed by type of rainfall estimator used (Grid-to-Grid model results are in brackets). | 239 |
| Table G.5 River Darwen catchments. R^2 performance statistics for the PDM (Grid-to-Grid results are in brackets) over calibration events listed by type of rainfall estimator used. | 240 |
| Table G.6 River Darwen catchments. R^2 performance statistics for the PDM over the case study extreme event 09:00 13 June to 09:00 16 June 2002, listed by type of rainfall estimator used (Grid-to-Grid model results are in brackets). | 240 |
| Table H.1 Details of the amplified storms created for the River Kent case study. Note that the rainfall amount, duration and FEH-estimated return period quoted relate to the River Kent at Victoria Bridge catchment. | 241 |
| Table H.2 Details of the amplified storms created for the River Darwen case study. Note that the rainfall amount, duration and FEH-estimated return period quoted relate to the River Darwen at Blue Bridge catchment. | 246 |
| Table H.3 Details of the amplified storms created for the Upper Thames case study. Note that the rainfall amount, duration and FEH-estimated return period quoted relate to the Sor at Bodicote catchment. | 252 |
| Table H.4 Details of the amplified storms created for the Stour at Shipston case study. Note that the rainfall amount, duration and FEH-estimated return period quoted relate to the Stour at Shipston catchment. | 256 |

1 Introduction

1.1 Objectives and approach

The main aim of this study is to develop a spatio-temporal extreme rainfall dataset based on raingauge and radar data, for historical storms and artificially-enhanced ones, for use in evaluating the performance of hydrological models during extreme events.

Two hydrological models are to be used in the evaluation and selected as being representative of the types of model likely to be encountered in practice, now or in the future. One is to be in operational use and of simple lumped form, and the other of spatially-distributed form and able to take full advantage of spatial weather radar data. Since many models share common elements, it will be possible to comment more broadly on the implications for other models.

A number of extreme storm events are to be selected that are sufficiently recent to include radar data coverage and some of which generated floods in catchments having historical flow records. The extreme storms and associated catchments are to be chosen to encompass the main classes of extreme event: convective, frontal and orographic. The catchments will ideally have gauging stations with good rating curves for high flows; however, the problem of rating extension will be considered as necessary.

The rainfall-runoff models are to be calibrated for the study catchments and used to carry out a detailed examination of catchment model behaviour - encompassing consideration of storm movement, storm coverage and soil moisture condition. Where deficiencies in model performance become apparent, ways of improving the model formulations will be sought.

A credible and practical approach to creating extreme rainfall datasets, through amplification of the historical data, will be developed taking into account areal extent and frequency-of-occurrence issues. Guidance on the estimation of extended flood flow ratings for assessing the impact of extreme rainfall events, and to allow forecasting systems to handle them, will be given if appropriate.

Use of the 'Extremes Dataset' for model destruction testing is an important application for the Environment Agency, as a procurer of hydrological models from third parties in support of its flood forecasting and warning systems. This application is to be given detailed consideration.

To aid this and other applications of the 'Extremes Dataset' (e.g. training, running 'what if?' scenarios), software will be developed to allow the dataset storms to be scaled (in magnitude) and transposed to any target catchment of interest.

The study is to provide guidelines and recommendations for rainfall-runoff modelling under extreme storm conditions.

1.2 Methodological framework

Figure 1.1 provides a broad methodological framework for addressing the objectives of the study. It identifies the need to select extreme events, to develop tools for rainfall transformation and areal rainfall estimation, and to apply these in a rainfall-runoff modelling context to assess model performance and behaviour.

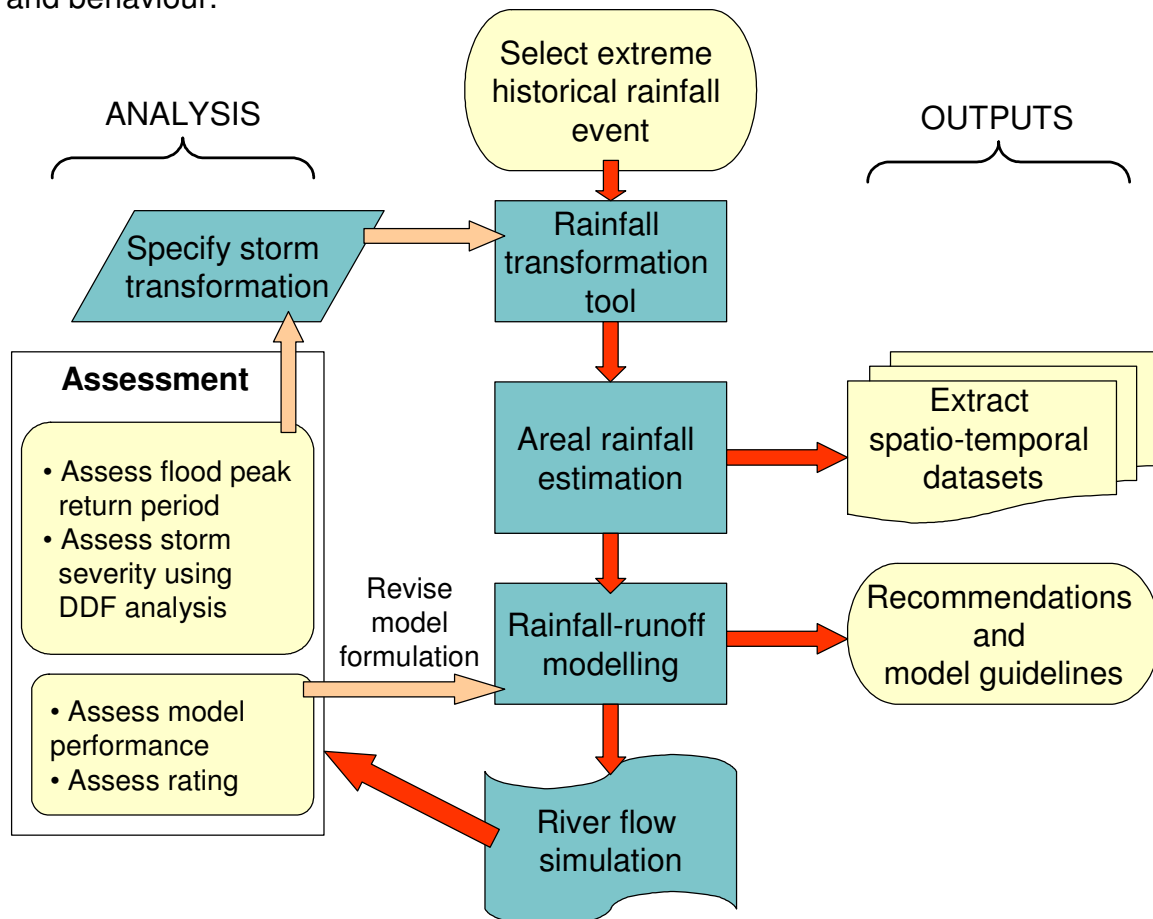


Figure 1.1 Methodological framework for the study

The rainfall transformation tool can be applied to consider storms more extreme than the historical event. Return periods of the associated catchment rainfalls and flood peaks can be assessed. Any failings identified in the model, taking account of possible shortcomings in rating curves, can be used to suggest and develop model improvements and the revised model reassessed.

The study outputs are generated within this framework in the form of the required extreme spatio-temporal rainfall dataset along with this report providing recommendations and model guidelines relevant to extreme flood event modelling. In addition, software has been developed that allows users to scale (in magnitude) and transpose any storm in the dataset to any catchment of interest.

1.3 Report overview

A brief outline of the report is given below, serving as a “roadmap” for what follows.

First, the issue of storm and case study selection is discussed in Section 2. An orographic, frontal and four convective rainfall events with radar coverage are selected from a broader menu of storms. As a result of consultation with Environment Agency hydrologists, three case study catchments experiencing extreme floods are identified, one for each type of rainfall. Hydrometric and weather data obtained to support the case studies are outlined. These data are included in the extreme dataset that forms an important output delivery of the study (Cole and Moore, 2006). Detailed descriptions of the case study rainfall events and catchments are given in Section 5.

Section 3 provides an outline of the lumped and distributed rainfall-runoff models selected for use in this study. The PDM (Probability Distributed Model) is chosen as representative of a lumped rainfall-runoff model and is used operationally by the Environment Agency. The Grid-to-Grid model, developed by CEH to exploit spatial information in gridded rainfall data and topographic datasets, is used as the distributed model.

Rainfall estimation and the creation of extreme spatio-temporal rainfall datasets are discussed in Section 4. Typically the input to lumped rainfall-runoff models is catchment average rainfall estimated by applying a set of linear weights to the point raingauge values. However, the main focus of the study is on providing spatial rainfall estimators. Section 6 considers areal rainfall estimates for catchment and grid-square areas obtained from weather radar data and by applying multiquadric interpolation methods to raingauge data alone or in combination with weather radar data.

A credible and practical approach to transforming historical spatial rainfall fields to more extreme ones is developed in Section 4.3. This results in a Rainfall Transformation Tool that can change the position, movement, orientation, size and shape of a spatio-temporal rainfall dataset. This is complemented by a 4D visualisation tool, developed to obtain animated displays of the transformed rainfall fields, and used to support the flood response studies.

The generation and application of extreme rainfall datasets for flood response experiments and model destruction testing requires an innovative methodology to assign return periods to both storms and floods. Building upon the Flood Estimation Handbook (FEH) research, Section 4.6 presents two approaches that use catchment specific return period estimates of both rainfall (amount and duration) and river flow.

The flood response of historical storm events is investigated using rainfall-runoff models in Section 7. For each case study, both rainfall-runoff models (PDM and Grid-to-Grid) are calibrated using, as alternative inputs, rainfalls obtained from the three rainfall estimators: radar-only, raingauge-only and raingauge-adjusted radar. The performance of the models is then assessed over the extreme flood

event and any failings noted. In one case, this acts as a catalyst to develop and trial a new prototype distributed formulation able to incorporate soil/geology property data.

Flood response experiments, using amplified storms as input to the rainfall-runoff models, are detailed in Section 8. A set of over 100 amplified storms are constructed using the Rainfall Transformation Tool. The experiments are designed to investigate complex storm to catchment interactions, and give improved understanding of extreme flood genesis helpful in identifying flood vulnerable situations.

An important output of the study is the 'Extremes Dataset' (Cole and Moore, 2006). The collated raingauge, radar, river flow/level and MORECS potential evaporation data together with the constructed spatial rainfall estimates (raingauge-only and raingauge-adjusted radar) has created a unique extreme storm dataset. For the flood response experiments the amplified spatio-temporal rainfalls are also included in the dataset. All the spatio-temporal rainfall data can be viewed through Hyrad. Also, software is provided to let users of the dataset scale (in magnitude) and move any of the historical or amplified storms to any catchment of interest. This allows users to perform their own flood response experiments with rainfall-runoff models used in practice.

2 Case study selection

2.1 Introduction

Firstly, a menu of recent storm events was identified jointly with the Met Office and is outlined in Section 2.2. The focus on recent events was to ensure radar coverage. Secondly, a final set of case studies, including catchments selected for rainfall-runoff modelling, was agreed after close consultation with Environment Agency regional hydrologists: these are outlined in Section 2.3. A detailed description of the case studies is given in Section 5.

2.2 Menu of storm events

Table 2.1 provides a menu of storm events identified using the following criteria:

- **Radar coverage:** The rainfall events had to be recent enough to be covered by radar data, preferably at a resolution of 2km or less.
- **Rainfall type:** Storms of orographic, frontal and convective type were required.
- **‘Extreme’ rainfall:** On account of the above criteria, the extreme rainfall threshold used in the Phase I Report of the “Extreme Rainfall and Flood Event Recognition Project” was considered too restrictive. Therefore other notable storms were considered as detailed below.

The events fall into three categories. The first are events identified in the Phase I Report that are recent enough to have radar records available for them. The second group of events are those studied as part of the Environment Agency/Met Office “Post Event Analysis Project” and carried out at the Joint Centre for Hydro-Meteorological Research, Wallingford. A third category of “Other Notable Events” encompass events that have been identified by CEH and the Met Office, based on past and recent experience of notable storms. Feedback has been sought and received from the Met Office on the meteorological suitability and priority of the events for the Project. The radar data requirements for the candidate events were initially checked with reference, in the first instance, to CEH’s own holdings of radar data; any missing data were subsequently requested from the Met Office.

Table 2.1 Menu of storm events

| Event date | Event location | Rainfall intensity | Rainfall type | Other information |
|--|---|--|--|--|
| Extreme Rainfall and Flood Event Recognition Report (2002) Events | | | | |
| 19 May 1989 (Table 3, ERFER) | Halifax Storm Walshaw Dean | 193 mm in 2 hours | Convective | Weather, 46(7), 1991 |
| 31 August 1994 (Table 3, ERFER) | Bungay (East Anglia) | 146 mm in 12 hours | Frontal | |
| 22-23 September 1992 (ERFER, p36) | Sleaford (Lincolnshire) | | Widespread, double frontal, embedded convection | Not extreme by Bilham. Silk Stream (Thames) very susceptible |
| Post Event Analysis Project Events | | | | |
| 14 June 2002 | Northwest | 25-40 mm in 2 hrs, >60 mm hr ⁻¹ rates | NW Thunderstorm | River Darwen (71/14: Blue Bridge, 71/13: Ewood) Flooding of Blackburn |
| New Year 2003 | Thames | | Frontal | Also affected Anglian, Southern, Southwest |
| 19 May 2003 | North Wales | | Intense rain in N Wales | Flood Watches on 20 th : Conwy, Dyfi, Afonydd Wnion/Mawddach, Upper Dee |
| 1 February 2004 | Capel Curig (Snowdonia) | 260 mm (96 hours to 2 February 2004) | Orographic | Also South Wales in Jan 2004 |
| Other Notable Events | | | | |
| 10 August 2003 (Met Office advised) | Carlton-in- Cleveland (North Yorkshire – Teesside Storm) | 49 mm in 15 minutes | Convective | Fast moving, accompanying large hail & squall Down Pennines & round NW corner of North York Moors |
| Easter 1998 (CEH Study Event) | Midlands | 66mm in 15 hours | Frontal | Stour at Shipston Studied by CEH with raw radar |
| Autumn 2000 (CEH Study Event) | Southern | | | Medway Studied by CEH but without radar |
| 16 August 2004 | Boscastle, North Cornwall | 154 mm in 6 hours | Orography & unstable air triggering convection | River Valency to Boscastle |

2.3 Identification of case studies

The menu of storm events was also considered for their hydrological suitability using the additional criterion:

- **Flood impact and catchment modelling:** Catchments affected by the storm had to be identified, if any, and their suitability for rainfall-runoff modelling assessed.

Hyrad displays of radar data have been used to visualise the storm development as a means of selecting gauged catchments for investigating the flood response via rainfall-runoff modelling. This initial event and catchment selection formed the basis of more detailed discussions with Environment Agency hydrologists in Welsh, Northwest and Northeast regions, with the aim of identifying case studies for rainfall-runoff modelling in frontal, convective and orographic extreme rainfall. This culminated in agreement on case studies to use and a formal request for river flow and raingauge data.

The outcome of these discussions are summarised below under each of the three rainfall type categories.

(i) Orographic Rainfall. The orographic Case Study in Wales on 1 February 2004 was abandoned for a number of reasons: the River Conwy is at long range from the Clee Hill radar and flow gauging is problematic; the flood warning impact in South Wales was not significant and the Dyfed radar is known to be problematic for measuring rainfall in the valleys under conditions of low level growth. Subsequent discussions with Northwest and Northeast regions identified, for the same storm system, significant orographic rainfall with associated flood impact affecting the River Kent and Kendal in the Lake District and the Upper Ure and Bainbridge in Yorkshire, with notable falls recorded at Tow Hill raingauge. The River Kent basin has a good hydrometric network with 5 gauging stations affected by the storm, thereby providing important information on the spatial development of the flood response. Detailed data requests for the River Kent were developed in association with Northwest Agency hydrologists.

(ii) Convective Rainfall. The Blackburn (Darwen) storm was the first Case Study to be identified and developed in discussion with the Environment Agency. This storm affected the River Darwen gauged at Blue Bridge and caused flooding at Blackburn. A second gauge in the headwaters at Ewood was seen as useful for gaining an understanding of flood response to rainfall as a function of catchment size. The suitability of these sites was discussed with the Agency, agreement reached on their use as a case study, a data request made and data received.

Three other convective storms in Table 2.1 – Halifax, Boscastle and Carlton-in-Cleveland - were included in the rainfall dataset but not developed as hydrological case studies due to the lack of gauged flow responses. These storms are still useful as the radar data for each are

used in creating the modified spatial rainfall datasets – see Section 4. Radar data for the day of the Halifax Storm was provided by the Met Office.

The fast moving convective storm on 10 August 2003, resulting in notable falls at Carlton-in-Cleveland, has been tracked using Hyrad to identify gauged catchments that were impacted. This identified the River Wiske but the Agency confirmed that only a small river stage rise of 0.5 m resulted. The event provides an example of how storm speed influences flood response and presents within the project the prospect of artificially slowing down the storm to amplify the modelled flood response. Analysis of this storm did reveal the upper limit of raw radar instantaneous measurement of 126 mm h^{-1} which transformed to variable values (138 mm h^{-1} was the highest observed) in the QC product.

(iii) Frontal Rainfall. Existing data archives at CEH have been used for the “Easter 1998” event as it impacted on the Stour at Shipston. This catchment, in Midlands Region and draining to the River Severn, was selected in the past by the Agency as of significant flood warning interest. In addition, two adjoining Thames Region catchments - the Sor at Bodicote and the River Cherwell at Banbury - were included to form an “Upper Thames and Stour” hydrological case study. Of particular interest are the differing responses of these neighbouring catchments.

Further investigation of Case Studies for frontal rain has highlighted that extreme floods are associated with large catchments and problems with radar coverage.

The final set of case studies and catchments selected for rainfall-runoff modelling are summarised in Table 2.2 along with the raingauge assessed rainfall magnitude. A comprehensive description of the rainfall events and the study catchments is given in section 1.

Table 2.2 Summary of case studies

| Event Date | Event location(s) | Rainfall magnitude | Study catchments |
|-----------------------------------|--|--|--|
| <i>Orographic rainfall</i> | | | |
| 30 Jan – 3 Feb 2004 | River Kent, Northwest Region | 229.2 mm in 96 hours, Brotherswater | 1. Kent at Sedgwick 2. Kent at Victoria Bridge 3. Sprint at Sprint Mill 4. Mint at Mint Bridge 5. Kent at Bowston |
| <i>Frontal rainfall</i> | | | |
| 8-9 Apr 1998 | Stour at Shipston, Midlands Region. River Cherwell and Sor, Thames Region | 76.6 mm in 14 hours, Pershore. 66 mm in 15 hours, Shipston. | 1. Stour at Shipston 2. Cherwell at Banbury 3. Sor at Bodicote |
| <i>Convective rainfall</i> | | | |
| 14 Jun 2002 | River Darwen, Blackburn. Northwest Region. | 31.4 mm in 1 hour, Darwen Sunnyhurst. | 1. Darwen at Blue Bridge 2. Darwen at Ewood |
| 10 Aug 2003 | Carlton-in-Cleveland, North Yorkshire, Northeast region. | 49 mm in 15 minutes, Carlton-in- Cleveland | N/A |
| 19 May 1989 | Halifax Storm, Northwest Region | 193 mm in 2 hours, Walshaw Dean | N/A |
| 16 Aug 2004 | Boscastle, Southwest Region. | 200.4 mm daily total, Otterham. 153.6 mm in 6 hours, Lesnewth (TBR) | N/A |

3 Hydrological model selection

3.1 Introduction

The spatio-temporal rainfall datasets are required to assess the performance of rainfall-runoff models under extreme storm conditions. Any failings in model response will serve as a catalyst to seek model improvement or alternative models. The model response studies may also lead to a better understanding of flood genesis from extreme storms and help recognise locations more vulnerable to flooding in relation to storm type and catchment form. For the purposes of this study there is a need to select two rainfall-runoff models that can be considered to be representative of other models likely to be considered for flood forecasting. One of the models should be lumped in form and used operationally for flood forecasting. The other should be a distributed rainfall-runoff model suitable for exploiting to the full weather radar data in grid-square form.

The PDM (Probability Distributed Model) has been selected as the lumped model in operational use. This is a popular conceptual model used throughout Northeast Region, part of Anglian Region, is an option for use in Thames Region, and is being calibrated for use in Southern Region under the National Flood Forecasting System initiative. It also performed well in a recent model intercomparison study commissioned by the Environment Agency (Moore *et al.*, 2000; Moore and Bell, 2001). One of the advantages of the PDM for the present study is that it provides a toolkit of model components which can be configured to accommodate a variety of behaviours of catchment flood response. Also some of the model components are generic forms of those used by other popular rainfall-runoff models, so the results will have more general relevance. A description of the PDM is given in Section 3.2.

The Grid-to-Grid model, a grid-based hydrological model, has been selected as representative of a distributed rainfall-runoff model capable of using grid-square weather radar data. The modelling framework has been specially prepared for use in this study to investigate flood responses to extreme rainfall provided in spatio-temporal (space-grid time-series) form. The model should prove of particular value in gaining an appreciation of the flood response associated with intense convective storms displaying marked spatial variability in rainfall. It is able to make full use of the spatially-distributed rainfall datasets developed as part of this study. The model employs Digital Terrain Model (DTM) data to support its configuration and parameterisation. It has a modular formulation which allows model revisions/extensions to be made to represent special flood response behaviours that might arise during extreme storms. It also supports modelling of nested and parallel catchments through adopting an area-wide formulation. The model formulation is outlined in Section 3.3.

3.2 The PDM (Probability Distributed Model)

The PDM is presented in Figure 3.1 in the structural form most commonly used in practice. Both fast and slow response routing components, here more loosely referred to as surface and subsurface storages, can be represented by the Horton-Izzard equation (Dooge, 1973). This equation results from continuity and the simple nonlinear storage form of momentum equation, $q=kS^n$, where q is flow rate per unit area, S is water storage per unit area and k^{-1} (the storage time-constant) and n are parameters of the relation. Solutions for different values of n are provided that cater for behaviours characteristic of channel and groundwater translation systems (see Appendix A of Moore and Bell, 2002). As an alternative to the Horton-Izzard formulation, either routing storage can be represented by a cascade of two linear reservoirs. Solution of this system takes the form of a Transfer Function (TF) model with dependence on two past outputs and the present and past input (Box and Jenkins, 1970; O'Connor, 1982). Whilst the TF model has four parameters, this is linked directly to the two physical time-constants of its equivalent reservoir storage model and its continuity constraint; imposing equality of time-constants reduces the parameters to one. In practice, the PDM is usually applied in a form that invokes a cubic storage ($n=3$) representation of the subsurface (groundwater) store and a cascade of two linear reservoirs (the TF model) for the surface (channel) storage.

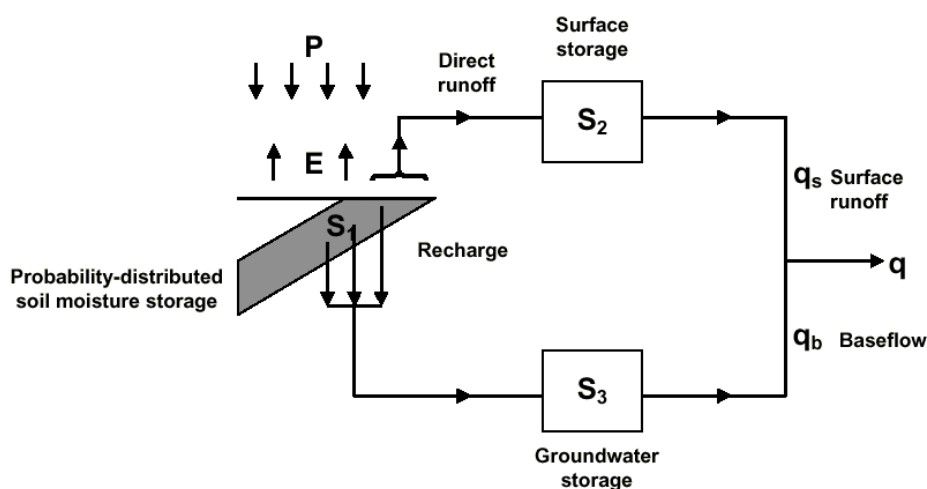


Figure 3.1 The PDM rainfall-runoff model

The runoff production component of the PDM assumes that runoff is generated via a saturation excess mechanism controlled by the combined absorption capacity of the soil, canopy and surface depressions. Infiltration capacity control on water entry into the soil is assumed not to be a dominant process (although a variant has been developed for this). It is recognised that absorption capacity will vary from point to point within a river basin and, whilst the geometric (location specific) form of this variation may be difficult to establish, the frequency of occurrence of capacities of different size can be readily parameterised. Thus by invoking a probability density distribution, $f(c)$, of absorption capacity, c , across the basin, then the proportion of the basin with point capacities less than or equal to C^* is given by the distribution function

$F(C^*) = \text{Prob}(c \leq C^*) = \int_0^{C^*} f(c)dc$. With A denoting the area of the basin, then $A F(C^*)$ is the contributing area of direct runoff. If the initial state of the basin is such that all stores of capacity less than C^* are full and net rainfall occurs at a rate π over an interval Δt , then the initial rate of runoff production per unit area is $q = \pi F(C^*)$ and the volume of runoff production per unit area over the interval is $V = \int_{C^*}^{C^* + \pi \Delta t} q(\tau) d\tau$. At the end of the interval all stores with capacities not greater than $C^* + \pi \Delta t$ are full and primed to generate runoff from more rain. The storage of water in the basin (expressed as a depth over the basin) at the start of the interval is $S = \int_0^{C^*} (1 - F(c))dc$ and at the end is given by continuity as $S + \pi \Delta t - V$. Some refinement of these expressions is required if the maximum storage capacity of the basin, S_{max} , is reached within the time-interval. It becomes a simple algebraic task to obtain solutions for the integral expressions, for chosen forms of density function, so as to calculate the volume of runoff generated at each time-step and maintain the basin storage water balance. A Pareto or truncated Pareto distribution is normally invoked for practical applications although the PDM toolkit offers a range of options. The probability-distributed theory and solutions to the integrals are developed further in Moore (1985, 1999) and Moore and Bell (2002). The net rainfall rate π is defined to make allowance for evaporation loss and drainage to groundwater, both as functions of moisture storage.

3.3 The Grid-to-Grid Model

The structure of the distributed Grid-to-Grid Model is summarised in Figure 3.2.

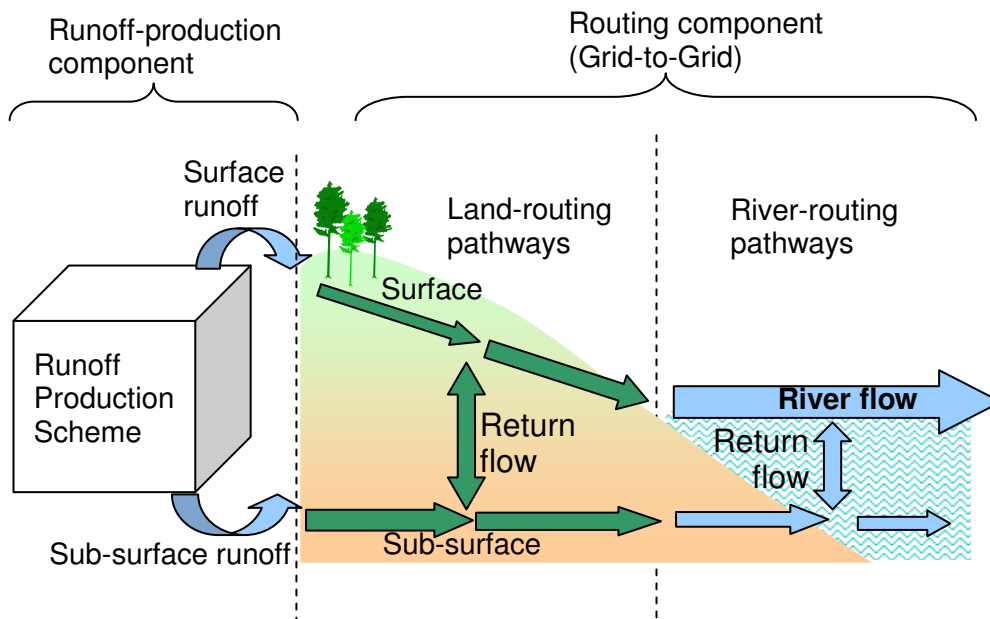


Figure 3.2 Schematic of the distributed model structure

The basic form of model employs a simple terrain-based runoff production scheme, based on methodology used in the CEH Grid Model (Bell and Moore, 1998a,b), to derive surface and sub-surface runoffs from gridded rainfall and potential evaporation inputs (see Section 3.3.1). The Grid-to-Grid water routing component employs a kinematic wave formulation that is equivalent in conceptualisation to a network cascade of linear reservoirs (see Section 3.3.2). Surface and sub-surface runoffs are routed via parallel fast and slow response pathways linked by a return flow component representing stream-soil-aquifer interactions. The terrain-following flow paths are configured using the DTM (see Appendix E).

3.3.1 Probability-distributed runoff production scheme for grid models

This section sets down the probability-distributed runoff production scheme employed within the Grid Model (Bell and Moore, 1998a,b) and used within the basic form of Grid-to-Grid Model. The scheme is based on the use of a probability-distributed store within a model grid-square to control runoff production, soil water storage, drainage and evaporation. The basic Grid Model runoff-production scheme is first outlined. The probability-distributed scheme is then developed as a variant.

Basic runoff production scheme

For a given grid square, the following linkage function is used to relate the maximum water storage capacity, S_{max} , and the average topographic gradient, \bar{g} , within the grid square:

$$S_{max} = c_{max} \left(1 - \frac{\bar{g}}{g_{max}} \right), \quad (3.1)$$

for $\bar{g} \leq g_{max}$. The parameters g_{max} and c_{max} are upper limits of gradient and storage capacity respectively and act as "regional parameters" for the runoff-production model. An estimate of mean slope for each grid square can be obtained from a DTM. In turn, this allows values for the structural parameter S_{max} for all grid squares to be determined using only the two regional parameters, g_{max} and c_{max} .

The soil column loses water as runoff, drainage and evaporation, as indicated in Figure 3.3. If the column is fully saturated from previous rainfall, then further addition of rain spills over as runoff and is routed via fast pathways. Drainage from the base of the column is dependent on the volume of water stored, S , and is routed via slow pathways. Finally, water is lost from the top of the column via evaporation.

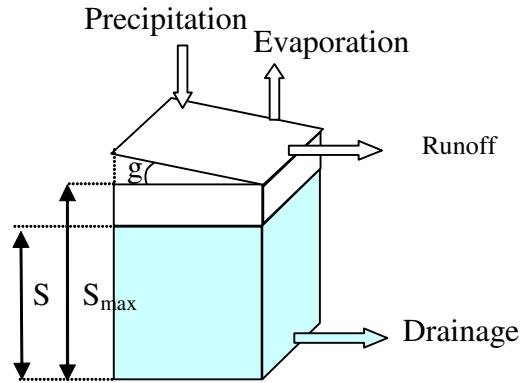


Figure 3.3 A typical grid-box storage illustrating the components of the water balance

Specifically a water balance is maintained for each grid square and time interval (ignoring time and space subscripts for notational simplicity) as follows. Evaporation loss from the soil column occurs at the rate, E_a , which is related to the potential evaporation rate, E , through the relation

$$E_a = E \left\{ 1 - \left(\frac{S_{\max} - S}{S_{\max}} \right)^2 \right\} \quad (3.2)$$

where S is the depth of water in store. Drainage from the grid-box occurs at the rate

$$d = \begin{cases} k_d (S - S_t)^\beta, & S - S_t > 0, \\ 0, & S - S_t \leq 0, \end{cases} \quad (3.3)$$

where the regional parameters are k_d a storage rate constant, S_t a soil tension threshold below which there is no drainage and β an exponent of the relation (often set to 3). If $S_{\max} < S_t$ then drainage from that grid square can never occur.

Finally, the (potential) water storage is given by the update equation

$$S = \max(0, S + p\Delta t - E_a\Delta t - d\Delta t), \quad (3.4)$$

where p is the rainfall rate. The direct runoff rate contributing to the fast pathways is then calculated as

$$q = \max(0, S - S_{\max}), \quad (3.5)$$

and the water storage S reset to S_{\max} if direct runoff is generated.

The inflows to the flow-routing scheme of equation (3.16), u_r or u_l , and u_{rb} or u_{lb} , comprise the surface and sub-surface runoff terms, q and d , in equations (3.5) and (3.3), depending on whether the grid-square is assigned land or river.

Probability-distributed runoff production scheme

In order to introduce heterogeneity of soil storage within a grid square, the probability-distributed soil moisture (PDM) formulation developed by Moore (1985, 1999) has been applied to an individual grid-square. A perceived benefit of introducing this additional level of complexity is that a certain proportion of the grid square is assumed to be saturated and generating runoff, even when rainfall amounts are small. Under the basic formulation outlined above, an entire grid-square has to become saturated before it generates runoff.

The probability-distributed extension to the basic runoff production scheme is developed as follows. Consider the simple empirical relation between gradient, g , and storage capacity, c , at a point

$$c = (1 - g/g_{\max}) c_{\max}, \quad (3.6)$$

where g_{\max} and c_{\max} are the maximum regional gradient and storage capacity values. For a given distribution of gradient within a grid-square, equation (3.6) can be used to derive the distribution of storage capacity over the square in terms of the parameters defining the distribution of gradient.

The choice of distribution can be guided by constructing frequency curves of topographic slope from DTM data, both for within-grid square areas and for whole regions. Particular distributions, such as truncated exponential or power, can be fitted to the slope frequency curve data. Parameters defining these distributions may then be used in the derived distribution for store capacity. The probability distributed formulation presented by Moore (1985) can then be used to obtain the proportion of each grid square which is saturated and in turn the volume of runoff generated.

The distribution function of store capacity for a power distribution of slope may be derived as follows. Consider slopes in the range $0 \leq g \leq g_{\max}$ which follow a power distribution of the form

$$F(g) = \text{Prob}(\text{slope} \leq g) = \left(\frac{g}{g_{\max}} \right)^b \quad 0 \leq g \leq g_{\max} \quad (3.7)$$

with the exponent b related to the mean slope \bar{g} by

$$b = \frac{\bar{g}}{g_{\max} - \bar{g}}. \quad (3.8)$$

The distribution function of storage capacity may be derived assuming equation (3.6) to hold, and takes the Pareto distribution form

$$F(c) = 1 - \left(1 - \frac{c}{c_{\max}}\right)^b \quad c \leq c_{\max}. \quad (3.9)$$

From the PDM methodology (Moore, 1985) it then follows that the soil moisture storage S and the critical capacity C^* are related by

$$S = \frac{c_{\max}}{b+1} \left[1 - \left(1 - \frac{C^*(t)}{c_{\max}}\right)^{b+1}\right]. \quad (3.10)$$

The critical capacity is that below which all stores of smaller capacity are full and generating surface runoff during rainfall. Note that the maximum possible value of soil moisture storage over the grid-square is given by

$$S_{\max} = \frac{c_{\max}}{b+1}, \quad (3.11)$$

which is also the mean store capacity, \bar{c} . It is this Pareto-based formulation that constitutes the probability-distributed variant of the basic runoff production scheme.

Note that the constraint $S_{\max} \geq \bar{c}_{\min}$ can be imposed to prevent any grid-square having a zero maximum storage capacity; here \bar{c}_{\min} is the minimum mean store capacity of a grid-square that is allowed and is treated as a regional parameter. For grid squares where this constraint applies, c_{\max} is recalculated using (3.1) with $S_{\max} = \bar{c}_{\min}$.

3.3.2 Grid-to-Grid flow routing scheme

The basic 1-D scheme

The 1-D kinematic wave equation relates channel flow, q , and lateral inflow per unit length of river, u , by

$$\frac{\partial q}{\partial t} + c \frac{\partial q}{\partial x} = cu, \quad (3.12)$$

where c is the kinematic wave speed and x and t are distance along the reach and time respectively. Consider time, t , and space, x , to be divided into discrete intervals Δt and Δx such that k and n denote positions in discrete time and space. Invoking difference approximations to the derivatives in (3.12) gives the discrete formulation

$$q_k^n = (1 - \theta)q_{k-1}^n + \theta(q_{k-1}^{n-1} + u_k^n) \quad (3.13)$$

where the dimensionless wave speed $\theta = c \Delta t / \Delta x$ and $0 < \theta < 1$. This is a recursive formulation which expresses flow out of the n 'th reach at time k , q_k^n , as a linear weighted combination of the flow out of the reach at the previous time with inflow to the reach from upstream (at the previous time) and the total lateral inflow along the reach (at the same time).

An alternative derivation of equation (3.13) can be sought from a simple hydrological storage approach. The n 'th reach can be viewed as acting as a linear reservoir with its outflow related linearly to the storage of water in the reach such that

$$q_k^n = \kappa S_k^n, \quad (3.14)$$

where κ is a rate constant with units of inverse time. If S_k^n is the storage in the reach just before flows are transferred at time k , then continuity gives

$$S_k^n = S_{k-1}^n + \Delta t (q_{k-1}^{n-1} - q_{k-1}^n + u_k^n) \quad (3.15)$$

and the equivalence to (3.13) follows, given $\theta = \kappa \Delta t$ with $\kappa = c / \Delta x$.

It is the above 1-D scheme that forms the basis of CEH's KW channel flow routing model (Moore and Jones, 1978; Jones and Moore, 1980) and is invoked to represent fast and slow pathway routing in the Grid Model of Bell and Moore (1998). It is a scheme based on a discrete approximation of the 1-D kinematic wave equation with lateral inflow as expressed by equation (3.13)

The 2-D Grid-to-Grid scheme

In the Grid-to-Grid Model it is assumed that a runoff-production scheme first partitions precipitation and evaporation fluxes into water stored in the soil and canopy, and water generated as surface and sub-surface runoff. The above kinematic routing scheme is then applied separately to these runoffs so as to represent parallel fast ("surface") and slow ("subsurface") pathways of water movement. The routing scheme also allows for different formulations over land and river pathways (initially just a different wave speed). The scheme as used for the Grid-to-Grid Model differs in two distinct ways from that implemented for the Grid Model. The first is that water is explicitly transferred from one grid to another based on topographic control. (In contrast, the Grid Model maps runoff from each grid onto a cascade of routing reaches defined via isochrones inferred from the DTM.) Secondly, a *return flow* term allows for flow transfers between the subsurface and surface pathways representing surface/sub-surface flow interactions on hillslopes and in river channels.

The Grid-to-Grid routing scheme equations in 1-dimension are:

$$\begin{aligned}
\frac{\partial q_l}{\partial t} + c_l \frac{\partial q_l}{\partial x} &= c_l (u_l + R_l) \\
\frac{\partial q_{lb}}{\partial t} + c_{lb} \frac{\partial q_{lb}}{\partial x} &= c_{lb} (u_{lb} - R_l) \\
\frac{\partial q_r}{\partial t} + c_r \frac{\partial q_r}{\partial x} &= c_r (u_r + R_r) \\
\frac{\partial q_{rb}}{\partial t} + c_{rb} \frac{\partial q_{rb}}{\partial x} &= c_{rb} (u_{rb} - R_r)
\end{aligned} \tag{3.16}$$

where q_l is flow over land pathways, q_r is flow over river pathways, R_l and R_r denote land and river return flow, and u_l and u_r are inflows for land and river, which include runoff generated by a runoff-production scheme. The additional subscript b denotes sub-surface (“baseflow”) pathways. The wave speed c can vary with the pathway and surface-type combination as indicated by the suffix notation.

The four partial differential equations are each discretised using a finite-difference representation similar to equation (3.13), but extended to include the return flow term R_k^n , such that

$$q_k^n = (1 - \theta) q_{k-1}^n + \theta (q_{k-1}^{n-1} + u_k^n + R_k^n). \tag{3.17}$$

For application to two dimensions, the q_{k-1}^{n-1} term, which represents inflow from the preceding grid-cell in space, is given by the sum of the inflows from adjacent grid-cells.

In practice, the routing is implemented in terms of an equivalent depth of water in store over the grid square, S_k^n , where $q_k^n = \kappa S_k^n$, and the inflow and return flow are also parameterised as water depths. The return flow to the surface is given by $R_k^n = r S_k^n$, where S_k^n is the depth of water in the subsurface store and r is the return flow fraction. This fraction takes a value between zero and one since it represents the proportion of the sub-surface store content that is routed to the surface, and can differ for land and river paths. For sub-surface routing, the return flow term is modified to subtract from water in store. Note that whilst return flow is normally positive, it can take negative values to represent influent, rather than the more normal effluent “stream” conditions. The flow-routing scheme allows for different values of the dimensionless wave speed, θ , for the different pathway (surface or subsurface) and surface-type (land or river) combinations.

4 Methodologies for constructing and using extreme spatio-temporal rainfall datasets

4.1 Introduction

Developing appropriate methodologies for constructing extreme spatio-temporal rainfall datasets and associating a frequency of occurrence to them constitute major challenges for this study. Use of the historical and amplified datasets in flood response studies and for model destruction testing also requires careful consideration. These issues are addressed in detail in this section whilst an outline of the section content is given below.

The extreme rainfall datasets created consist of two parts: historical rainfall data and artificially generated rainfall data. For the historical case study storms (previously identified in Section 2.3) there are three principle types of rainfall estimator available: radar data, raingauge-only data and raingauge-adjusted radar data; these estimators are discussed in Section 4.2. Two forms of artificially generated rainfall data are considered. Firstly a practical methodology for “amplifying” historical rainfall data to generate more extreme artificial storms is developed in Section 4.3. This form is used for the main flood response experiments described in Section 7. Secondly, simple synthetic temporal rainfall profiles of a rectangular or triangular composition are considered for input into lumped models: an example is given in Section 4.6.1.

Methodologies developed for constructing extreme rainfall datasets are detailed in Section 4.6. The rainfall datasets and river flow (observed or modelled) need to be placed in a frequency of occurrence context. The Phase 1 Report used the Flood Studies Report (FSR) to derive a UK-wide point rainfall threshold for classifying historical storms as extreme. Whilst this UK-wide threshold was clearly useful for identifying historical extreme storms it becomes less relevant for the specific catchment case studies of interest here. The Flood Estimation Handbook (FEH), and subsequent developments, provide methodologies for deriving consistent catchment specific return period estimates of both rainfall and river flow which are exploited in this report. The frequencies of occurrence of rainfall and river flow are discussed in Section 4.4 and 4.5 respectively.

Finally the use of extreme rainfall datasets for destruction testing of rainfall-runoff models is discussed in Section 4.7.

4.2 Rainfall estimators

4.2.1 Point rainfall estimators

Raingauges provide estimates of rainfall at a point. These can be used directly to estimate the catchment average rainfall for input into lumped rainfall-runoff models by applying a set of linear weights to the point raingauge values. Various options can be used to derive these weights. Thiessen weighted catchment average rainfall (Thiessen, 1911) is the most common form of rainfall input used operationally for lumped rainfall-runoff modelling. This weighting method is considered as part of the historical model performance assessment in Section 7. However, utilising point raingauge values within a distributed grid-based model - which is intentionally designed to exploit spatial information - is not a straightforward task and is discussed in the following section.

4.2.2 Spatial rainfall estimators

Spatial rainfall estimators are the main form of rainfall input used for rainfall-runoff modelling in this report. This is partly driven by wanting to exploit the distributed formulation of the Grid-to-Grid model. Allied to this, spatial rainfall estimators provide increased flexibility, compared to point rainfall estimators, for the options available for storm amplification (e.g. altering the spatial location and extent of storms). This allows the flood response experiments to investigate complex storm to catchment interactions and to give improved understanding of extreme flood genesis.

Three principle types of historical spatial rainfall estimator are considered in this study:

1. **Radar data.** The finest resolution single-site radar data available. Preferably Nimrod Quality Controlled (Nimrod QC) data.
2. **Raingauge-only surface.** A gridded spatial surface fitted to point raingauge values every 15 minutes with a 1km resolution.
3. **Raingauge-adjusted radar.** Raingauge adjustment factors are calculated for radar grid-squares coincident with raingauge locations. A surface of adjustment factors are fitted to these point values and applied to the radar image. This is repeated at 15 minute intervals.

The gridded rainfall data can be immediately used as input to distributed rainfall-runoff models such as the Grid-to-Grid model used in this study. Also catchment average rainfalls can easily be calculated from the gridded rainfall datasets for use as input to lumped rainfall-runoff models.

The multiquadric surface fitting technique used to generate the gridded surfaces is detailed in Appendix C. The relative performance of the three types of spatial rainfall estimator, from a rainfall perspective, is discussed in Section 6. Their

relative performance from a hydrological perspective, when used for rainfall-runoff modelling, is discussed in Section 7.

4.3 Rainfall amplification

A credible and practical methodology has been developed to transform historical spatial rainfall fields so they are made more extreme, including their areal extent. The approach essentially takes historical grid-square rainfall data and “amplifies” each time-frame to create a modified storm that is also output in a gridded format that replicates the radar data. A summary of the storm transposition and modification options that have been developed are given below. Their application for “amplifying” historical storms and for the flood response studies are also discussed.

Relative spatial position. Storms can be relocated to any location, e.g. from one case study catchment to another and/or to different locations relative to a given catchment.

Relative temporal position. Storms can be relocated to any point in time, e.g. a different month of the year or after a period of high/low flow, allowing investigation of the impact antecedent moisture conditions can have on flood response.

Relative direction and speed of travel. Storms paths can be created with altered directions and speed of travel relative to the original, e.g. slowing down a storm so that the point rainfalls generated are greater but the total areal extent of the storm path is less. This modification can have a particular relevance for the catchment or river network in question, e.g. following a river from the source to the catchment outlet or vice versa.

Scaling of amounts. The rainfall rates of the original storm are scaled by a factor. Normally used to create storms with greater rainfall intensities and accumulations.

Spatial squeezing (preserving rainfall amounts). Spatial squeezing is performed preserving the rainfall total i.e. rainfall rates are adjusted. The main application would be to make the storm have a smaller spatial extent but with increased rainfall rates, e.g. spatially squeezing a convective cell to create a more localised and intense storm.

Spatial expansion (*not* preserving rainfall amounts). Spatial expansion is performed preserving rainfall rates i.e. the rainfall total will change. The main application would be to make the storm have a larger spatial extent but with the same rainfall rate, e.g. spatially expanding a convective cell to create a more spatially extensive storm whilst preserving rainfall rates.

Time squeezing (preserving rainfall amounts). Time squeezing is performed preserving the rainfall total i.e. rainfall rates are adjusted. The

main application would be to make the storm have a shorter duration with increased rainfall rates, e.g. time squeezing a convective cell to create a shorter, more intense storm.

Time expansion/contraction (*not* preserving rainfall amounts).

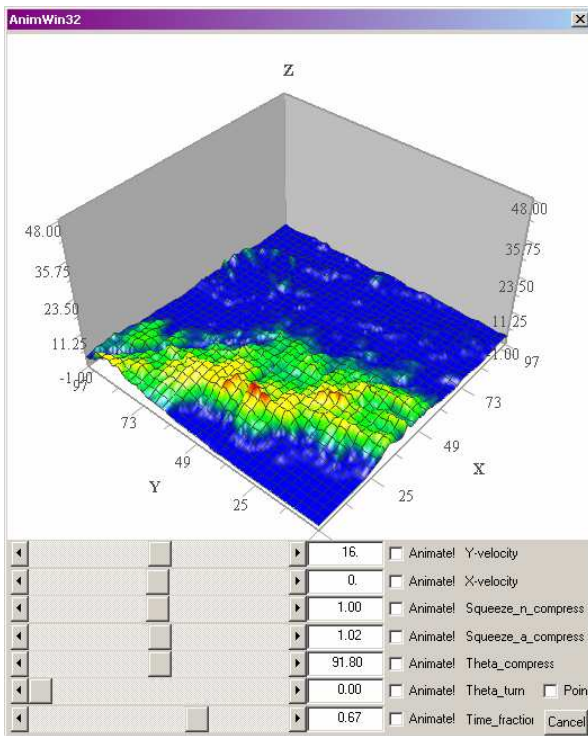
Temporal expansion/contraction is performed preserving the rainfall rates i.e. the rainfall total will change. The main application would be to make the storm have a longer duration but using the same rainfall rates, therefore increasing the total rainfall amount, e.g. time expanding a frontal event to create a longer duration storm with greater storm total whilst using the original rainfall rates.

A full description of the storm transposition and modification options available, including the mathematical formulae used, is given in Appendix A and B. Note that the changes to storm movement and areal coverage required for the flood response studies are encompassed by the proposed transformation methodology.

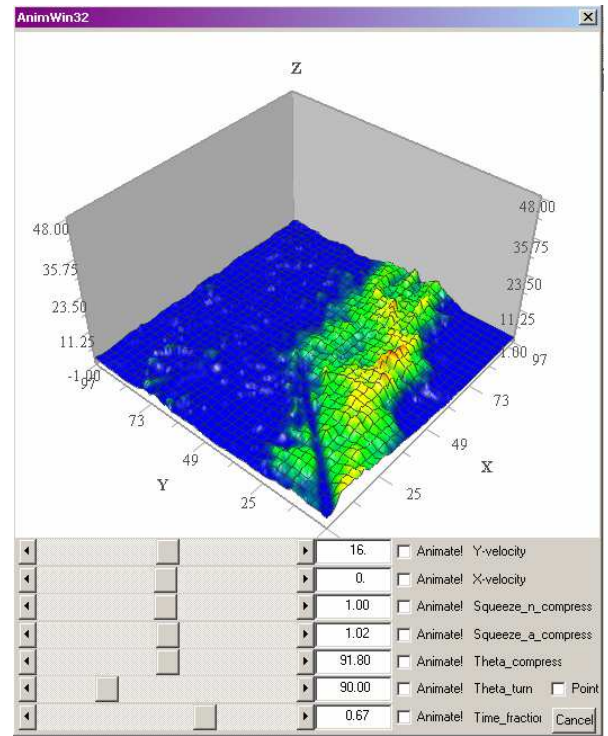
These options can be used in isolation or in conjunction with each other and have been coded up to form a Rainfall Transformation Tool that can be applied to spatio-temporal rainfall datasets to obtain artificially-enhanced fields. This 4D visualisation software allows easy exploration of the different modification options and aided the generation of amplified storms with desired properties. Static examples of this temporally-animated visualisation, using different forms of field transformation, are shown in Figure 4.1.

In order to apply the modifications a set of historical storm characteristics were derived from sequences of radar data for the case study storms. Details of these are listed in Section 8.2 along with guidelines for applying the modifications. A catalogue of the amplified storms that form part of the extreme spatio-temporal rainfall dataset can be found in Appendix H.

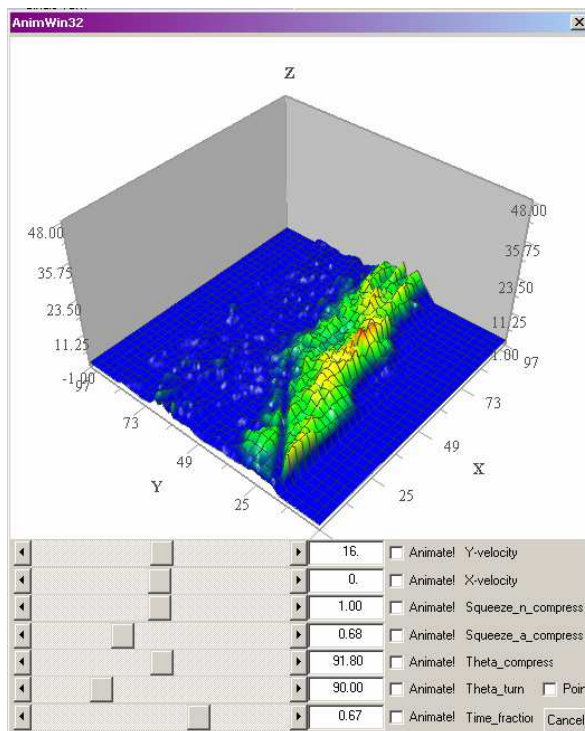
(a) Initial rainfall field



(b) Rotate by 90°



(c) Lateral-compression normal to band



(d) Lateral-compression along band

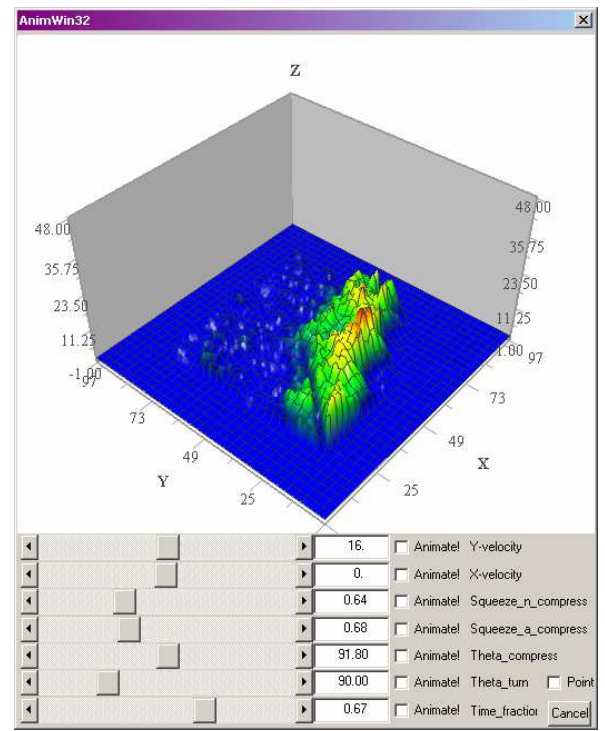


Figure 4.1 Rotation and compression of a radar rainfall field using the Rainfall Transformation Tool

4.4 Rainfall datasets and frequency of occurrence

A methodology is required that places the rainfall datasets in a frequency of occurrence context. This issue is not straightforward to resolve and demands an innovative solution. Section 4.4.1 reviews the UK-wide extreme point rainfall threshold used in the Phase 1 Report and explains why an alternative catchment specific approach, detailed in Section 4.4.2, is used here.

4.4.1 Phase 1 classification of ‘extreme’ rainfall events

The UK-wide extreme point rainfall threshold used in the Phase 1 Report is given here in the final row of Table 4.1 and is derived using the Flood Studies Report (FSR). For durations of 24 hours or greater the extreme threshold values were the 1 in 100 year return period rainfalls taken from Table 3.4 of the FSR Vol. II for the Average Annual Rainfall (AAR) range 2000-2800 mm. For durations of 1 hour or less the FSR ‘maximum fall possible’ was used for the AAR range 1400-2800 mm. Table 4.1 of FSR Vol. II expresses these as percentages of the estimated 2 hour maximum rainfall. For the purposes of the Phase 1 report this was conveniently assumed to be 100 mm. In fact there are no estimated 2 hour maximum rainfalls given for each AAR range since the 2 hour maximum rainfalls vary spatially and do not necessarily correlate with AAR. The intention of the FSR methodology is to identify the 2 hour maximum rainfall for the point location of interest and then apply the appropriate percentages based on the AAR of the location in order to derive the maximum rainfall amounts for durations less than 2 hours.

Table 4.1 M100, M1000 and M10000 rainfall amounts, growth factors (that are applied to M5 rainfall) and estimated M5 rainfall for the AAR range 2000-2800 mm. These are derived from FSR Vol. II.

| Duration | 15 min | 30 min | 60 min | 2 hr | 6 hr | 12 hr | 24 hr | 48 hr | 72 hr | 96 hr |
|--|---------------|---------------|---------------|-------------|-------------|--------------|--------------|--------------|--------------|--------------|
| Estimated M5 rainfall (mm) | 11 | 15 | 21 | 30 | 50 | 68 | 94 | 131 | - | - |
| M100 growth factor | 1.95 | 1.99 | 1.97 | 1.91 | 1.77 | 1.66 | 1.57 | 1.47 | - | - |
| M1000 growth factor | 3.19 | 3.30 | 3.27 | 3.09 | 2.69 | 2.43 | 2.17 | - | - | - |
| M10000 growth factor | 5.19 | 5.49 | 5.42 | 5.00 | 4.10 | 3.57 | 3.01 | - | - | - |
| M100 rainfall amount (mm) | 21 | 30 | 42 | 57 | 88 | 113 | 148 | 193 | 219 | 247 |
| M1000 rainfall amount (mm) | 35 | 49 | 69 | 93 | 135 | 165 | 204 | - | - | - |
| M10000 rainfall amount (mm) | 57 | 82 | 114 | 150 | 205 | 243 | 283 | - | - | - |
| Extreme rainfall threshold (mm) | 45 | 62 | 79 | 94 | 117 | 132 | 152 | 193 | 219 | 247 |

However, an alternative approach using the FSR is possible for deriving return period rainfalls for durations less than 24 hours. This is useful as it puts the extreme rainfall threshold used into context. The approach is outlined below and uses the FSR notation *duration M return period* (for example, the 24 hour, 100 year return period rainfall is 24 hour M100).

1. The ratio, r , of (60 minute M5)/(2 day M5) is given in Table 3.6 of FSR Vol. II for each AAR range. It is 0.17 for the AAR range 2000-2800 mm.
2. Table 3.4 of FSR Volume II lists the estimated 2 day M5 for each AAR range. It is 124 mm for the AAR range 2000-2800 mm.
3. Table 3.10 of FSR Volume II gives the M5 rainfall for durations up to 48 hours as a percentage of the 2 day M5 rainfall for various values of r . The value $r=0.17$ is not explicitly listed but can be obtained by linearly interpolating between the values for $r=0.15$ and $r=0.18$. Applying these ratios to the approximate 2 day M5 value of 124 mm gives the M5 rainfall amount for the AAR range 2000-2800 mm, as presented in the top row of Table 4.1.
4. The growth factors used to obtain the M100, M1000 and M10000 rainfall are derived by averaging the appropriate growth factors from Table 2.7 (growth factors for England and Wales) and Table 2.9 (growth factors for Scotland and Northern Ireland) of FSR Vol. II. These growth factors, and the associated rainfall amounts, are given in Table 4.1.

Table 4.1 clearly shows that the UK-wide extreme rainfall threshold used in the Phase 1 Report increases in return period with decreasing duration. Allied to this, atmospheric disturbances show storms lasting about 1 hour have a typical scale of 10 km, while those lasting around 12 hours have a typical scale of 100km and those lasting 3 days have a typical scale of 1000 km. Extreme storms generally occur not when these scales are violated, but rather when the storm is quasi-stationary, so that the area over which the rain falls is minimised. So, for a given area and return period (e.g. 100 years), one would expect far more 100 year return period storms of 1 hour duration than 12 hour and far more 100 year return period storms of 12 hour duration than 3 day. Therefore, the property of the extreme threshold increasing in return period for decreasing duration had a practical benefit for the historical extreme storm identification task carried out as part of the Phase 1 Study as it restricted the number of storms identified at the shorter durations.

However, in terms of catchment flood response it is the return period of the rainfall that is of primary importance and therefore the lower rainfall amounts of the M100 storms are still a useful benchmark for assessing historical storms, albeit a UK-wide based estimate. Figure 4.2 displays the rainfall amount and duration of the 50 most extreme rainfall events of the 20th century, taken from the Phase 1 Report, along with the extreme rainfall threshold used for the classification of “extreme rainfall”. The rainfall amounts and durations for the extreme rainfall events used here are overlaid for comparison (see Table 4.2 for details) along with the M100 threshold.

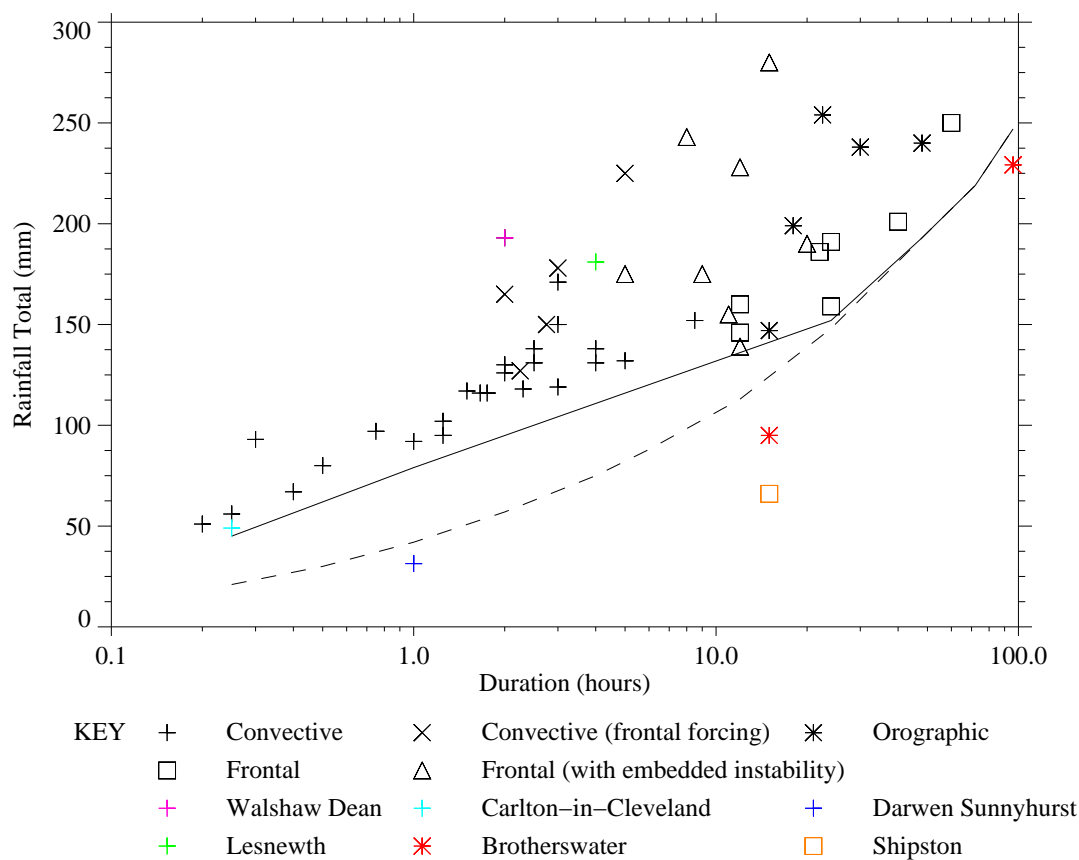


Figure 4.2 Rainfall amount (mm) versus duration (hours) (on a logarithmic scale) for the 50 most extreme rainfall events of the 20th Century using data from the Phase 1 Report. See key for event category. The solid line indicates the extreme rainfall threshold used in the Phase 1 Report and the dashed line shows the 100 year return period derived from the FSR. Raingauge totals relating to the case studies are also shown.

The FSR methodology has the advantage of providing UK-wide estimates of point rainfall depth for different durations and return periods and allows a sensible definition of a UK-wide extreme point rainfall threshold. However, the FSR methodology for estimating return period of rainfall has been updated as part of the Flood Estimation Handbook (FEH). The FEH methodology allows estimation of both point *and* catchment average rainfall return periods, over a given duration, at any location in the UK, taking into account the spatial variability that is averaged out in the UK-wide extreme point rainfall threshold. As the present study uses specific catchments and examines their flood response to storm rainfall, it is appropriate to use the FEH methodology to estimate the return periods of the historical extreme rainfalls on a catchment-by-catchment basis. The FEH approach is summarised in the following section.

4.4.2 Flood Estimation Handbook approach

When investigating the flood response of a given catchment to a given storm, it is the return period of the rainfall at the given location that is of primary interest. Therefore a location (or catchment) focussed approach to estimating rainfall return periods is need, rather than a UK-wide extreme point rainfall threshold.

The FSR methodology for estimating return periods of rainfall has been updated as part of the Flood Estimation Handbook. The Depth-Duration-Frequency (DDF) model that resulted is incorporated into the FEH CD-ROM software and allows estimation of both point *and* catchment average rainfall return periods, over a given duration, at any location in the UK. As the present study uses specific catchments and examines their flood response to storm rainfall, it is appropriate to use the DDF model to estimate the return periods of the historical extreme rainfalls. These return periods are given in Table 4.2.

Table 4.2 FEH estimated return periods for the historical extreme storms, based on raingauge records

| Event Date | Rainfall location | Rainfall depth and duration | FEH estimated return period |
|-----------------------------------|--------------------------|------------------------------------|------------------------------------|
| <i>Orographic rainfall</i> | | | |
| 30 Jan – | Brotherswater | 229.2 mm in 96 hours | 8.8 years |
| 3 Feb 2004 | Watchgate | 159.4 mm in 96 hours | 38 years |
| | Catchment average | 168.5 mm in 96 hours | 39 years |
| <i>Frontal rainfall</i> | | | |
| 8-9 Apr 1998 | Shipston | 66 mm in 15 hours | 31 years |
| | Byfield | 64 mm in 15 hours | 19 years |
| <i>Convective rainfall</i> | | | |
| 14 Jun 2002 | Darwen Sunnyhurst | 31.4 mm in 1 hour | 19 years |
| | Holden Wood | 25.4 mm in 1 hour | 10 years |
| 10 Aug 2003 | Carlton-in-Cleveland | 49.1 mm in 15 mins | 600 years (approx) |
| | Carlton-in-Cleveland | 49.4 mm in 20 mins | 500 years (approx) |
| 19 May 1989 | Walshaw Dean | 193 mm in 2 hours | > 5000 years |
| 16 Aug 2004 | Lesnewth (corrected TBR) | 181 mm in 4 hours | 4500 years (approx) |

The theory of the DDF model, including the FORGEX pooling method used to derive growth curves, is well documented in Volume 2 of the FEH. However, some key points relating to the method and the information contained on the FEH CD-ROM are set down below.

Parameters of the DDF model at a point

The FEH CD-ROM includes point values of the six parameters of the rainfall DDF model on a 1km grid across the UK, i.e. any point location within a given 1km grid square has the same DDF parameters.

Catchment-average parameters of the DDF model

For estimating catchment rainfall it is necessary to know the rainfall for a typical point in a catchment. The FEH CD-ROM includes values of the six parameters of the rainfall DDF model for a typical point in all UK catchments draining an area of at least 0.5 km². The catchment average DDF model parameters are evaluated by taking a weighted average of the 1 km grid of point values.

The areal reduction factor

Since rainfall is rarely uniform, particularly in extreme storms, the T-year rainfall at a point is bound to be larger than the T-year rainfall over an area. Viewed another way, the atmosphere has to work much harder to exceed a given rainfall depth over a 100 km² catchment than it does to exceed the same depth at one raingauge location. The T-year point rainfall, derived using the DDF parameters for a typical point in the catchment, must therefore be reduced by an *areal reduction factor* (ARF) to estimate the T-year catchment rainfall.

The ARF used in the FEH is that defined in the FSR Vol II. It is assumed to vary only with area and rainfall duration, not with return period or geographical position within the UK.

4.5 River flows and frequency of occurrence

Observed river flows and those derived from model simulations need to be placed in a frequency of occurrence context. This is relevant for historical extreme events and when using amplified forms of the historical storms or synthetically generated rainfalls in the flood response experiments. The Flood Estimation Handbook statistical method for estimating the flood peak of a specified return period at almost any site, gauged or ungauged, on the UK river network has been automated as part of the Defra Report FD1603. Following this work datasets containing estimated flood peaks for return periods of 2, 5, 10, 25, 50, 100, 200, 250 and 1000 years are available at a 50m grid resolution across the UK for catchments that drain areas in excess of 0.5km². These datasets are used here to assess the frequency of occurrence of both observed and modelled river flows.

4.6 Generation and application of extreme spatio-temporal rainfall datasets for flood response experiments

Two approaches are used to generate and apply extreme rainfall datasets for the catchment flood response experiments. The first approach focuses on the rainfall frequency of occurrence whilst the second focuses on the simulated flood frequency of occurrence.

Approach 1: For a given catchment rainfall datasets are generated, either synthetically or by amplifying historical storms, to attain FEH catchment average rainfall amounts for given durations and return periods. The return periods focussed on here are 100, 200, 500 and 1000 years whilst the durations used depend on the storm and catchment considered. The resulting model simulations of river flow can be assessed for their frequency of occurrence using the automated FEH approach (see Section 4.5).

For given return period and duration of rainfall, several storms with differing characteristics can be created and used to explore which characteristics cause more extreme modelled response. These storms can also be applied to a range of initial soil moisture conditions to encompass the effect of antecedent conditions on flood response.

Benefits of this approach for generating extreme rainfall datasets are that it uses return periods of rainfall specific to the catchment in question, using the FEH approach it can be applied consistently across different catchments and it can be applied independent of the rainfall-runoff model used. A drawback is that it does not focus on the return period associated with the flood response which is of practical interest to flood management.

Approach 2: For a given catchment, the automated FEH methodology (see Section 4.5) is used to estimate the flood peaks corresponding to required return periods, e.g. 100, 200 or 1000 years. Rainfalls are generated, either synthetically or by amplifying historical storms, so that the corresponding modelled flood peak matches the value for a given return period.

A number of rainfall datasets with varying characteristics and transformed from different types of historical storm or generated synthetically (e.g. simple triangular or rectangular profiles), are determined in this way. These rainfall datasets are then representative of the types of rainfall conditions likely to lead to a flow event of a given rarity.

Note that by choosing different soil moisture conditions for initialising the rainfall-runoff model, different sets of artificial storms are derived for a chosen flood rarity, thus encompassing the effect of antecedent conditions on flood response. The return

periods of the rainfall associated with each generated storm can be assessed using standard FEH methodology (see Section 4.4.2).

Benefits of this approach for generating extreme rainfall datasets are the focus on the return period associated with the flood response (which is of practical interest to flood management) and the FEH methodology can be consistently applied across different catchments. Drawbacks are that the generated rainfall datasets are dependent on the rainfall-runoff model used and therefore more difficult to create.

Approach 1 has been used to generate the extreme rainfall datasets for the flood response experiments that involve historical storms, and amplified forms of them, in Section 7. This is because using approach 2 would introduce the problem of rainfall-runoff model dependence and make the generation of the datasets too computationally and time expensive, especially when using distributed models. However, when using simple synthetically generated rainfall profiles, e.g. rectangular or triangular, for input into a lumped model it is possible to apply approach 2 more easily and a brief example is given in the following section.

4.6.1 Simplified rainfall profiles and their use in flood response studies

This section illustrates the value in constructing simple synthetic rainfall datasets, particularly for use with lumped rainfall-runoff models. Here approach 2, outlined in the previous section, is used i.e. space-time rainfall datasets are created using simple rainfall profiles and a rarity is associated to them with reference to the resulting model flood response. Simple rainfall profiles of a triangular or rectangular nature, characterised by intensity, temporal duration and spatial extent (and possibly spatial speed) are obvious candidates. Such storm profiles, when used as input to a rainfall-runoff model, can support flood response studies through analysing the modelled flow to investigate simple relations such as peak flow for a given storm duration. Graphs can be constructed of these model-derived quantities as functions of the characteristics of the rainfall profile; variants for wet, medium or dry catchment states can be obtained by varying the initial conditions of the rainfall-runoff model. The graphs can be a useful tool for representing the general characteristics of the response of a catchment to a foreseen rainfall event where the details of the forecasts are not very well defined. Appendix D shows how graphs can be constructed that serve as diagnostic tools in model destruction testing.

A demonstration of this approach has been developed using rectangular profile storms of different duration and magnitude and employing the PDM as the rainfall-runoff model. The motivation is to find the characteristics of rainfall events likely to lead to flooding problems for a catchment at risk. Critical flow-rates are first determined for the catchment at risk using the automated FEH methodology (see Section 4.5). A special version of the PDM program has been developed that determines the total amount of rainfall required for the peak flow to reach these threshold flows. These results depend on the duration over

which the rainfall event happens (with rainfall assumed constant within the event), and the starting conditions for the rainfall-runoff model.

Some example plots of the results of the procedure are shown in Figures 4.3 to 4.6. These show the critical rainfalls as a function of event duration (for selected initial flows) and as functions of the initial flows (for selected event durations). The lines shown are labelled with the recurrence interval of the critical flow threshold to be reached. In the plots showing critical rainfall as a function of initial flow, the highest initial flow included is equal to the 2-year flow. Examples are given for the Rhondda at Trehafod and for the Lavant at Graylingwell. The Lavant is groundwater-dominated with little response to rainfall unless the catchment is already wet, and any surface-flow response tends to be much slower than for the Rhondda. Hence the event-duration has little effect in the case of the Lavant compared to the faster-responding Rhondda.

The initial conditions for the PDM are specified via a single value of flow at the start of the simulation: values for the water contents of the model stores are derived from this on the basis that the conditions are relatively static. For low starting flows, flow is assumed to derive wholly from baseflow, surface-flow stores being empty and the soil store set to initially recharge the baseflow at a rate equal to the outflow from the baseflow store. For higher initial flows, the initial flow is divided between baseflow and surface-flow on the basis that it is all provided by baseflow up to a limit set by the maximum rate of recharge from the soil store, if this were full, after which the remaining contribution is attributed to the surface water stores. The initial status of the surface water-stores is determined on the basis that the flow has just peaked at the start of the simulation run. The rainfall event is specified as beginning immediately at the start of the run, with preceding rainfalls being zero. However, the rainfall event is subject to the time-delay that is built into the rainfall-runoff model and which is fitted as part of the model calibration. The difficulties in providing suitable starting conditions for the rainfall-runoff model are a limitation on how specific the overall procedure can be made to ongoing situations for operational use.

4.7 Destruction testing of rainfall-runoff models using extreme rainfall datasets

A special and important use of extreme rainfall datasets for the present study is for destruction testing of rainfall-runoff models. This special use is dealt with in detail in this section.

4.7.1 Model setup

For destruction testing, it is important that models are implemented exactly as they would be for routine use. Problems can be expected to arise in relation to the time-step length used within numerical calculations, and thus must be left as for routine use. Rainfall-runoff models usually employ a fixed time-step for internal calculations; only in unusual cases will a model implementation include automatic adjustment of the lengths for sub-steps within the basic time-step. Rainfall-runoff models will have usually been calibrated against observational

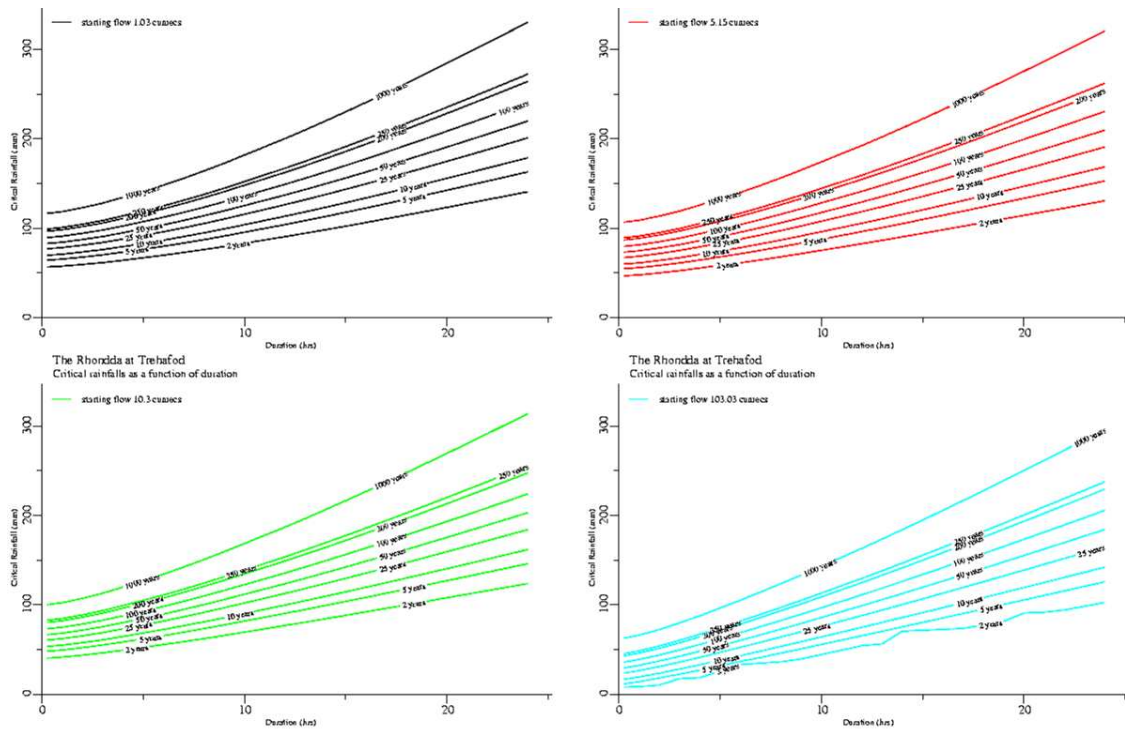


Figure 4.3 Critical Rainfall (mm) as a function of Duration (hrs), for different Starting Flows: River Rhondda at Trehafod

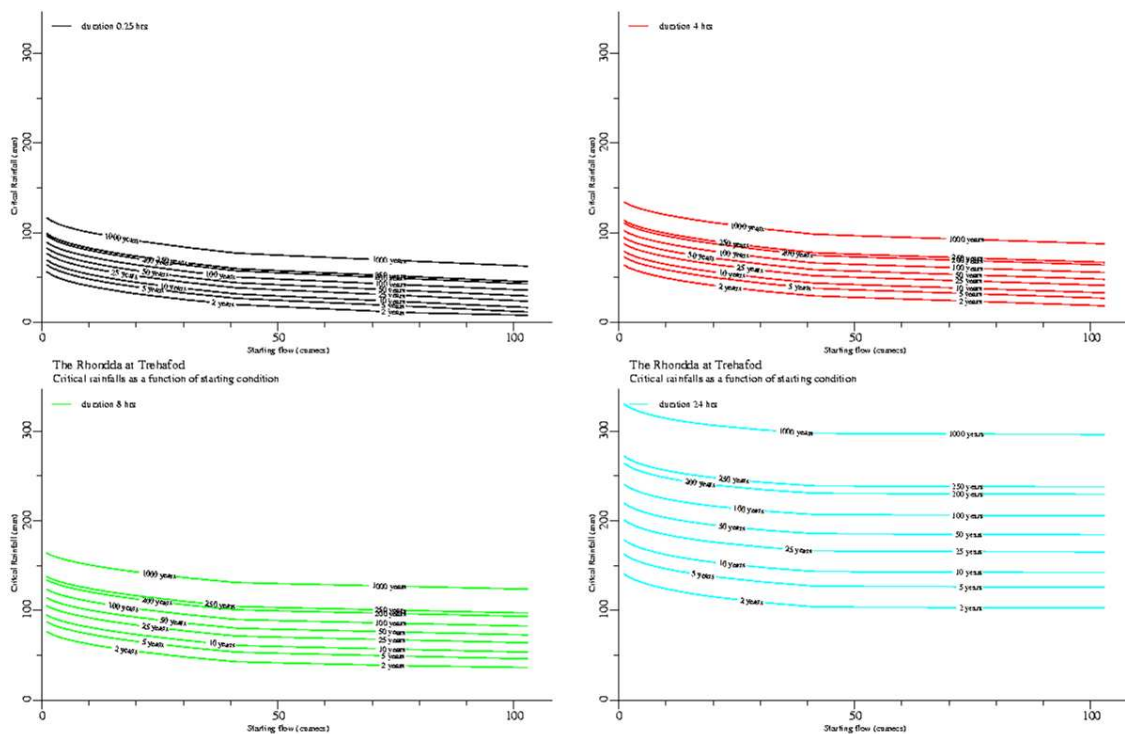


Figure 4.4 Critical Rainfall (mm) as a function of Starting Flow ($m^3 s^{-1}$) for a given Duration: River Rhondda at Trehafod

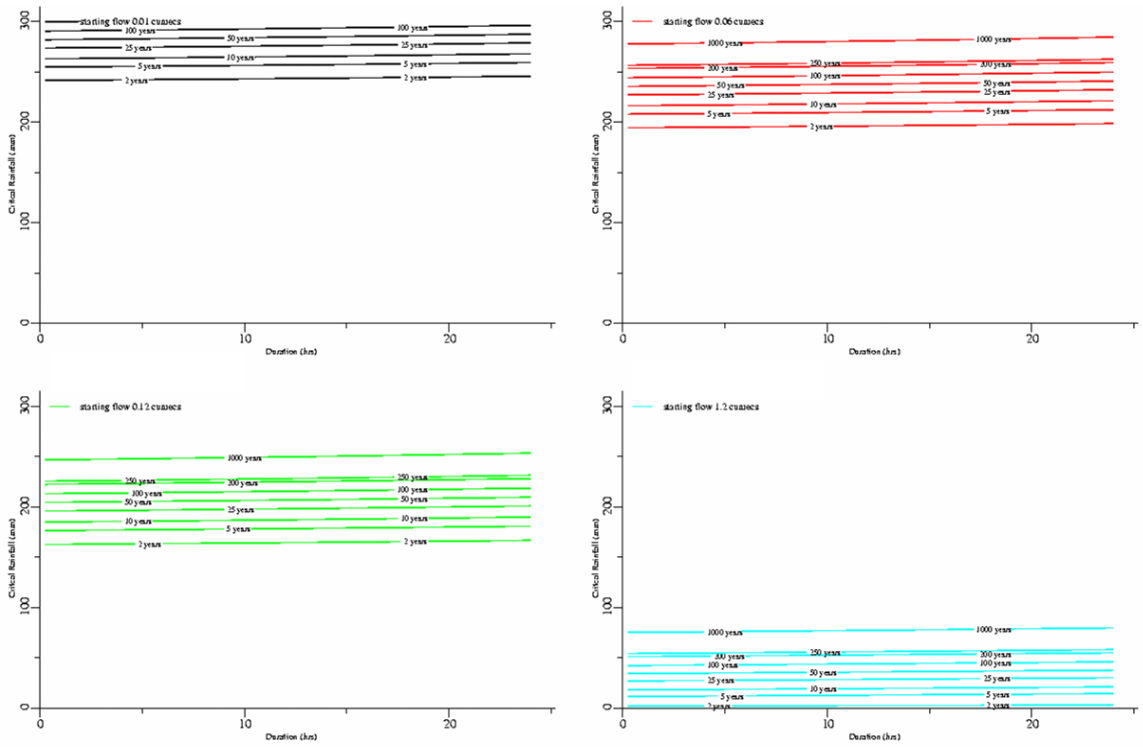


Figure 4.5 Critical Rainfall (mm) as a function of Duration (hrs), for different Starting Flows: River Lavant at Graylingwell

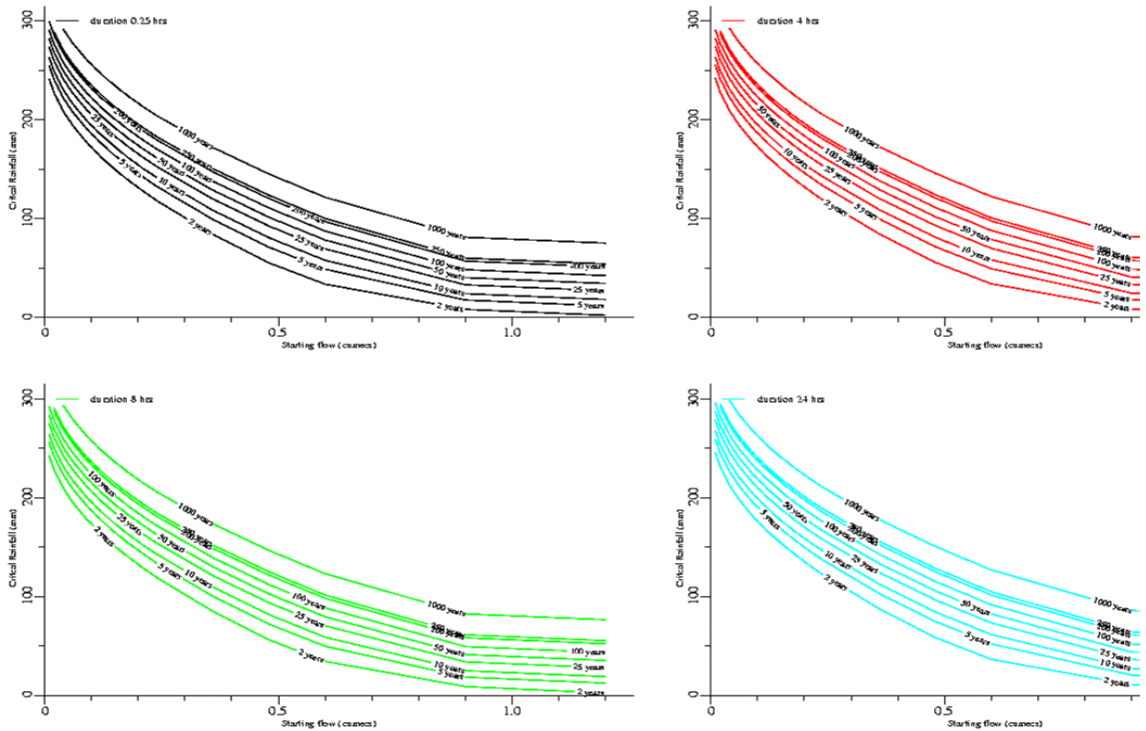


Figure 4.6 Critical Rainfall (mm) as a function of Starting Flow (m^3s^{-1}) for a given Duration: River Lavant at Graylingwell

records. Settings for time-step lengths within the calibration procedures should be the same as used for operational versions of the models. Given calibrated model parameters, the model should produce a realistic response for rainfall-inputs within the range experienced in the record used for calibration.

4.7.2 Classification of model failure

Model failure is said to occur if either:

- (a) the model execution fails to complete or
- (b) if the model results fail to display a physically realistic response to the rainfall input or
- (c) if different calibrated rainfall-runoff models significantly disagree when exposed to the same rainfall data

The chief concern of hydrological modelling is that the models should provide a reasonably good representation of the real-world hydrological responses over a range of conditions. Failure can be attributed to many causes but the main ones are poor coding of the model, inappropriate selection of model parameter values, model configuration, missing physical processes in the model and/or a model limitation. Understanding of model failure is key to improving both the conceptual development of models and their robustness under extreme rainfall.

4.7.3 Methods of testing

Two approaches are considered for the destruction testing of rainfall-runoff models:

Method 1: The approach taken here to model destruction testing is that the models should be run in the same way as usual, except that unusually large rainfall values are supplied as input. The destruction testing applied here runs the rainfall-runoff model over a relatively short time-period, but subject to a number of different versions of rainfall input. Each version is obtained from a basic source rainfall dataset by applying a multiplying factor to it. In this case a specific definition of unphysical model behaviour can be given:

A rainfall-runoff model is said to fail to produce a realistic response if the modelled flow (at a fixed time-point) ever decreases as the multiplying factor increases.

This type of criterion is appropriate for a range of modelling contexts, but not to models where catastrophic changes occur (for example dam and embankment failures in hydrodynamic models and snowpack break-up in snowmelt models). An example using this method is given in Appendix D using a simple model which has been set-up and deliberately coded to exhibit poor behaviour when subject to large rainfalls. Even though it has been poorly coded

model failure only occurs for unrealistically large rainfalls in excess of 15 metres in 12 hours.

Method 2: The approach taken here to model destruction testing is that the models are run in the same way as usual but only exposed to realistic extreme rainfalls generated following approach 1 of Section 4.6. These storms have given FEH return periods of up to 1000 years. Failure is deemed to occur if either the model execution fails, the model exhibits unphysically realistic behaviour or two calibrated models significantly disagree. The latter two criteria are not explicitly defined. This method is used during the flood response experiments in Section 8 and model failure is noted as and when it occurs.

5 The case study storms and catchments

In Section 2 case study storms were selected encompassing orographic, convective and frontal types of extreme rainfall. Table 2.2 provided a summary of the storms, including the magnitude of rainfall involved and details of the associated study catchments used for flood response modelling. In this section, the extreme storms and catchment details are discussed in more detail following the same order as used in Table 2.2. Each storm event is discussed in terms of the reasons for selection, the synoptic conditions pertaining, the rainfall intensity records and their return period, associated flood damage, and details of the hydrological case study catchments.

5.1 Orographic events

5.1.1 Event 1: 30 January to 3 February 2004, River Kent

Why selected?

- Long lasting Orographic event
- Considerable flood impact:
 - highest levels on record along the River Kent, Cumbria
 - the Environment Agency also reported that the River Ure flooded at Boroughbridge, North Yorkshire
- Good hydrometric network around the River Kent catchment - 5 river gauging stations and 9 raingauges
- Served by 2km resolution radar

Meteorological synopsis

A low pressure system to the west dominated the final two days of January causing heavy rain and gales to sweep across England and Wales from a westerly direction. The first four days of February were dominated by a deep depression to the north or north-west which drove a broad south-westerly flow across the region. This was responsible for record-breaking warm temperatures during the first week of February. It also caused a sequence of wet and windy weather to pass across the UK with exceptional amounts of orographic rain in Wales, Cumbria and South-West Scotland.

Rainfall intensity

Figure 5.1 (a) shows the 4-day rainfall accumulation across North Wales and Northern England for the period up to 12:00 3 February 2004 obtained using the Nimrod composite analysis. This clearly highlights the orographically-enhanced rainfall over Snowdonia and Cumbria with peak grid-square accumulations of 243 and 313 mm respectively.

The raingauges that were selected to support the hydrological case study for this event are mapped in Figure 5.1 (b). A cumulative hyetograph for a selection of raingauges over the event is given in Figure 5.2 (a). The Brotherswater rain gauge recorded the heaviest rainfall with a fall of 229.2 mm in the 4 days up to 11:00 3 February 2004, 95 mm falling in the final 15 hours. These have FEH-derived return periods of 8.8 and 5.8 years respectively and are, surprisingly, not particularly noteworthy. However, in terms of FEH-derived return periods, the most significant point rainfall occurred at the Watchgate rain gauge where 159.4 mm fell in 96 hours giving an estimated return period of 38 years. The return period of the rain gauge-based catchment average rainfall of 168.5 mm in 96 hours for the River Kent to Sedgwick (see Hydrological Case Study 1(a)) was estimated to be 39 years.

(a) North Wales and Northern England

(b) River Kent

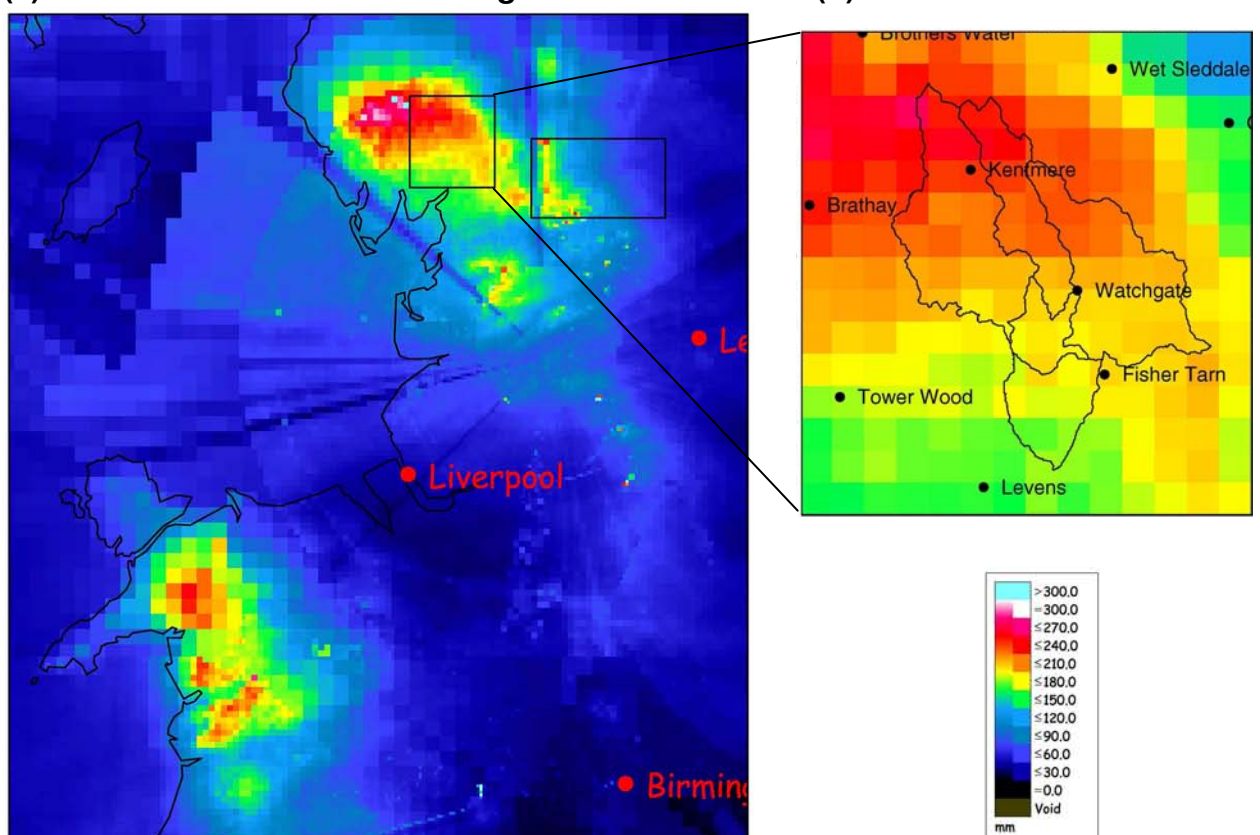
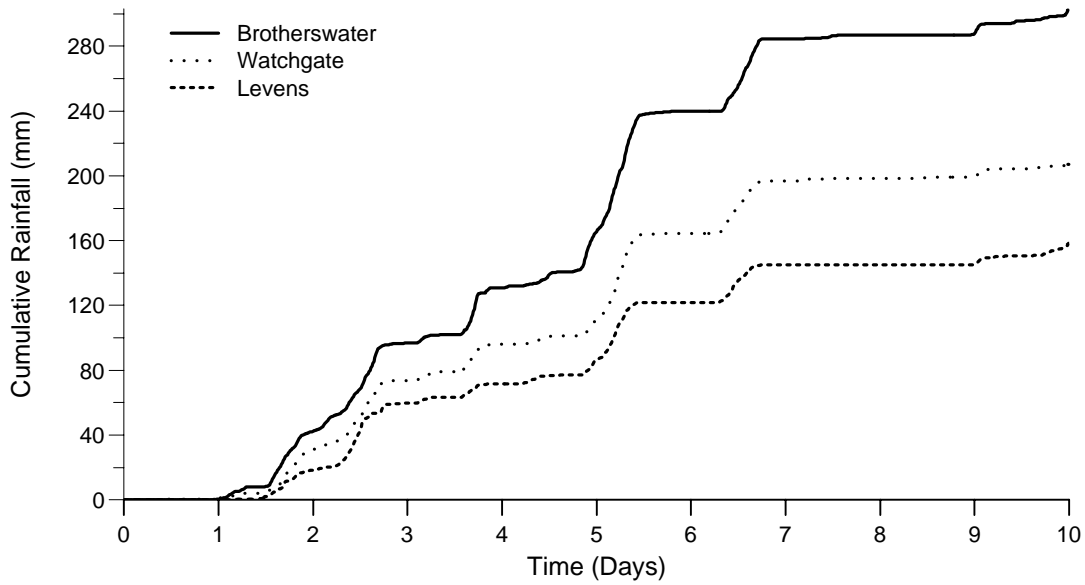


Figure 5.1 Rainfall accumulation (in mm), using Nimrod composite analysis, for Event 1: 96 hours to 12:00 GMT 3 February 2004. Image (a) shows the orographic enhancement over Snowdonia and Cumbria. Image (b) shows the River Kent catchments. Rain gauge locations are marked with solid circles.

(a) Cumulative hyetographs



(b) Flow hydrograph for the River Kent at Sedgwick

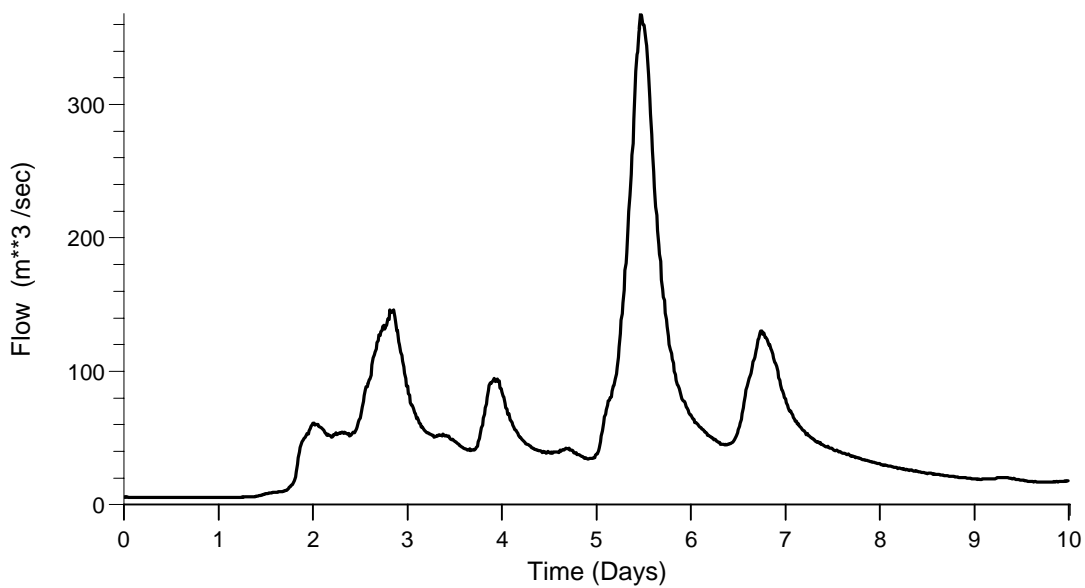


Figure 5.2 Cumulative hyetographs for a selection of raingauges in and around the Kent and Upper Ure catchments, and the flow response of the River Kent at Sedgwick, for the period 29 January to 8 February 2004.

Comparison with results of the Phase 1 Study

Figure 4.2 of Section 4.4.1 marks the rainfall totals for Brotherswater (red stars), showing that this rainfall event would not have been classified as extreme; however, the 96-hour total of 229.2 mm would classify this event as a near miss.

There are 5 orographic events within the set of 50 extreme events identified in the Phase 1 Study. All 5 occurred between November and January and were characterised by a strong west to southwest flow and a region of high pressure over the Bay of Biscay or over Greece with a ridge to Spain. The surface pressure charts during the first four days of February 2004 (contained in the Met Office Daily Weather Summaries) show a ridge of high pressure over Spain with a strong south-westerly airflow. This indicates that the meteorological conditions for the case study are similar to those for the extreme orographic rainfall events identified in the Phase 1 Study.

Flood damage?

Although this event was just below the classification threshold for extreme rainfall it had an extensive flooding impact with rivers in North Wales, Cumbria and Yorkshire all going out-of-bank. A brief summary of reported flooding is given below.

Wales: The River Conwy in North Wales suffered serious flooding. The villages of Trefriw and Llanrwst were completely cut off during the flood and three motorists were airlifted to safety. Rail services on Welsh Valley lines were disrupted due to damaged embankments.

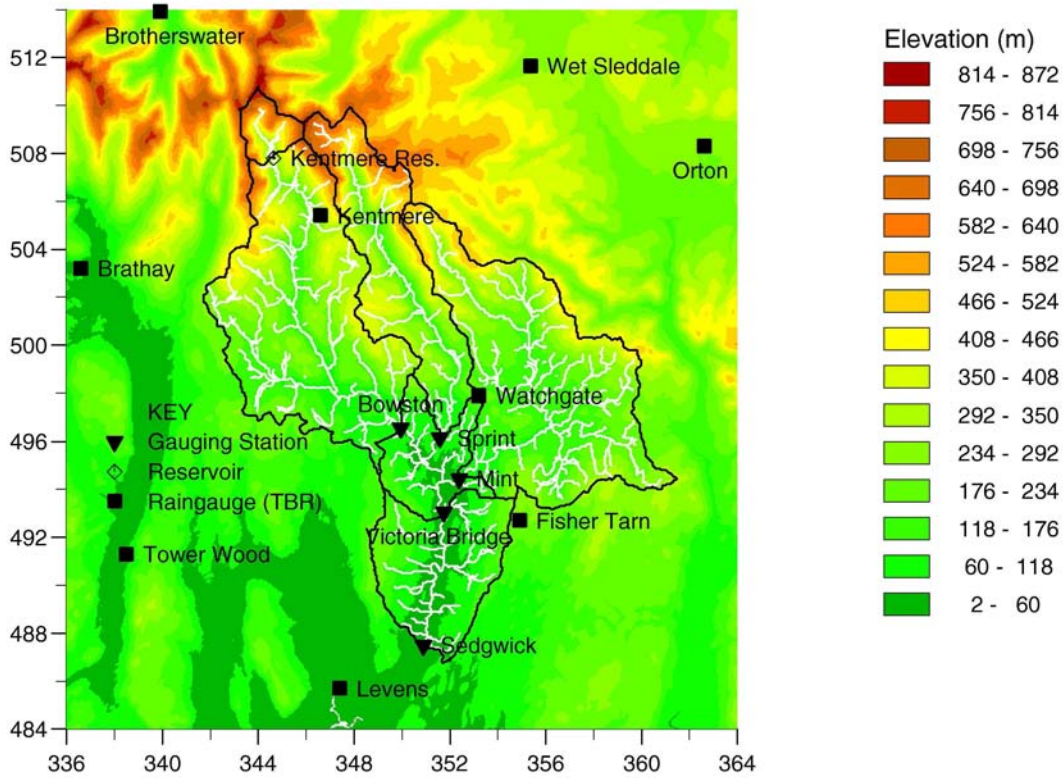
Cumbria: The River Eden at Carlisle went out-of-bank. Other areas in Cumbria suffered serious localised flooding, notably the River Kent at Kendal, and the River Derwent at Bass Lake. The flood response of the River Kent at Sedgwick (downstream of Kendal) is shown in Figure 5.2 (b) and resulted in the highest stage on record

Yorkshire: The River Ure flooded at Boroughbridge, North Yorkshire. Also the River Ouse (of which the River Ure is a tributary) went out-of-bank flooding parts of the centre of York.

5.1.2 Hydrological Case Study 1: River Kent, Northwest Region

The River Kent rises in the southeast part of the Cumbrian hills (Figure 5.3) with the river eventually feeding into Morecambe Bay. For the purposes of this case study, the River Kent is taken to comprise the catchment upstream of the gauging station at Sedgwick, encompassing an area of 212 km² with an altitude ranging from 19 to 812 m.

(a) Relief map



(b) SAAR map

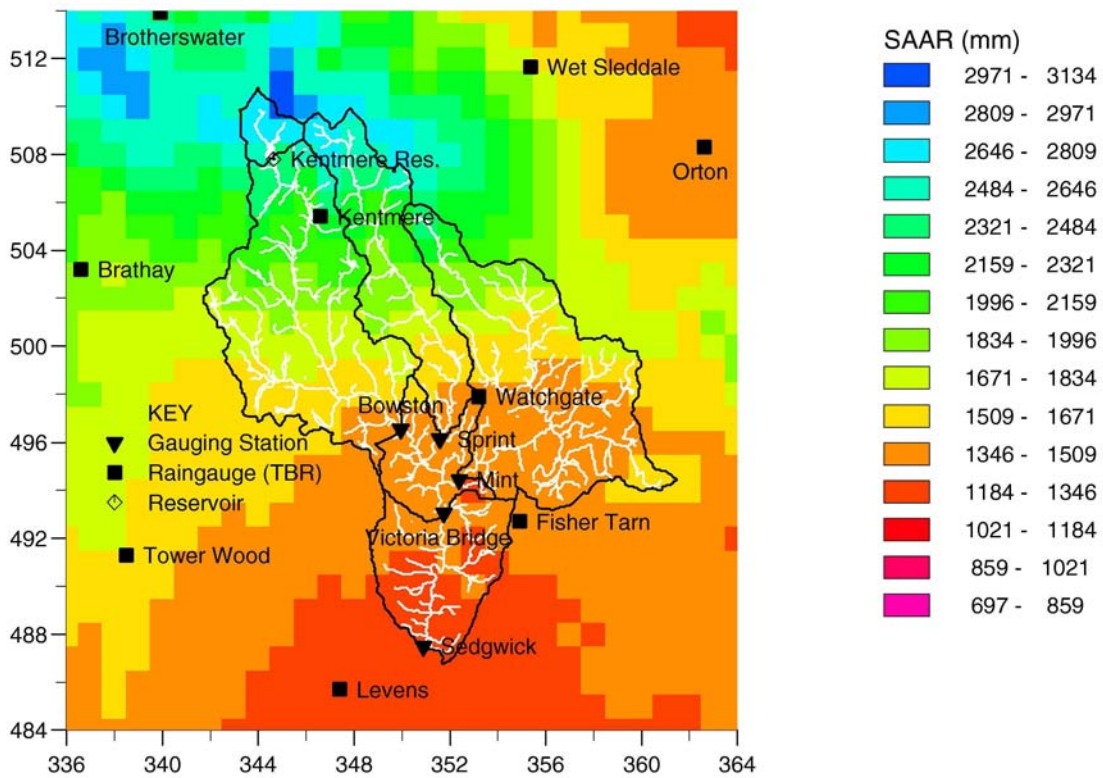


Figure 5.3 Maps of relief and SAAR (1km grid) for the River Kent catchment and surrounding area.

The upper reaches of the River Kent and its tributaries descend steeply to Kendal, the only major town within the catchment, and are fast flowing. The upper reaches also have very high relief (Figure 5.3 (a)) and are generally wet (Figure 5.3 (b)).

The very northern part of the catchment consists of volcanic and low-grade metamorphic rocks of Ordovician age. Moving south to Kendal these are overlain by a wide tract of rocks of Silurian age, comprising of slates and grits, which are predominantly impermeable and covered by heather moorland and peat. From Kendal southwards a Carboniferous Limestone Series occurs: this consists of thick limestone layers interbedded with low-permeability shales and mudstones and provides good grazing. The only significant reservoir within the catchment is the Kentmere Reservoir (NY 447 078) at the head of the River Kent with a drainage area of 5.02 km². Currently it is owned by a single mill owner who is entitled to release water for their own industrial needs although none has been released in recent years (Environment Agency, 2004).

The hydrological case study is concerned with modelling river flows at five locations within the River Kent basin, each corresponding to an established river gauging station. Figure 5.3 maps the station locations and the position of the Kentmere Reservoir in relation to the river network. Also shown are the boundaries of their drainage areas and the locations of the telemetry raingauges. The station at Bowston is on the River Kent upstream of Kendal. Gauging stations at Sprint Mill and Mint Bridge are on tributaries which join the River Kent upstream of Kendal. The station at Victoria Bridge is within Kendal. Kendal itself is situated on the natural floodplain of the River Kent and has suffered several serious floods, most notably in 1898 and 1954. Flood defences were improved during the Kendal Flood Relief Scheme (1972-1978) which included widening a stretch of the river in Kendal and the dredging of gravel. Also a large lagoon was constructed at the confluence of the River Kent and River Mint to act as a gravel trap.

The Environment Agency issued The Kent Catchment Abstraction Management Strategy (CAMS) in March 2004 which detailed abstractions and discharges affecting the River Kent basin. In summary, it reported that currently there is very little abstraction upstream of the gauging stations at Bowston, Sprint Mill and Mint Bridge. However there is significant abstraction in the lower Kent for industrial purposes and water supplies of around 12 MI d⁻¹. There are also significant discharges from the sewage treatment works at Kendal of 14 MI d⁻¹: this is important as a majority of public water is imported from outside of the catchment.

River gauging stations

Table 5.1 lists the location, station number, catchment area and Standard Average Annual Rainfall for each gauging station in terms of total drainage area (i.e. *including* the Kentmere Reservoir drainage area) and natural drainage area (i.e. *excluding* the Kentmere Reservoir drainage area). The latter is most appropriate for modelling purposes. Note that the total catchment areas are

Table 5.1 River gauging stations: River Kent

| Station | National Grid Reference | Station Number | Total Catchment | | Naturally Draining | |
|-------------------------------|-------------------------|----------------|-------------------------|-----------|-------------------------|-----------|
| | | | Area (km ²) | SAAR (mm) | Area (km ²) | SAAR (mm) |
| River Kent at Bowston | SD 4994 9653 | 730120 | 70.61 | 1925 | 64.78 | 1868 |
| River Sprint at Sprint Mill | SD 5148 9610 | 730203 | 34.60 | 2019 | 34.60 | 2019 |
| River Mint at Mint Bridge | SD 5241 9447 | 730404 | 65.80 | 1599 | 65.80 | 1599 |
| River Kent at Victoria Bridge | SD 5181 9307 | 730507 | 183.0 | 1786 | 179.71 | 1761 |
| River Kent at Sedgwick | SD 5088 8742 | 730511 | 209.0 | 1727 | 207.31 | 1705 |

those given by the Environment Agency whilst the naturally draining areas have been derived using the CEH Digital Terrain Model.

River level measurements at 15 minute intervals are available for conversion to flows using rating equations derived from historical current meter readings made at a range of flows. Table 5.2 gives details of the rating equation available for each station. The form of the rating equation is $Q = \alpha(h+d)^\beta$ for $h < h_t$, where Q is the flow in m^3s^{-1} , h is the stage in m with h_t the threshold stage for validity, and α , d and β are parameters of the relation. Table 5.2 also gives comments on the reliability of the rating equations along with the flood peak of the case study event. Encouragingly the rating equations appear to be reasonably accurate for all stations with the exception of high flows at Sprint Mill and Victoria Bridge.

The case study flood event is certainly rare as it created the highest levels on record at all stations. To help assess the return period of the flood, FEH estimates of the 2, 5, 10, 25, 50, 100, 250 and 1000 year floods have been listed for each gauging station in Table 5.3. These are formed from using an automated procedure based on the FEH methodology as detailed in Defra Report FD1603. Interestingly, Table 5.3 shows that the flood peak for a given return period actually decreases between the gauging station at Victoria Bridge and the downstream station at Sedgwick. Although such a phenomenon can be accounted for by attenuation of flood peaks with downstream distance travelled it may also be a signature of spatial incoherence issues that arise from the automated procedure. Of course, one must always be cautious when comparing peak flows derived from extrapolated rating curves to the estimated FEH return periods. However, it is still a useful and worthwhile line of inquiry. For the case study event the peak flows at the upstream stations of Sprint Mill and Mint Bridge are certainly very rare with an estimated return period in excess of 100

Table 5.2 Rating equations: River Kent

| Station | h_r | α | d | β | Bankfull (m) | Flood Peak |
|-------------------------------|---|----------|---------|--|--------------|---|
| River Kent at Bowston | 0.141 | 138.4886 | 0.0070 | 2.9289 | 3.0 | 2.042 m 102.6 m ³ s ⁻¹ * |
| | 0.584 | 40.0442 | -0.0390 | 1.8905 | | |
| | 1.575 | 38.3577 | -0.1050 | 1.4881 | | |
| <i>Comments</i> | Rating is generally good at all levels. *Treat extrapolation to bankfull with caution. | | | | | |
| River Sprint at Sprint Mill | 0.363 | 45.2272 | 0.0180 | 2.9721 | 2.0 | 1.624 m 72.3 m ³ s ⁻¹ * |
| | 0.722 | 34.2065 | -0.1200 | 1.8328 | | |
| | <i>Comments</i> | | | | | |
| | | | | Flat V Crump profile weir. Rating curve based on flow measurements up to a level of 0.722m. Higher levels have been gauged and show that the rating curve *underestimates high flows by up to 20%. | | |
| River Mint at Mint Bridge | 0.561 | 16.3055 | 0.0070 | 2.6298 | 2.4 | 2.250 m 112.8 m ³ s ⁻¹ |
| | 1.765 | 21.2738 | -0.1100 | 2.1929 | | |
| | <i>Comments</i> | | | | | |
| | | | | Flow controlled by a stable flat V Crump profile weir. Rating improved following a set of high flow gaugings during winter 98/99. Good at all flows and extrapolation to bankfull should be reasonable. | | |
| River Kent at Victoria Bridge | 1.200 | 0.0984 | 0.0000 | 11.1966 | 4.1 | 3.244 m 214.1 m ³ s ⁻¹ * |
| | 2.957 | 62.3969 | -1.1280 | 1.6450 | | |
| | <i>Comments</i> | | | | | |
| | | | | Rating is working satisfactorily at low to medium flows. However, recent gaugings and comparison with flows downstream at Sedgwick indicate that *high flows are underestimated by approximately 30% and should be used with caution. | | |
| River Kent at Sedgwick | 0.311 | 13.1894 | -0.0300 | 1.3443 | 4.0 | 2.841 m 368.3 m ³ s ⁻¹ |
| | 0.913 | 43.8227 | -0.0200 | 2.3552 | | |
| | 2.202 | 41.3127 | -0.0070 | 2.1002 | | |
| <i>Comments</i> | Flow controlled by a compound broad-crested weir. Rating gives good results at all levels and extrapolation to bankfull should be reasonable. | | | | | |

years. (Note that no attempt to account for the underestimation of high flows at Sprint Mill is made since observations from the station are included in the FEH automated estimates.) The peak flow at Bowston, the other station upstream of Kendal, was not so exceptional with an estimated return period of around 20 years. Taking into account the likely 30% underestimation at Victoria Bridge the more realistic peak flow of approximately 300 m³s⁻¹ has an estimated return period of 50 to 100 years (increasing the peak flow at Victoria Bridge is valid since observations from the station were not included in the automated technique whereas observations from Sprint Mill were). Finally the peak flow at Sedgwick is estimated to have a return period well in excess of 250 years. This seems unlikely given the upstream return period estimates and the spatial distribution of the rainfall (Figure 5.1). It is more likely that a return period of around 50-100 years is appropriate, implying that either the FEH-estimated return periods for Sedgwick are too low or that the extrapolation of the rating

Table 5.3 FEH-estimated flows (m^3s^{-1}) for given return periods (years) for gauging stations: River Kent

| Station | 2 | 5 | 10 | 25 | 50 | 100 | 250 | 1000 | Flood Peak |
|-----------------------------|-------|-------|-------|-------|-------|-------|-------|-------|------------|
| River Kent at Bowston | 61.3 | 78.1 | 90.1 | 107.0 | 121.4 | 137.5 | 161.8 | 207.1 | 102.6 |
| River Sprint at Sprint Mill | 32.4 | 40.9 | 46.9 | 55.4 | 62.6 | 70.5 | 82.5 | 104.7 | 72.3 |
| River Mint at Mint Bridge | 39.2 | 50.0 | 57.5 | 68.1 | 76.9 | 86.7 | 101.3 | 128.0 | 112.8 |
| River Kent at Vic. Bridge | 142.3 | 180.7 | 207.6 | 245.2 | 276.8 | 311.6 | 363.9 | 459.2 | 214.1 |
| River Kent at Sedgwick | 116.7 | 147.7 | 169.5 | 200.2 | 226.0 | 254.7 | 297.9 | 377.1 | 368.3 |

curve is incorrect and is over-estimating the flow at very high stages. In this instance the FEH-estimated return periods from the automated technique are likely to be too high. Overall this analysis confirms that the event is most certainly rare.

Raingauge network

The River Kent catchment and surrounding area is served by a network of 9 telemetry tipping-bucket raingauges. Their locations are indicated in Figure 5.3. Raingauge data are recorded in time-of-tip form at a resolution of 0.2 mm. The location, height, SAAR and Environment Agency's station number for each raingauge are listed in Table 5.4.

Table 5.4 Telemetry raingauges: River Kent

| Raingauge | National Grid Reference | Station Number | Height (m) | SAAR (mm) |
|------------------|-------------------------|----------------|------------|-----------|
| Brathay Hall | NY 366 032 | 586898 | 51 | 1842 |
| Tower Wood | SD 385 913 | 587552 | 46 | 1571 |
| Brothers Water | NY 3990 1390 | 600140 | 230 | 2379 |
| Kentmere | NY 466 054 | 585022 | 266 | 1464 |
| Levens | SD 474 857 | 586056 | 4 | 1464 |
| Watchgate | SD 5320 9790 | 585512 | 196 | 1276 |
| Fisher Tarn Res. | SD 549 927 | 584772 | 224 | 2215 |
| Wet Sleddale | NY 5535 1165 | 600986 | 271 | 1721 |
| Orton | NY 626 083 | 580058 | 238 | 1386 |

Radar data

At the time of the extreme event, 2km resolution data coverage from the Hameldon Hill radar was available for all the River Kent catchments. Both 2km raw and 2km Nimrod QC radar are used for this case study.

5.2 Frontal events

5.2.1 Event 2: 9 to 10 April 1998, Upper Thames and Stour

Why selected?

- Caused widespread flooding during Easter 1998
- Highest levels on record at several stations including the River Stour at Shipston and River Cherwell at Banbury
- Reasonable hydrometric network
- Partially served by 2km resolution radar

Meteorological synopsis

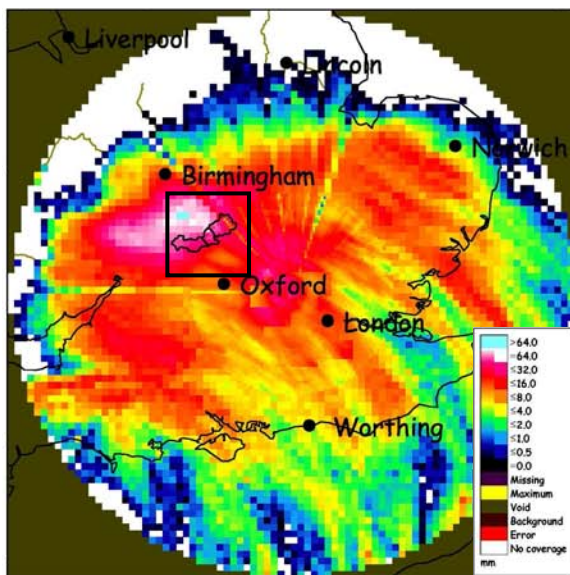
Following the 'Easter 1998 Floods' the Environment Agency commissioned an independent report (Bye, 1998), including details of the meteorological conditions which are summarised here. The first week of April was particularly wet across the Midlands with 20 to 30 mm of rain falling. On 8 April a depression that originated near Iceland moved south across the UK and resulted in falls of rain up to 10 mm. This, combined with the earlier wet weather, caused serious antecedent wetness conditions with many catchments close to saturation.

During the 9th the depression centre remained almost stationary over Brittany and had two frontal systems associated with it. Firstly a front to its north marked the boundary of very cold air over northern England and Scotland which edged slowly southwards. Secondly an occluded front, spiralling outwards in a clockwise direction around the depression, moved slowly north across southern England. The weather system created a frontal rainband over central England and Wales and, as the occluded front moved north, thundery showers broke out ahead of it and added further intense downpours to the pre-existing frontal rainband. As the two fronts collided and merged they created a very slowly moving and intense frontal zone which produced prolonged and heavy rainfall across central England and into Wales. The majority of the rainfall is attributed to the slowly moving fronts rather than the embedded convection.

Rainfall intensity

Heavy rainfall fell in a 100km wide band between the Black Mountains in south Wales and north Cambridgeshire. Figure 5.4 presents rainfall accumulations using 2 and 5 km Nimrod data from the Chenies radar for the 18 hours to 18:00

(a) Chenies



(b) Stour, Sor and Cherwell

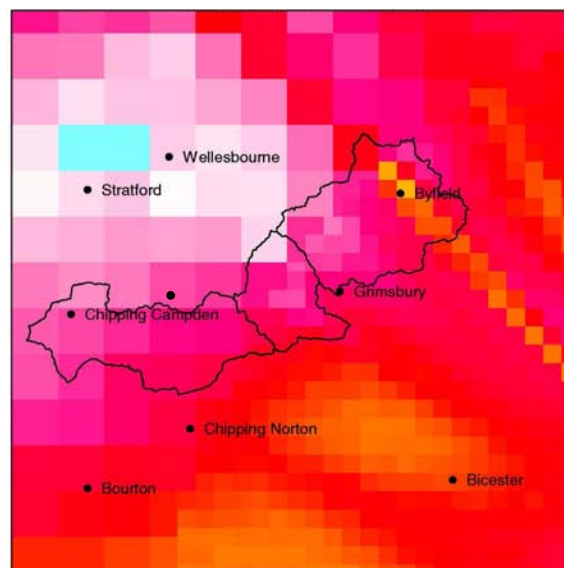


Figure 5.4 Rainfall accumulation (in mm), using 2 and 5km Nimrod single site radar data from Chenies for Event 2: 18 hours to 18:00 GMT 9 April 1998. Image (a) shows the heavy rainfall affecting Central England. The square region in (a) is enlarged in image (b) to show the Stour, Sor and Cherwell catchments and the raingauge locations (marked with solid circles).

9 April 1998. This image clearly shows the large and widespread rainfall totals affecting central parts of England with a peak grid-square accumulation of 71 mm.

The most notable raingauge total was 76.6 mm at Pershore (SO 972 500) in the 14 hours to 19:00 9 April 1998. This raingauge is not specifically used in the following hydrological studies but has an FEH-estimated return period of 102 years. Other notable raingauge totals from gauges used in the hydrological modelling were 66 mm recorded at Shipston in the 15 hours to 19:00 9 April 1998 and 64 mm recorded at Byfield in the 15 hours to 19:30 9 April 1998. These have FEH-estimated return periods of 31 and 19 years respectively. The raingauges selected to support this case study are listed later in Tables 5.8 and 5.12. Cumulative hyetographs for the raingauges closest to the study catchments (see hydrological case studies below) are given in Figures 5.7 and 5.8 and their locations are mapped in Figure 5.5.

Comparison with results of the Phase 1 study

This rainfall event was not classified as extreme in the Phase 1 Study Report.

Flood damage?

As recorded in the Environment Agency 'Bye Report' (Bye, 1998), the Easter 1998 floods caused extensive and widespread damage across Wales and central parts of England, with an estimated financial cost (at the time) of £350m.

Tragically 5 people died as an apparent consequence of the flooding. The most severe floods occurred in an area of some 5000km², bounded by Bedford to the east, Evesham to the west, Peterborough to the north and Oxford to the south and, in many places, were the worst on record.

5.2.2 Hydrological case study 2(a): River Cherwell and Sor Brook, Thames region

The River Cherwell rises at Charwelton in Northamptonshire flowing through Banbury and eventually joining the Thames at New Hinksey, South Oxford. Along its southwards flow it is joined by several tributaries including Sor Brook. This case study is concerned with two catchments: The River Cherwell at Banbury and Sor Brook at Bodicote. As Figure 5.5 shows, the two gauging stations are situated upstream of the confluence of the Sor Brook with the Cherwell whilst the Sor Brook catchment shares boundaries with the Stour catchment (see case study 2(b)) to the west and the Cherwell catchment to the east.

The relief map of Figure 5.5 shows that Sor Brook rises in the relatively steep slopes of the Cotswolds. Its catchment to Bodicote ranges in altitude from 225m to 90m and drains an area of approximately 89km². The Cherwell to Banbury covers a similar range of altitude from 224m to 90m but drains a larger area of around 202km² and has less steep tributaries. Standard Average Annual Rainfall for the region, mapped in Figure 5.6, shows a close association with elevation. Figure 5.6 also locates the hydrometric network relative to the river network.

Predominantly the catchments lie on Liassic formations with a majority being clay, in particular Lower Lias clay to the North of Banbury. Apart from the town of Banbury the catchments are mainly rural in character but both flow regimes are affected by abstraction. Also the flow at Banbury is affected by intakes and returns from the Oxford canal and by a sewage treatment works. Both catchments are responsive in nature with field flooding common in the Bodicote catchment.

Despite the flow regimes for the catchments being affected by unnatural influences, the case study is still valuable because of the extreme flood peaks recorded and that the widespread frontal event was well captured by radar and raingauge data.

River gauging stations

Table 5.5 lists the location, station number, catchment area and Standard Average Annual Rainfall for each gauged catchment used in this case study. Note that the areas have been derived using the CEH Digital Terrain Model.

Calculated river flow data were provided by the Thames Region of the Environment Agency. Exact details of the rating equations were not requested

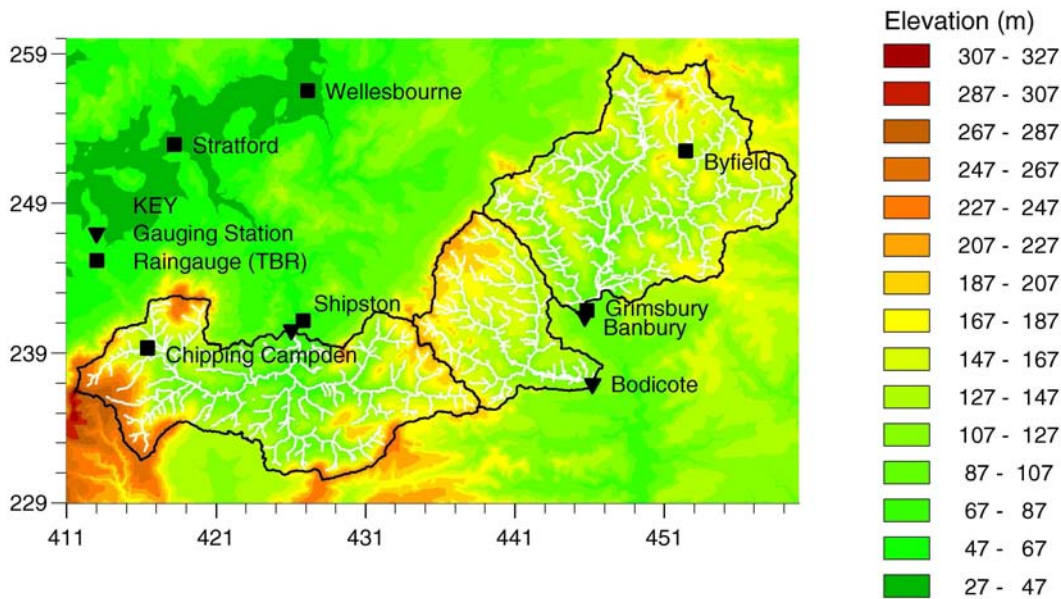


Figure 5.5 Relief map of the Stour, Sor and Cherwell catchments showing the river network, catchment boundaries and the hydrometric network.

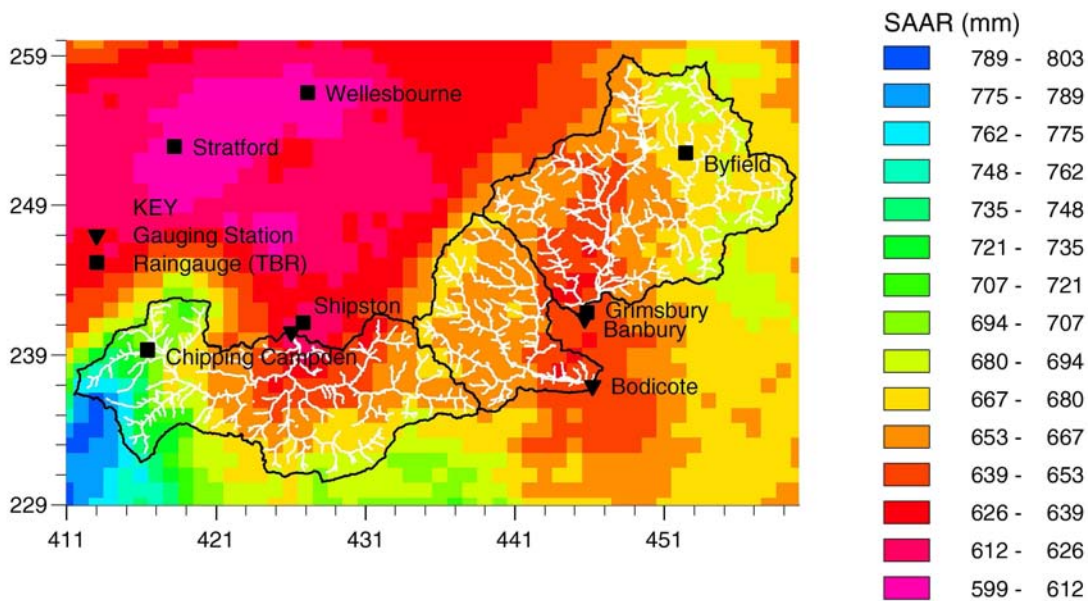


Figure 5.6 Map of SAAR (1km grid) for the Stour, Sor and Cherwell catchments. Heavy lines show the catchment boundaries.

but details of the gauging stations, along with the peak flow, are given in Table 5.6.

The gauging station of the Cherwell at Banbury dates back to 1966. During the Easter 1998 flood the river level recording floats ‘jammed’ and some levels were estimated. The estimated upstream peak level at Banbury was 2.75m, well above the bankfull height of 0.874m and the previous highest recorded level of 1.72m. The flow peak of $90\text{m}^3\text{s}^{-1}$ was derived using an extrapolated rating curve

Table 5.5 River gauging stations: Upper Thames

| Station | NGR Coords | Station Number | Catchment Area (km ²) | SAAR (mm) |
|---------------------------|------------|----------------|-----------------------------------|-----------|
| River Cherwell at Banbury | SP 458 411 | 1420 | 201.9 | 665 |
| Sor Brook at Bodicote | SP 462 369 | 1437 | 88.8 | 660 |

Table 5.6 Rating equation details: Upper Thames

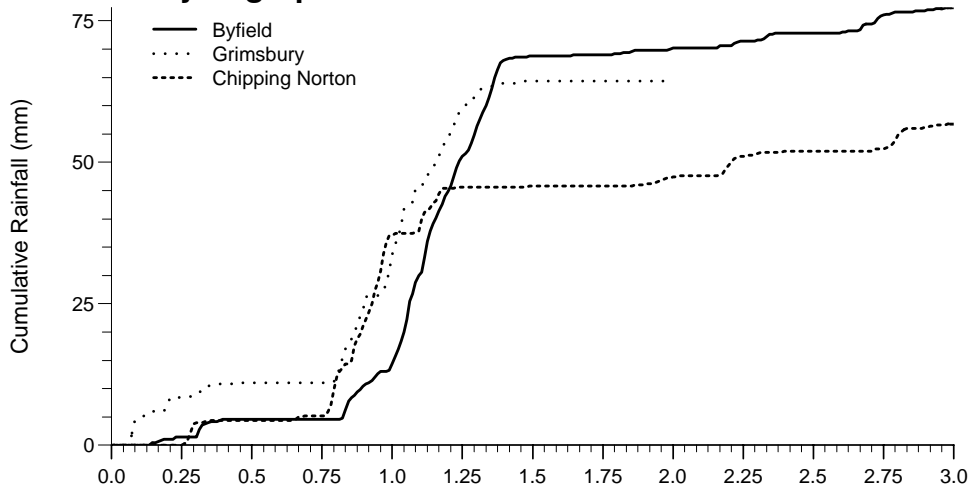
| Station | Bankfull (m) | Flood Peak | Comments |
|---------------------------|--------------|---|---|
| River Cherwell at Banbury | 0.874 | 2.75 m* 90.8 m ³ s ⁻¹ * | Asymmetrical compound Crump style weir with a modular limit of around 22 m ³ s ⁻¹ or 1.1 m. Upstream and downstream flows monitored. Maximum gauged level (flow) is 2m (56 m ³ s ⁻¹). * Peak levels estimated as level floats 'jammed' during flood but are largest since station records began in 1966. |
| Sor Brook at Bodicote | N/A | 1.219 m* 14.9 m ³ s ⁻¹ * | Crump weir with upstream and downstream flows used to derive flow. Largest flood peak at station since records began in 1995. Limit of rating equation unknown.*Peak flow affected by upstream level float 'jamming' during flood, evident in hydrograph Figure 5.7 (b) |

beyond the highest current meter gauging at 2m. The flood response hydrograph at Banbury is given in Figure 5.7 (b).

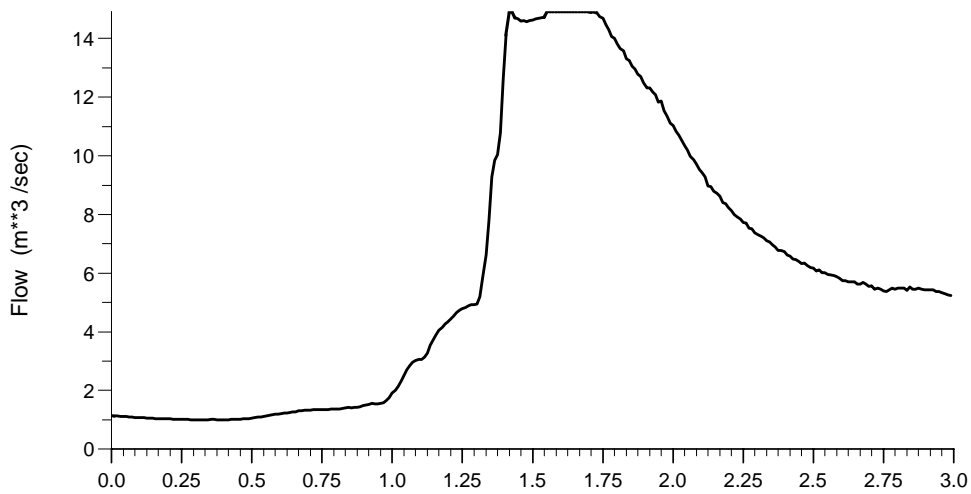
The Sor Brook at Bodicote gauging station was commissioned in 1995 and replaced the station at Adderbury which ran from 1967 to 1988. During the flood event the upstream river level float at Bodicote also suffered from 'jamming'. This is evident in the flood response hydrograph given in Figure 5.7 (c) by the flattened peak. As a result the *actual* flood peak was estimated in the Bye Report to have been around 16.6m³s⁻¹, slightly above the recorded peak of 14.9m³s⁻¹. Given the short record, it is not surprising that the Easter 1998 flood was also the largest on record for the Sor Brook at Bodicote.

The Bye Report on the Easter 1998 flood estimated the return period of the peak of the Cherwell at Banbury to be around 100 years. This was based on the gauging record dating back to 1966 and knowledge of other historical floods, such as the major flood of 1947. A specific return period for the Sor Brook at Bodicote was not given due to the short gauging record but inferred to be around 100 years also.

(a) Cumulative hyetographs



(b) Flow hydrograph for the Sor at Bodicote



(c) Flow hydrograph for the River Cherwell at Banbury

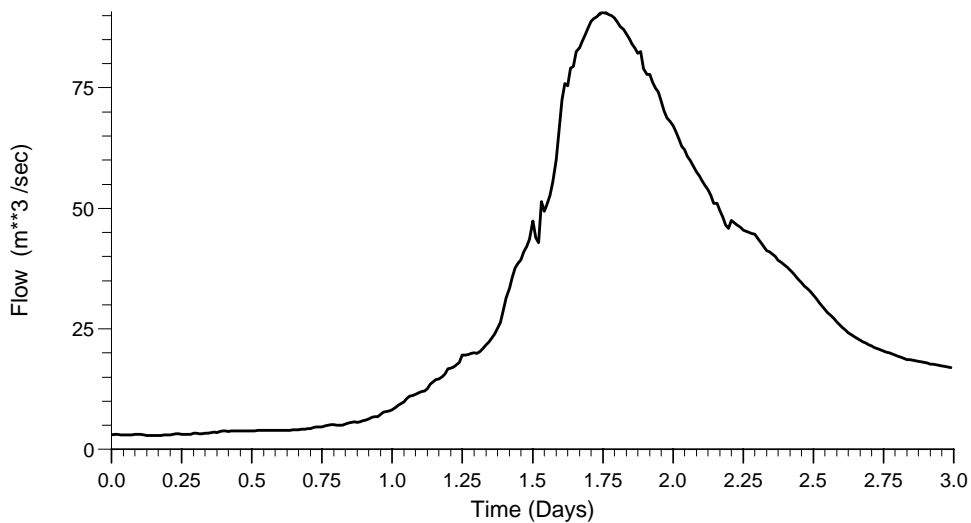


Figure 5.7 Cumulative hyetographs for raingauges in and around the Upper Thames and the flow response of the River Cherwell at Banbury, for the period 09:00 8 April to 09:00 11 April 1998.

The estimated return period flows for Banbury and Bodicote are derived using the methodology of Defra Report FD1603 and presented in Table 5.7. The gauging station record at Banbury was used within the FEH automated procedure whilst the record at Bodicote was not. Using Table 5.7 the return period of the observed flood flow peaks at both Bodicote and Banbury are estimated by the FEH automated procedure to be well in excess of a thousand years which, although the flood was the largest on the gauging stations' records, appears to be an overestimate. A return period of around 100 years, as indicated by the Bye Report, would seem more realistic and in keeping with other known historical events *before* gauging records began.

Table 5.7 FEH-estimated flows (m^3s^{-1}) for given return periods (years) for gauging stations: Upper Thames

| Station | 2 | 5 | 10 | 25 | 50 | 100 | 250 | 1000 | Flood Peak |
|-----------------------|------|------|------|------|------|------|------|------|------------|
| Cherwell at Banbury | 16.5 | 23.7 | 28.7 | 35.7 | 41.6 | 48.1 | 57.8 | 75.4 | 90.8 |
| Sor Brook at Bodicote | 4.2 | 5.7 | 6.7 | 8.1 | 9.2 | 10.3 | 11.9 | 14.7 | 14.9 |

Raingauge network

The Cherwell to Banbury and Sor Brook to Bodicote catchments are principally served by three telemetry raingauges in the Thames Region: Byfield, Grimsbury and Chipping Norton. However, since the rainfall event was a widespread frontal event, data from other Thames Region telemetry raingauges further from the catchments were provided for creating raingauge-only estimated rainfall fields. The locations of the raingauges closest to the study catchments are mapped in Figure 5.6. All raingauge data received were 15 minute accumulations at 0.2 mm resolution. The location, height, SAAR and Environment Agency's station number for each raingauge are listed in Table 5.8.

Radar data

At the time of the extreme event, 2km resolution data from the Chenies radar covered all but the north-west edges of the Banbury and Bodicote catchments. These gaps in coverage were filled in by 5km resolution data. Figure 5.4 (b) shows the combined 2 and 5km Nimrod data from the Chenies radar and the switch between the two types of data over the study catchments is just visible.

Table 5.8 Telemetry raingauges: Upper Thames

| Raingauge | NGR Coords | Station Number | Height (m) | SAAR (mm) |
|------------------|-------------------|-----------------------|-------------------|------------------|
| Grimsbury | SP 458 418 | 257038 | 91.8 | 642 |
| Byfield | SP 524 525 | 256340 | 136.7 | 676 |
| Chipping Norton | SP 294 268 | 254829 | 138.2 | 694 |
| Stanford | SU 343 929 | 260221 | 69.5 | 626 |
| Bicester | SP 581 212 | 259110 | 62.2 | 620 |
| Osney | SP 504 058 | 256229 | 54.6 | 637 |
| Shorncote | SU 034 971 | 248331 | 93.4 | 745 |
| Chipping Norton | SP 294 268 | 254829 | 138.2 | 694 |
| St Johns | SU 222 990 | 251530 | 71.4 | 646 |
| Abingdon | SU 493 952 | 261021 | 50.0 | 582 |
| Wheatley | SP 608 052 | 263541 | 60.2 | 629 |
| Rodbourne | SU 132 855 | 249744 | 93.7 | 682 |
| Worsham | SP 301 105 | 253860 | 110.0 | 682 |
| Bourton | SP 182 203 | 253339 | 128.5 | 741 |
| Maddle Farm | SU 305 817 | 268103 | 152.7 | 735 |
| Rapsgate | SO 996 105 | 248965 | 240.0 | 862 |
| Eynsham | SP 445 087 | 254336 | 60.0 | 635 |
| West Ilsley | SU 457 829 | 411411 | 149.7 | 728 |
| Benson | SU 613 913 | 264253 | 42.6 | 594 |
| Stokenchurch | SU 746 971 | 413413 | 242.7 | 768 |
| Cleeve | SU 601 818 | 264845 | 44.7 | 650 |

5.2.3 Hydrological case study 2(b): River Stour, Midlands Region

The Stour is situated in the Midlands Region and forms a major tributary of the Worcester Avon draining an area of 348 km² to its confluence with the Avon. This case study is concerned with the Stour catchment to the gauging station at Shipston, draining an area of approximately 185 km². The catchment is mainly agricultural and lies on Lower Lias and Cotswold Oolite. The river flows primarily northwards with a relatively narrow floodplain and steep gradient. Elevation ranges from 61m to over 300m as shown by the relief map of Figure 5.5. Standard Average Annual Rainfall for the region is mapped in Figure 5.6 which also locates the hydrometric network relative to the river network.

River gauging stations

The Stour case study centres on the single river gauging station at Shipston, a site used only for flood forecasting purposes. The location, station number, catchment area and Standard Average Annual Rainfall for the catchments drainage area are given in Table 5.9. The rating equation used is of the form $Q = \alpha(h + d)^\beta$ for $h < h_T$, where Q is the flow in m^3s^{-1} , h is the stage in m with h_T the threshold stage for validity, and α , d and β are parameters of the relation. The details of the rating equation are presented in Table 5.10 along with the flood peak flow. This indicates that the observed flood level (4.205m) was considerably above bankfull (2.5m) and the inferred flow was extrapolated well beyond the highest gauged level (2.8m). The flood response at Shipston is given in Figure 5.8 (b).

Table 5.9 River gauging station: River Stour at Shipston

| Station | NGR Coords | Station Number | Catchment Area (km ²) | SAAR (mm) |
|-------------------------|------------|----------------|-----------------------------------|-----------|
| River Stour at Shipston | SP 260 405 | 2029 | 185 | 676 |

Table 5.10 Rating equation: River Stour at Shipston

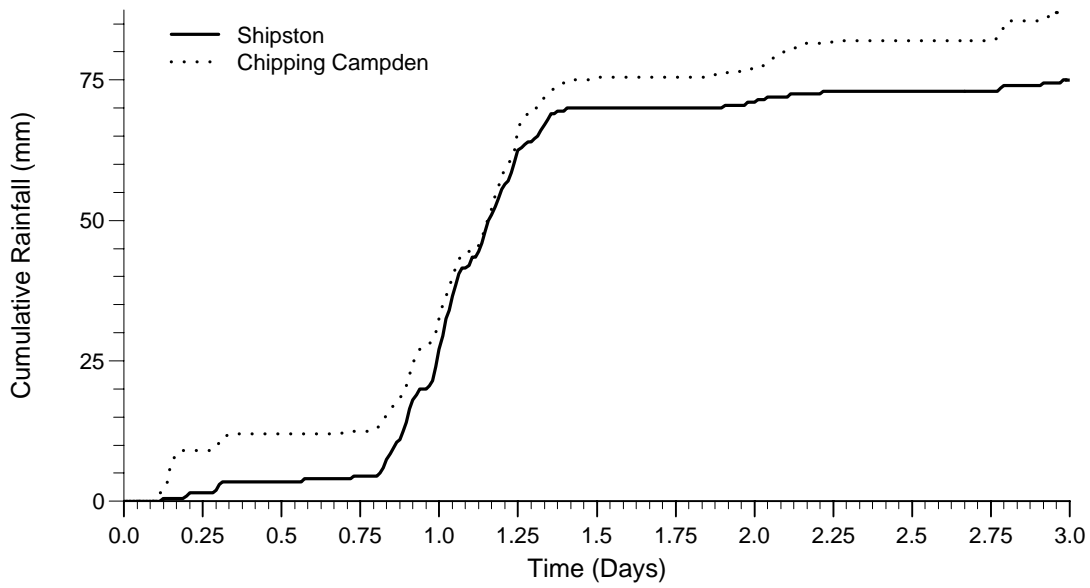
| Station | h_T | α | d | β | Bankfull (m) | Flood Peak |
|-------------------------|--|----------|--------|---------|--------------|---|
| River Stour at Shipston | 0.31 | 6.861 | 0.038 | 2.192 | 2.5 | 4.205 m 91.3 m^3s^{-1} * |
| | 0.55 | 5.419 | -0.166 | 1.072 | | |
| | 2.58 | 5.733 | -0.084 | 1.418 | | |
| | 2.80 | 1.295 | -0.039 | 2.983 | | |
| <i>Comments</i> | Open channel station with cableway. During dry periods stilling well bottoms out. Only one gauging above bankfull. *Peak flow out of bank. | | | | | |

The gauging station record was not used as part of the FD1603 report and therefore the FEH-estimated return period flows presented in Table 5.11 were obtained using the automated procedure outlined in FD1603. Using Table 5.11 the return period of the observed flood flow peak is estimated by the FEH automated procedure to be well in excess of a thousand years which, although the flood was the largest on record at Shipston, would appear to be an overestimate. Previously, direct analysis of the record at Shipston gave a more realistic estimated return period of between 40 and 80 years.

Table 5.11 FEH-estimated flows (m^3s^{-1}) for given return periods (years) for the gauging station at Shipston

| Station | 2 | 5 | 10 | 25 | 50 | 100 | 250 | 1000 | Flood Peak |
|-------------------------|------|------|------|------|------|------|------|------|------------|
| River Stour at Shipston | 20.8 | 28.9 | 34.2 | 41.2 | 46.9 | 52.9 | 61.4 | 76.1 | 91.3 |

(a) Cumulative hyetographs



(b) Flow hydrograph for the Stour at Shipston

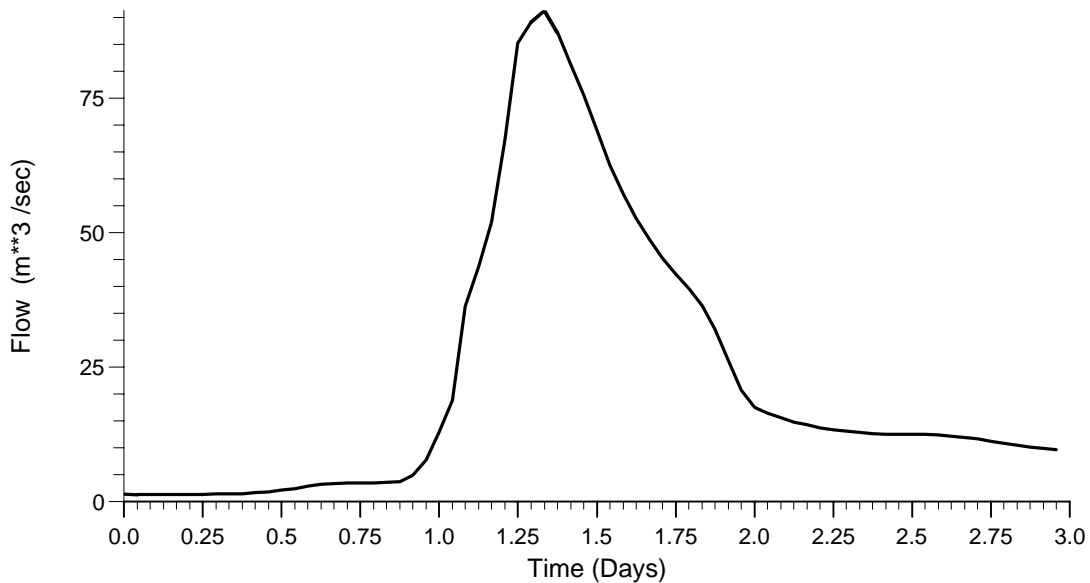


Figure 5.8 Cumulative hyetographs for the relevant raingauges in and around the Shipston catchment, and the flow response of the River Stour at Shipston, for the period 09:00 8 April to 09:00 11 April 1998.

Raingauge network

The Stour to Shipston catchment is served by five raingauges in the Midlands Region. Their locations are mapped in Figure 5.6. All raingauge data received were in time-of-tip format and at a resolution of 0.5 mm. The location, height, SAAR and Environment Agency's station number for each raingauge are listed in Table 5.12. The Midlands Region raingauges were used in conjunction with the Thames Region raingauges from hydrological case study 2(a) to form the raingauge-only spatial fields of rainfall.

Table 5.12 River Stour catchment: Raingauges

| Raingauge | NGR Coords | Station Number | Height (m) | SAAR (mm) |
|------------------|-------------------|-----------------------|-------------------|------------------|
| Shipston | SP 268 411 | 1087 | 64.5 | 623 |
| Chipping Campden | SP 164 393 | 1761 | 122.7 | 710 |
| Langley | SP 005 282 | 1005 | 170.0 | 763 |
| Stratford | SP 182 529 | 1086 | 42.3 | 603 |
| Wellesbourne | SP 271 565 | 1165 | 43.6 | 606 |

Radar data

At the time of the extreme event, only the western tip of the Stour to Shipston catchment was covered by 2km resolution data from the Clee Hill radar. The entire catchment was covered by 5km resolution data from both Clee Hill and Chenies radars. Since the Chenies radar is used for hydrological case study 2(a) Chenies 5km data were used for the entire Stour catchment as well.

5.3 Convective events

5.3.1 Event 3: 14 June 2002, River Darwen

Why selected?

- Identified by the Met Office and Environment Agency for Post Event Analysis
- Considerable urban flood impact from both river levels and surface runoff, including the River Darwen through Blackburn
- Good hydrometric network around the River Darwen catchment - 2 river gauging stations and 8 raingauges
- Served by 2 and 1km resolution radar data. The availability of 1km radar data captured finer details of the convective storm and was desirable for the storm modification experiments and for inclusion in the spatial datasets.

Meteorological synopsis

A cold front passed quickly in a north-east direction across England and Wales. Very warm moist air to the south-east collided with colder air from the Atlantic causing the sudden onset of thunderstorms along the front. These thunderstorms, some of which were very intense, primarily affected the northern parts of England. The speed of the front prevented any one location being affected by heavy rainfall for longer than a couple of hours. In particular a region centred on Blackburn was subject to the passage of an intense thunderstorm but there was no report of hail.

Antecedent wetness conditions played an important role. The runoff rate of the storm in the Lancashire area was increased by low soil moisture deficits, estimated to be around 6 mm on 11 June, following a wet May and early June.

Rainfall intensity

In north-west England between 25 and 40 mm of rainfall was recorded in many urban areas in a swathe between Wigan, Blackburn and Burnley. This is evident in the accumulation of the 1km raw radar presented in Figure 5.9. In the Blackburn area a majority fell within one hour. The most notable recorded catches were 25.4 mm at Holden Wood in the hour to 17:15 GMT, with 15 mm recorded in the 15 minutes ending at 16:45. These have FEH-estimated return periods of 10 years and 8.2 years respectively. The raingauge at Darwen Sunnyhurst recorded the largest hourly total with 31.4 mm in the hour to 16:15 GMT, with an estimated return period of 18.7 years.

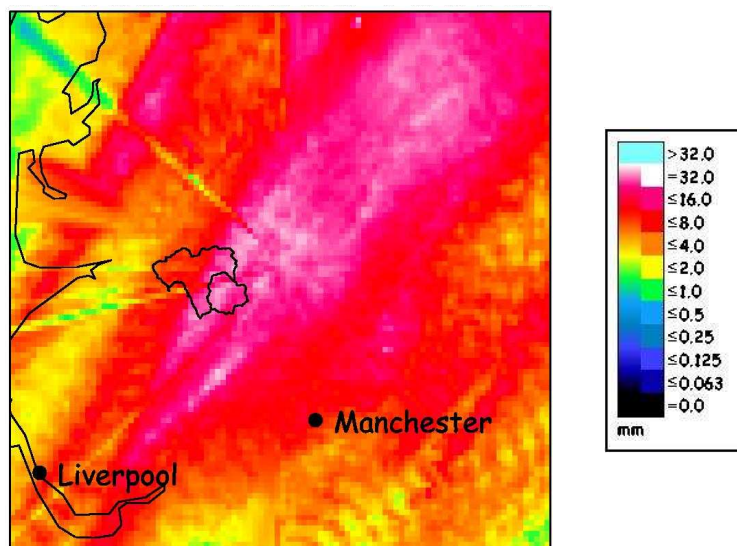


Figure 5.9 Rainfall accumulation (in mm), using 1km raw radar data from Hameldon Hill for Event 3: 4 hours to 18:30 GMT, 14 June 2002. The River Darwen catchments are also shown.

Although the maximum recorded hourly total was 31.4 mm the instantaneous rain-rates were much larger than this and hourly catches were limited by the quick passage of the thunderstorm. This is confirmed by the sequence of 1km raw radar data images in Figure 5.10 which show several grid squares with an

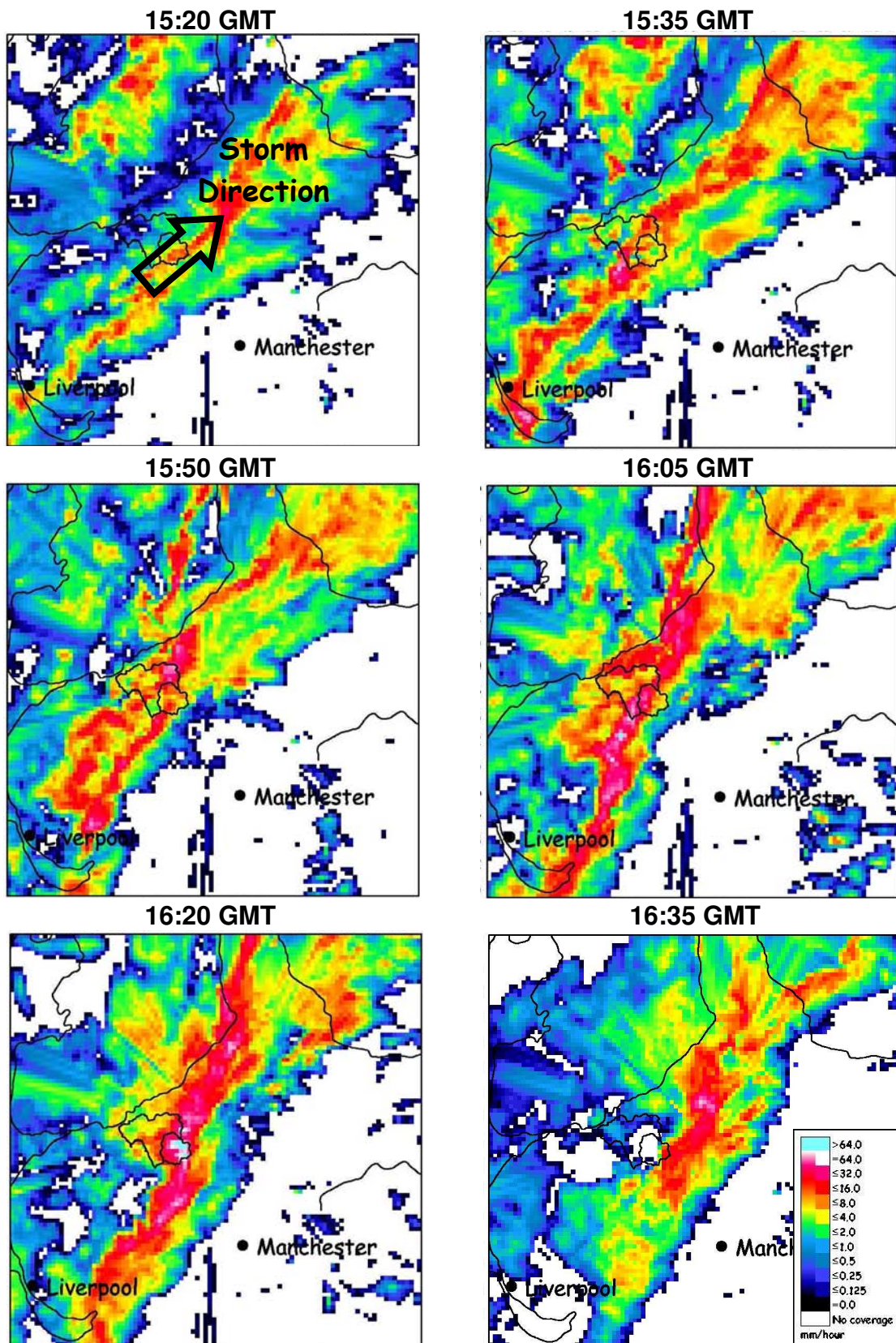


Figure 5.10 A sequence of 1km raw radar images, at time intervals of 15 minutes, from 15:20 GMT to 16:55 GMT on 14 June 2002. The River Darwen catchments are also shown. The first image indicates the storm direction of travel.

estimated rain-rate in excess of 64 mm hr^{-1} and an inferred storm velocity of 50 to 60 km hr^{-1} .

The raingauges selected to support this case study are listed later in Table 5.17. Cumulative hyetographs for these raingauges and catchment average radar estimated rainfalls are presented later in Figure 5.14 (a), confirming the storm effected the Darwen catchment for only a short period.

Comparison with results of the Phase 1 Study

This storm would not have met the extreme threshold criteria of the Phase 1 Study Report.

Flood damage?

The Post Event Analysis and North West Regional Summary Report were made available from the Met Office and Environment Agency respectively. They report that the storm caused the flooding of around 300 properties with the areas of Blackburn, Darwen and Leigh being the worst hit.

5.3.2 Hydrological case study 3: River Darwen, North West Region

The River Darwen has its source in the Southwest Pennines in Lancashire. The case study focuses on the catchment to the river gauging station at Blue Bridge, draining an area of circa 136 km^2 with an altitude range between 11m and just over 400m. A second gauging station within the catchment at Ewood drains an area of about 39 km^2 . The headwaters are steep and contain several small reservoirs draining about 15% (20 km^2) of the catchment area to Blue Bridge. Table 5.13 provides a summary of the catchment and reservoir areas and the areas that are naturally drained.

Table 5.13 Catchment, reservoir and natural drainage areas: River Darwen

| Catchment (total area) | Reservoir (reservoir catchment area, km^2) | | | | | Natural drainage area (km^2) |
|--------------------------------------|--|---------------------------|---------------------------|-----------------------------|------------------------|--|
| | 1. Roddlesworth (6.49) | 2. Hoddleson (5.28) | 3. Rokebrook (3.77) | 4. Pickup Bank (2.03) | 5. Earnsdale (2.02) | |
| Darwen at Ewood (38.99) | | | | | | 29.66 |
| Darwen at Blue Bridge (135.68) | | | | | | 116.09 |

The catchment is underlain mainly by Carboniferous grits except near Blue Bridge where the bedrock is Permo-Triassic sandstone. Superficial deposits are predominantly glacial clays and gravel. The upper catchment is almost entirely urbanised by the towns of Blackburn and Darwen whilst the lower half is mainly agricultural. Figures 5.11 and 5.12 map the elevation and Standard Average

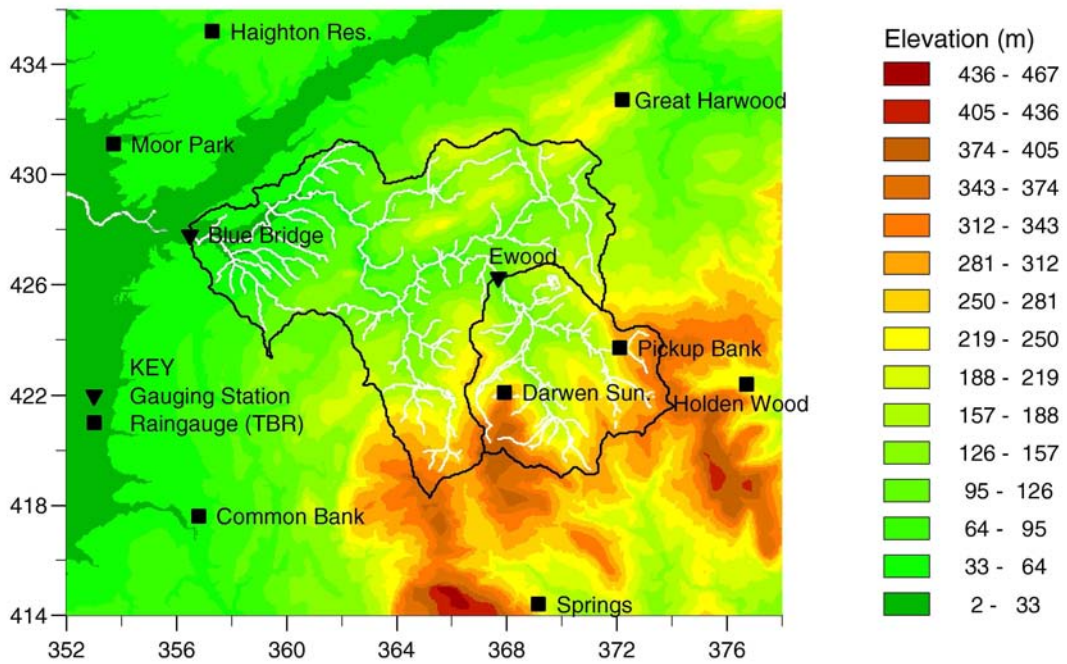


Figure 5.11 Relief map of the Darwen catchment showing the river network, catchment boundaries and the hydrometric network.

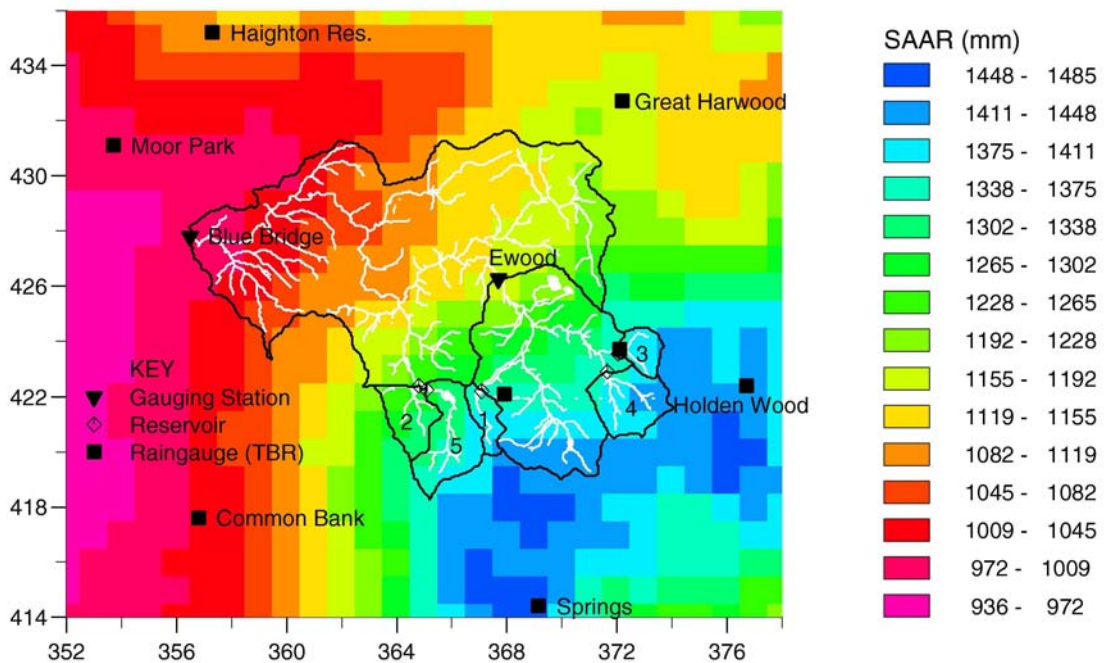


Figure 5.12 Map of SAAR (1km grid) for the Darwen catchment. Heavy lines show the reservoir drainage areas (1-5) and naturally draining areas (others).

Annual Rainfall for the area of interest and also locates the hydrometric network relative to the river network.

River gauging stations

Table 5.14 lists the location, station number, catchment area and Standard Average Annual Rainfall for each gauging station in terms of total drainage area (i.e. including reservoir drainage areas) and natural drainage area (i.e. excluding the reservoir drainage areas). The latter is most appropriate for modelling purposes. Note that the areas have been derived using the CEH Digital Terrain Model.

Table 5.14 River gauging stations: River Darwen

| Station (Station Number) | Grid Ref. | Total Catchment | | Naturally Draining | |
|-----------------------------------|------------|----------------------------|--------------|----------------------------|--------------|
| | | Area (km ²) | SAAR (mm) | Area (km ²) | SAAR (mm) |
| Darwen at Ewood (713120) | SD 677 262 | 38.99 | 1339 | 29.66 | 1322 |
| Darwen at Blue Bridge (713122) | SD 565 278 | 135.68 | 1198 | 116.09 | 1171 |

Both river gauging stations convert level readings to flows using established rating equations, of the standard form previously defined. Table 5.15 gives details of the rating equation parameters and the flood peak values for comparison.

Table 5.15 Rating equations: River Darwen

| Station | h_T | α | d | β | Bankfull (m) | Flood Peak |
|--------------------------------|--|----------|--------|---------|-----------------|--|
| River Darwen at Blue Bridge | unknown | 24.1833 | -0.084 | 1.7963 | 2.2 | 2.754 m 141 m ³ s ⁻¹ * |
| <i>Comments</i> | Controlled by V profile weir (modified from an old mill weir). Levels measured 800m upstream. *Maximum validity of rating equation unknown, also flow out of bank. | | | | | |
| River Darwen at Ewood | 1.334 | 17.751 | -0.123 | 2.3841 | 3.8 | 1.898 m 69.7 m ³ s ⁻¹ * |
| <i>Comments</i> | Open channel velocity-area station. Vertical concrete wall forms left bank, high natural right bank. *Flood peak is from an extrapolation. | | | | | |

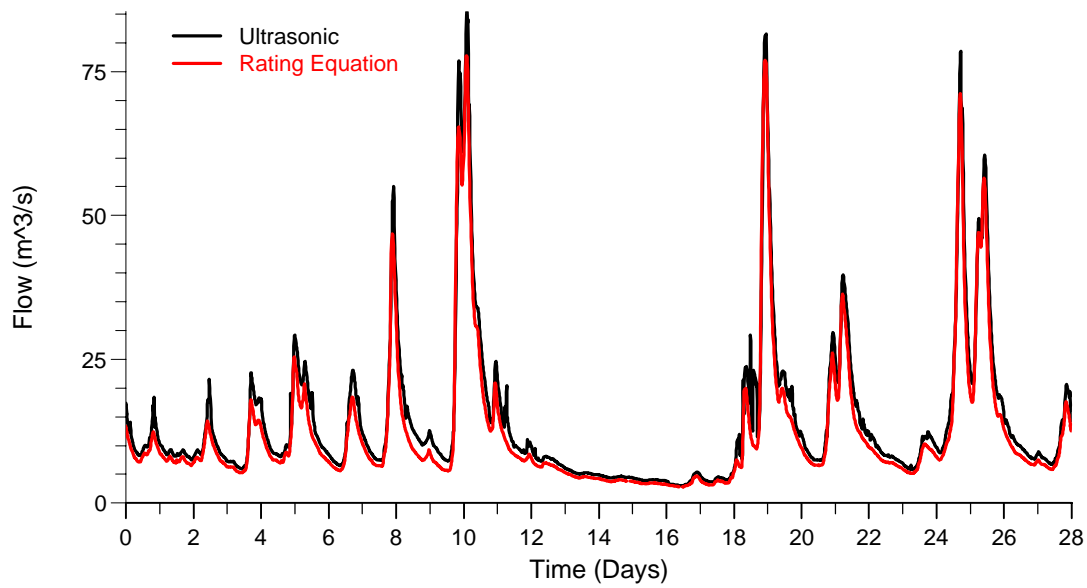
In addition, the Blue Bridge gauging station is also served by an ultrasonic flow measuring device. Analysis of data for 2002 shows the agreement of the ultrasonic recorded flows with the rating equation inferred estimates is generally good, which is reassuring, but there is a distinct temporal jump. Prior to July 2002 the ultrasonic recorded flows have a tendency to be higher than the rating equation inferred estimates, as shown by Figure 5.13 (a) for February 2002, whilst onwards from July 2002 the agreement is very good, an example being August 2002 given in Figure 5.13 (b). This temporal change in agreement between the two sources of flow estimation occurs very close to the date of the event, suggesting that the flood, or some side effect thereof, may have had a positive impact on the performance of the ultrasonic device. However, without further investigation this remains a conjecture. Unfortunately the ultrasonic record is missing for part of the flood peak but agrees well with the rating-inferred flows when available: see Figure 5.14 (b).

In assessing the return period of the flood event it is noted that both stations were used in the FD1603 report and therefore the return period estimates contained in the associated digital datasets should be reliable as they are essentially based on the historical records of the stations. These estimates of flood peaks for given return periods are listed in Table 5.16 along with the observed flow peaks. This indicates that the flood was more severe for the upstream catchment at Ewood with an estimated return period in excess of 100 years whereas the larger downstream catchment at Blue Bridge showed a less extreme response with an estimated return period between 5 and 10 years. The spatial difference in the rarity of the flood response is consistent with the spatial distribution of rainfall accumulations observed by radar (see Figure 5.9), which shows that the headwaters of the catchment were most severely affected.

Table 5.16 FEH-estimated flows (m^3s^{-1}) for given return periods (years) for gauging stations: River Darwen

| Station | 2 | 5 | 10 | 25 | 50 | 100 | 250 | 1000 | Flood Peak |
|-----------------------------|-------|-------|-------|-------|-------|-------|-------|-------|------------|
| River Darwen at Blue Bridge | 113.4 | 139.1 | 157.2 | 182.8 | 204.5 | 228.5 | 265.1 | 332.3 | 141.0 |
| River Darwen at Ewood | 30.2 | 37.8 | 43.1 | 50.6 | 56.8 | 63.8 | 74.1 | 93.0 | 69.7 |

(a) February 2002



(b) August 2002

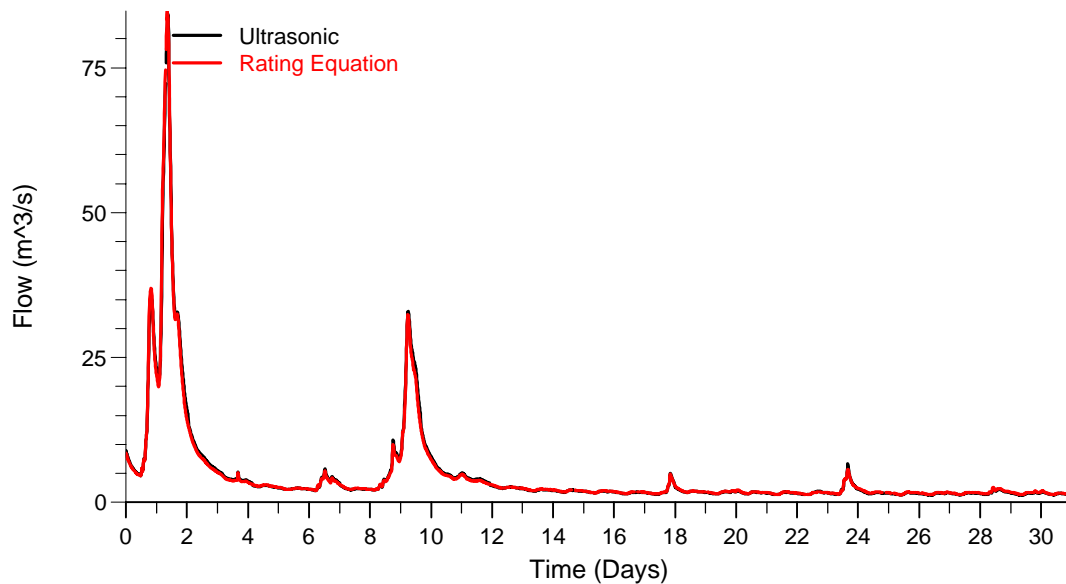
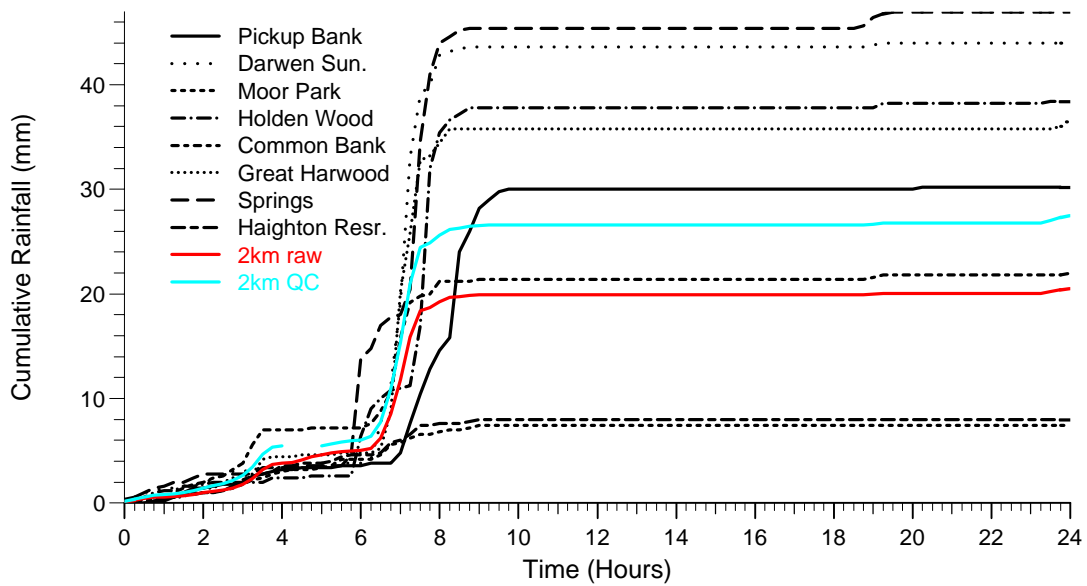


Figure 5.13 Flow hydrographs from the River Darwen at Blue Bridge comparing ultrasonic flow estimates and rating equation inferred estimates: (a) shows February 2002 data and (b) shows August 2002 data.

(a) Cumulative hyetograph



(b) Flow hydrograph from the River Darwen at Blue Bridge

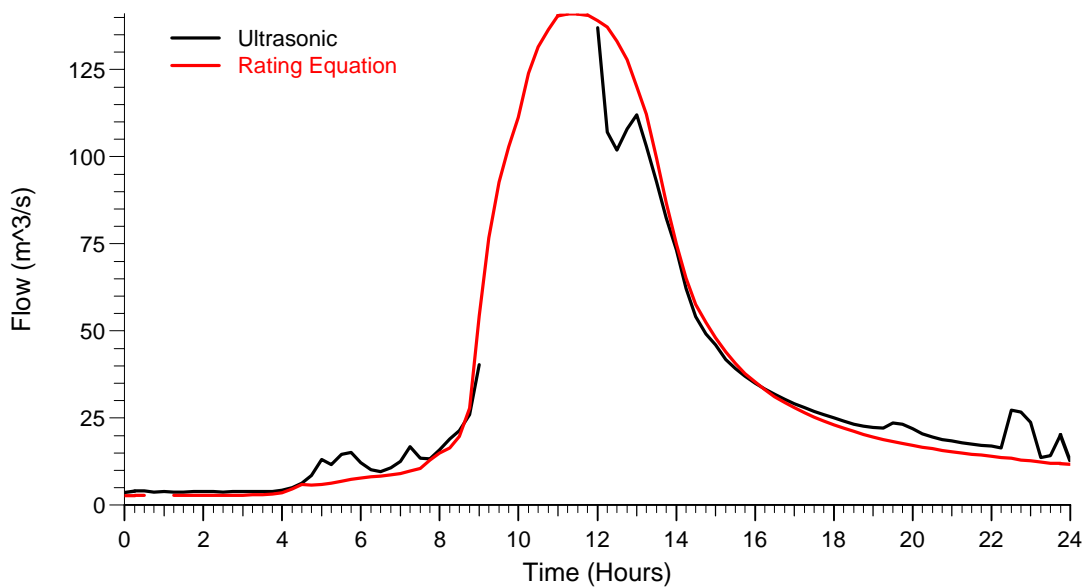


Figure 5.14 (a) Cumulative hyetograph of raingauges in and around the River Darwen catchment and catchment average rainfall derived from 2km raw and 2km QC radar data. (b) The flow response of the River Darwen at Blue Bridge as measured by an ultrasonic flow gauge and inferred from a rating equation. Both plots relate to the 24 hours starting at 09:00 14 June 2002.

Raingauge network

The River Darwen catchment and surrounding area is served by a network of 8 telemetry tipping-bucket raingauges. Their locations are indicated in Figure 5.11. All raingauge data received were in time-of-tip format and at a resolution of 0.2 mm. The location, height, SAAR and Environment Agency's station number for each raingauge are listed in Table 5.17.

Table 5.17 Telemetry raingauges: River Darwen

| Raingauge | NGR Coords | Station Number | Height (m) | SAAR (mm) |
|-------------------|-------------------|-----------------------|-------------------|------------------|
| Common Bank | SD 568 176 | 570788 | 49.0 | 1014 |
| Great Harwood | SD 722 327 | 575384 | 202.9 | 1172 |
| Darwen Sunnyhurst | SD 679 221 | 575935 | 272.3 | 1348 |
| Pickup Bank | SD 721 237 | 575975 | 227.1 | 1343 |
| Haighton Resr. | SD 573 352 | 576578 | 79.0 | 1099 |
| Moor Park | SD 537 311 | 576635 | 32.6 | 997 |
| Springs | SD 691 144 | 562341 | 239.1 | 1453 |
| Holden Wood | SD 767 224 | 560943 | 212.5 | 1436 |

Radar data

1km raw radar data from Hameldon Hill are used for the River Darwen case study. Note that 1km Nimrod QC data were not available at the time of the extreme event.

5.3.3 Event 4: 10 August 2003, Carlton-in-Cleveland

Why selected?

- Primarily for the exceptional raingauge record at Carlton-in-Cleveland
- Although no serious associated flooding it is a prime candidate for the storm modification experiments and should be included in the spatial datasets
- Partly captured by 2km resolution radar data – the storm eventually exceeds the range (from the radar site) of 2km resolution data

Meteorological synopsis

A detailed account of this storm from a meteorological observer is given by Cinderey (2005). In summary, a weak cold front moved across the north-west of

the British Isles in a south-easterly direction. The front pushed aloft the cooler, unstable air ahead of it. The 10th was also noteworthy as being the hottest day on record with 38.1°C recorded at both Kew Gardens and Gravesend.

Early in the morning thunderstorm activity broke out over parts of western Britain, moving north-eastward to affect most of northern England in the following hours. Some thunderstorms were heavy with hail mixed in. In particular one extremely intense cloudburst affected North Yorkshire and Teesside and is the focus of this event. The storm moved generally in a north-east direction with considerable velocity but appeared to slow as it reached the north-western edge of the North York Moors. The sequence of 2km Nimrod QC radar images, from the Hameldon Hill radar, contained in Figure 5.15 show the storm track and the estimated storm velocity is 60km hr⁻¹.

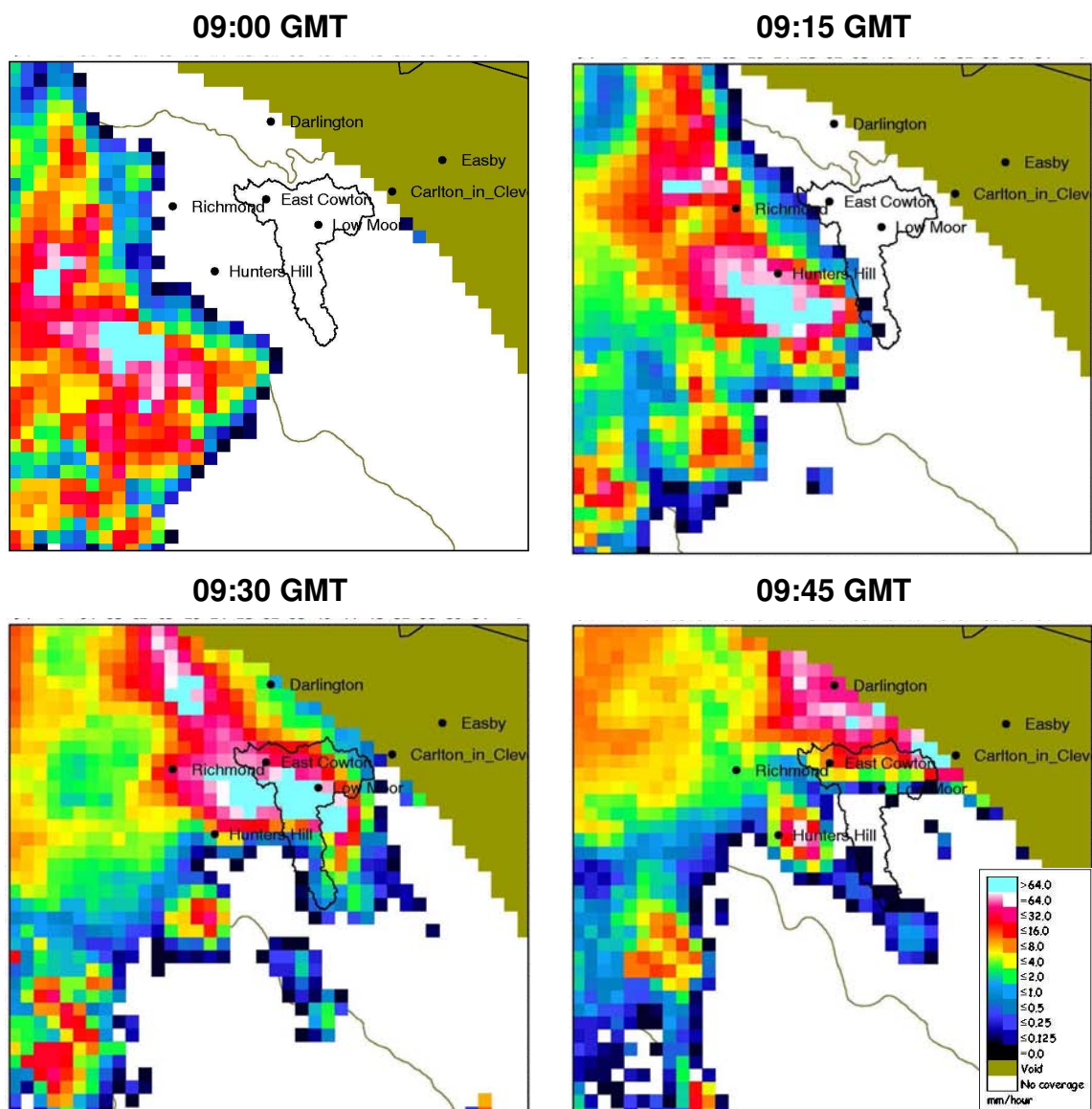


Figure 5.15 A sequence of 2km Nimrod QC radar images, at time intervals of 15 minutes, from 09:00 GMT to 09:45 GMT on 10 August 2003. The Wiske catchment and the local raingauge network are also shown.

Rainfall intensity

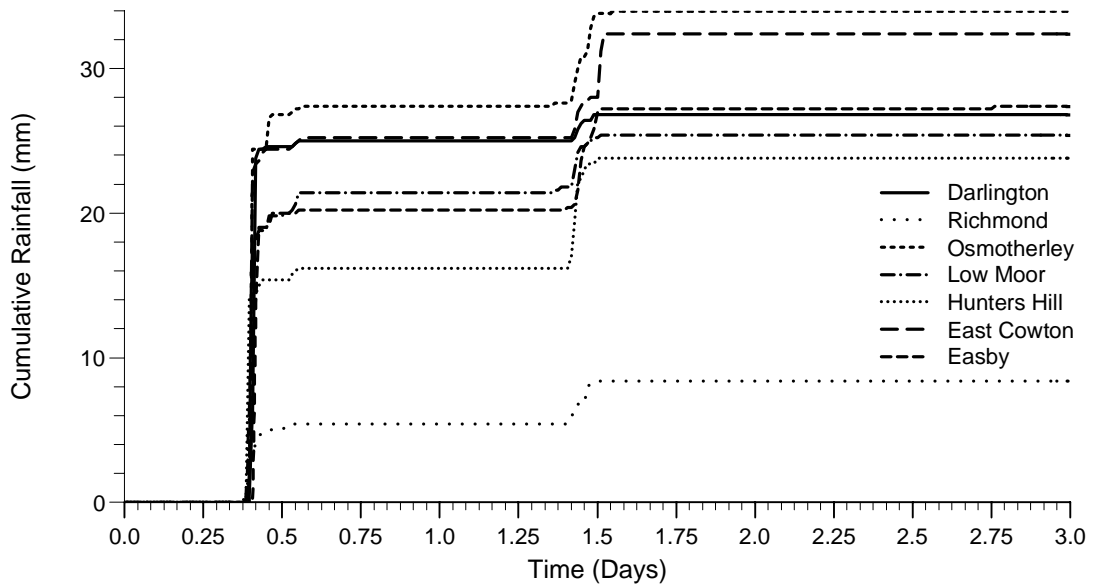
A detailed investigation of the rainfall intensity and distribution is given by Cinderey (2005), which is summarised below. The intense cloudburst deposited considerable rainfall at several raingauges in a 20km band between Leeming and Hartlepool. In particular a well exposed 'standard' climatological raingauge (Met Office Mark 2) located at Carlton-in-Cleveland recorded 49.4 mm between 9:00 and 10:00 GMT. Using the trace from a recording tilting-siphon gauge, located some 60m west-southwest of the 'standard' gauge, for the temporal segregation of the 'standard' gauge record gives a rainfall of 49.1 mm between 09:35 and 09:50 GMT and a total rainfall of 49.4 mm between 09:35 and 09:55 GMT. These have FEH-estimated return periods of approximately 600 and 500 years respectively. The event is extremely rare as it establishes new UK depth-duration extremes for periods of 8 and 10 minutes. The raingauge record also indicates peak intensities in excess of 350 mm hr^{-1} . These high intensities, combined with the presence of hail, makes quantitative rainfall estimation by radar very difficult. In fact, analysis of the instantaneous raw radar images revealed that the upper limit of 126 mm hr^{-1} was attained for several grid squares, transforming into variable values for the QC product (138 mm hr^{-1} was the highest observed). This has led to a general underestimate of the radar accumulations when compared to raingauge readings. However the spatial information contained in the radar data is evident in Figure 5.15 and shows the value of the data for the storm modification experiments.

The network of telemetry raingauges selected to support this case study is detailed later in Table 5.18. Cumulative hyetographs for the telemetry raingauges are presented in Figure 5.16 for a period of three days which includes the event, seen as near vertical lines, and a less intense short duration storm the following day. Other notable 15 minute observed totals during the event were 24.4 mm at Osmotherley and 21.4 mm at East Cowton in the 15 minutes to 09:45 GMT. These have FEH-estimated return period of 60 and 38 years respectively.

Comparison with results of the Phase 1 Study

This event occurred after the Phase 1 Study. The rainfall of 49.1 mm recorded in 15 minutes is comparable with several short convective events that took place in the last century. Namely the Hindolveston storm in 1959 where 63 mm fell in 18 minutes, the Bolton storm in 1964 where 56 mm fell in 15 minutes and the Wisbech storm in 1970 where 51 mm fell in 12 minutes. The storm is indicated in Figure 4.2 (Section 4.4.1) by a light blue cross.

(a) Cumulative hyetographs



(b) Flow hydrograph for the River Wiske at Kirby Wiske

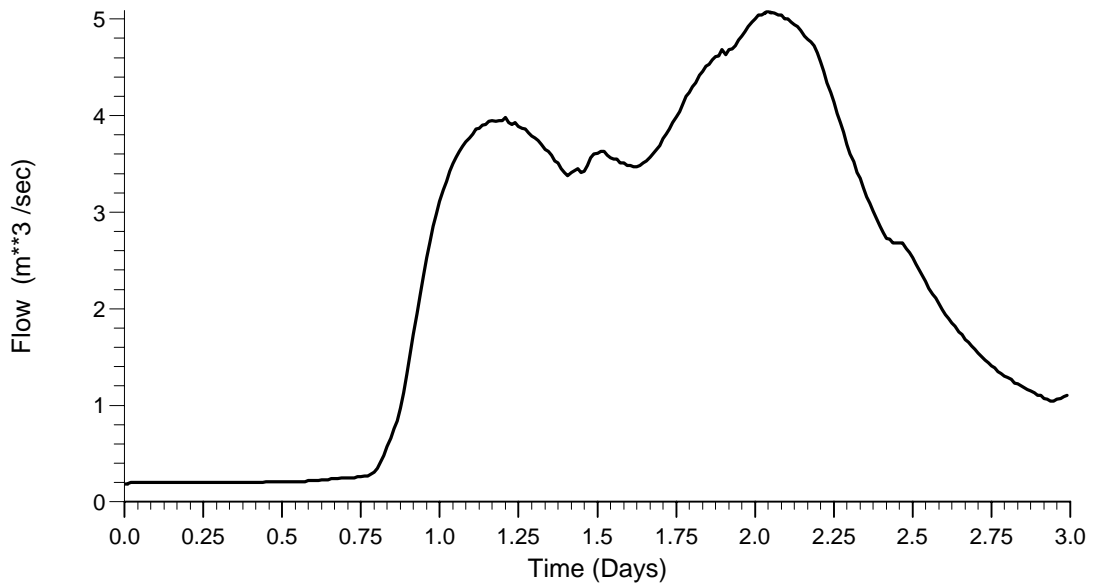


Figure 5.16 Cumulative hyetographs for the telemetry rain gauge network in and around the River Wiske catchment and the flow response of the River Wiske at Kirby Wiske for the period 00:00 10 August to 00:00 13 August 2003.

Flood damage?

No serious flooding occurred although sewer and localised runoff flooding were reported. Gauged river levels showed little response: for example the River Wiske at Kirby Wiske only rose by approximately 0.5m (see Figure 5.16(b)). Therefore this storm event was not progressed to a hydrological case study. Significant storm damage did result from the accompanying large hail and strong winds.

Raingauge network

The raingauge at Carlton-in-Cleveland is principally a daily gauge and does not provide time-of-tip data or 15 minute totals. However, for this event, two 15 minute totals have been derived using the information from Cinderey (2005) for modelling purposes. They are 41.5 mm in the 15 minutes up to 09:45 GMT and 7.9 mm in the 15 minutes up to 10:00 GMT.

The River Wiske catchment and the surrounding area are served by a network of 7 tipping-bucket raingauges. Of these, 3 have been recently installed: Low Moor and Easby in March 2003 and Hunters Hill Farm in July 2003. Their locations are mapped in Table 5.17. Data from this raingauge network have been used to create a spatial rainfall surface at 15 minute intervals which forms part of the spatial dataset. All raingauge data received were in time-of-tip format and at a resolution of 0.2 mm. The location, height, SAAR and Environment Agency's station number for each raingauge are listed in Table 5.18.

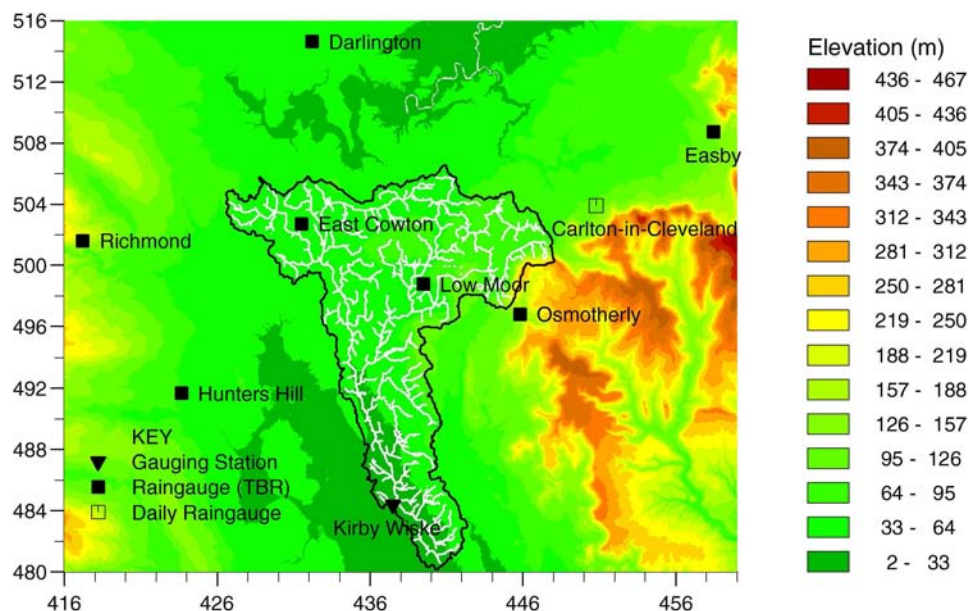


Figure 5.17 Relief map of the Wiske catchment showing the river network, catchment boundary and the hydrometric network.

Table 5.18 Raingauges: River Wiske

| Raingauge | National Grid Reference | Station Number | Height (m) | SAAR (mm) |
|------------------------------------|--------------------------------|-----------------------|-------------------|------------------|
| Osmotherley | SE 458 968 | 55223 | 147.7 | 757 |
| Richmond | NZ 172 016 | 52287 | 187.0 | 785 |
| Darlington | NZ 322 146 | 30377 | 52.5 | 606 |
| Easby | NZ 584 087 | 31555 | 112.5 | 755 |
| East Cowton | NZ 315 027 | 54371 | 38.9 | 617 |
| Hunters Hill | SE 237 917 | NE059 | 59.0 | 667 |
| Low Moor | SE 395 988 | 54507 | 55.6 | 649 |
| Carlton-in-Cleveland (daily gauge) | NZ 508 039 | 31971 | 103.7 | 713 |

Radar data

2km Nimrod QC data from Hameldon Hill weather radar are used for the Carlton-in-Cleveland case study.

5.3.4 Event 5: 19 May 1989, Walshaw Dean

Why selected?

- Exceptional raingauge record at Walshaw Dean (not confirmed by the Met Office)
- Caused serious flooding in Halifax and surrounding villages; also caused serious erosion of hillsides and river banks
- Captured by 2km resolution radar data – although radar data quality has improved since 1989 the record is still valuable for the spatial datasets and modification experiments

Meteorological synopsis

Acreman (1989) gives a detailed report of the storm and its impact, including a meteorological account which is summarised here. A high pressure system was building over the North Sea and the remnants of a front lay close to the Scottish borders with very warm and humid air to the south. Thunderstorms and lightning were reported across a wide area of Yorkshire. One extremely intense storm broke out in West Yorkshire, seriously affecting Halifax and the villages to the west, and is the focus of this case study. The rainfall associated with this storm was very localised and intense, resulting in exceptional amounts being recorded along its path. This is confirmed by the accumulated radar image, presented in Figure 5.18. Eyewitness accounts report large dark clouds forming across the

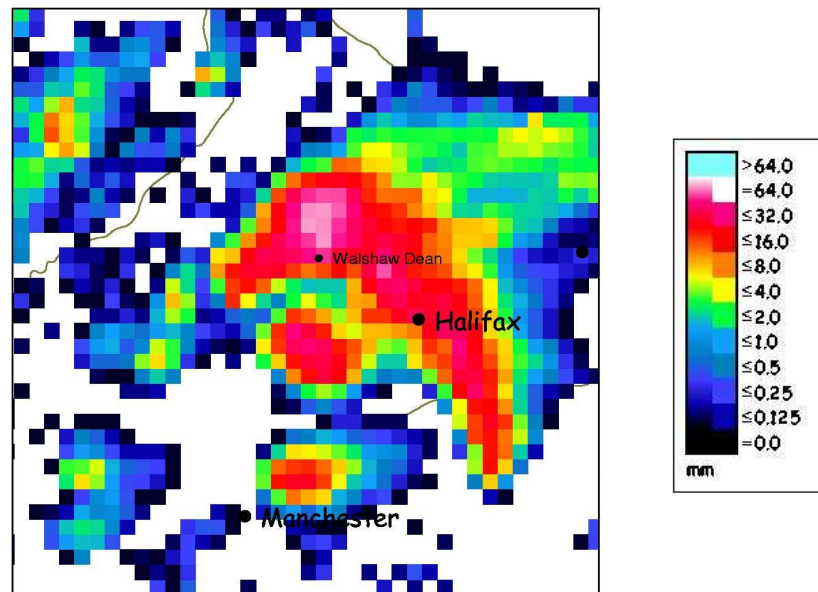


Figure 5.18 Rainfall accumulation (in mm), using 2km raw radar data from Hameldon Hill for Event 5: 5 hours up to 19:00 GMT, 19 May 1989

hills above the Walshaw Dean reservoirs. Residents near Walshaw Dean spoke of “sheets of water” covering the hillsides and suggest that the rain fell in a period of two hours commencing at 14:00 GMT with hail mixed in. This is corroborated by the 2km radar image sequence given in Figure 5.19 which shows the storm remaining almost stationary for the first two hours before moving slowly eastwards and then gaining speed as it arced its path southwards and passed over Halifax. Finally the storm petered out around 19:00 GMT.

Rainfall intensity

Acreman (1989) gives a detailed account of the raingauge recordings for the storm, the spatial pattern of which agrees qualitatively with the 2km radar accumulation over the storm. The storage raingauge situated at Walshaw Dean Lodge (SD 963 336) recorded an astonishing 193 mm for the 24 hour period including the storm. This is thought to be entirely due to the storm as local residents reported no other rainfall during the period. Investigation of the gauge showed no signs of inflow from surface flow or other malfunction. However, despite the considerable flood damage and erosion in the area, the Met Office would not accept this total stating, in a letter to the *New Civil Engineer* (6 July 1989, page 45), that following “a detailed study of this storm using all sources of information currently available” they had “reluctantly come to the conclusion that this total does not appear acceptable”. If indeed 193 mm did fall at Walshaw Dean in 2 hours, the estimated return period from DDF analysis would be in excess of 5000 years making it one of the most extreme rainfalls on record. Even though there is some controversy over the actual rainfall total at Walshaw Dean, Acreman (1989) concludes that although the indirect evidence from river

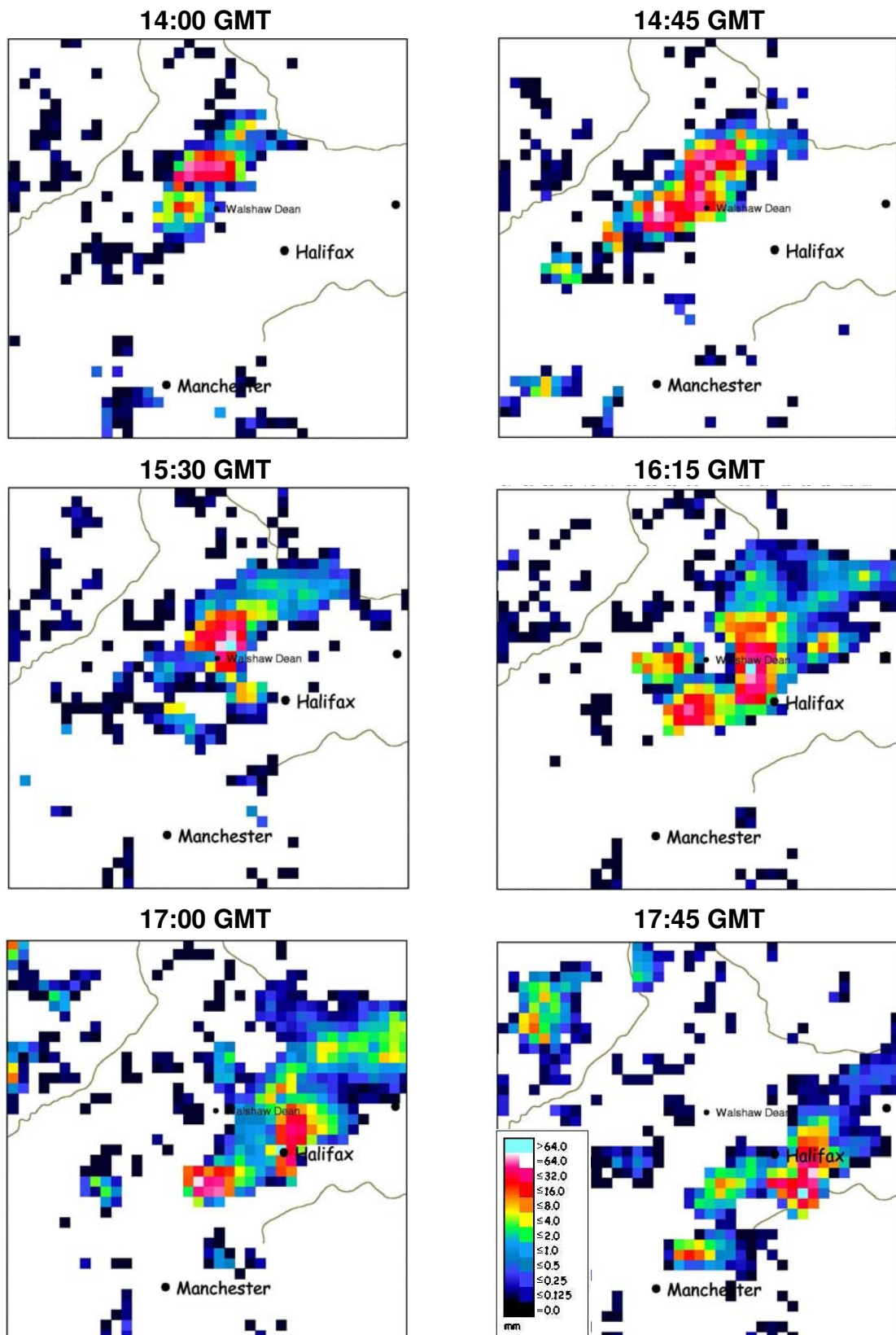


Figure 5.19 A sequence of 2km raw radar images, at time intervals of 45 minutes, from 14:00 GMT to 17:45 GMT on 19 May 1989. The location of the Walshaw Dean raingauge is also shown.

flows, reservoir levels and geomorphological response provide only rough guesses, these support a figure in excess of 100 mm. This certainly exceeds the estimated 100 year 2 hour duration return period rainfall for Walshaw Dean of 60 mm.

The storm was not progressed to a historical hydrological case study for several reasons. The main reason is the lack of hydrometric data: the telemetry raingauge network did not capture the storm sufficiently and not all river level records for the period have been digitised.

Flood damage?

The flash floods associated with the storm caused serious damage to Halifax and the villages upstream. The damage was documented by Acreman (1989) and summarised here. The village of Ludden was seriously affected by various culverts exceeding capacity. This caused gardens to be washed away and roads to become like rivers. Hebble Brook was particularly affected with water levels up to 4 m, that is 2 m above bankfull between Salterhebble and Lee Bridge Mill. Other flooding in Halifax was mainly due to inadequate surface drainage rather than high river levels. The Halifax *Evening Courier* reported that roads were impassable due to direct runoff, fallen trees and paving slabs which had been swept off the pavement.

Comparison with results of the Phase 1 Study

The Halifax storm was included in the Phase 1 Study Report and stood out for its short duration, as indicated in Figure 4.2 (Section 4.4.1) by the magenta cross.

Raingauge network

As the telemetry raingauge network did not capture the storm coverage, raingauge data were not requested and no spatial rainfall surfaces fitted to raingauge values were created.

Radar data

2km raw data from Hameldon Hill weather radar were used for the Halifax case study. Note that at the time of the extreme event Nimrod QC radar data did not exist.

5.3.5 Event 6: 16 August 2004, Boscastle

Why selected?

- Exceptional raingauge totals recorded at Lesnewth and Otterham
- Caused serious flooding and destruction in Boscastle and Crackington Haven; also caused serious erosion of hillsides and river banks
- Captured by 2km resolution radar data; although no direct river level/flow data are available the storm is still useful to include within the spatial datasets

Meteorological synopsis

Following the devastating floods associated with the extreme rainfall of the Boscastle and North Cornwall storm, the Met Office produced a comprehensive meteorological analysis (Golding, 2005) and an article in *Weather* (Golding *et al.* 2005) which are briefly summarised here. The heavy rainfall which affected North Cornwall predominantly fell between 12:00 and 16:00 GMT and was produced by a sequence of convective storms that developed along a coastal convergence line caused by the change in friction between the land and sea. This effect was heightened by solar heating over land. The exact storm path of each heavy rain cell varied slightly but the variation between the Camel Estuary and Bude was sufficiently small that the heaviest rain fell on the same small coast-facing catchments throughout the period. This is evident in Figure 5.20 which shows the rainfall accumulation using radar data over the event and the Boscastle and Crackington Haven catchments.

That successive storms followed the same path increased the efficiency of subsequent storms as residual clouds from earlier storms were incorporated into later ones. The sequence of 2km radar images presented in Figure 5.21 clearly shows the almost stationary heavy rainfall over the Boscastle catchment during the succession of storm cells. The sequence of radar images are discussed in much more detail in Golding (2005).

Rainfall intensity

The extreme rainfall event was captured by a network of tipping-bucket raingauges and daily storage gauges. Three gauges were situated near the core of the storm. In the 24 period to 09:00 GMT 17 August 2004, the daily storage gauge at Otterham (SX 169 916) recorded 200.4 mm, the daily storage gauge at Lesnewth (SX 134 900) recorded 184.9 mm and the tipping-bucket raingauge at Lesnewth (SX 134 900) recorded 155.2 mm.

The tipping-bucket raingauge data at Lesnewth provides information about the time profile of the storm. The discrepancy between this and the Lesnewth daily raingauge totals is most likely to be due to known problems with tipping-bucket raingauges during intense rainfall events. During heavy rainfall such raingauges

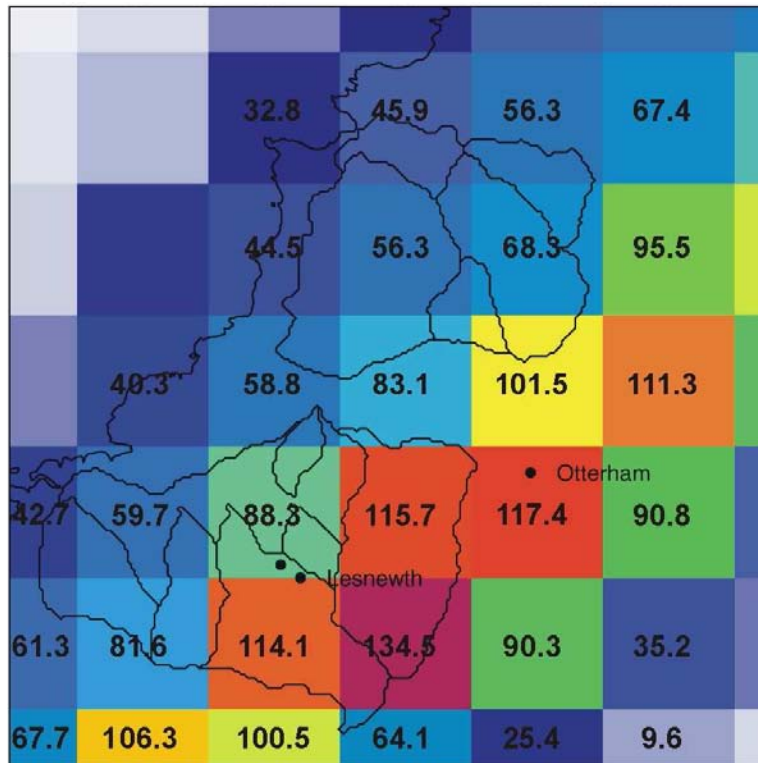


Figure 5.20 Rainfall accumulation, using 2km Nimrod QC data from the Cobbacombe Cross radar, for Event 6: 5 hours up to 17:00 GMT, 16 Aug 2004. Figures give actual radar grid square values. The Boscastle and Crackington Haven catchments are highlighted and solid circles mark the location of the daily and telemetry raingauges in the vicinity.

can underestimate rainfall because of *dead time* when the bucket is emptying. For example at a rain rate of 200 mm hr^{-1} the bucket empties every 3.6 seconds and a daily total of 155.2 mm results from 776 tips. The recommendation from Golding (2005) is to scale the tipping-bucket rainfall amounts at Lesnewth to the daily gauge total.

Table 5.19 presents the values of maximum rainfall accumulation for periods of one to five hours using the uncorrected and corrected Lesnewth tipping-bucket rain gauge data taken from Golding (2005). Also given are the FEH-derived return periods which show the 4 hour duration maximum was the most extreme with an estimated return period in excess of 2000 years (note the FEH recommends that calculated rainfall return periods in excess of 2000 years should be referred to as having 'return period in excess of 2000 years'). A peak rainfall intensity of nearly 300 mm hr^{-1} was recorded at the Lesnewth tipping-bucket rain gauge at 15:35 GMT. Cumulative hyetographs (using 15 minute accumulations) for a selection of tipping-bucket rain gauges in and around the Boscastle catchment are presented in Figure 5.22 emphasising the notable rain-rates and amounts recorded at Lesnewth.

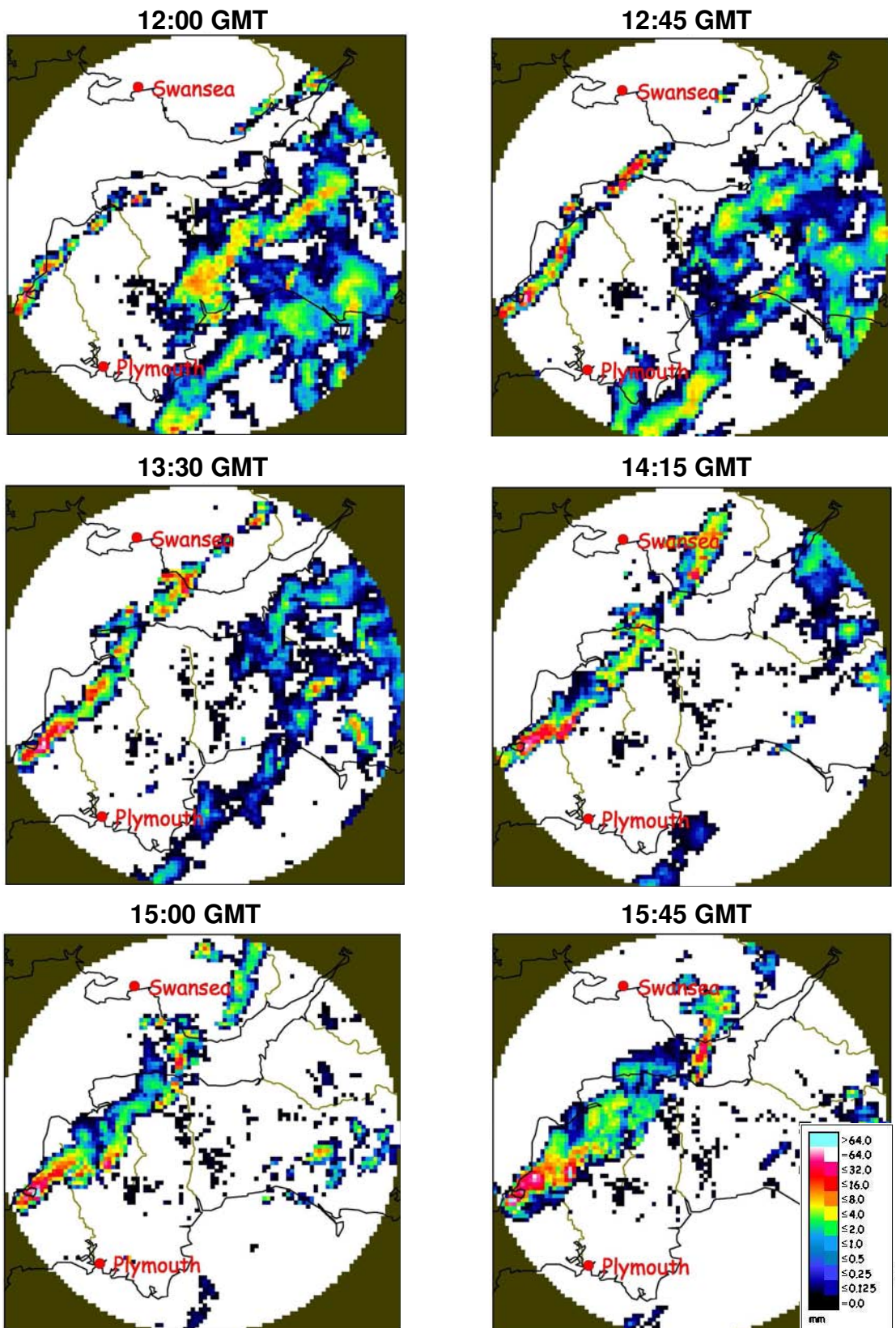


Figure 5.21 A sequence of 2km Nimrod QC images from the Cobbacombe Cross radar, at time intervals of 45 minutes, from 12:00 GMT to 15:45 GMT on 16 Aug 2004. The Boscastle catchment is also shown.

Table 5.19 Rolling peak maximum rainfall accumulations for the Lesnewth raingauge and FEH estimated return periods.

| | Duration (hours) | | | | |
|--------------------------------------|------------------|------|-------|-------|-------|
| | 1 | 2 | 3 | 4 | 5 |
| Lesnewth uncorrected TBR (mm) | 68 | 94 | 123 | 150 | 152 |
| Estimated return period (yrs) | ~400 | ~700 | ~1300 | ~2200 | ~1900 |
| Lesnewth corrected TBR (mm) | 72 | 100 | 148 | 181 | 183 |
| Estimated return period (yrs) | ~750 | ~850 | ~2500 | ~4500 | ~4000 |

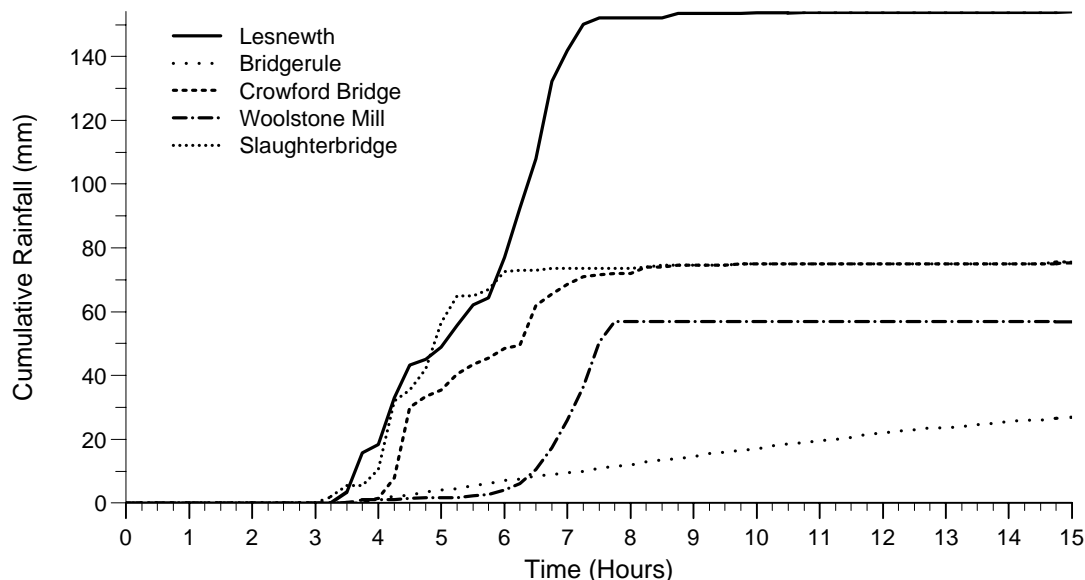


Figure 5.22 Cumulative hyetographs for selected tipping-bucket raingauges in and around the Boscastle catchment for the period 09:00 16 August to 00:00 17 August 2004.

Flood damage?

Several catchments across North Cornwall were affected by flooding. The most severe flooding occurred on the Valency and Crackington Stream but the rivers Ottery and Neet also flooded. Following the event the Environment Agency commissioned a detailed consortium study lead by HR Wallingford. The study report (HR Wallingford, 2005) contains a detailed account of the considerable damage caused to Boscastle and Crackington Haven. Flash flooding affected at least 100 homes and businesses with a total of six properties being destroyed. Roads, bridges and other infrastructure were badly damaged and 115 vehicles

were swept away. Fortunately, due to the quick response of the emergency services, no lives were lost but around 100 people were rescued by helicopter. Notable effects of the flash flood were the numerous trees swept away, causing trash dams and several new paths cut by the flows.

Comparison with results of the Phase 1 Study

The Boscastle storm occurred after the Phase 1 Study so did not feature in the study report. The three and five hour rolling peak totals of 148 and 183 mm from the corrected Lesnewth tipping-bucket raingauge record certainly confirms that the storm was extreme according to the Phase 1 Study Report classification and are marked in Figure 4.2 (Section 4.4.1). Comparison with other extreme convective events of the 20th century shows that the three hour total is comparable with the Camelford storm of 1957 (138 mm in 2.5 hours) but did not reach the 3 hour totals of 171 mm at Hampstead in 1975 and 178 mm at Horncastle in 1960. The 5 hour total does stand out from other pure convective events, except for the much shorter duration storm at Halifax where 193 mm fell in 2 hours (see Event 5).

Raingauge network

As noted above, the most notable rainfall amounts were recorded at Lesnewth and Otterham. However, a wider network of tipping-bucket raingauges in the vicinity of Boscastle also captured some aspects of the storm. Data from this tipping-bucket network have been used to create a spatial rainfall surface at 15 minute intervals which forms part of the spatial datasets. The tipping-bucket record from Lesnewth has been scaled up to meet the daily gauge total as suggested by Golding (2005).

Data were received from the Environment Agency in a variety of formats. The data from gauges at Lesnewth, Roserrow and Bude were in time-of-tip format with the remaining data provided as 15 minute totals. The resolution of tip size also varied with Bude, De Lank, Roserrow, Lesnewth, Wadebridge and Woolstone Mill using a 0.2 mm tip size and the others using a 0.5 mm tip size. The location, height, SAAR and Environment Agency's station number for each raingauge are listed in Table 5.20. Data were provided for a raingauge at Bridgrule (SS 272 024) but examination of the cumulative hyetograph given in Figure 5.22 revealed that the raingauge did not record properly over the event and was therefore not used.

Radar data

2km Nimrod QC data from Cobbacombe Cross weather radar were used for the Boscastle case study.

Table 5.20 Raingauges: Boscastle area

| Raingauge | National Grid Reference | Station Number | Height (m) | SAAR (mm) |
|------------------|--------------------------------|-----------------------|-------------------|------------------|
| Bastreet | SX 2443 7639 | R12592_FW | 230.2 | 1688 |
| Bude | SS 2079 0629 | 27A04 | 9.4 | 857 |
| Canworthy Water | SX 2284 9168 | R12588_FW | 101.5 | 1139 |
| Crowford | SX 2905 9910 | R12586_FW | 84.5 | 1097 |
| De Lank | SX 1326 7655 | N/A | 228.6 | 1486 |
| Roserrow | SW 9458 7803 | N/A | 33.1 | 952 |
| Slaughterbridge | SX 1094 8572 | R25578_FW | 203.4 | 1410 |
| Tamarstone | SS 2823 0564 | R12583_FW | 102.7 | 1106 |
| Lesnewth (TBR) | SX 1340 9000 | N/A | 210.0 | 1286 |
| Lesnewth (daily) | SX 1340 9000 | 385700 | 210.0 | 1286 |
| Wadebridge | SW 9883 7271 | 25A06 | 3.6 | 1025 |
| Woolstone Mill | SS 2273 0181 | R27582_FW | 20.3 | 945 |
| Yeolmsbridge | SX 3171 8738 | R12587_FW | 66.6 | 1167 |
| Otterham (daily) | SX 1690 9160 | 371160 | 202.3 | 1244 |

6 Rainfall estimators for the case studies

Spatial rainfall estimators are well suited for use as input to distributed rainfall-runoff models but also allow increased flexibility for ‘amplifying’ storms and for use in catchment flood response experiments. This section assesses the relative performance, from a rainfall perspective, of the three spatial rainfall estimators used in this report. These estimators are:

1. **Radar rainfall:** The finest resolution single site rainfall radar data available. Preferably Nimrod Quality Controlled (Nimrod QC) data.
2. **Raingauge-only rainfall surface:** A gridded spatial rainfall surface fitted to point raingauge values every 15 minutes with a 1km resolution.
3. **Raingauge-adjusted radar rainfall:** Raingauge adjustment factors are calculated for radar grid-squares coincident with raingauge locations. A surface of adjustment factors are fitted to these point values and applied to the radar image. This is repeated at 15 minute intervals.

The multiquadric surface fitting technique used to generate the gridded surfaces is detailed in Appendix C and its application for generating the raingauge-only surface and raingauge-adjusted radar data are detailed in Section 6.1. The objective is to determine the optimum forms of the raingauge-only surface and raingauge-adjusted radar data. It is not to determine which rainfall estimator performs best: this will ultimately be assessed in Section 7 through rainfall-runoff modelling over the case study extreme events.

The method of performance assessment used for each type of rainfall estimator is also given in Section 6.1. The performance assessment framework allows the optimisation of the incidental parameters associated with the multiquadric surface applications. These parameters are optimised over a long period of data (11-20 months) that includes different seasons as well as the extreme rainfall event of interest. In addition, the spatial rainfall estimators generated have been viewed (through Hyrad) to visually inspect their characteristics and to identify any other traits not evident from the statistics.

Sections 6.2 to 6.4 present the results of the different rainfall estimators for each of the three case study catchments: the River Darwen, the River Kent and the Upper Thames and Stour. Finally Section 6.5 details recommended forms of the raingauge-only surface and raingauge-adjusted radar for each catchment.

6.1 Spatial rainfall estimators and performance assessment

This section details application of the multiquadric surface fitting technique to a network of raingauges for generating the raingauge-only rainfall surface and the raingauge-adjusted radar rainfall data. The performance assessment of each spatial rainfall estimator is also detailed including unadjusted radar data.

6.1.1 Radar rainfall data

For each case study catchment the finest resolution raw radar data are used and, if available, the Nimrod quality controlled radar data are also considered.

Performance assessment

The performance assessment for the radar rainfall data is made by comparing the 15 minute raingauge totals to the radar-based estimates for the grid square coincident with the raingauge.

Since 15 minute raingauge data are derived by counting the number of tips of a tipping-bucket made within the 15 minute interval, the values may be in error by $\pm 0.8 \text{ mm hr}^{-1}$ for a 0.2 mm capacity bucket. To compensate for this, the criteria used for assessing the accuracy of the radar data are based on the quantised-adjusted error which effectively rounds the raingauge value towards the radar data by an amount equal to the bucket capacity. Let r_i denote the unadjusted radar estimate of rainfall rate for the grid-square coincident with the i^{th} raingauge and let R_g^i denote the actual rainfall rate for the i^{th} raingauge.

Formally, using the i^{th} raingauge value as 'truth' and given $\delta_g = (\text{bucket capacity in mm}) / (\text{time interval in hrs})$ is the rainfall intensity quantisation error for the time interval considered, then the quantised-adjusted error of the radar data at the i^{th} raingauge location is:

$$e_i = \begin{cases} R_g^i - r_i - \delta_g & R_g^i - r_i > \delta_g \\ R_g^i - r_i & |R_g^i - r_i| \leq \delta_g \\ R_g^i - r_i + \delta_g & R_g^i - r_i < -\delta_g \end{cases} \quad (6.1)$$

For a single time-frame these errors can be obtained at each of the N raingauge locations. A subtle question is which timeframes and/or raingauges to include in the analysis? In this study statistics were calculated for each of the following criteria.

- 1. All rain >1 mm:** Only considers time-frames where the *maximum* rainfall recorded at any raingauge in the network exceeds 1 mm hr^{-1} . For this case the errors are calculated at every available gauge (even if $R_g^i < 1 \text{ mm hr}^{-1}$).
- 2. Medium Rain:** Errors are only calculated for raingauges where $4 < R_g^i < 12 \text{ mm hr}^{-1}$.
- 3. Heavy Rain:** Errors are only calculated for raingauges where $R_g^i > 12 \text{ mm hr}^{-1}$.

For each criterion, errors are calculated over all time-frames for the periods considered. The mean quantised-adjusted error (me) of the radar data is the

average of these errors whilst the root mean square quantised-adjusted error (rmse) is the square root of the average of these errors. Hence

$$\text{me} = \frac{1}{n} \sum e_i \quad (6.2)$$

$$\text{rmse} = \left(\frac{1}{n} \sum e_i^2 \right)^{1/2} \quad (6.3)$$

where n is the total number of errors (across all raingauges and time-frames). This allows performance comparison between different spatial rainfall estimators.

6.1.2 Raingauge-only rainfall estimation

When constructing a spatial rainfall estimator based on a network of raingauges, the key question posed is how to infer the spatial distribution of the rainfall and, in particular, how to construct the grid-square average rainfall totals? One option is to fit a multiquadric surface to the observed raingauge totals at each model time-step and then calculate, for each grid-square, the grid-square average rainfall total. However, Section C.3 indicates that the average rainfall total for a given grid-square will be the same linear combination of raingauge totals for every time-step: that is the weights will be the same regardless of the actual raingauge values being combined. Therefore, it is far more efficient to simply calculate the linear set of raingauge weights for each grid-square in turn at the outset and then use these weights at each time-step to construct the grid-square average rainfall totals required by the distributed rainfall-runoff model. In practice these weights (but not the volumes as these remain constant and only need to be calculated once) are recalculated each time a raingauge in the network comes in to or out of service.

Depending on the extent of the region of interest it may not be appropriate to use the entire network of raingauges for all grid squares. The approach used for deriving the weights for a given grid-square is outlined in the decision flowchart presented in Figure 6.1.

Performance assessment

Based on earlier studies of constructing spatial rainfall from raingauge-only data (Moore *et al.*, 1989) the raingauge values are transformed, using a modified logarithmic form, before the grid-square averages are calculated. Then the reverse transformation is applied and any negative rainfall that results is set to zero.

Let R_g^i denote the actual rainfall rate for the i^{th} raingauge, f denote the rainfall transformation function and $\hat{R}_g^i = f(R_g^i)$ denote the transformed rainfall for the i^{th} raingauge. The latter are used as the data points z_i in the multiquadric surface fitting techniques discussed earlier. The transformed rainfall is given by

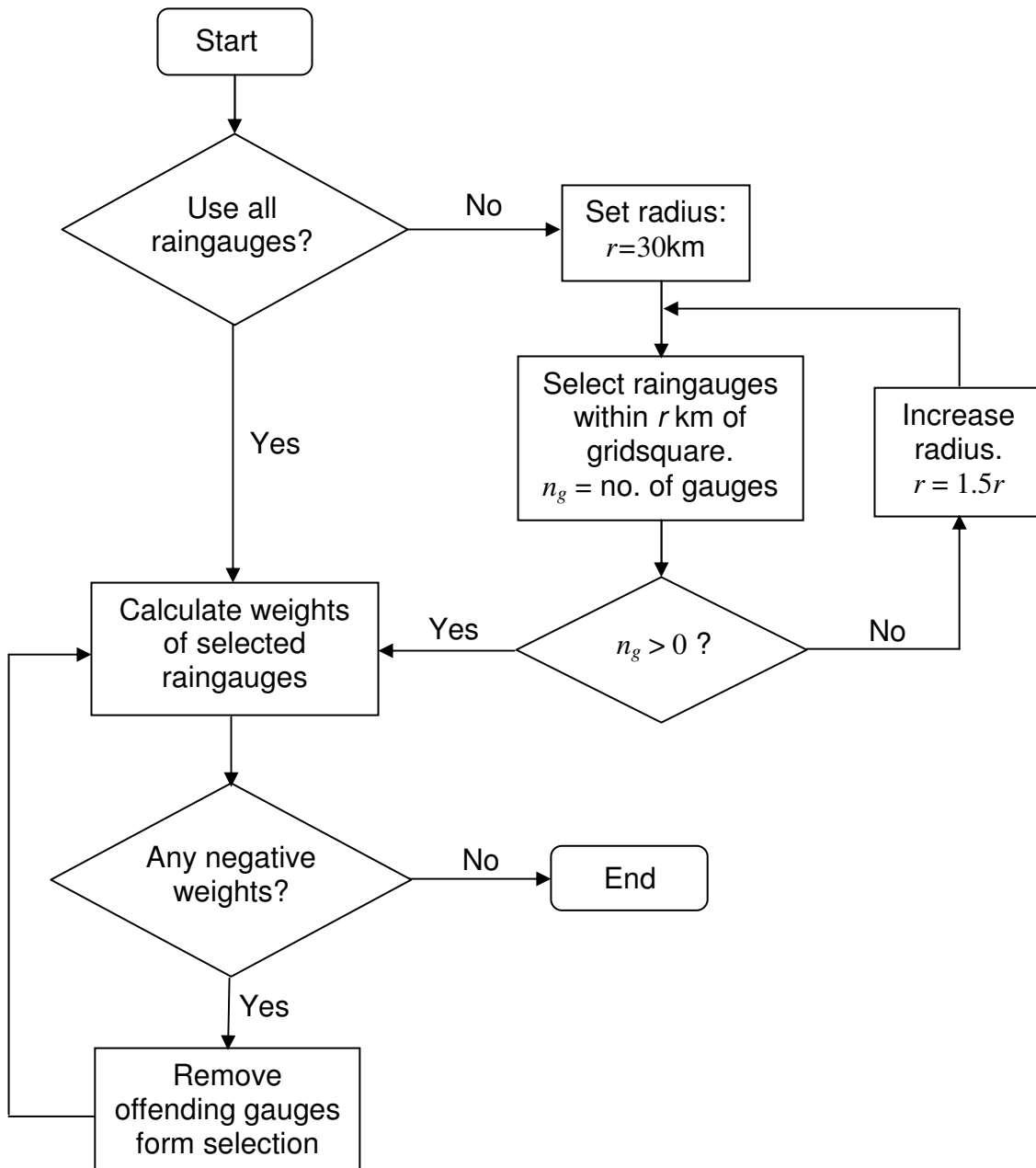


Figure 6.1 Flowchart for deriving raingauge weights for a given grid-square

$$\hat{R}_g^i = f(R_g^i) = \begin{cases} \log(R_g^i) & \text{for } R_g^i > R_0 \text{ mm/hr} \\ \log(R_0) + \frac{R_g^i}{R_0} - 1 & \text{for } R_g^i \leq R_0 \text{ mm/hr} \end{cases} \quad (6.4)$$

where R_0 is another parameter that is empirically estimated from the data. The inverse transformation is then given by:

$$f^{-1}(\hat{R}_g^i) = \begin{cases} 10^{\hat{R}_g^i} & \text{for } \hat{R}_g^i > \log(R_0) \\ \max\{R_0(\hat{R}_g^i + 1 - \log(R_0)), 0\} & \text{for } \hat{R}_g^i \leq \log(R_0) \end{cases} \quad (6.5)$$

The criteria used for assessing the accuracy of the rainfall surface is based on the quantised-adjusted error (see equation (6.1)). Of course deriving a raingauge-only surface from a network of raingauges and then comparing this to the network of raingauges would be nonsensical. Therefore the method of 'selective deletion' is applied: Here r_i in equation (6.1) denotes the surface-derived rainfall rate at the i^{th} raingauge location, where the surface has been derived **excluding** the i^{th} raingauge from the set of data points and the inverse rainfall transformation, equation (6.5), has been applied.

The mean quantised-adjusted error (me) of the derived surface and the root mean square quantised-adjusted error (rmse) are used for performance assessment of the raingauge-only rainfall surface.

6.1.3 Raingauge-adjusted radar estimations

Radar estimates of rainfall capture the spatial variability of rainfall well, in comparison to the point estimates of a raingauge network (unless a very dense network is available). However, a downside is that the accuracy of radar estimation is significantly less than that of raingauge-based estimation at the location of the raingauge. Therefore, the objective is to adjust radar estimations using information from the raingauge network in an attempt to obtain a more accurate spatially varying rainfall field.

Static gauge-adjustment of radar

This approach attempts to improve the radar data by identifying the long-term bias of a radar dataset and then correcting for it. This is known as **static gauge-adjustment of radar**, as a single factor is applied to the entire radar dataset.

For the i^{th} raingauge the long term bias, B_i , is defined to be the arithmetic mean ratio calculated over n time frames:

$$B_i = \frac{1}{n} \sum \frac{R_g^i}{R_r^i} \quad (6.6)$$

where R_r^i is the unadjusted radar estimate for the grid-square coincident with the i^{th} raingauge. In practice the ratio is only calculated if both R_r^i and R_g^i are greater than 1 mm hr^{-1} . This minimises discretisation errors and the influence of anomalous propagation. It also ensures that the ratio is defined. Averaging this over the n raingauges gives the long-term bias, B , of the radar:

$$B = \frac{1}{N} \sum B_i . \quad (6.7)$$

Applying this factor to the entire radar dataset gives the statically-adjusted radar dataset.

Dynamic gauge-adjustment of radar

For the case of dynamic gauge-adjustment of radar the data points z_i that the multiquadric surface is fitted to are adjustment factors. This is known as dynamic gauge-adjustment as the surface is constructed at each time-step. There are several options for the form of the gauge-adjustment factor: in this study two related forms are considered. The first is defined as a modified ratio of the rainfall at the i^{th} raingauge, R_g^i , to the radar estimate, R_r^i , for the grid-square coincident with the raingauge:

$$z_i = \frac{R_g^i + \varepsilon_g}{R_r^i + \varepsilon_r} \quad (6.8)$$

where ε_g and ε_r are positive constants such that the ratio is defined for all values of R_g^i and R_r^i . This form was found to be most effective in previous studies of the Chenies radar (Moore *et al.*, 1989) and is referred to as **standard dynamic gauge-adjustment of radar**.

An extended form (Wood *et al.*, 2000) that takes account of the long-term bias is also considered that modifies the gauge-adjustment factor (6.8) to

$$z_i = \frac{R_g^i + \varepsilon_g}{\kappa R_r^i + \varepsilon_r} \quad (6.9)$$

where κ is the long-term static adjustment factor (see equation (6.7)). In this case $\varepsilon_g = \varepsilon_r = \varepsilon$. This is referred to as **dynamic adjustment of radar including mean bias**. An important point is that, for this form of adjustment factor, the long-term bias is accounted for and therefore the surface fitted should tend to an adjustment factor of 1 (i.e. no adjustment) at large distances. As such, only the exponential form of the Euclidean distance and the inverse distance measures should be used with the no adjustment at large distances boundary condition.

For both forms of dynamic gauge-adjustment the derived surface of adjustment ('calibration') factors can be applied to the radar estimate to obtain the raingauge-adjusted radar estimate. Note that unlike for the raingauge-only case, the raingauge rainfall is kept in its original form. The derivation of the weights required for the grid-square average adjustment factors follows the same procedure as the raingauge-only case, outlined in Figure 6.1.

Performance assessment

The mean quantised-adjusted error and the root mean square quantised-adjusted error are again used as the measure of the performance. This is identical to that explained in Section 6.1.2 except that r_i corresponds to the gauge-adjusted radar estimate using 'selective deletion', rather than the derived rainfall surface. Note that when the rmse and me statistics are calculated for a *radar-only* estimate of rainfall (e.g. the raw radar data or Nimrod radar data) the notion of 'selective deletion' no longer applies.

6.2 The River Darwen case study

For this case study the single site 1km raw radar data from Hameldon Hill were used. Raingauge data were only available from 1 January 2002 to 30 November 2002. The results given here are for this 11 month period when there were 26868 observations for the all rain > 1 mm category, 1929 observations for the medium rainfall category and 99 observations for the heavy rainfall category.

Raingauge-only rainfall estimation

The optimal results were obtained by primarily minimising the rmse statistics for the medium rain case for many different combinations of the incidental parameters R_0 , K and L . The final results were further refined by taking in to account the rmse statistics for the heavy rainfall and the all rain > 1 mm hr^{-1} categories. Clearly there was a subjective element in the final selection as the optimum incidental parameter set for each rainfall category were not necessarily the same.

The results are detailed in Table 6.1. These show that changing the distance measure or surface type of the raingauge-only rainfall estimate have little effect on the optimal rmse statistic. The mean error statistics contained in Table 6.1 show that the raingauge-only estimate of rainfall consistently underestimates rainfall, particularly for the heavy rain events. The latter is not surprising since the heavy rainfall events are generally associated with convective storms which, by their nature, have a very varied spatial structure. Therefore, for a given fifteen minute interval, convective storms may not always register a significant reading at more than one (if indeed any) raingauge in the network. Of course this is dependent on the raingauge density in the region but is a valid point for the Darwen case study where there are 8 gauges covering a region of approximately 520 km^2 . In a situation where only one gauge receives a significant reading, the method of 'selective deletion' will, inevitably, lead to a significant underestimation of the rainfall by the fitted surface and is the likely explanation for the poorer performance of the raingauge-only rainfall estimator for heavy rainfall.

The rmse statistics are also given for the 1 km raw radar estimate; however it should be noted that this is not strictly a like-for-like comparison since the radar estimate actually *samples* the rainfall at the raingauge location whereas, in the 'selective deletion' approach, the raingauge-only rainfall estimator is actually

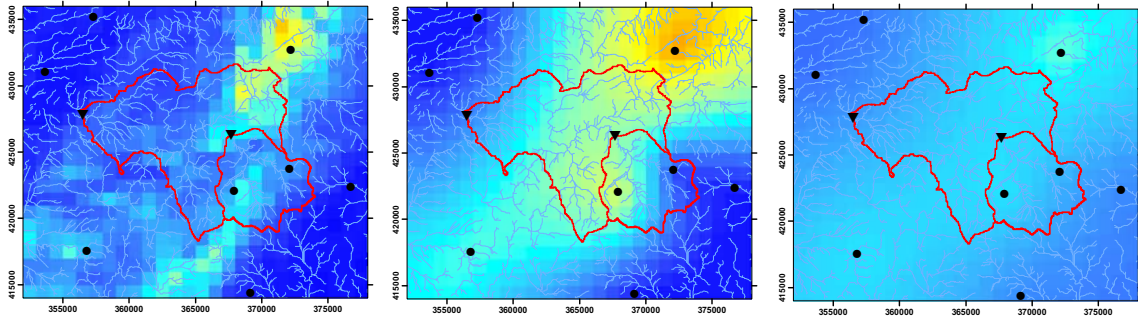
Table 6.1 Optimal parameter sets and rainfall estimation performance for raingauge-only rainfall estimation: River Darwen case study. The performance of the 1km raw radar and the zero parameter surface are given for comparison.

| Distance Measure | Surface Type | RMSE (ME) | | | Incidental parameters |
|--|---------------------------------|---------------------------------|--------------------------------------|------------------------------------|---|
| | | All rain >1 mm hr ⁻¹ | Medium rain 4-12 mm hr ⁻¹ | Heavy rain >12 mm hr ⁻¹ | |
| Euclidean distance | Flatness constraint | 1.561 (0.137) | 2.841 (1.961) | 20.240 (17.247) | $R_0 = 7.5 \text{ mm hr}^{-1}$, $K = 18 \text{ km}$ |
| Exponential form of Euclidean distance | Flatness constraint | 1.560 (0.139) | 2.843 (1.963) | 20.246 (17.280) | $R_0 = 7.5 \text{ mm hr}^{-1}$, $K = 0.32, L = 35 \text{ km}$ |
| | Zero rainfall at large distance | 1.567 (0.131) | 2.847 (1.936) | 20.250 (17.311) | $R_0 = 7.5 \text{ mm hr}^{-1}$, $K = 0.12, L = 35 \text{ km}$ |
| Inverse distance | Flatness constraint | 1.560 (0.138) | 2.841 (1.960) | 20.242 (17.272) | $R_0 = 7.5 \text{ mm hr}^{-1}$, $K = 0.17, L = 65 \text{ km}$ |
| | Zero rainfall at large distance | 1.560 (0.137) | 2.840 (1.953) | 20.238 (17.267) | $R_0 = 7.5 \text{ mm hr}^{-1}$, $K = 0.1, L = 55 \text{ km}$ |
| Raw 1km radar | | 1.420 (-0.046) | 2.765 (0.919) | 11.536 (7.333) | |
| Zero parameter raingauge surface (Euclidean distance) | | 1.680 (0.064) | 2.952 (1.737) | 19.203 (15.971) | No rainfall rate transformation, $K = 0 \text{ km}$ |

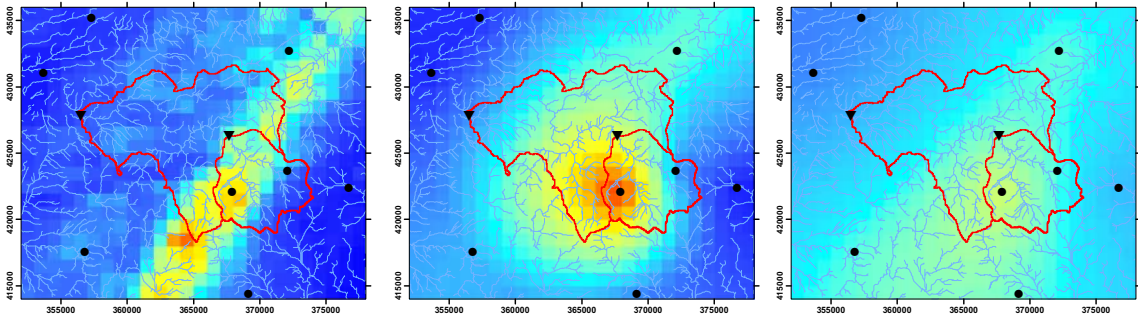
estimating the rainfall at the raingauge location by fitting a surface. This difference is highly relevant for the heavy rainfall case. However, the comparison is still informative and shows the raingauge-only estimator is only slightly worse than radar for medium rain but is considerably worse, as expected, for heavy rainfall.

Visualising the raingauge-only surface using the optimal parameters for the Euclidean distance ($R_0 = 7.5 \text{ mm hr}^{-1}$ and $K = 18 \text{ km}$) revealed good qualitative and reasonable quantitative agreement with the 1 km raw radar data for stratiform rainfall events. However, this agreement deteriorated significantly for spatially-localised convective events because the raingauge-only surface underestimated the peak intensities and the spatial extent was overestimated. A typical example, during the convective event of 14 June 2002, is given in Figure 6.2. The right hand column is the raingauge-only surface derived using the optimal parameters and the left hand column is the corresponding 1km radar accumulations; note the significantly lower scale used for the raingauge-only surface. The poor performance of the raingauge-only surface is due to the

(a) 16:00



(b) 16:15



(c) 16:30

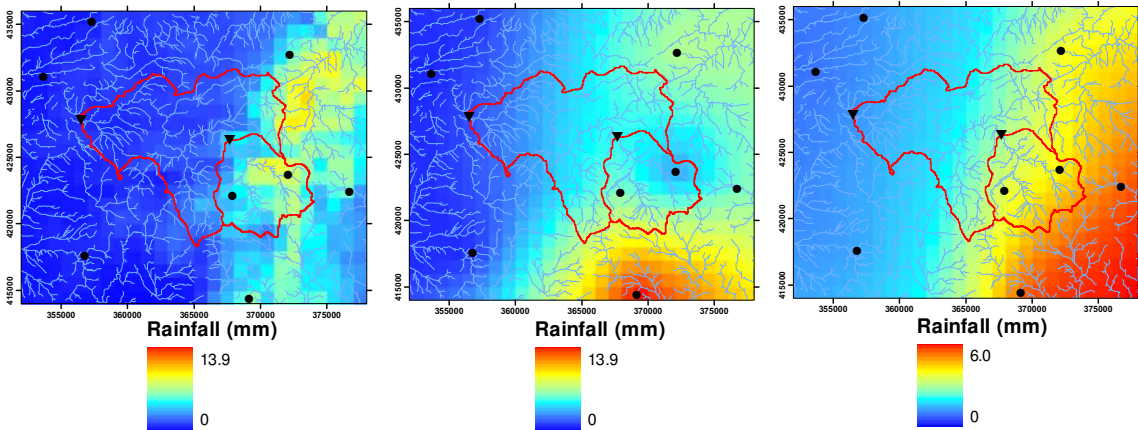


Figure 6.2 15 minute rainfall accumulations derived using different rainfall estimators for the convective storm affecting the River Darwen on 14 June 2002. Left column: raw 1km radar. Middle column: raingauge-only estimator using the Euclidean distance measure with a zero offset parameter ($K=0$ km) and no rainfall rate transformation. Right column: optimised raingauge-only estimator using the Euclidean distance measure with an offset parameter of $K=18$ km and a rainfall rate transformation with $R_0=7.5$ mm hr⁻¹. Circles denote raingauges and triangles denote gauging stations. Note that the right hand column uses a significantly smaller intensity scale.

optimal parameters selected. In particular, the offset parameter of $K=18$ km has the effect of smoothing the surface and lowering/raising the maximum/minimum of the fitted surface relative to the maximum/minimum raingauge totals. This effect is evident in Figure 6.2.

The visual analysis raised the question: 'Is it possible to improve the raingauge-only surface for convective events without a significant adverse impact on the stratiform events?'. Since the optimised parameters yielded an unsatisfactory performance over convective storms, a surface that had no incidental parameters was used, namely the Euclidean distance measure with a zero offset parameter, $K=0$ km, and with no rainfall transformation (i.e. no need for the incidental parameter R_0). A zero offset parameter ensures that the fitted surface attains the maximum totals observed by the raingauge network, hopefully improving performance over convective events. The rmse results for this 'zero parameter' surface are given in the final row of Table 6.1 and show that the performance over heavy rainfall is improved (bearing in mind the earlier comments about 'selective deletion') relative to the optimal parameter surfaces by around 5% whilst performance over the other categories is worsened by between 4 and 8%. Visual comparison of the 'zero parameter' surface ($K=0$ km, no R_0) with the optimised Euclidean surface ($R_0=7.5$ mm hr⁻¹, $K=18$ km) revealed only small differences for stratiform events but large improvements for convective events. The earlier example given in Figure 6.2 clearly shows the significant improvement of the 'zero parameter' raingauge surface (middle column), relative to the optimised Euclidean raingauge surface (right hand column), at capturing the spatial extent (given by 1km raw radar data, left hand column) and magnitude of convective events.

In conclusion the significant performance improvement of the 'zero parameter' surface over convective rainfall events outweighs the slight loss in performance over stratiform rainfall events. This highlights that rmse statistics should not be used alone in determining the best raingauge-only surface but should be used in conjunction with visual inspection of the generated surfaces.

Gauge-adjustment of radar

Firstly the long-term bias of the radar was calculated to be approximately 1.2, using the methodology presented in 6.1.3. The results for the 11 month period studied are presented in Table 6.2 along with bias statistics on a month-by-month basis. The monthly statistics show no obvious seasonality in bias but do show some variability. The 11 month period biases for each gauge are closely correlated with elevation: the three highest raingauges - Darwen Sunnyhurst, Springs and Pickup Bank - have noticeably higher bias statistics whilst the three lowest gauges - Moor Park, Common Bank and Houghton Reservoir - show considerably less bias.

The rmse statistics for the 1km raw radar and the static gauge-adjustment (using a bias of 1.2) are given in Table 6.3. This shows that the static gauge-adjustment makes some improvement for the heavy rainfall category (by 7%) but worsens the medium rainfall category (by 12%). This is in keeping with the results found by Wood *et al.* (2000) for the Brue catchment, although they

Table 6.2 Long-term bias statistics for each raingauge location (final column, second table): River Darwen case study. Bias statistics for individual months are also given.

| Raingauge | Bias <i>Number of observations</i> | | | | | | | | | | | |
|---------------------|------------------------------------|----|--------|-----|--------|----|--------|----|--------|-----|----------|--|
| | Jan 02 | | Feb 02 | | Mar 02 | | Apr 02 | | May 02 | | Jun 02 | |
| Haighton Reservoir | 1.040 | 83 | 1.042 | 113 | N/A | | 0.791 | 53 | 0.982 | 50 | 1.114 63 | |
| Great Harwood | 1.198 | 90 | 1.052 | 256 | 0.935 | 43 | 0.819 | 52 | 1.000 | 101 | 1.171 48 | |
| Pickup Bank | 1.335 | 98 | 1.163 | 237 | 1.016 | 40 | 1.062 | 68 | 1.143 | 142 | 1.608 47 | |
| Darwen Sunnyhurst | 1.349 | 93 | 1.287 | 214 | 1.352 | 36 | 1.216 | 76 | 1.202 | 140 | 1.398 57 | |
| Holden Wood | 1.279 | 95 | 1.250 | 257 | 0.986 | 56 | 1.094 | 87 | 1.128 | 134 | 1.181 61 | |
| Common Bank | 0.963 | 55 | 1.254 | 194 | 1.254 | 8 | 1.119 | 65 | 1.031 | 11 | 1.190 51 | |
| Springs | 1.238 | 63 | 1.391 | 229 | 1.655 | 5 | 1.016 | 84 | 1.235 | 68 | 1.840 67 | |
| Moor Park | 1.163 | 59 | 1.204 | 202 | 1.093 | 25 | 0.856 | 48 | 1.035 | 98 | 1.163 46 | |
| Average over gauges | 1.196 | | 1.204 | | 1.184 | | 0.997 | | 1.095 | | 1.333 | |

| Raingauge | Bias <i>Number of observations</i> | | | | | | | | | | | |
|---------------------|------------------------------------|-----|--------|----|--------|----|--------|-----|--------|-----|---------------|-------------|
| | Jul 02 | | Aug 02 | | Sep 02 | | Oct 02 | | Nov 02 | | Jan 02-Nov 02 | |
| Haighton Reservoir | 1.122 | 74 | 1.372 | 95 | 1.386 | 40 | 0.937 | 140 | 1.169 | 114 | 1.088 | 825 |
| Great Harwood | 1.149 | 107 | 1.412 | 90 | 1.219 | 38 | 1.057 | 149 | 1.172 | 117 | 1.107 | 1091 |
| Pickup Bank | 1.953 | 17 | N/A | | 1.374 | 16 | 1.248 | 95 | 1.301 | 108 | 1.234 | 868 |
| Darwen Sunnyhurst | 1.308 | 92 | 1.753 | 71 | 1.368 | 41 | 1.115 | 150 | 1.461 | 122 | 1.315 | 1092 |
| Holden Wood | 1.251 | 95 | 1.501 | 71 | 1.509 | 29 | 0.973 | 172 | 1.237 | 135 | 1.191 | 1192 |
| Common Bank | 1.149 | 70 | 1.338 | 68 | 1.329 | 28 | 0.906 | 135 | 1.138 | 117 | 1.141 | 802 |
| Springs | 1.462 | 96 | 1.443 | 65 | 1.604 | 32 | 1.083 | 159 | 1.645 | 153 | 1.378 | 1021 |
| Moor Park | 1.373 | 77 | 1.455 | 71 | 0.946 | 36 | 0.744 | 86 | 1.359 | 114 | 1.157 | 862 |
| Average over gauges | 1.346 | | 1.468 | | 1.342 | | 1.008 | | 1.310 | | 1.201 | |

recorded a 40% improvement for the heavy rainfall for 2km resolution radar data and used a period of 30 months to derive the long-term bias.

Standard dynamic gauge-adjustment results are also presented in Table 6.3 and, as for the raingauge-only results, show little variation with differing surface type or distance measure. The optimal sets of incidental parameters were also arrived at in the same manner as those for the raingauge-only case. Encouragingly the results show a significant improvement over the raw radar estimates for all categories of rainfall with a 7% improvement for the heavy rain category and 13% for the rest. The standard dynamic gauge-adjustment results also outperform the static gauge-adjustment ones for all but the heavy rainfall category.

Finally the results of the dynamic gauge-adjustment *including* the mean bias are given in Table 6.3. As for the previous surface fitting results the effect of distance measure type appears to be negligible. These results, not surprisingly in light of the previous discussion, perform the best out of all estimators for the heavy rainfall case improving the rmse by 10%. This method also performs well for the medium rain and all rain $> 1 \text{ mm hr}^{-1}$ cases, with improvements in rmse of 7 and 8% respectively, but these are not as good as the standard dynamic gauge-adjustment results.

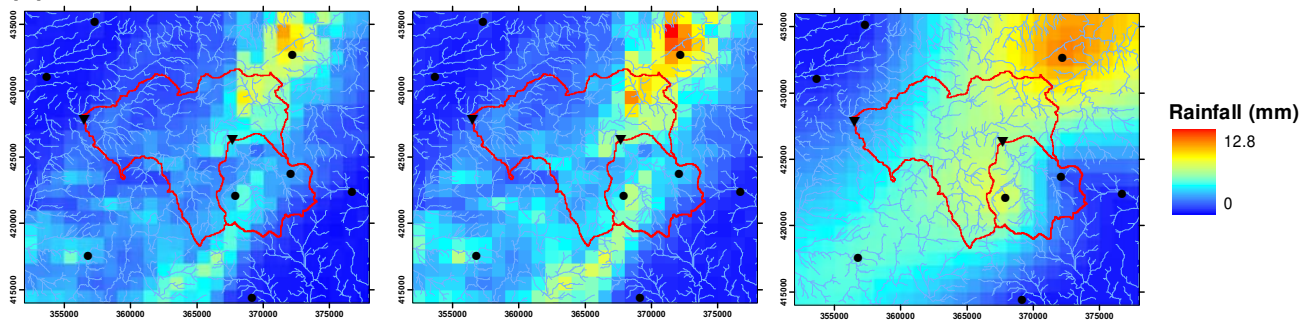
In conclusion the standard dynamic gauge-adjustment with a Euclidean distance measure has been selected as the method for deriving gauge-adjusted radar estimates for the Darwen case study since it provides good rmse improvements for all categories of rainfall. Visual comparison of the standard dynamic gauge-adjustment data 1km raw radar and raingauge-only estimators revealed that the standard dynamic gauge-adjustment method worked well for all types of rainfall. An example showing 15 minute accumulations for different rainfall estimators over a convective event is presented in Figure 6.3 and clearly shows the successful merging of raw radar data with raingauge data.

A subtle point worth mentioning is that the use of an offset parameter introduces a degree of smoothing to the fitted surface, resulting in the maximum/minimum values of the fitted surface being lower/larger than the maximum/minimum values of the individual points being fitted to. Although this effect had an undesirable consequence for the raingauge-only surfaces over convective events, as discussed earlier, it has desirable properties when fitting a calibration surface since calibration surfaces with large peaks or troughs can give very unrealistic gauge-adjusted surfaces.

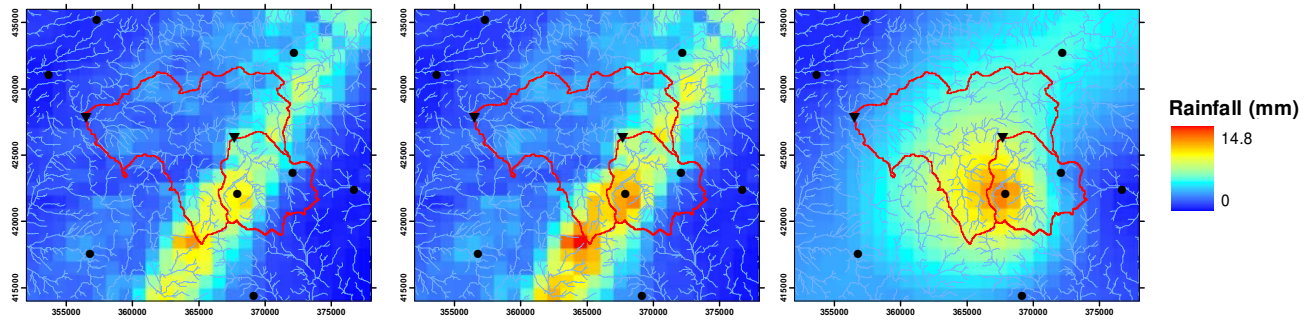
Table 6.3 Optimal parameter sets and rainfall estimation performance for gauge-adjusted radar rainfall estimation: River Darwen case study. The performance of the 1km raw radar is given for comparison.

| Distance Measure | Surface Type | RMSE | | | Incidental parameters |
|--|-----------------------------------|---------------------------------|--------------------------------------|------------------------------------|--|
| | | All rain >1 mm hr ⁻¹ | Medium rain 4-12 mm hr ⁻¹ | Heavy rain >12 mm hr ⁻¹ | |
| Static gauge-adjustment of radar ($\kappa=1.2$) | | | | | |
| N/A | N/A | 1.639 | 3.107 | 10.675 | N/A |
| Standard dynamic gauge-adjustment of radar ($\kappa=1$) | | | | | |
| Euclidean distance | Flatness constraint | 1.231 | 2.429 | 10.765 | $\varepsilon_g = 3 \text{ mm hr}^{-1}$, $\varepsilon_r = 3 \text{ mm hr}^{-1}$, $K = 60 \text{ km}$ |
| Exponential form of Euclidean distance | Flatness constraint | 1.231 | 2.427 | 10.757 | $\varepsilon_g = 3 \text{ mm hr}^{-1}$, $\varepsilon_r = 3 \text{ mm hr}^{-1}$, $K = 0.8, L = 40 \text{ km}$ |
| | Zero adjustment at large distance | 1.231 | 2.429 | 10.770 | $\varepsilon_g = 3 \text{ mm hr}^{-1}$, $\varepsilon_r = 3 \text{ mm hr}^{-1}$, $K = 0.15, L = 400 \text{ km}$ |
| Inverse distance | Flatness constraint | 1.229 | 2.425 | 10.769 | $\varepsilon_g = 3 \text{ mm hr}^{-1}$, $\varepsilon_r = 3 \text{ mm hr}^{-1}$, $K = 0.9, L = 30 \text{ km}$ |
| | Zero adjustment at large distance | 1.231 | 2.428 | 10.762 | $\varepsilon_g = 3 \text{ mm hr}^{-1}$, $\varepsilon_r = 3 \text{ mm hr}^{-1}$, $K = 0.1, L = 500 \text{ km}$ |
| Dynamic gauge-adjustment of radar including mean bias ($\kappa=1.2$) | | | | | |
| Exponential form of Euclidean distance | Zero adjustment at large distance | 1.311 | 2.567 | 10.347 | $\varepsilon_g = \varepsilon_r = 3 \text{ mm hr}^{-1}$, $K = 0.15$ $L = 400 \text{ km}$ |
| Inverse distance | Zero adjustment at large distance | 1.311 | 2.567 | 10.347 | $\varepsilon_g = \varepsilon_r = 3 \text{ mm hr}^{-1}$, $K = 0.1,$ $L = 500 \text{ km}$ |
| Raw 1km radar | | 1.420 | 2.765 | 11.536 | N/A |

(a) 16:00



(b) 16:15



(c) 16:30

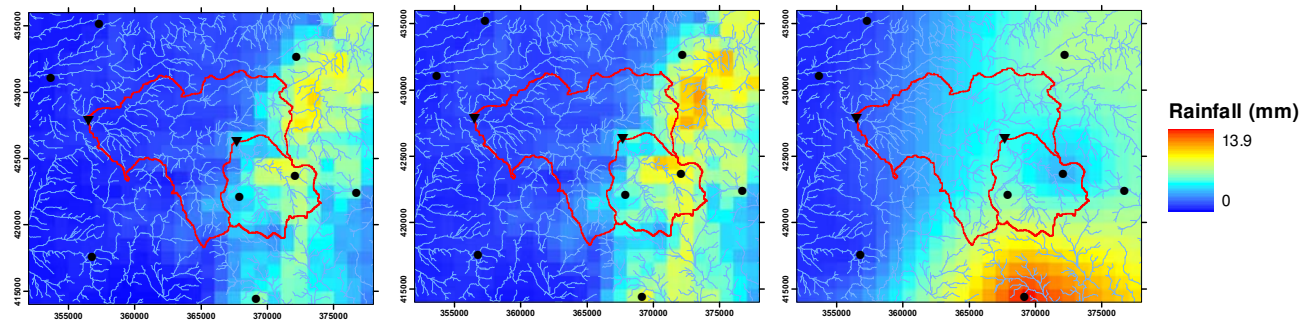


Figure 6.3 15 minute rainfall accumulations derived using different rainfall estimators for the convective storm affecting the River Darwen on 14 June 2002. Left column: raw 1km radar. Middle column: dynamically gauge-adjusted 1km radar using the optimised Euclidean distance. Right column: zero parameter raingauge-only estimator. Circles denote raingauges and triangles denote gauging stations.

6.3 The River Kent case study

For this case study the single site 2km raw and 2km Nimrod Quality Controlled (QC) data from the Hameldon Hill radar were used. Raingauge data were available from 1 January 2003 to 29 August 2004. Over this period the set of data considered, for the different rainfall estimating methods, was restricted to only include 15 minute intervals where both the 2km raw and QC products were available to allow meaningful comparisons. This resulted in 59511 observations for the all rain $> 1 \text{ mm hr}^{-1}$ category, 4678 for the medium rainfall category and 187 for the heavy rainfall category.

Raingauge-only rainfall estimation

The optimal incidental parameters were determined by the same parameter search approach outlined in Section 6.2. As in the Darwen case, the optimal rmse statistics of the raingauge-only rainfall estimation showed little dependence on surface type or distance measured used. Therefore only the results for the Euclidean distance are given in Table 6.4. The performance of the 2km raw and 2km Nimrod QC radar estimates are also given for comparison. The results for the Kent case study, contained in Table 6.4, show some similarities to the results for the Darwen case study (Table 6.1): such as the heavy rainfall being better estimated by the radar and the raingauge-only estimate generally underestimating the observed rainfall. However, there are also some key differences. For the River Kent case study the raingauge-only estimate performs better than either radar estimate during medium rainfall whilst for the all rain $> 1 \text{ mm hr}^{-1}$ category it performs better than the raw radar estimate but worse than the QC estimate.

Table 6.4 Optimal parameter sets and rainfall estimation performance for raingauge-only rainfall estimation: River Kent case study. The performance of the radar estimates and the zero parameter raingauge-only surface are given for comparison.

| Distance Measure | Surface Type | RMSE (ME) | | | Incidental parameters |
|--------------------|--|----------------------------------|---------------------------------------|-------------------------------------|--|
| | | All rain $>1 \text{ mm hr}^{-1}$ | Medium rain $4-12 \text{ mm hr}^{-1}$ | Heavy rain $>12 \text{ mm hr}^{-1}$ | |
| Euclidean distance | Flatness constraint | 1.307 (0.126) | 2.610 (1.656) | 16.867 (15.056) | $R_0=7.5 \text{ mm hr}^{-1}$, $K=10 \text{ km}$ |
| | Raw 2km radar | 1.579 (-0.091) | 3.871 (0.194) | 10.354 (4.999) | N/A |
| | 2km Nimrod QC radar | 1.197 (0.039) | 2.827 (0.906) | 11.126 (8.110) | N/A |
| | Zero parameter raingauge surface (Euclidean distance) | 1.402 (0.073) | 2.691 (1.477) | 16.053 (13.867) | No rainfall rate transformation, $K=0 \text{ km}$ |

The rmse performance of the 'zero parameter surface' which uses the Euclidean distance measure with a zero offset parameter and no rainfall rate transformation is given in the last row of Table 6.4. It shows an improvement in the heavy rainfall category of 5% whilst only worsening the all rain and medium rain categories by 7 and 3% respectively. Visual comparison of the zero parameter raingauge surface with the optimised raingauge-only surface showed improvements for convective type events with little change for the stratiform rainfall event. This is very similar to the Darwen case study. An example during an orographic rainfall event in early 2004 is presented in Figure 6.4. Comparing the zero parameter surface (the middle column) to the optimised parameter surface (the right hand column) reveals little difference, except for slightly less smoothing occurring for the zero parameter surface. It is the convective rainfall events where the improvements due to the zero parameter surface are most apparent, as indicated by the heavy rainfall rmse in Table 6.4. Once again the improved performance of the zero parameter surface over convective events outweighs the slight loss of performance over the stratiform events. Therefore, the zero parameter rainfall surface was selected as the raingauge-only estimator of rainfall. This is also consistent with the surface used for the Darwen case study and gives some confidence that the zero parameter surface could be applied successfully to other raingauge networks.

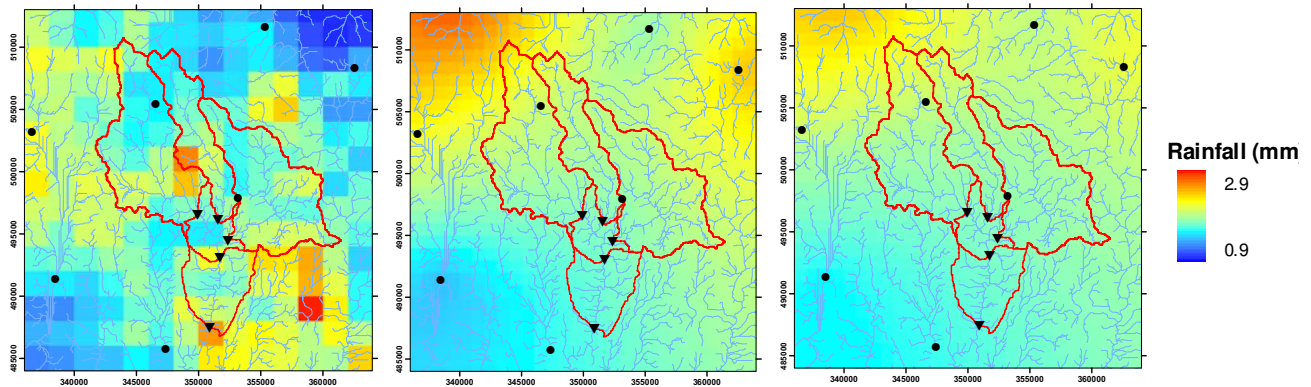
Gauge-adjustment of radar

The long-term bias of the 2km raw and 2km Nimrod QC radar estimates of rainfall over the 20 month case study were calculated using the methodology outlined in Section 6.2 and are presented in Table 6.5. There was no evidence of significant seasonality in the bias. However, there is still a general positive correlation with elevation which is more noticeable in the raw radar estimates.

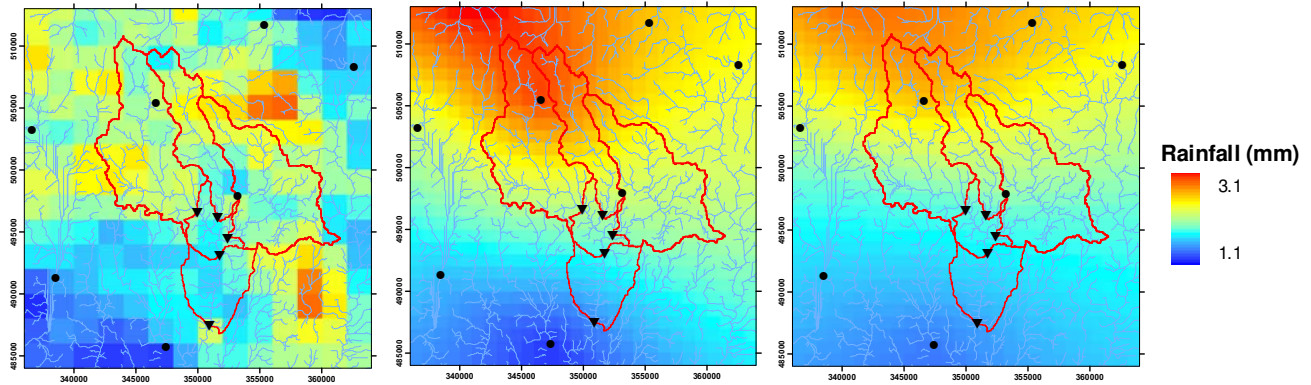
The results for the gauge-adjustment of radar are grouped by radar type: the 2km raw radar results are presented in Table 6.6 and the 2km Nimrod QC radar results are presented in Table 6.7. Applying the appropriate long-term bias factor to either radar estimate caused a general decrease in the performance and only improved the heavy rainfall rmse statistic for the 2km Nimrod QC case (by 5%).

Standard dynamic gauge-adjustment results are also presented in Table 6.6 and Table 6.7. Again, the optimal rmse statistics showed little variation with surface type or distance measure and therefore only a selection are presented in the results. Table 6.6 shows that the standard dynamic gauge-adjustment of raw radar makes a significant improvement to the rmse statistics for the all rain $> 1 \text{ mm hr}^{-1}$ category (30%) and the medium rainfall category (35%) and a modest improvement of 1% for the heavy rainfall category. This pattern of improvement is also evident in the standard dynamic gauge-adjustment of 2km Nimrod QC radar results presented in Table 6.7. The improvement in the 2km Nimrod QC is not as dramatic since the initial estimate of the Nimrod QC radar is significantly better than that of the raw estimate.

(a) 07:00



(b) 07:15



(c) 07:30

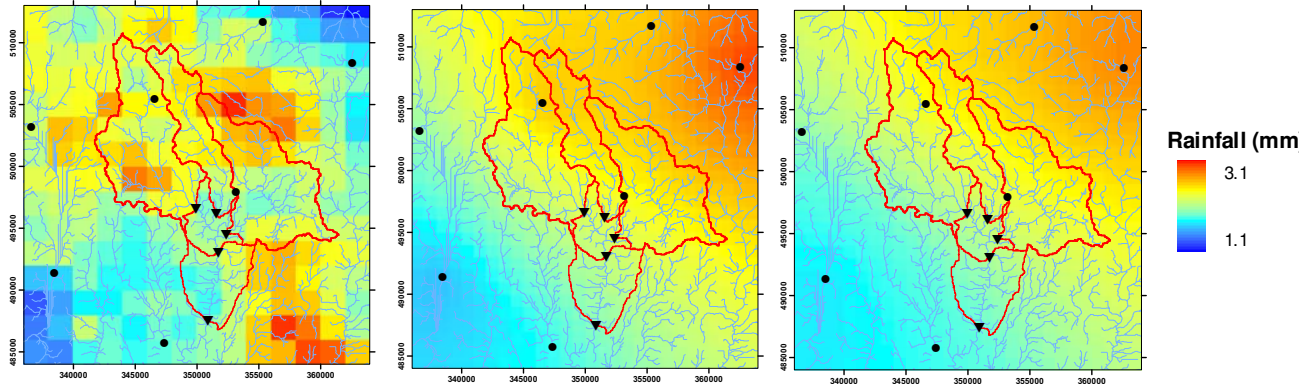


Figure 6.4 15 minute rainfall accumulations derived using different rainfall estimators for the orographic storm affecting the River Kent on 3 February 2004. Left column: raw Nimrod 2km QC radar. Middle column: raingauge-only estimator using the Euclidean distance measure with a zero offset parameter ($K=0$ km) and no rainfall rate transformation. Right column: optimised raingauge-only estimator using the Euclidean distance measure with an offset parameter of $K=10$ km and a rainfall rate transformation with $R_0=7.5$ mm hr⁻¹. Circles denote raingauges and triangles denote gauging stations

Table 6.5 Long-term bias statistics of 2km raw and 2km Nimrod QC radar data for each raingauge location: River Kent case study. Raingauge elevations are also listed.

| Raingauge | Elevation (m) | Bias for Jan 2003 – Aug 2004 <i>Number of observations</i> | | | |
|---------------|---------------|---|------|---------------|------|
| | | 2km raw | | 2km Nimrod QC | |
| Levens | 4 | 0.942 | 1526 | 1.148 | 1488 |
| Tower Wood | 46 | 1.066 | 1722 | 1.247 | 1770 |
| Brathay Hall | 51 | 1.138 | 1937 | 1.157 | 2223 |
| Watchgate | 196 | 1.038 | 1631 | 1.168 | 1714 |
| Fisher Tarn | 224 | 0.968 | 1559 | 1.151 | 1566 |
| Brotherswater | 230 | 1.400 | 1944 | 1.391 | 2251 |
| Orton | 238 | 1.361 | 1214 | 1.432 | 1341 |
| Kentmere | 266 | 1.165 | 1977 | 1.248 | 2168 |
| Wet Sleddale | 271 | 1.223 | 1748 | 1.325 | 1847 |
| Gauge average | | 1.144 | | 1.252 | |

Table 6.6 Optimal parameter sets and rainfall estimation performance for gauge-adjusted 2km raw radar rainfall estimation: River Kent case study. The performance of the unadjusted 2km raw radar is given for comparison.

| Distance Measure | Surface Type | RMSE | | | Incidental parameters |
|---|-----------------------------------|------------------------------------|---|---------------------------------------|--|
| | | All rain >1 mm hr ⁻¹ | Medium rain 4-12 mm hr ⁻¹ | Heavy rain >12 mm hr ⁻¹ | |
| Static gauge-adjustment of 2km raw radar ($\kappa=1.14$) | | | | | |
| N/A | N/A | 1.824 | 4.489 | 10.598 | N/A |
| Standard dynamic gauge-adjustment of 2km raw radar ($\kappa=1$) | | | | | |
| Euclidean distance | Flatness constraint | 1.103 | 2.504 | 10.262 | $\varepsilon_g=3$ mm hr ⁻¹ , $\varepsilon_r=3$ mm hr ⁻¹ , $K=25$ km |
| Exponential form of Euclidean distance | Zero adjustment at large distance | 1.106 | 2.520 | 10.217 | $\varepsilon_g=4$ mm hr ⁻¹ , $\varepsilon_r=4$ mm hr ⁻¹ , $K=0.15$ $L=120$ km |
| Dynamic gauge-adjustment of raw 2km radar including mean bias ($\kappa=1.14$) | | | | | |
| Exponential form of Euclidean distance | Zero adjustment at large distance | 1.169 | 2.666 | 10.269 | $\varepsilon_g=\varepsilon_r=3$ mm hr ⁻¹ , $K=0.15$ $L=400$ km |
| Raw 2km radar | | 1.579 | 3.871 | 10.354 | N/A |

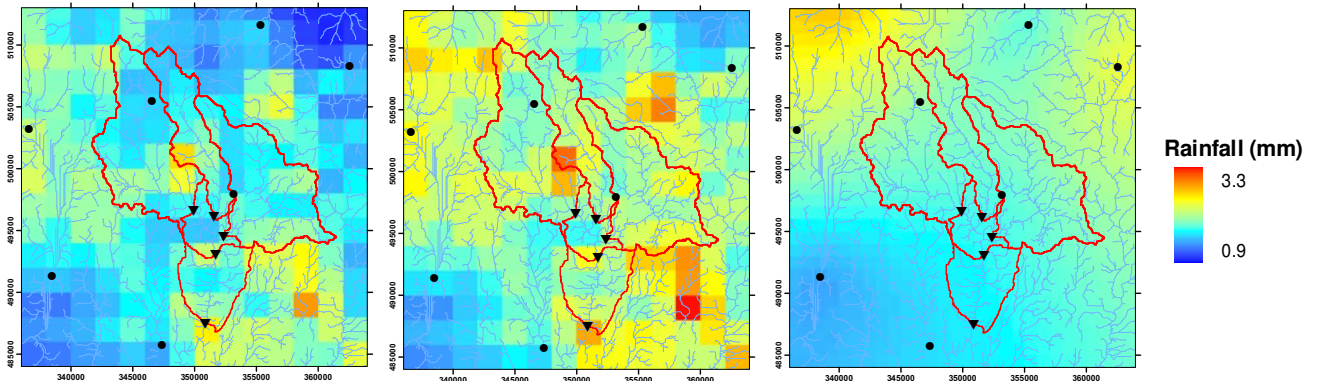
Table 6.7 Optimal parameter sets and rainfall estimation performance for gauge-adjusted 2km Nimrod QC radar rainfall estimation: River Kent case study. The performance of the unadjusted 2km Nimrod QC radar is given for comparison.

| Distance Measure | Surface Type | RMSE | | | Incidental parameters |
|--|-----------------------------------|------------------------------------|---|--|--|
| | | All rain >1 mm hr ⁻¹ | Medium rain 4-12 mm hr ⁻¹ | Heavy rain >12 mm hr ⁻¹ | |
| Static gauge adjustment of 2km Nimrod QC radar ($\kappa=1.25$) | | | | | |
| N/A | N/A | 1.416 | 3.291 | 10.545 | N/A |
| Standard dynamic gauge-adjustment of 2km Nimrod QC radar ($\kappa=1$) | | | | | |
| Euclidean distance | Flatness constraint | 1.026 | 2.340 | 10.788 | $\varepsilon_g = 4 \text{ mm hr}^{-1}$, $\varepsilon_r = 4 \text{ mm hr}^{-1}$, $K = 40 \text{ km}$ |
| Exponential form of Euclidean distance | Zero adjustment at large distance | 1.023 | 2.354 | 10.766 | $\varepsilon_g = 4 \text{ mm hr}^{-1}$, $\varepsilon_r = 4 \text{ mm hr}^{-1}$, $K = 0.6, L = 60 \text{ km}$ |
| Dynamic gauge-adjustment of 2km Nimrod QC radar <i>including</i> mean bias ($\kappa=1.25$) | | | | | |
| Exponential form of Euclidean distance | Zero adjustment at large distance | 1.079 | 2.473 | 10.511 | $\varepsilon_g = \varepsilon_r = 3 \text{ mm hr}^{-1}$, $K = 0.6, L = 70 \text{ km}$ |
| 2km Nimrod QC radar | | 1.197 | 2.827 | 11.126 | N/A |

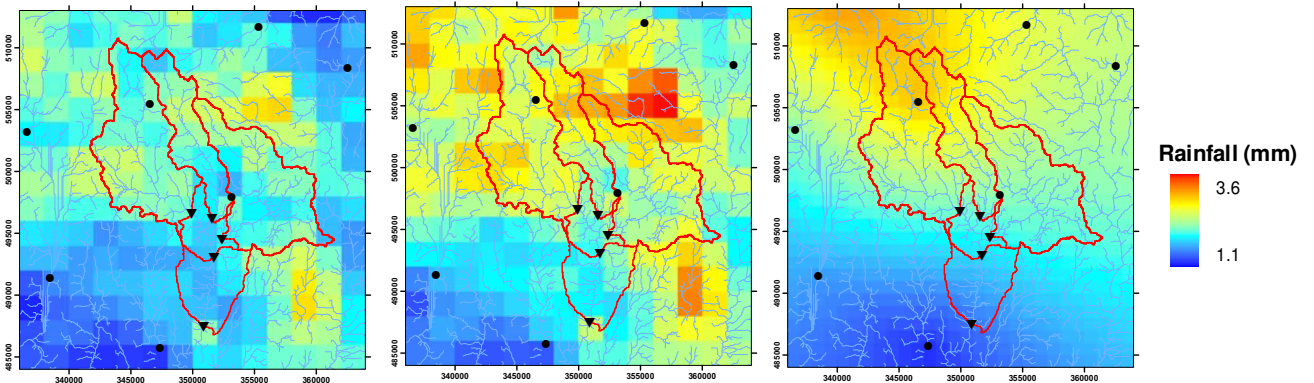
The results for the dynamic gauge-adjustment *including* the mean bias factor are presented in Table 6.6 and Table 6.7 as well. These show an improvement on the initial radar estimate for both 2km raw and 2km Nimrod QC radar cases but, generally, the standard dynamic gauge-adjustment performs best. This is consistent with the Darwen case study results for 1km raw radar.

Overall the best performing gauge-adjusted radar estimate is the standard dynamic adjustment of 2km Nimrod QC radar and the Euclidean distance measure has been selected as the method for deriving gauge-adjusted radar estimates for the Kent case study. This provides good rmse improvements for all categories of rainfall. Visual examination of the standard dynamic gauge-adjustment with a Euclidean distance and comparison with the Nimrod 2km QC radar and raingauge-only estimators revealed that the standard dynamic gauge-adjustment method worked well for all types of rainfall. An example showing 15 minute accumulations for different rainfall estimators over an orographic event is presented in Figure 6.5. The left hand column shows Nimrod 2km QC radar, the middle column shows the optimised standard dynamic gauge-adjustment using a Euclidean distance and the right hand column shows the zero parameter raingauge-only surface. The example, together with the accuracy assessment in Table 6.7, clearly shows the successful merging of the radar and raingauge data.

(a) 07:00



(b) 07:15



(c) 07:30

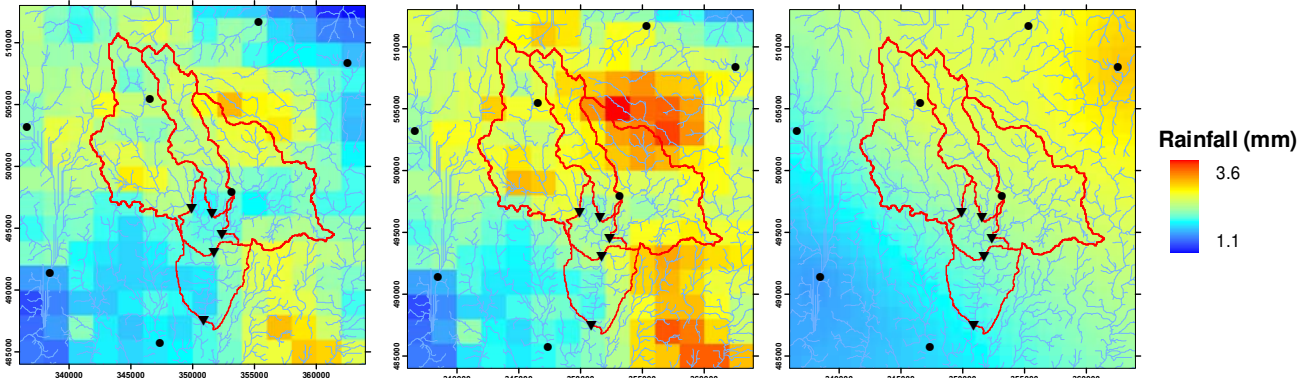


Figure 6.5 15 minute rainfall accumulations derived using different rainfall estimators for the orographic storm affecting the River Kent on 3 February 2004. Left column: Nimrod 2km QC radar. Middle column: dynamically gauge-adjusted 2km QC radar using the optimised Euclidean distance. Right column: zero parameter raingauge-only estimator using the Euclidean distance measure with an offset parameter of $K = 0$ km and no rainfall rate transformation. Circles denote raingauges and triangles denote gauging stations. The scales used for each time period are given.

6.4 The Upper Thames case study

For this case study the single site 2km and 5km raw data from the Chenies radar were used. Since the study catchments were not entirely contained within the 2km range of the Chenies radar a composite using 2km and 5km radar data was used. This study covered the twelve month period from 1 September 1997 to 31 August 1998, encompassing the Easter 1998 flood. Over this period the set of data considered, for the different rainfall estimating methods, was restricted to only include 15 minute intervals where both the 2km and 5km raw products were available to allow meaningful comparisons. However, since the 5km data are available for longer ranges than the 2km data, they cover more raingauge locations and therefore, for the 5km data, more raingauge observations were available. For this study there were data available from 12 raingauge locations for the 2km data and from 23 for the 5km data. This resulted in 32132 (96223) observations for the all rain $> 1 \text{ mm hr}^{-1}$ category, 1103 (2589) for the medium rainfall category and 57 (107) for the heavy rainfall category for the 2 km (5 km) data. There are relatively fewer observations for each category for raingauges in the Thames Region compared to those in the North West region used for the Kent and Darwen studies. This is explained by the lower long-term average (1961-1990) rainfalls experienced in the Thames Region (668 mm) relative to the North West Region (1201 mm). Note that for this study period the Stokenchurch raingauge was not operational and that the data from the Byfield raingauge are not included as its location is affected by a beam blockage. There was not scope within the project to investigate infilling of the beam blockage.

Raingauge-only rainfall estimation

The optimal incidental parameters were determined by the same parameter search approach outlined in Section 6.2. As in the previous case studies, the optimal rmse statistics of the raingauge-only rainfall estimation showed little dependence on surface type or distance measure used. Therefore only the results for the Euclidean distance are given in Table 6.8. This can be directly compared to the performance of the 5km raw radar estimate as the same network of raingauges is covered. The performance of the 2km raw radar estimates are also given for comparison, although this is not strictly a like-for-like comparison as a smaller network of raingauges is covered by the 2km data.

When considering only the raingauge and 5km raw radar results the Upper Thames case study shows, as in the other case studies, that the heavy rainfall rmse statistics are better for the raw radar estimate but the earlier comments relating to 'selective deletion' (Section 6.2) should be borne in mind. In fact, for the Upper Thames case study, the results in Table 6.8 show that the fitted raingauge surface rmse statistics outperform those for the 5km raw data for all rainfall categories. This result differs from the earlier case studies and is mainly due to the larger resolution radar data (5km rather than 2km) being used and that the region is located at a longer range from the radar.

Table 6.8 Optimal parameter sets and rainfall estimation performance for raingauge-only rainfall estimation: Upper Thames and Stour case study. The performance of the radar estimates is given for comparison.

| Distance Measure | Surface Type | RMSE (ME) | | | Incidental parameters |
|--------------------|----------------------|---------------------------------|--------------------------------------|------------------------------------|--|
| | | All rain >1 mm hr ⁻¹ | Medium rain 4-12 mm hr ⁻¹ | Heavy rain >12 mm hr ⁻¹ | |
| Euclidean distance | Flatness constraint | 0.856 (0.068) | 3.166 (0.856) | 18.062 (15.872) | $R_0=8.5$ mm hr ⁻¹ , $K=12.5$ km |
| | Raw 2km radar | 1.555 (-0.045) | 4.264 (2.007) | 16.281 (13.811) | N/A |
| | Raw 5km radar | 1.161 (-0.033) | 3.699 (1.512) | 16.886 (14.402) | N/A |

Gauge-adjustment of radar

The long-term bias of the 2km and 5km raw radar estimates of rainfall over the 12 month case study were calculated using the methodology outlined in Section 6.1.3 and are presented in Table 6.9. Again, like the earlier case studies, there was no strong evidence of seasonality in the bias. The mean bias for raingauges within both the 2km and 5km range show a close agreement for most cases and the overall mean bias of both types of data are remarkably similar. There is no apparent correlation between elevation and bias.

The results for the gauge-adjustment of radar are grouped by radar type: the 2km raw radar results are presented in Table 6.10 and the 5km raw radar results are presented in Table 6.11. Applying the appropriate long-term bias factor to either radar estimate (static gauge-adjustment) caused a general decrease in performance. The only marginal improvement (2-4%) was for the heavy rainfall rmse statistics.

The optimal rmse statistics for the standard dynamic gauge-adjustment results show little variation with surface type or distance measure used, so only a selection are given in Table 6.10 for the 2km raw radar and Table 6.11 for the 5km raw radar. The results show that dynamic gauge-adjustment has a significant positive impact on the rmse performance for both 2 and 5km raw radar. In particular the rmse statistics for the all rain > 1 mm hr⁻¹ and the medium rainfall categories are drastically improved by between 18 and 23%. The heavy rainfall rmse statistics are also improved but to a lesser degree: 7% for the 2km raw radar and 5% for the 5km raw radar.

The results for the dynamic gauge-adjustment *including* the mean bias factor are also presented in Table 6.10 for the 2km raw radar and Table 6.11 for the 5km raw radar. These show an improvement over the raw radar estimates, especially for the heavy rainfall category (7-9%). However, the overall

Table 6.9 Long-term bias statistics of 2km and 5km raw radar data for each raingauge location for the Upper Thames and Stour case study. Raingauge elevations are also listed.

| Raingauge | Elevation (m) | Bias for Sep 1997 – Aug 1998 | | | |
|------------------|---------------|-------------------------------|-----|---------|-----|
| | | <i>Number of observations</i> | | | |
| | | 5km raw | | 2km raw | |
| Stratford | 42.3 | 1.315 | 432 | N/A | N/A |
| Benson | 42.6 | 1.289 | 275 | 1.289 | 284 |
| Wellesbourne | 43.6 | 1.177 | 539 | N/A | N/A |
| Cleeve | 44.7 | 1.497 | 302 | 1.427 | 294 |
| Abingdon | 50.0 | 1.408 | 288 | 1.255 | 257 |
| Osney | 54.6 | 1.287 | 327 | 1.231 | 337 |
| Eynsham | 60.0 | 1.252 | 364 | 1.353 | 331 |
| Wheatley | 60.2 | 1.363 | 360 | 1.325 | 352 |
| Bicester | 62.2 | 1.322 | 331 | 1.344 | 291 |
| Shipston | 64.5 | 1.285 | 427 | N/A | N/A |
| Stanford | 69.5 | 1.291 | 337 | 1.263 | 298 |
| St Johns | 71.4 | 1.311 | 366 | N/A | N/A |
| Grimsbury | 91.8 | 1.143 | 303 | 1.122 | 297 |
| Shorncote | 93.4 | 1.179 | 407 | N/A | N/A |
| Rodbourne | 93.7 | 1.353 | 389 | N/A | N/A |
| Worsham | 110.0 | 1.354 | 420 | 1.343 | 398 |
| Chipping Campden | 122.7 | 1.476 | 447 | N/A | N/A |
| Bourton | 128.5 | 1.232 | 460 | N/A | N/A |
| Chipping Norton | 138.2 | 1.260 | 436 | N/A | N/A |
| West Ilsley | 149.7 | 1.360 | 268 | 1.337 | 280 |
| Maddle Farm | 152.7 | 1.296 | 301 | 1.182 | 288 |
| Langley | 170.0 | 1.192 | 453 | N/A | N/A |
| Rapsgate | 240.0 | 1.349 | 456 | N/A | N/A |
| Gauge average | | 1.304 | | 1.289 | |

Table 6.10 Optimal parameter sets and rainfall estimation performance for gauge-adjusted 2km raw radar rainfall estimation: Upper Thames and Stour case study. The performance of the unadjusted 2km raw radar is given for comparison.

| Distance Measure | Surface Type | RMSE | | | Incidental parameters |
|--|-----------------------------------|------------------------------------|---|--|---|
| | | All rain >1 mm hr ⁻¹ | Medium rain 4-12 mm hr ⁻¹ | Heavy rain >12 mm hr ⁻¹ | |
| Static gauge-adjustment of 2km raw radar ($\kappa=1.29$) | | | | | |
| N/A | N/A | 1.931 | 4.883 | 15.902 | N/A |
| Standard dynamic gauge-adjustment of 2km raw radar ($\kappa=1$) | | | | | |
| Euclidean distance | Flatness constraint | 1.191 | 3.473 | 15.039 | $\varepsilon_g=5$ mm hr ⁻¹ , $\varepsilon_r=6$ mm hr ⁻¹ , $K=38$ km |
| Exponential form of Euclidean distance | Zero adjustment at large distance | 1.193 | 3.440 | 15.042 | $\varepsilon_g=5$ mm hr ⁻¹ , $\varepsilon_r=6$ mm hr ⁻¹ , $K=0.2$ $L=140$ km |
| Dynamic gauge-adjustment of 2km raw radar <i>including</i> mean bias ($\kappa=1.29$) | | | | | |
| Exponential form of Euclidean distance | Zero adjustment at large distance | 1.416 | 3.717 | 14.882 | $\varepsilon_g = \varepsilon_r = 6$ mm hr ⁻¹ , $K=0.1$ $L=120$ km |
| Raw 2km radar | | 1.555 | 4.264 | 16.281 | N/A |

improvements are not as significant as those for the standard dynamic gauge-adjustment.

The pattern of qualitative changes to the rmse statistics, depending on the method of gauge-adjustment used, is consistent across the 2km and 5km raw radar and with the previous case studies. The standard dynamic gauge-adjustment using a Euclidean distance measure has been selected as the method for deriving gauge-adjusted radar estimates for the Upper Thames case study since it provides good rmse improvements for all categories of rainfall. The 2km and 5km raw radar data will be dynamically adjusted separately and then merged to form the final rainfall estimate. The merging process simply uses the 5km data where 2km data is not available (i.e. at long distances from the radar location).

Table 6.11 Optimal parameter sets and rainfall estimation performance for gauge-adjusted 5km raw radar rainfall estimation: Upper Thames and Stour case study. The performance of the unadjusted 5km raw radar is given for comparison.

| Distance Measure | Surface Type | RMSE | | | Incidental parameters |
|---|-----------------------------------|---------------------------------|--------------------------------------|------------------------------------|--|
| | | All rain >1 mm hr ⁻¹ | Medium rain 4-12 mm hr ⁻¹ | Heavy rain >12 mm hr ⁻¹ | |
| Static gauge-adjustment of 5km raw radar ($\kappa=1.30$) | | | | | |
| N/A | N/A | 1.449 | 4.307 | 16.284 | N/A |
| Standard dynamic gauge-adjustment of 2km raw radar ($\kappa=1$) | | | | | |
| Euclidean distance | Flatness constraint | 0.916 | 2.947 | 16.037 | $\varepsilon_g = 4 \text{ mm hr}^{-1}$, $\varepsilon_r = 4 \text{ mm hr}^{-1}$, $K = 22 \text{ km}$ |
| Exponential form of Euclidean distance | Zero adjustment at large distance | 0.916 | 2.934 | 16.046 | $\varepsilon_g = 4 \text{ mm hr}^{-1}$, $\varepsilon_r = 4 \text{ mm hr}^{-1}$, $K = 0.15$ $L = 100 \text{ km}$ |
| Dynamic gauge-adjustment of 5km raw radar including mean bias ($\kappa=1.30$) | | | | | |
| Exponential form of Euclidean distance | Zero adjustment at large distance | 0.992 | 3.046 | 15.682 | $\varepsilon_g = \varepsilon_r = 3 \text{ mm hr}^{-1}$, $K = 0.1$ $L = 100 \text{ km}$ |
| Raw 5km radar | | 1.161 | 3.699 | 16.886 | N/A |

6.5 Conclusions

The objective of this section has been to derive the best methods for forming the raingauge-only surface and raingauge-adjusted radar data. The objective has not been to determine which spatial rainfall estimator performs best as the different rainfall estimators cannot be compared objectively, via rmse statistics, in a consistent manner. This is because the raingauge locations used for calculating the rmse statistics are systematically ignored by the surface fitting techniques due to 'selective deletion', whereas the estimates using radar data actually *sample* the rainfall at these locations. Ultimately the best spatial rainfall estimator, from a hydrological perspective, will be addressed through rainfall-runoff modelling in the next Section.

The following conclusions have been grouped by rainfall estimator.

Raingauge-only rainfall surface

- Once incidental parameters had been optimised for each case study, there was little difference between the rmse performance for the various distance measures used.
- All raingauge surfaces using optimised incidental parameters showed poor performance over spatially localised convective events, both in rmse statistics and by visual inspection. This is primarily due to the non-zero offset parameters smoothing the fitted surface and lowering/raising the maximum/minimum of the surface relative to the maximum/minimum of the raingauge totals.
- A 'zero parameter' raingauge-only surface, using the Euclidean distance measure with no offset parameter ($K=0\text{km}$) and no rainfall transformation, gave much improved performance over convective events and only slight loss over the stratiform rainfall events when compared to the optimised surfaces. The 'zero parameter' raingauge surface has been used for all case studies and is recommended for use over other raingauge networks where spatial rainfall estimators are needed.

Gauge-adjustment of rainfall radar data

- Standard dynamic gauge-adjustment of radar using optimised incidental parameters and applied at 15 minute intervals gave best results. Encouragingly it provided improved rmse statistics, compared to the unadjusted radar data, for all rainfall types and all case studies. Again there was little dependence on the type of distance measure used; the Euclidean has been used for all case studies.
- There is no obvious link between optimal incidental parameters and radar data type (e.g. 1km raw 2km Nimrod QC) and/or case study catchment. Therefore, incidental parameters have to be derived on a case study region-by-region basis.
- The improvements offered by standard dynamic gauge-adjustment of radar are more pronounced for the raw radar data products compared to the Nimrod QC product as would be expected.

7 Flood response modelling using case study storms

7.1 Introduction

This section focuses on the performance of the rainfall-runoff models over the case study extreme events, using historical rainfall and flow data. A split sample methodology has been used where distinct *calibration* and *evaluation* events are identified. Calibration events, capturing different seasons and rainfall types that produce a range of river flows, have been selected from the data provided by the Environment Agency. These are used to calibrate the models by achieving a ‘best fit’ between simulated flows and observed records. Evaluation events consist of the case study extreme events. These are used to evaluate model performance and robustness over an event previously unseen during the calibration process. The split sample methodology is commonly used within the Environment Agency for calibrating and testing models. Here the methodology recreates the common operational scenario where calibrated models are exposed to events more extreme than those contained in the historical record and therefore provides a realistic test of model robustness.

The calibration process and performance methodology is explained in more detail in Section 7.2. Model results over calibration and evaluation events are given for each case study in Sections 7.3 to 7.5. The case studies also use different spatial rainfall estimators and provide a hydrological test for assessing which rainfall estimator performs best. Whilst the performance over the calibration events is not of primary interest, it is still important to report as it puts the performance over evaluation events into context. The assessment process identifies model failure as and when it occurs (see Method 2 of Section 4.7.3) and attempts to rectify any shortcomings where appropriate. This has identified difficulties in modelling lowland catchments (Upper Thames and Stour case study) where soil/geology provide the primary control on flood response and topographic controls are secondary. This has led to developing a prototype area-wide distributed model, as an extended variant of the Grid-to-Grid model. Its formulation allows incorporation of soil/geology datasets with the aim of improving model robustness when applied over large, possibly heterogeneous, areas (Section 7.6). This model development is particularly relevant to understanding the genesis of lowland flooding, at a regional scale, resulting from extreme widespread frontal rainfall events. Finally some conclusions are set down in Section 7.7.

7.2 Model calibration and performance assessment methodology

The approach for calibrating models and assessing their performance is the same for each case study and is outlined in the following sections.

7.2.1 Model calibration

Data:

- Hydrometric data (raingauge and level/flow data) for each case study were received from the EA for periods of up to 5 years with the aim of limiting the amount of data processing required whilst retaining a long enough record to support model calibration.
- Calibration events, which aimed to capture different seasons and rainfall types (excluding the case study event), were selected from the available data by analysing hydrographs.
- Once calibration events had been selected radar data were retrieved for them from CEH data holdings.

Probability Distributed Model (PDM):

- *Model form.* The standard form of the PDM was initially used for all case studies with a cubic baseflow storage, a cascade of two unequal reservoirs for the surface storage and a truncated Pareto distribution of soil/vegetation absorption capacity. For catchments with a significant baseflow component, such as the Sor at Bodicote, alternative baseflow modelling and surface routing were considered. Where appropriate the soil tension capacity, S_t , influencing drainage to groundwater and evaporation, was allowed to be non-zero and modelling of catchment returns/abstractions was invoked through adding a constant flow, q_c . Section 3.2 provides a more comprehensive model description. Note that in this study the PDM is used in *simulation-mode* only, computing flows based solely on “actual” rainfall and potential evaporation inputs (i.e. not forecasts). The calibrated model parameters for each catchment are listed in Appendix F.
- *Raingauge input.* The PDM is a lumped conceptual model and requires catchment average rainfall as input. Operationally this is usually estimated by deriving a set of linear weights to apply to the available network of raingauges. An initial estimate of the weights was obtained by using the Thiessen method (based on a nearest-neighbour principle) and a multiquadric surface fitting technique (using a Euclidean distance measure with a zero offset parameter). These weights were refined during the calibration process and are listed in Appendix F. Appendix C provides more detail of the surface fitting technique.
Of course there is not a spatial rainfall surface, needed for input into the distributed Grid-to-Grid model, that is equivalent to the set of calibrated linear raingauge weightings. Therefore, for a strictly fair comparison to the Grid-to-Grid modelling, the catchment average rainfall from the raingauge surface used as an input into the distributed Grid-to-Grid model was also used as a rainfall input into the PDM. Generally the PDM results using this method differed little from using the linear set of raingauge weights.
- *Radar rainfall input.* The finest resolution radar data were used and a catchment average rainfall calculated. In these case studies it is either 1km raw radar, 2km raw radar, 2km Nimrod QC radar or a composite of 2 and 5km raw data. For all case studies gauge-adjusted radar data were also considered.

- *Potential evaporation.* The PDM default option of a sine curve profile was first tried. However, catchment average estimates of potential evaporation derived from MORECS PE data (available as monthly values on a 40 km grid) were used if they improved the model simulations.
- *Model initialisation.* Model initialisation is performed using observed flows at the station of interest. Usually only a short warm-up period of 1 day is discounted from the R^2 statistics. For slowly responding catchments a longer warm-up period of up to 2 months is used.
- *Calibration.* If the PDM had not previously been calibrated for the case study, weighted raingauge data were used for model calibration. Calibration events were selected to encompass different seasons and a range of flows without covering the extreme event of interest. For other rainfall estimators the set of model parameters calibrated using the weighted raingauge data were used **except** for the rainfall factor which was reassessed over the calibration events. Where a case study involved more than one catchment the largest was calibrated first by initially manually adjusting the model parameters followed by, where suitable, automatic optimisation. This then acted as a basis for calibration of the neighbouring and/or smaller sub-catchments.
- *Model evaluation over the extreme event.* Model performance over the extreme event of interest is assessed for all types of rainfall estimator.

Grid-to-Grid Model:

- *Model form:* Section 3.3 provides a full model description whilst the calibrated model parameters are listed in Appendix F.
- *River Network.* The Grid-to-Grid model requires flow directions at a 1km resolution. Initially these are derived by the Fekete method (Fekete, 2001) which is an automated procedure that utilises IHDTM (Integrated Hydrological Digital Terrain Model, Morris and Flavin, 1990) information at the finer resolution of 50m. These are then compared to the 50m resolution flow paths and hand-corrected as appropriate. Appendix E provides further details.
- *Raingauge rainfall input.* Essentially a multiquadric surface is fitted at each time-frame to observations from the available network of raingauges and averaged over 1km grid squares for input into the distributed model. The Euclidean distance was used with a zero offset parameter (see Section 6).
- *Radar rainfall input.* The finest resolution radar data were used and a catchment average rainfall calculated. In these case studies it is either 1km raw radar, 2km raw radar, 2km Nimrod QC radar or a composite of 2 and 5km raw data. For all case studies gauge-adjusted radar data were also considered: Section 6 provides further details.
- *Potential evaporation.* MORECS PE data, available as monthly values over a 40 km grid, were used for all case studies.
- *Model initialisation.* Model initialisation is performed using observed flows from the furthest downstream station. Due to difficulties in initialising distributed models a long warm-up period of up to 2 months is used for all events.

- Calibration.* Since the Grid-to-Grid model had not previously been calibrated for any of the case study catchments it was manually calibrated for all case studies using raingauge data. The same calibration events as the PDM were used. For other rainfall estimators the raingauge-based model parameters were used. Where a case study involved nested catchments, the flow at the furthest downstream station was primarily used for calibration. As the Grid-to-Grid model is a distributed model it is possible to obtain the flow at all the sub-catchment locations simultaneously and therefore, although the furthest downstream station was used primarily for calibration, the flow at the other stations is also checked with the aim of achieving a consistent 'regionally' calibrated model.

For case studies where the catchments are neighbouring but not nested, e.g. the Upper Thames, the station for the largest catchment would initially be used for calibration. The model results for the neighbouring catchment's station locations were then checked with the hope of achieving a consistent 'regionally' calibrated model.

If the results at the neighbouring catchment/sub-catchment locations were not satisfactory then the Grid-to-Grid model would be calibrated for each gauging station location independently.

Note that, unlike the PDM, automatic optimisation is not currently available for the Grid-to-Grid model due to computational demands.
- Model evaluation over the extreme event.* Model performance over the extreme event of interest is assessed for all types of rainfall estimator.

7.2.2 Method of performance assessment

Performance measures used for assessing the quality of a model are constructed by comparing the observed and modelled flows at each time-step of an event. The principle performance measure used in this study is the R^2 statistic. Let the observed and modelled flows at time t be denoted by Q_t and q_t respectively and let n denote the total number of observations. Then the error at time t is $e_t = Q_t - q_t$. The R^2 statistic over n observations is then defined to be

$$R^2 = 1 - \frac{\sum_{t=1}^n e_t^2}{\sum_{t=1}^n (Q_t - \bar{Q})^2}$$

where \bar{Q} is the mean of the observed flows over the n observations. The R^2 statistic is a dimensionless measure which gives the proportion of variability in observed flows accounted for by the model simulation and allows comparison across different events, catchments and models. A value of 1 indicates a perfect model. Note that the R^2 statistic is period/event specific due to the calculation of \bar{Q} and can be negative if the modelled flow is worse than that provided by the (unknown) mean observed flow. The actual R^2 statistics for each event, model and rainfall type are listed in Appendix G but are presented graphically within this section to aid comparison and identification of patterns in performance.

In addition to the R^2 statistic, inspection of the modelled hydrograph and comparison with the observed flows is a very informative and complementary means of model assessment.

Performance measures are also used within the automatic optimisation procedure used in automatically calibrating the PDM model parameters. The goal of automatic optimisation is to minimise an *objective function*. In this study the objective function used is the root mean square error (*rmse*) of the differences between observed and modelled flows at each time-step t . Over n observations the *rmse* is given by

$$rmse = \left(\frac{1}{n} \sum_{t=1}^n e_t^2 \right)^{1/2}$$

and has the same units as the flow (usually m^3s^{-1}). The automatic optimisation employs a robust and straightforward simplex minimisation procedure (Nelder and Mead, 1965) modified to incorporate the ideas suggested by Gill, Murray and Wright (1981).

In addition to R^2 and *rmse* statistics, a visual analysis of model performance is also given. Model hydrographs presented show the total simulated river flow (solid line), 'baseflow' (dashed line) and soil moisture deficit (solid line below axis). The definitions of these quantities are model dependent and are given in Table 7.1.

Table 7.1 Definition of modelled quantities for the PDM and Grid-to-Grid models

| Modelled quantity | PDM definition | Grid-to-Grid definition |
|-----------------------------|--|--|
| Total river flow | Total outflow from surface storage (surface runoff) and groundwater storage (baseflow) | Routed surface flow at grid-square modelling location derived from surface runoffs and subsurface return flows |
| Baseflow | Outflow from groundwater storage | Component of routed surface flow at grid-square modelling location derived only from subsurface return flows |
| Soil Moisture Deficit (SMD) | Catchment average soil moisture deficit | Soil moisture deficit is calculated for each grid-square store and then averaged over the catchment |

7.3 Hydrological case study 1: River Kent (Orographic)

7.3.1 PDM model calibration – weighted raingauge data

The PDM had not previously been calibrated for any of the River Kent catchments. Hydrometric data were obtained for the years 2003 and 2004 from which two calibration events were selected. The dates of the calibration events are listed in Table 7.2. These events were from different seasons and encompassed a reasonable range of flows.

Table 7.2 Periods used for model calibration and periods encompassing the extreme storms

| Hydrological case study | Calibration events | Extreme events |
|-------------------------|---|----------------------|
| 1. River Kent | 25 Oct – 30 Dec 2003 15 Jun – 30 Aug 2004 | 29 Jan - 8 Feb 2004 |
| 2a. Upper Thames | 1 Sep 2000 – 1 Jun 2001 | 6 Apr - 19 Apr 1998 |
| 2b. Stour at Shipston | 8 Jan - 8 Apr 1990 1 Nov 1991 - 1 May 1992 | 6 Apr - 19 Apr 1998 |
| 3. River Darwen | 17 Feb – 9 Mar 2002 26 Jul – 16 Nov 2002 | 13 Jun – 16 Jun 2002 |

Analysis of the raingauge data identified that observations from the Fisher Tarn raingauge were missing for a significant period of the orographic rainfall event: therefore this gauge was excluded when deriving the set of linear weights.

In the light of the Kent CAMS report, modelling of catchment returns/abstractions was invoked through adding a constant flow, q_c , to obtain the total modelled flow at the catchment outlet. Also, model performance was improved by allowing the soil tension capacity, S_t - influencing drainage to groundwater and water loss to evaporation - to be non-zero. Using 15 minute data between events to maintain a water balance, in order to provide initial conditions for the next event, had limited effect on model performance. As a consequence, each event was automatically initialised starting from a low period of flow without recent rainfall and with a 24 hour warm-up period discounted from the R^2 efficiency performance measure.

The Kent catchment to Sedgwick was calibrated first. This is the largest catchment and the calibrated model provided a basis for the calibration of its four sub-catchments. As a set of calibration parameters did not exist, calibration was started from guideline values. Parameters were initially manually adjusted and then automatically optimised over both calibration events. The calibration process revealed that the model was not overly sensitive to the set of linear raingauge weights used. This suggests that the raingauge network provides good coverage for the storms experienced and, in general, good catchment

average rainfall estimates are obtained. The final set of raingauge weights used in the PDM is listed in Appendix F.

The calibration results achieved for the Kent at Sedgwick were excellent with R^2 values of 0.967 and 0.952, as shown in Figure 7.1. The modelled flow from the calibrated PDM for Sedgwick is compared to the observed flow in Figure 7.2 when using the raingauge rainfall surface as the rainfall estimator: this confirms their good agreement, particularly for the large flow peaks. These simulations are very similar to those using the weighted raingauge data and are presented to allow a like-for-like comparison with the Grid-to-Grid model performance. There are instances where the model performance is not as good. One noticeable failing during the second calibration event occurs on 24 August 2004 when the modelled flow is significantly less than observed. Inspection of radar data for this event as displayed via HYRAD revealed this to be a convective, spatially-varying event whose intensity was not fully captured by the raingauge network, resulting in the model underestimating the observed flow.

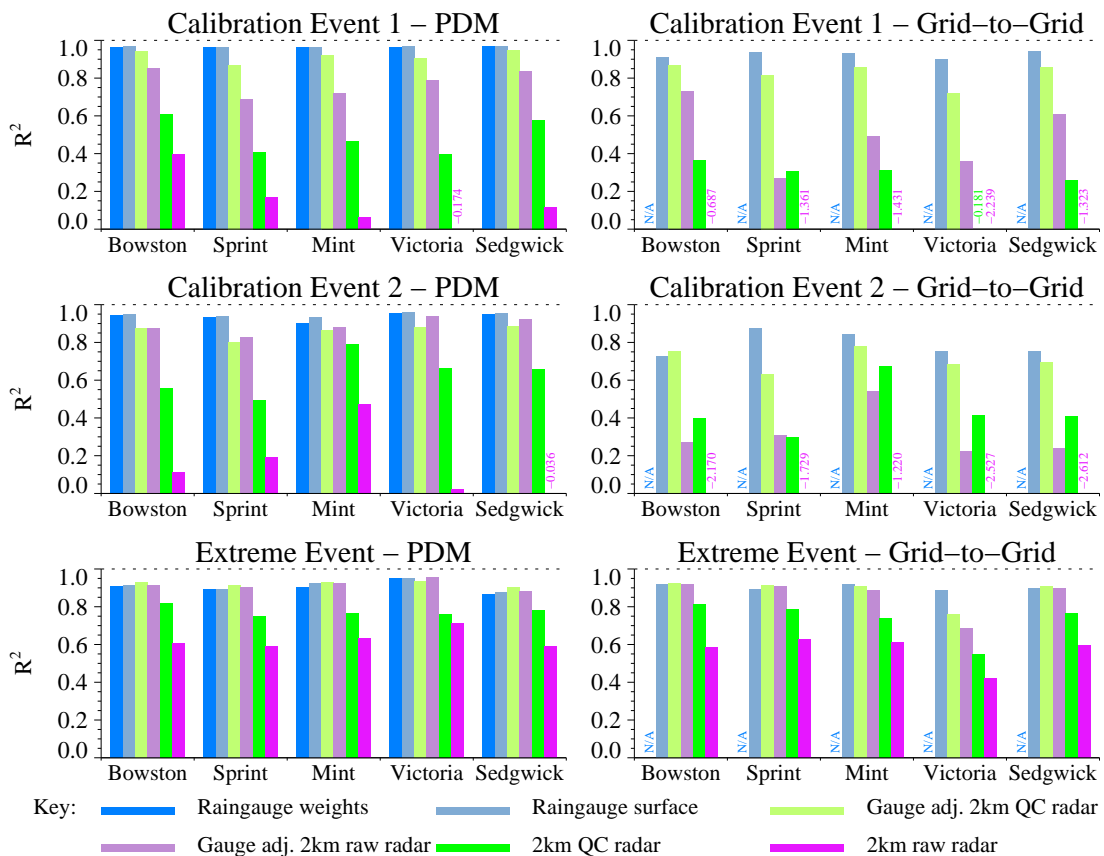


Figure 7.1 River Kent catchments: R^2 statistics for PDM and Grid-to-Grid models using different rainfall estimators.

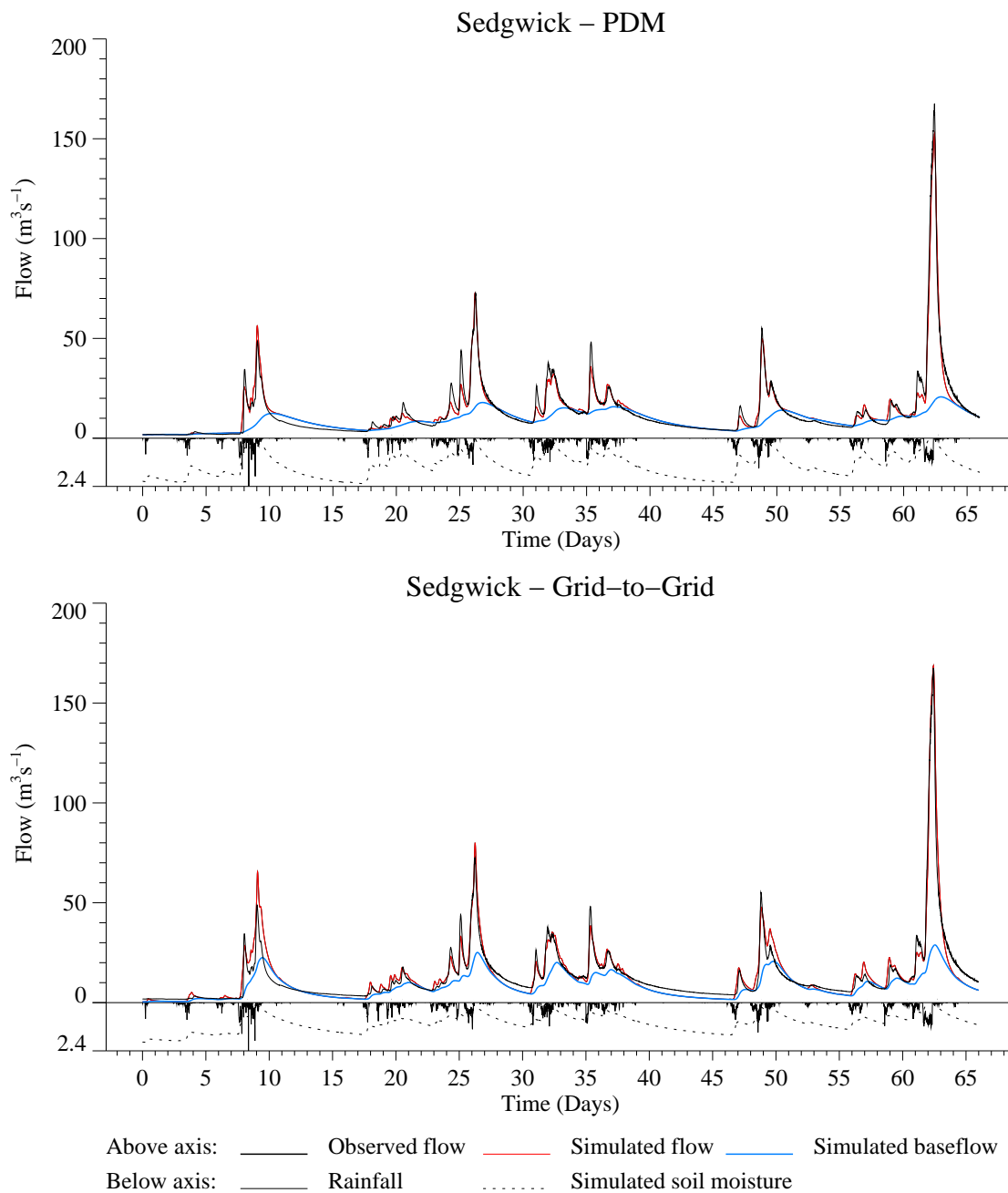


Figure 7.2 River Kent at Sedgwick: Hydrographs for the PDM and Grid-to-Grid models over the calibration event: 25 October to 30 December 2003. The rainfall estimator used is the raingauge rainfall surface. The figure below the axis is the maximum 15 minute catchment average rainfall for that event.

The calibrated PDM parameters for the Kent at Sedgwick provided the basis for subsequent calibrations for the Kent at Victoria Bridge and at Mint Bridge. The parameter transference was very good and only a small amount of automatic optimisation was required to obtain excellent results at these upstream stations. This is reflected in the R^2 values shown in Figure 7.1 which are greater than 0.9. The only significant difference is the poorer performance of the Mint Bridge calibration over the second event. This is attributable to the convective event on 24 August 2004, mentioned previously, with rainfall confined to the Mint Bridge catchment. The Mint Bridge calibration was used as a basis for the calibrations at Sprint Mill and Bowston. Again there was very good parameter transference and the final calibrations gave R^2 values in excess of 0.93, as shown in Figure 7.1.

Hydrographs comparing modelled and observed flow are not given for the stations upstream of Sedgwick as they are very similar to Figure 7.2. This similarity is reflected in the R^2 statistics as seen in Figure 7.1. The set of calibrated parameters, listed in Appendix F, indicate that generally the parameters transfer well across all catchments. However, there are some exceptions such as with the surface routing parameters where k_2 noticeably decreases with catchment size, reflecting the flashier response of the smaller catchments. Another interesting feature of the model calibration is the time delay parameter, τ_d , which ranges between 1.3 and 2.25 hours across the catchments. This considerable delay acts as a “free” short-range forecast (before rainfall forecasts are required as input to the PDM) and has obvious benefits for flood warning purposes.

7.3.2 PDM model calibration – other rainfall estimators

Five other rainfall estimators were investigated for the River Kent case study: namely using a fitted raingauge rainfall surface, 2km raw radar, gauge-adjusted 2km raw radar, 2km Nimrod QC radar and gauge-adjusted 2km QC radar. For each different rainfall estimator only the rainfall factor was reassessed: these are listed in Appendix F.

The rainfall factors for the raingauge rainfall surface, 2km QC and the gauge-adjusted 2km QC rainfall estimators are all very similar to the rainfall factor calibrated using the raingauge weights as input. The rainfall factor for the 2km raw and gauge-adjusted 2km raw radar data tended to be a little lower than the rainfall factor used for weighted raingauge data.

The R^2 statistics over the calibration events are presented for all rainfall estimators and catchments in Figure 7.1. The statistics show that the raingauge weights or ‘raingauge rainfall surface’ rainfall estimators give the best model performance for both calibration events and all catchments. The results for the radar-based rainfall estimators are slightly hampered due to missing data during precipitating periods. Over the 40610 5 minute intervals used for calibration 2299 (5.7%) of 2 km Nimrod QC images were missing and 3181 (7.8%) of the 2 km raw images were missing. The R^2 statistics also clearly show the significant benefit afforded to model performance by applying gauge-adjustment to radar

data, giving performance statistics comparable with the raingauge-only estimators. As would be expected, the benefit is more marked for the 2 km raw data.

7.3.3 Grid-to-Grid model calibration – Raingauge data

For this case study the furthest downstream river gauge at Sedgwick was primarily used to calibrate the distributed Grid-to-Grid model. Initial modelling revealed a time lag of the modelled response at Sedgwick. Further investigation revealed that the distributed Grid-to-Grid model could not route water to the catchment outlet quick enough when using a 15 minute routing time-step. This is due to the stability criterion of the 1-D kinematic wave which, for a given routing time-step and spatial grid resolution, effectively provides an upper limit for the wave speeds. This problem was easily rectified by reducing the routing time-step to 5 minutes, allowing faster wave speeds to be used.

Once the routing time-step had been reduced a good manual calibration was achieved at Sedgwick. Since the Grid-to-Grid model is a distributed model, river flow estimates can be obtained for any grid-square in the region: it allows simulated flow to be compared to gauged flow at the gauging stations upstream of Sedgwick.

Figure 7.1 presents the R^2 statistics for each gauging station over the two calibration events when using the raingauge rainfall surface as the rainfall estimator. A warm-up period of 1 month was discounted from the R^2 efficiency performance measure. These statistics indicate that the model performance at the upstream locations were comparable to the results at Sedgwick, confirming that the distributed model is performing well across the entire catchment. The statistics also indicate that the model performs better over the first calibration event.

The Grid-to-Grid modelled flow at Sedgwick using the raingauge rainfall surface as the rainfall estimator is presented in Figure 7.2 for the first calibration event. It shows the good agreement between observed and simulated flows and allows comparison with the PDM simulation. Figure 7.1 also allows comparison with the PDM results and shows that over the calibration events the PDM consistently outperforms the Grid-to-Grid model when using the raingauge rainfall surface as the rainfall estimator. This is not entirely surprising since, due to the computation time involved, automatic optimisation of the Grid-to-Grid parameters is not currently possible. However, the R^2 statistics for the Grid-to-Grid model are still very respectable. The calibrated parameter values are listed in Appendix F. The rapid response nature of the Kent catchment is reflected in the reasonably quick wave speeds.

7.3.4 Grid-to-Grid model calibration – other rainfall estimators

The R^2 statistics for the Grid-to-Grid model using the different rainfall estimators available are presented in Figure 7.1. They broadly follow the same pattern as described for the PDM in Section 7.3.2 with the raingauge-based rainfall

estimator giving the best model performance. However, for a given rainfall estimator and catchment, the PDM consistently performs best.

7.3.5 Model evaluation over the extreme event – Raingauge data

Up to this point the calibrated PDM and Grid-to-Grid models have not been exposed to the case study extreme event. This sub-section is concerned with how the models perform over the extreme orographic rainfall event of January/February 2004 and if there are any signatures of “model failure”. Note that in this section the raingauge rainfall surface is used as the rainfall estimator.

The most informative method of assessing model performance is to study the hydrographs produced by the models and to compare these to the observed flows. These hydrographs have been produced for each catchment and are shown in Figure 7.3 for the PDM and Figure 7.4 for the Grid-to-Grid model. These should be assessed in conjunction with the corresponding R^2 performance statistics for the ‘raingauge rainfall surface’ rainfall estimator presented in Figure 7.1. Warm-up periods of 24 hours and 1 week were used for the PDM and Grid-to-Grid models respectively.

The hydrographs for both models show a very good agreement between the simulated and observed flows, particularly in the period before the main flood peak, up to the flow associated with the maximum validated stage of the rating curve (indicated by a dashed horizontal line) for all catchments. Beyond this limit agreement is not so good with the modelled flows consistently underestimating the “observed” flood peak flows. The agreement after the flood peak is reasonable but all modelled flows tend to underestimate that observed: although the underestimate is reasonably large for some stations it does not constitute a “model failure”.

The possible reasons for the difference during and after the flood peak are numerous and it is difficult to identify a single cause. Around the flood peak there is significant uncertainty about the extrapolation of the rating curve and the validity of the “observed flows”. There are also other uncertainties concerning the hydrometric data. Could a ponding effect or mobilised sediment affect the level reading? Deposits of the latter could affect readings after the main flood peak. Raingauge data can also be uncertain and prone to underestimation in heavy rain (normally of a convective nature). However, this is thought unlikely since the instantaneous rain-rates associated with this orographic case study are well within raingauge operating limits. Of course there is model uncertainty as well, especially as the model was not exposed to such a large flood peak during calibration. In support of the modelling, the PDM and Grid-to-Grid model simulations are very similar and both agree very well with the observed flows in the build-up to the peak. Also, the PDM modelled peaks at different stations provide a consistent picture, in terms of volumes, across the catchments (this consistency is assured for the Grid-to-Grid model because of its distributed formulation). On the downside, the magnitude of the simulated peaks do not constitute a particularly rare event (i.e. in excess of the 1 in 100 year flood estimate from the FEH method, see Table 5.3) for any of the

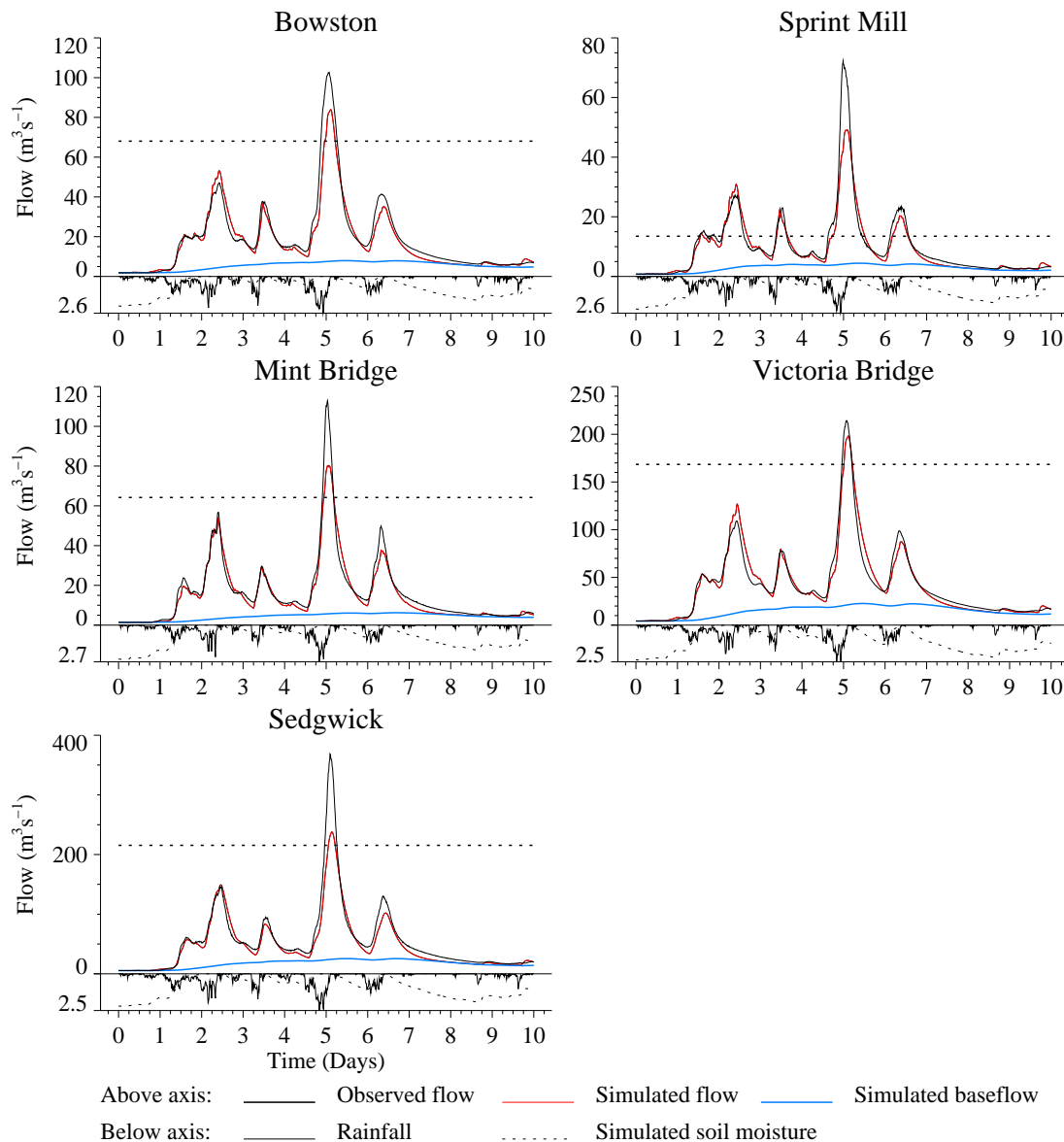


Figure 7.3 River Kent catchments: Hydrographs for the PDM models over the case study extreme event: 29 January to 8 February 2004. The rainfall estimator used is the raingauge surface. The figure below the axis is the maximum 15 minute catchment average rainfall for that catchment. The dashed line above the axis indicates the flow associated with the maximum stage used to derive the rating equation for that catchment.

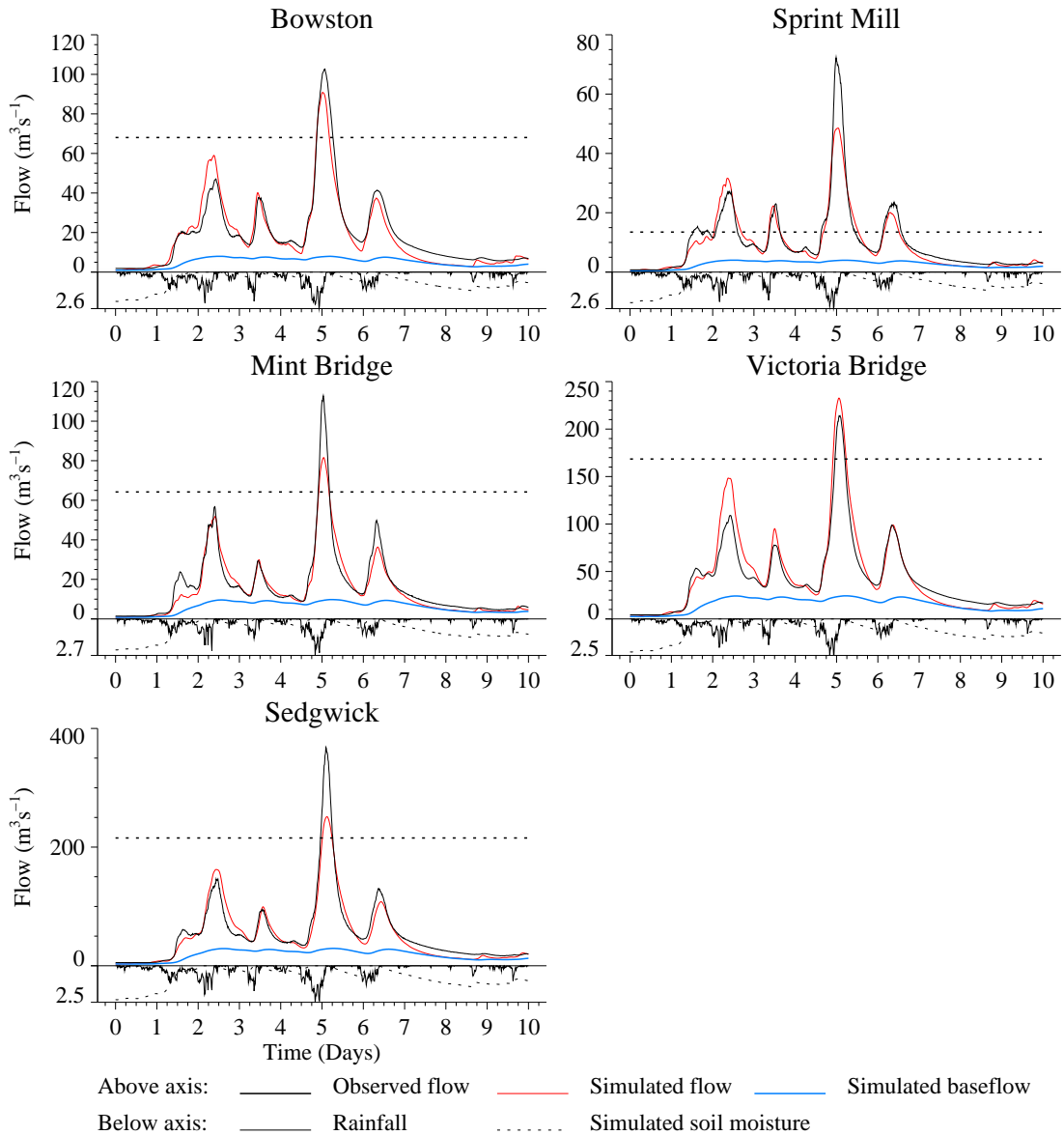


Figure 7.4 River Kent catchments: Hydrographs for the Grid-to-Grid model over the case study extreme event: 29 January to 8 February 2004. The rainfall estimator used is the raingauge surface. The figure below the axis is the maximum 15 minute catchment average rainfall for that catchment. The dashed line above the axis indicates the flow associated with the maximum stage used to derive the rating equation for that catchment.

stations except Sedgwick where there is anyway some doubt over the FEH estimates. However, this is not necessarily surprising since the “observed” flow records of the stations are used in the FEH estimation method.

Overall the agreement between modelled and observed flows over the case study extreme event is good and well within the performance expectations of the models. This agreement is reflected in the R^2 performance statistics, as presented in Figure 7.1. Interestingly the statistics also show that not one model performs best over all catchments when using the raingauge rainfall surface as input. This is in contrast to the calibration events where the PDM consistently outperforms the Grid-to-Grid model.

7.3.6 Model assessment – other rainfall estimators

Model performance over the case study extreme event is assessed for all rainfall estimators. Simulated flows for the River Kent at Sedgwick using 2km raw radar data, gauge-adjusted 2km raw radar data, 2km Nimrod QC radar data, gauge-adjusted 2km QC data and a raingauge rainfall surface are shown for the PDM model in Figure 7.5 and for the Grid-to-Grid model in Figure 7.6. In addition the PDM model simulation using weighted raingauge data is given in Figure 7.5. The R^2 performance statistics over the extreme event are presented for both models over all catchments and rainfall estimators in Figure 7.1. Encouragingly the radar data records were almost entirely complete over the case study and so there was no impact from missing radar data on the model simulations over the extreme event.

The simulated hydrographs give an informative insight into the characteristics of the different rainfall estimators and their use for hydrological modelling. Analysing Figure 7.5, which relates to the PDM, shows that model simulations using 2 km raw radar have five flow peaks of comparable magnitude with some observed peaks overestimated and the observed extreme flood peak being significantly underestimated. This intermittent over- and under-estimation also highlights some of the difficulties that can be encountered when trying to calibrate hydrological models using raw radar data. Returning to Figure 7.5 the simulated hydrograph using the 2 km Nimrod QC radar data shows a marked improvement compared to using the 2 km raw data. The only noticeable overestimation is during the fourth day of the event. This shows that the Nimrod QC product is adding value by providing more ‘stable’ rainfall estimates (i.e. fewer periods of over-/under-estimation) and is therefore more likely to give a successful model calibration.

The simulated hydrographs in Figure 7.5 that use the gauge-adjusted rainfall estimators are clear proof of the added benefit that merging raingauge data with radar data can give for model performance over using unadjusted radar estimates. In fact the model simulations using gauge-adjusted radar data can perform as well or better than simulations using raingauge data. These comments are reflected in the R^2 performance statistics for the different rainfall estimators presented in Figure 7.1, confirming that there is little difference in model performance between using the raingauge rainfall surface or gauge-

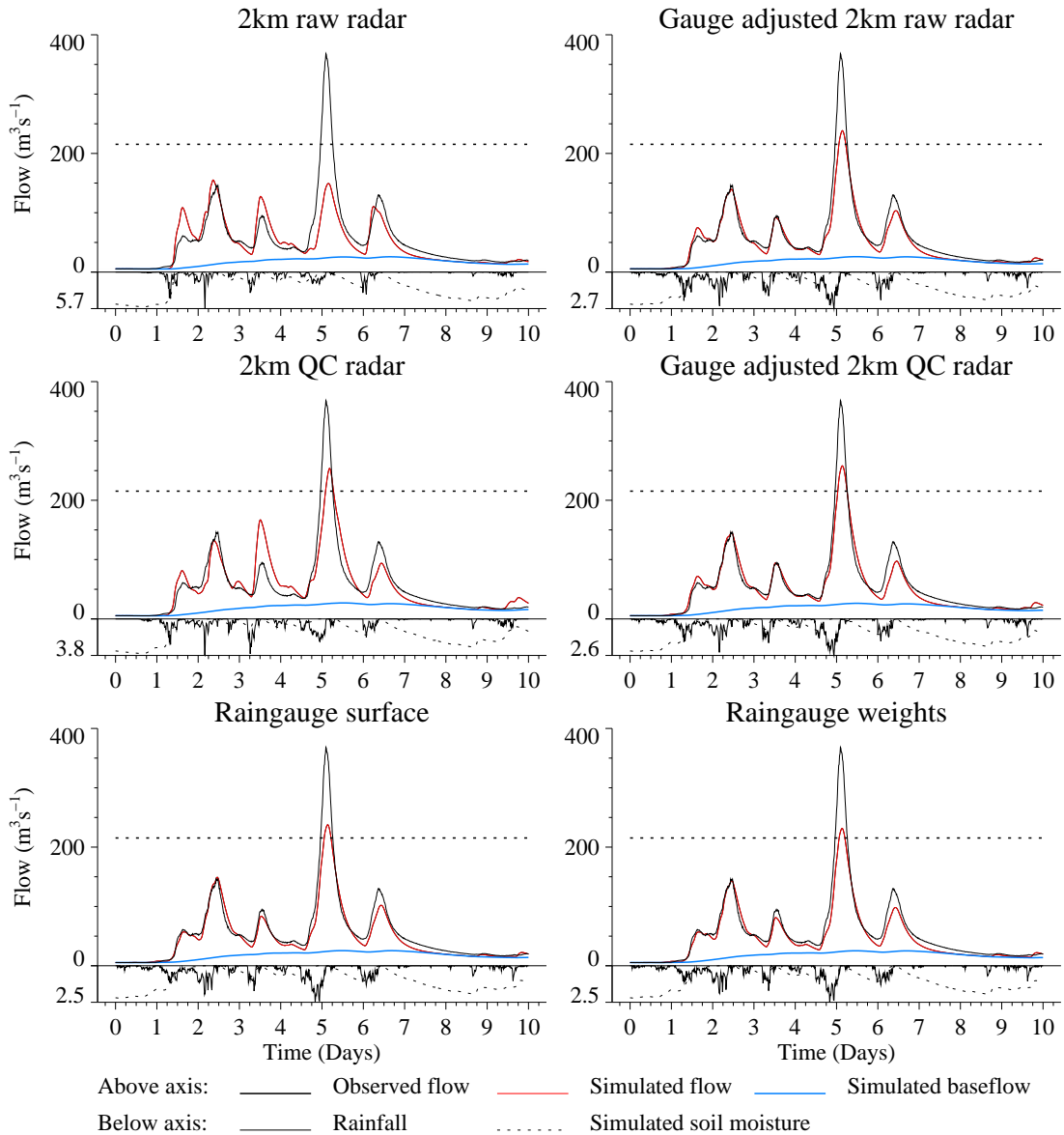


Figure 7.5 River Kent at Sedgwick: Hydrographs for the PDM model over the case study extreme event 29 January to 8 February 2004 for different rainfall estimators. The figure below the axis is the maximum 15 minute catchment average rainfall for that catchment. The dashed line above the axis indicates the flow associated with the maximum stage used to derive the rating equation.

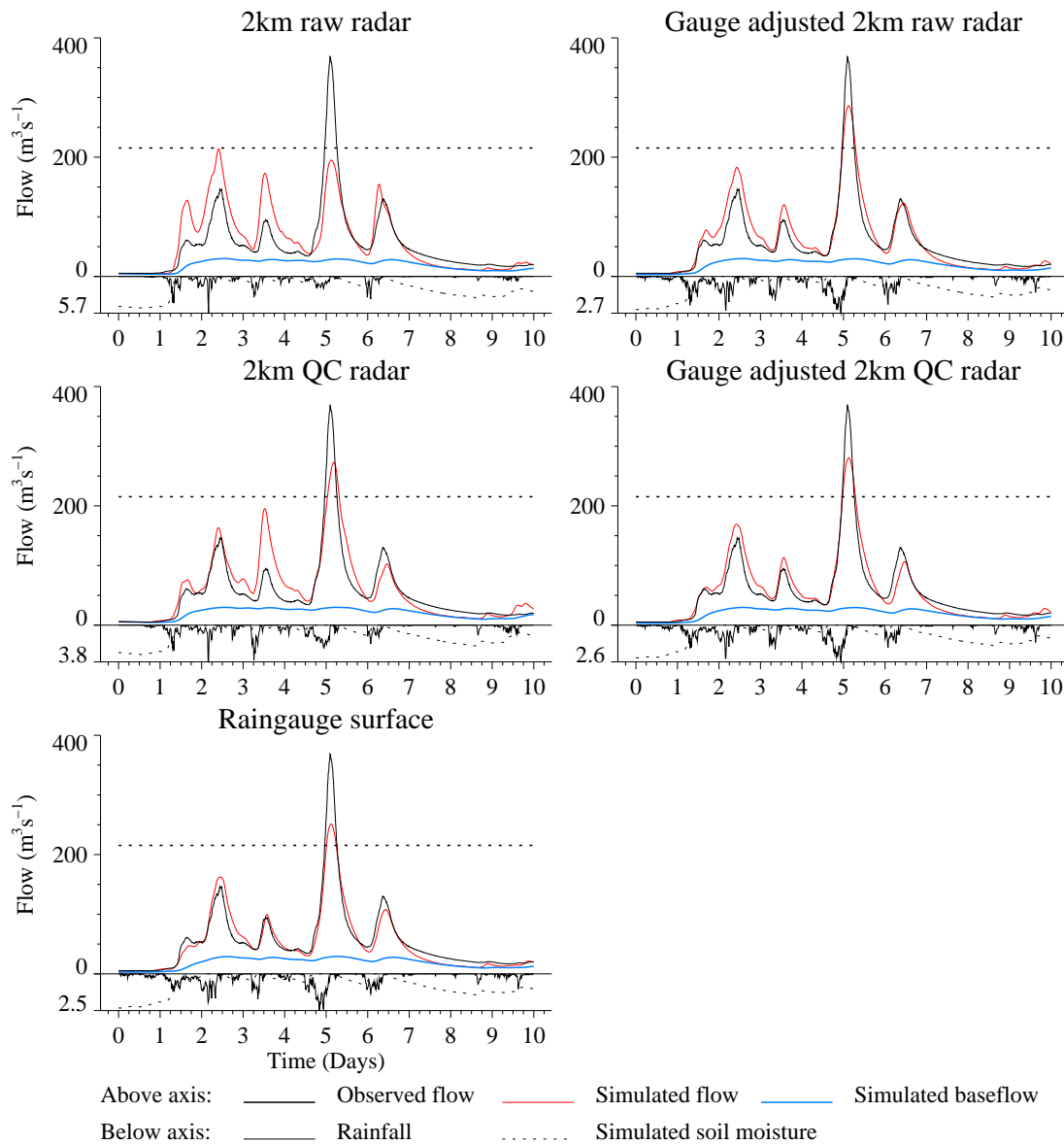


Figure 7.6 River Kent at Sedgwick: Hydrographs for the Grid-to-Grid model over the case study extreme event 29 January to 8 February 2004 for different rainfall estimators. The figure below the axis is the maximum 15 minute catchment average rainfall for that catchment. The dashed line above the axis indicates the flow associated with the maximum stage used to derive the rating equation.

adjusted radar data as the rainfall estimator but that generally the gauge-adjusted 2km Nimrod QC data performs best. The R^2 statistics also reveal that the PDM and Grid-to-Grid models perform similarly for a given catchment and rainfall estimator with neither model consistently outperforming the other.

7.4 Hydrological case study 2: Upper Thames and Stour (Frontal)

Three catchments were selected for this case study: the Stour at Shipston, the Sor at Bodicote and the Cherwell at Banbury. The latter two catchments eventually feed into the River Thames and are hence referred to as the *Upper Thames* catchments. The PDM or Grid-to-Grid models have not previously been calibrated for either of the Upper Thames catchments. The PDM has previously been calibrated for the Stour at Shipston as part of the R&D Technical Report W242 *Comparison of Rainfall-Runoff Models for Flood Forecasting* and the model performance over the Easter 1998 flood was also studied. The event periods used for this case study are listed in Table 7.2.

7.4.1 PDM model calibration – weighted raingauge data

Upper Thames catchments

Hydrometric data were obtained for the years 1997 to 2001 inclusive. Inspection of the hydrographs revealed that both catchments were responsive to rainfall and emphasised the significant baseflow component to the flow records at Bodicote: see the observed flows presented later in Figure 7.10. Therefore a long calibration event of 9 months from 1 September 2000 to 1 June 2001 was selected to encompass a reasonable range of flows and the subsequent recession. The less significant baseflow contribution at Banbury, despite bordering the Bodicote catchment, can be attributed to the differing catchment soil types. Although both catchments lie mostly on Lias clay bedrock with low permeability, the HOST (Hydrology of Soil Types) data, presented in Figure 7.7, reveals that the soil covering the Bodicote catchment is generally much deeper than that over the Banbury catchment and is responsible for the slowly responding baseflow component at Bodicote. More details of the HOST classification system is given by Boorman *et al.* (1995).

Model calibration was performed using raingauge data. The final sets of raingauge weights derived during calibration are given in Appendix F. Note that to be consistent with current operational practice, only raingauges within Thames Region were considered when deriving the weights. Investigations revealed that using MORECS potential evaporation data, rather than the standard sine curve profile, provided a modest improvement to model performance.

Since the flow at Bodicote has a relatively large baseflow component the model performance can be sensitive to when it is initialised. As a result, each catchment model was automatically initialised starting from a low period of flow

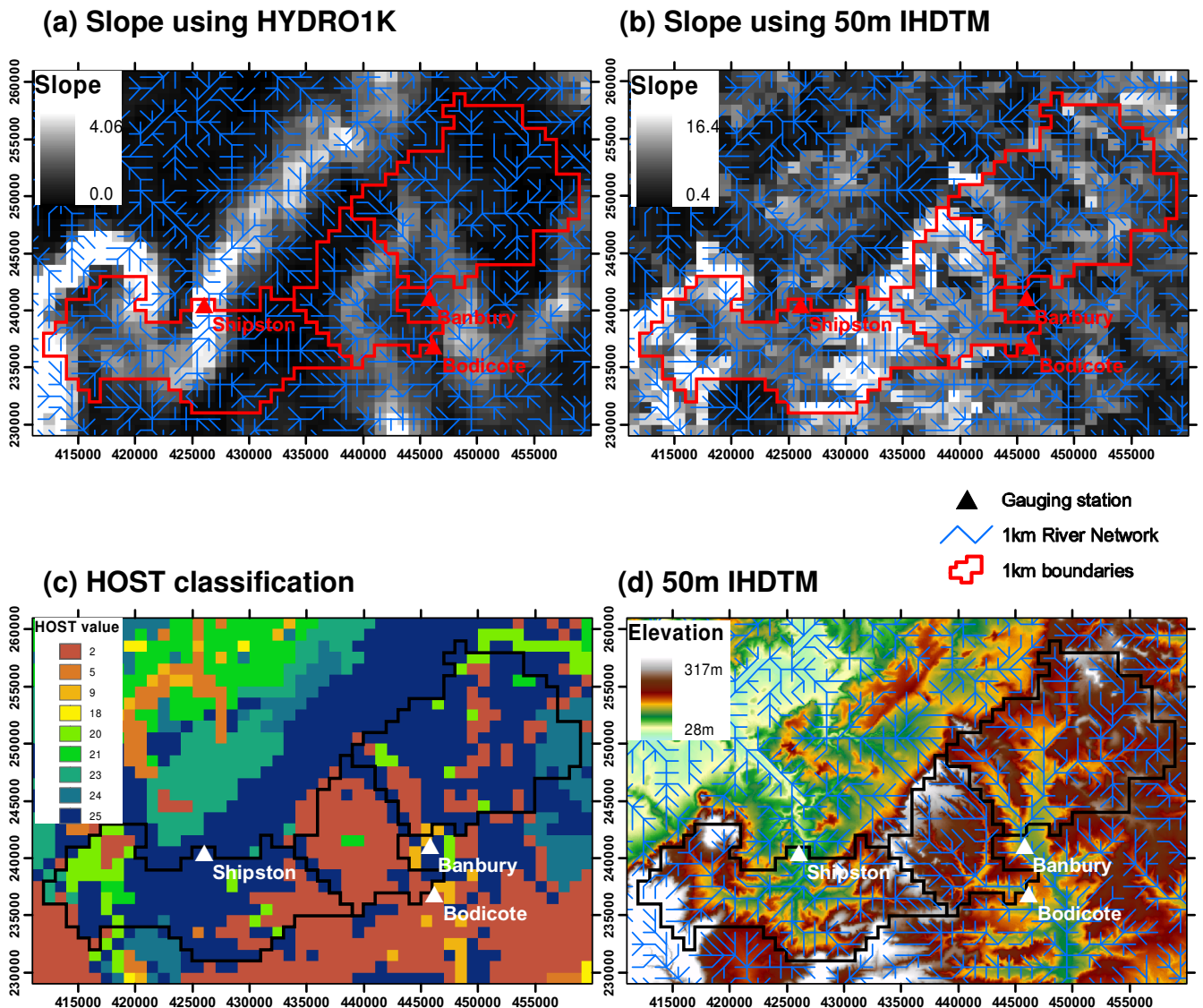
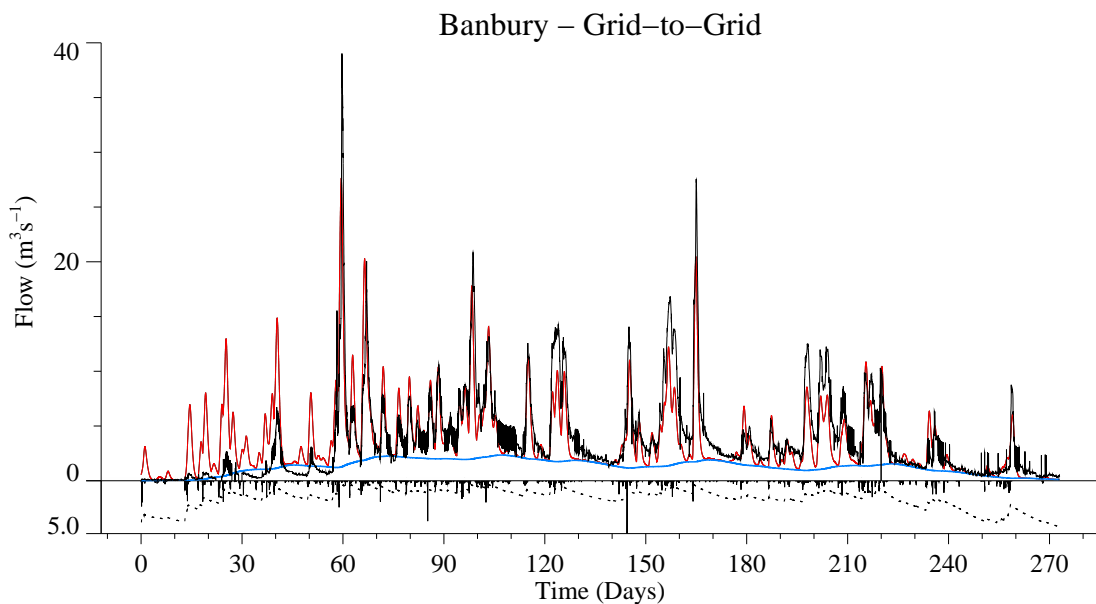
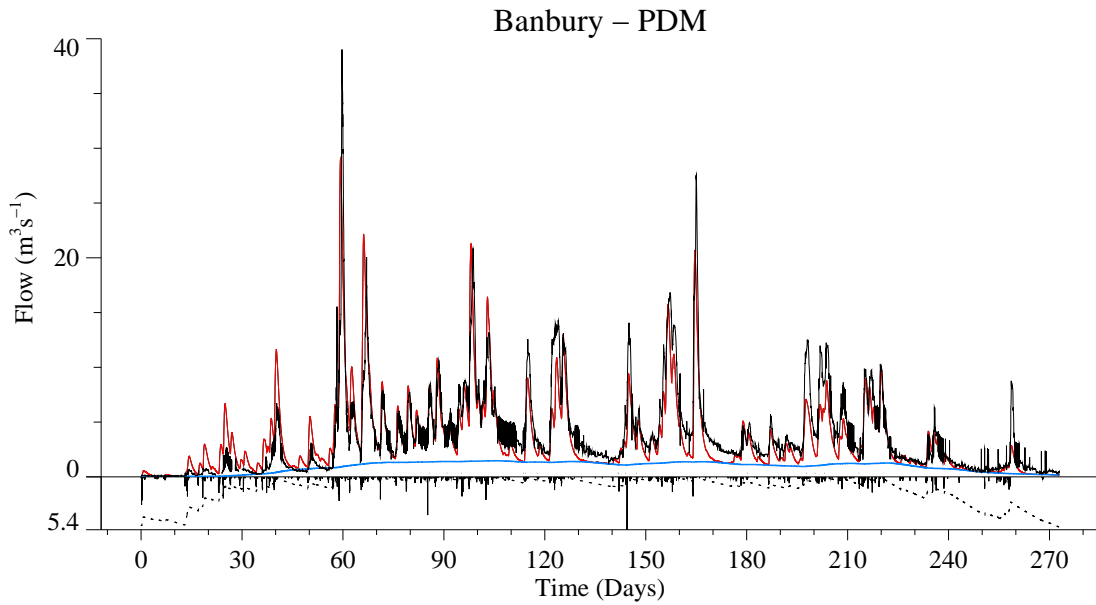


Figure 7.7 Digital datasets for the Upper Thames and Stour catchments. The 1 km river network and associated catchment boundaries are also shown.

without recent rainfall and a 2 month warm-up period discounted from the R^2 efficiency performance measure. Model performance was improved by invoking a soil tension capacity, S_t , allowing more loss of soil water to evaporation.

The Cherwell to Banbury is the largest catchment and was calibrated first. Although mainly rural in character there is significant human influence through water abstractions, sewage treatment works and intakes or returns from the Oxford canal. These influences are the most likely reason for the occasional oscillatory behaviour and erroneous peaks in the historical flow records and are evident during the calibration period: see Figure 7.8. As a result, the model



Above axis: ——— Observed flow ——— Simulated flow ——— Simulated baseflow
 Below axis: ——— Rainfall ····· Simulated soil moisture

Figure 7.8 Cherwell at Banbury hydrographs for the PDM and Grid-to-Grid models over the calibration event 1 September 2000 to 1 June 2001. The rainfall estimator used is the raingauge rainfall surface. The figure below the axis is the maximum 15 minute catchment average rainfall for that event.

calibration process at Banbury proved to be very difficult and only manual optimisation was possible. In particular, obtaining a consistent agreement between the observed and simulated time-of-peak was challenging and a time delay of 3 hours was needed. Alternative runoff generation and surface routing configurations were investigated but the standard PDM formulation gave best results. Modelled flow from the calibrated PDM for Banbury is compared to the observed flow in Figure 7.8 where the raingauge rainfall surface is the rainfall estimator (the simulations are very similar to the weighted raingauge rainfall estimator and are presented to allow a like-for-like comparison with the Grid-to-Grid model). This highlights the difficulty in obtaining consistent model performance over the entire calibration event and is reflected in the R^2 performance statistic of 0.748: see Figure 7.9. The final set of manually calibrated parameters for Banbury is listed in Appendix F. Of particular interest is the large soil tension value of 40 mm.

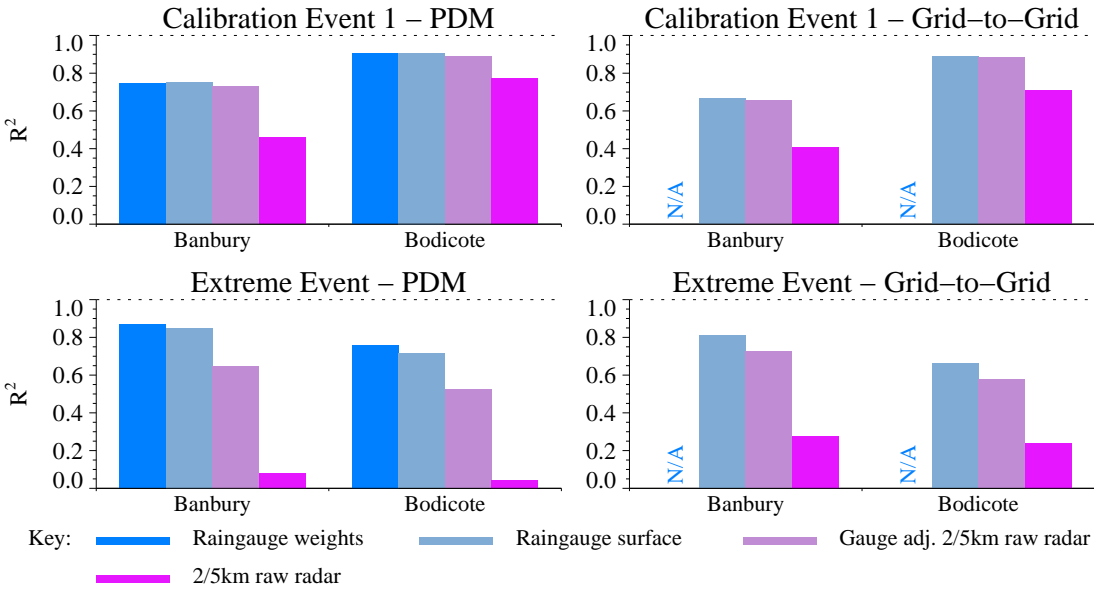


Figure 7.9 Upper Thames catchments: R^2 statistics for PDM and Grid-to-Grid models using different rainfall estimators.

The final set of calibration parameters for Banbury were initially trialled for Sor at Bodicote but, due to the differing flood responses, this proved unhelpful and the calibration at Bodicote was actually started from recommended parameter values. Investigations revealed that an alternative surface routing configuration of a single cubic store improved model performance considerably, allowing the shape and magnitude of the peaks to be more successfully modelled. Also, only manual optimisation was used. In order to obtain the slow model baseflow component of the simulation a relatively deep maximum soil depth, c_{max} , of 225 mm was needed. To get the catchment water balance of the model correct a large soil tension value of 60 mm was required to allow evaporation to deplete more of the soil moisture store. The final set of manually calibrated parameters for Bodicote is listed in Appendix F. The calibration results at Bodicote were very good giving an R^2 performance statistic of 0.906: see Figure 7.9. The good agreement between modelled and observed flows over the calibration event is clearly shown in Figure 7.10 where the raingauge rainfall surface has been

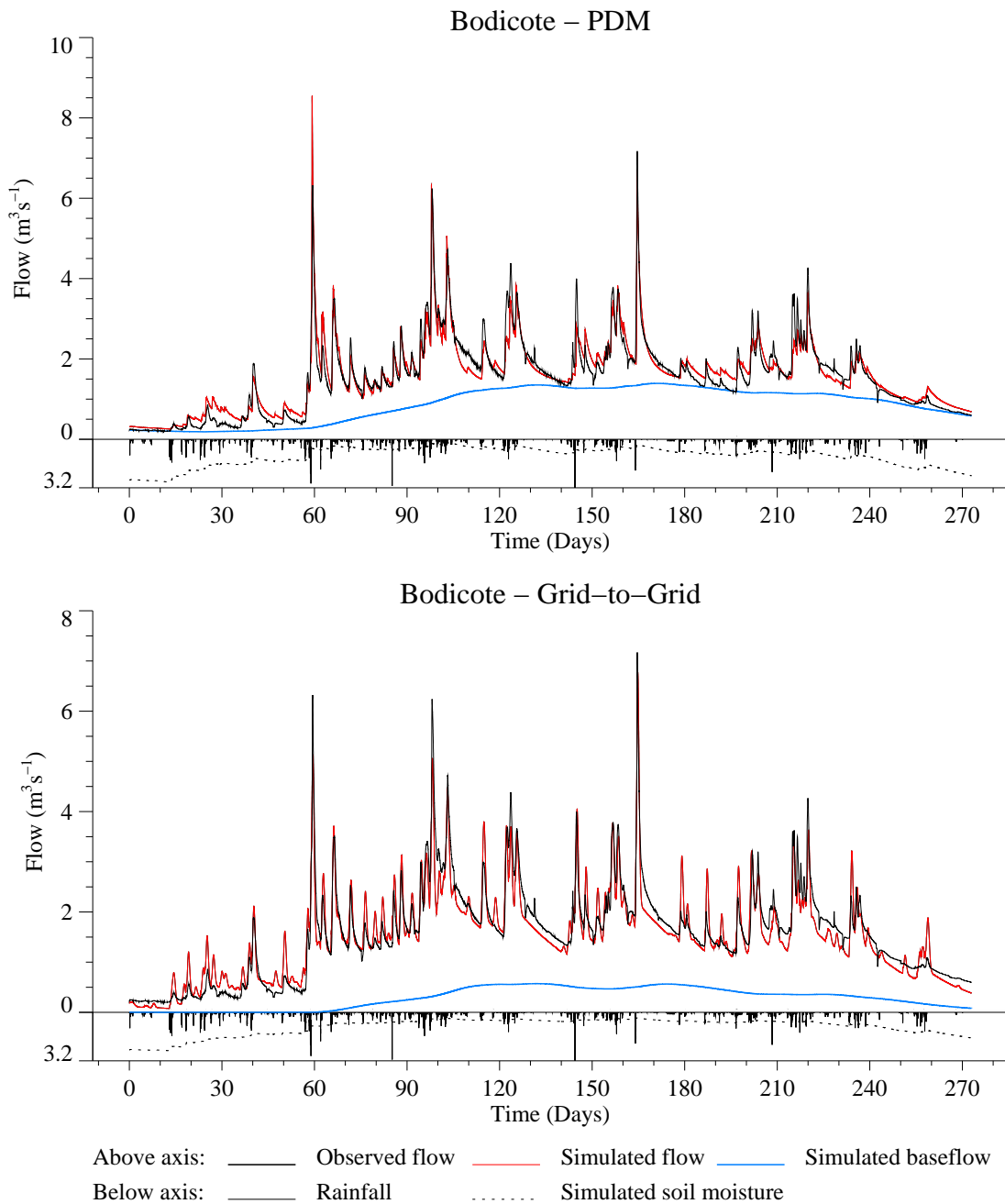


Figure 7.10 Sor at Bodicote hydrographs for the PDM and Grid-to-Grid models over the calibration event 1 September 2000 to 1 June 2001. The rainfall estimator used is the raingauge rainfall surface. The figure below the axis is the maximum 15 minute catchment average rainfall for that event.

used as the rainfall estimator (the simulations are very similar to the weighted raingauge rainfall estimator). This also shows the successful modelling of the baseflow over long time-scales.

Stour at Shipston

The PDM had previously been calibrated for the Stour at Shipston: Appendix F lists the calibrated model parameters. The set of raingauge weights used are also listed in Appendix F along with the Thiessen and multiquadric derived weights for comparison. Note that to be consistent with current operational practice, only raingauges within Midlands region were considered when deriving the weights. MORECS potential evaporation data has been used as input.

The R^2 performance statistics are presented for the two calibration events in Figure 7.11 and show a better performance over the first event. Good agreement between the modelled and observed flows over the first calibration event is evident in Figure 7.12 where the raingauge rainfall surface has been used as the rainfall estimator (the simulations are very similar to the weighted raingauge rainfall estimator). In comparison to the Upper Thames catchments, the Stour is

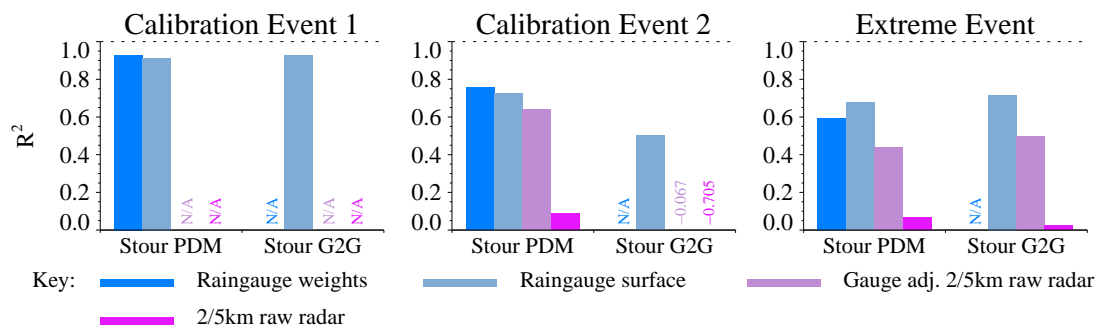


Figure 7.11 Stour at Shipston: R^2 statistics for PDM and Grid-to-Grid (G2G) models using different rainfall estimators.

slightly more responsive to rainfall and this is reflected in the small surface routing parameters (see Appendix F) and a shorter warm-up period of 24 hours.

7.4.2 PDM model calibration – other rainfall estimators

Three other rainfall estimators were investigated for the Upper Thames and Stour case study, namely using a fitted raingauge rainfall surface, a composite of 2 and 5 km raw radar and a composite of gauge-adjusted 2 and 5 km raw radar data. Radar rainfall data from Chenies weather radar was used for this case study. For each different rainfall estimator only the rainfall factor was reassessed: these are listed in Appendix F. Note that for the Stour, radar rainfall data were only available for the second calibration event.

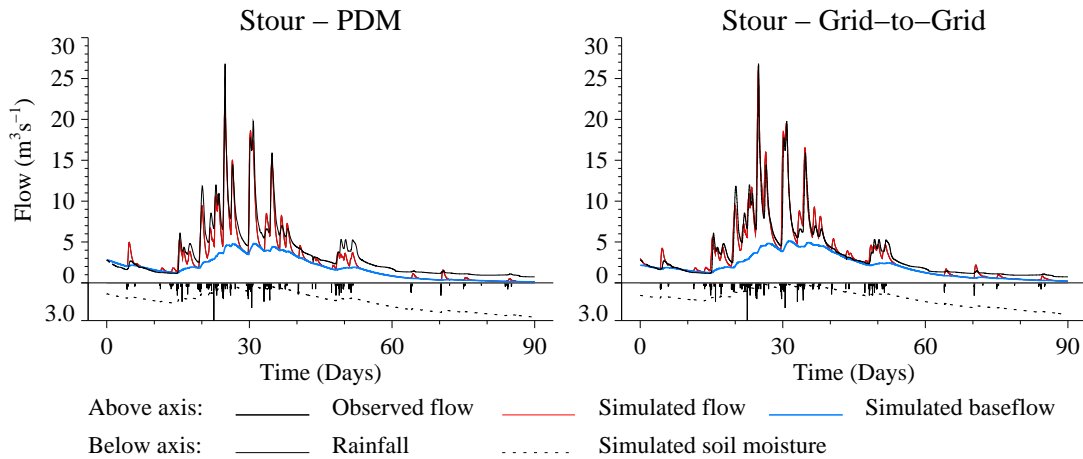


Figure 7.12 Stour at Shipston hydrographs for the PDM and Grid-to-Grid models over the calibration event 8 January to 8 April 1990. The rainfall estimator used is the raingauge rainfall surface. The figure below the axis is the maximum 15 minute catchment average rainfall for that event.

For the Upper Thames catchments the rainfall factors for the other estimators were very close to the rainfall factors derived using the weighted raingauge data as input. For the Stour the rainfall factors for the other estimators were not so close ranging from 0.70 for the composite of gauge-adjusted 2 and 5 km raw radar to 0.84 for the fitted raingauge rainfall surface.

The R^2 performance statistics over the calibration events are presented for all rainfall estimators in Figure 7.9 for the Upper Thames catchments and Figure 7.11 for the Stour at Shipston. The statistics show that the raingauge weights or 'raingauge rainfall surface' rainfall estimators give the best model performance for all calibration events and all catchments.

For the Upper Thames catchments the R^2 statistics again show the benefit given to the simulations when applying gauge-adjustment to radar rainfall data, resulting in performance statistics comparable with the raingauge-only estimators. Over the Upper Thames calibration event, only 2401 out of 78624 (3.1%) 2 km images were missing and 1108 out of 26208 (4.2%) 5 km images were missing from the Chenies radar data.

For the Stour at Shipston the R^2 statistics show that the raw radar data does not perform particularly well but model performance is considerably improved by applying gauge-adjustment. However, the raingauge-based estimators perform significantly better. A contributing factor to this is the relatively 'early' radar data used for the calibration event (1991/1992) compared to the calibration event used for the Upper Thames catchments (2000/2001). Over the Stour calibration event the Chenies radar data were reasonably complete with only 1487 out of 52416 (2.8%) 2 km images missing and 508 out of 17472 (2.9%) 5 km images missing.

7.4.3 Grid-to-Grid model calibration – Raingauge data

For this case study the gauging station record for the Cherwell at Banbury was first used to calibrate the distributed Grid-to-Grid model. Initial trials revealed that a consistent model over both the Upper Thames catchments and the Stour was not possible within the basic Grid-to-Grid model formulation. As a result attention first focussed on the digital datasets used to configure the model to see if any improvement could be made to give a regionally consistent model.

In particular the mean 1 km grid-square gradient, \bar{g} , was identified as being important since it is used within each grid-square runoff production scheme to derive the parameters of the soil store capacity distribution. Previously (and for all other case studies presented in this report) the mean gradient of a grid square has been calculated using HYDRO1K elevation data by constructing 1km resolution flow paths and then calculating the gradient between connected 1km grid squares. With the availability of 50m resolution DTMs it is possible to calculate a better estimate of \bar{g} by constructing 50m resolution flow paths, calculating the gradient between connected 50m squares and then averaging these over the 1km grid squares.

Estimates of \bar{g} derived using both the HYDRO1k and 50m IHDTM data are presented in Figure 7.7 and clearly show the extra spatial variability found using the latter. The 50m DTM base data are also presented in Figure 7.7 for comparison. Using estimates of \bar{g} based on the 50m IHDTM improved model performance and have been used for this case study only. Estimates of \bar{g} based on the 50m DTM are recommended for use in future applications of the Grid-to-Grid model.

However, even using the improved estimates of mean grid-square gradient, the Grid-to-Grid model still could not give consistent performance across all catchments. As previously mentioned the flood response of these lowland catchments are dominated by heterogeneous soil and geology controls rather than topographic controls. Since the basic Grid-to-Grid formulation only uses topographic datasets it is not surprising that the model parameters calibrated at Banbury are not successfully applied to the Bodicote catchment. Therefore, a separate set of Grid-to-Grid model parameters have been calibrated for each of the Upper Thames and Stour catchments. A prototype distributed model that incorporates soil/geology control, in addition to topographic control, is under development as a new variant of the Grid-to-Grid model. Preliminary results from this prototype model applied over the Upper Thames and Stour catchments are presented in Section 7.6.

The final Grid-to-Grid model calibration parameters for the Upper Thames and Stour catchments are given in Appendix F. Since the flood responses are not as 'flashy' as for the Kent or Darwen case studies, slower wave speeds and drainage constants were used and, for the Upper Thames catchments, a routing time-step of 15 minutes was adequate. Also a deeper regional maximum point store, C_{max} , was required, particularly for the Bodicote catchment (as suggested

by the HOST data). Calibration of the Grid-to-Grid model at Banbury and Bodicote was further aided by invoking a soil tension storage capacity, S_t , which increases the effect of evaporation on the water balance. Note that, for a given grid-square, if S_t is bigger than the maximum soil storage capacity, S_{\max} , then water from the soil storage can only be lost through evaporation and not drainage.

The R^2 statistics over the calibration events, when using the raingauge rainfall surface as the rainfall estimator, are presented in Figure 7.9 for the Upper Thames and Figure 7.11 for the Stour. Warm-up periods for each catchment have been discounted from the R^2 efficiency performance measure. These statistics show good model performance at Bodicote and for the first calibration event at Shipston. The difficulties calibrating the Grid-to-Grid model at Banbury are reflected in the lower R^2 statistics, as was the case for the PDM. The simulated flow from the calibrated Grid-to-Grid model is compared to the observed flow for both Upper Thames catchments in Figure 7.10 and Figure 7.8 and over the first calibration event for Shipston in Figure 7.12.

The R^2 statistics allow comparison between the PDM and the Grid-to-Grid model over the calibration events. There is little difference between the two models but the PDM generally performs slightly better when using the raingauge rainfall surface. Visual inspection of the simulated hydrographs in Figures 7.8 and 7.12 reveals the similarity between the different model simulations.

7.4.4 Grid-to-Grid model calibration – other rainfall estimators

Three other rainfall estimators were investigated for the Upper Thames and Stour case study: using a fitted raingauge rainfall surface, a composite of 2 and 5 km raw radar and a composite of gauge-adjusted 2 and 5 km raw radar data. Radar rainfall data from Chenies weather radar were used for this case study. The R^2 statistics for the Grid-to-Grid model over the calibration events are presented for all rainfall estimators in Figure 7.9 for the Upper Thames and Figure 7.11 for the Stour. The statistics show a similar qualitative pattern to the PDM results discussed in Section 7.4.2. One noticeable difference, compared to the PDM results, is the significantly poorer performance for the Stour when using radar or gauge-adjusted radar data. Overall the raingauge rainfall surface gives the best results for the Grid-to-Grid model and, for a given catchment and rainfall estimator, the PDM usually offers a slight improvement in model performance.

7.4.5 Model evaluation over the extreme event – Raingauge data

This section is concerned with the PDM and Grid-to-Grid model performance over the extreme frontal event during Easter 1998 which affected a wide area including the Upper Thames and Stour catchments. Note that the raingauge rainfall surface is used as the rainfall estimator in this section.

The simulated model hydrographs are compared to the observed flows in Figure 7.13 for all catchments and both models. These should be used in conjunction with the corresponding R^2 statistics, presented in Figure 7.9 for the Upper Thames and Figure 7.11 for the Stour, when assessing model performance. Warm-up periods of up to 3 months were used and discounted from the R^2 statistics.

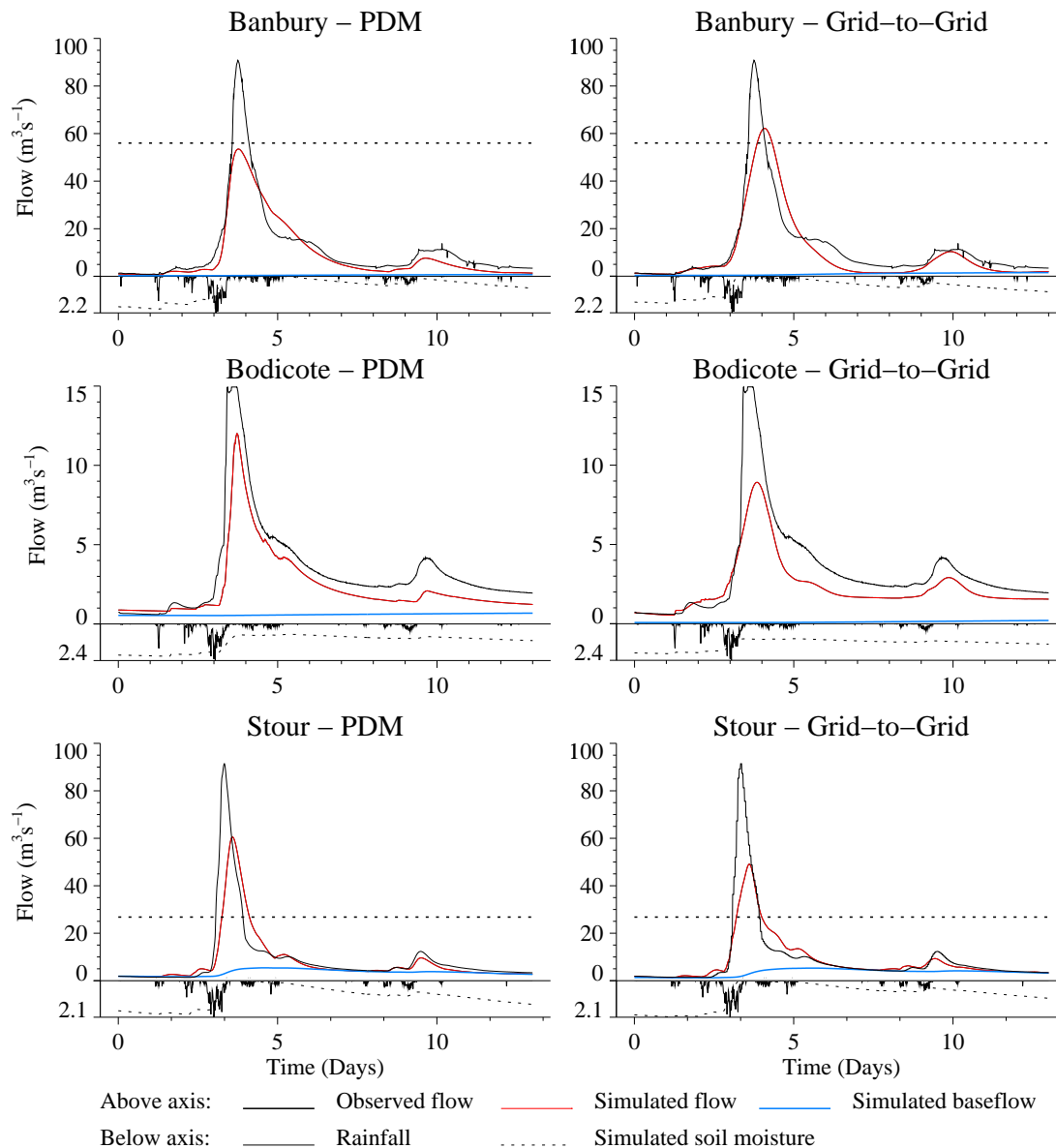


Figure 7.13 Upper Thames and Stour catchment hydrographs for the PDM and Grid-to-Grid models over the case study extreme event: 6 to 19 April 1998. The rainfall estimator used is the raingauge rainfall surface. The figure below the axis is the maximum 15 minute catchment average rainfall for that catchment. The dashed line above the axis indicates the flow associated with the maximum stage used to derive the rating equation for that catchment.

Both model simulations at Banbury perform reasonably well with good R^2 statistics in excess of 0.8; however, both underestimate the 'observed' flood peak. The Grid-to-Grid model gives a larger simulated peak flow than the PDM but is slightly late on the timing.

At Bodicote the model performance is not as good, as reflected in the lower R^2 statistics. Both models underestimate the 'observed' flood peak. The PDM gives the larger simulated flow peak and a better shape to the simulated hydrograph. This is mainly due to the cubic surface storage option used for the Bodicote model. The Grid-to-Grid model gives a better fit to the second peak, around day 10, but does not have a sharp enough response over the main flood peak. The peak timings of both models are in good agreement with the observed. The model results at Bodicote show that the soil moisture deficit of the catchment never reaches zero for either model: see Figure 7.13. This is due to the deep soil stores used by both models and implies that a significant proportion of the rain entering the models infiltrates into the soil stores rather than entering as direct runoff to the fast surface flow paths. Note the model simplification of the PDM version used here, where runoff is only generated from full stores as saturation excess runoff; prolonged moderate rain-rate events might lead in practice to infiltration excess runoff from unfilled stores as near-surface infiltration rates reduce over time.

For the Stour at Shipston both models underestimate the flood peak and are slightly late in the peak timing. The PDM predicts a larger flow peak whilst the Grid-to-Grid model has better agreement with the observed flow on the rising limb, particularly below the rating equation threshold, resulting in a better R^2 statistic.

In summary both models perform reasonably well at all catchments, particularly Banbury, but noticeably they underestimate the 'observed' flows at all catchments. The raingauge network in the vicinity of the Upper Thames and Stour catchments is dense enough that the magnitude of this widespread frontal event has been sufficiently spatially sampled. Also the rain-rates experienced were well within the measuring capabilities of the raingauges. Therefore, the difference between the model and 'observed' peaks must be due to either the extrapolated rating curves overestimating the observed flows or the models underestimating the simulated flows or a combination of both, rather than an underestimate of the rainfall estimator.

7.4.6 Model evaluation over the extreme event – other rainfall estimators

Model performance over the extreme frontal event is assessed for all rainfall estimators. Simulated flows for the River Cherwell at Banbury using composite 2 km and 5 km raw radar data, gauge-adjusted radar data and a raingauge rainfall surface are shown for the PDM and Grid-to-Grid models in Figure 7.14. The R^2 performance statistics over the extreme event are presented in Figure 7.9 for the Upper Thames and Figure 7.11 for the Stour, using both models and all rainfall estimators. Over the extreme rainfall event only 116 out of 3744

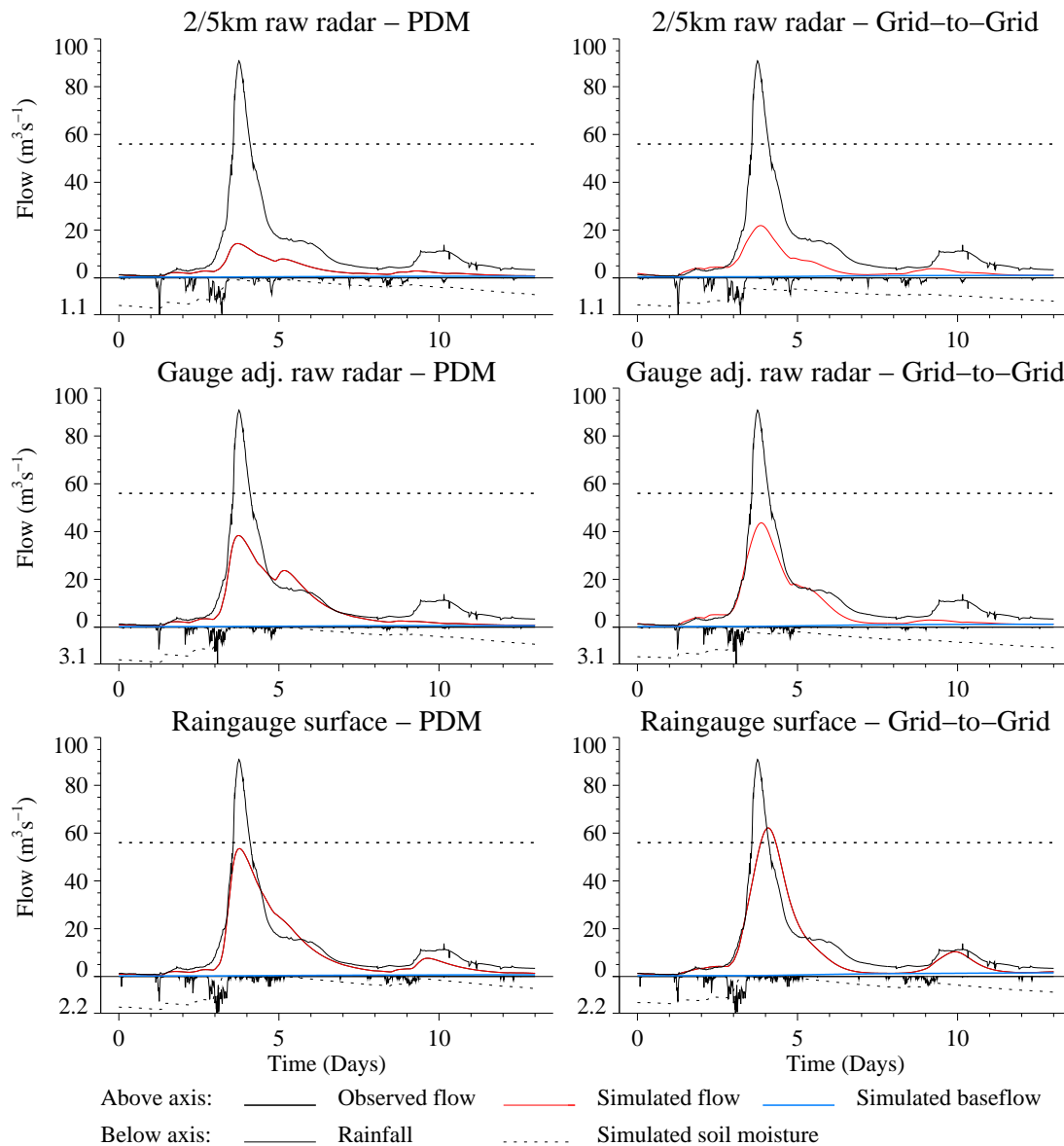


Figure 7.14 River Cherwell at Banbury hydrographs for the PDM and Grid-to-Grid models over the case study extreme event: 6 to 19 April 1998 for different rainfall estimators. The figure below the axis is the maximum 15 minute catchment average rainfall for that catchment. The dashed line above the axis indicates the flow associated with the maximum stage used to derive the rating equation.

(3.1%) 2 km images were missing and 31 out of 1248 (4.2%) 5 km images were missing from the Chenies radar data. Encouragingly most of these did not occur during the main period of rainfall (8 and 9 April 1998) and so there was no significant impact from missing radar data on the model simulations over the extreme event.

The simulated hydrographs give an informative insight into the characteristics of the different rainfall estimators and their use for hydrological modelling. Analysing Figure 7.14 clearly shows both models seriously underestimating the

observed peak when the composite 2 and 5 km raw data are used. This is due to the raw radar data underestimating the rainfall: for example the peak 15 minute catchment average rainfall estimated by the raw radar data is 1.1 mm compared to 2.2 mm for the raingauge rainfall surface. The model performance is significantly improved when gauge-adjusted raw radar data are used and provides more proof of the benefits gauge-adjustment can have. The R^2 performance statistics reveal that the 'raingauge rainfall surface' rainfall estimator gives best modelling results by a considerable margin. The R^2 statistics also show that the PDM and Grid-to-Grid models perform similarly for a given catchment and rainfall estimator with neither model consistently outperforming the other.

7.5 Hydrological case study 3: River Darwen (Convective)

7.5.1 PDM model calibration – weighted raingauge data

The PDM had not previously been calibrated for either of the River Darwen catchments. Hydrometric data were obtained for the year 2002 from which two suitable calibration periods were selected by inspection of the hydrographs and which did not include the flood event of interest. The dates of the calibration events selected are listed in Table 7.2: these encompass different seasons and a reasonable range of flows. Calibration was performed using raingauge data. The final set of raingauge weights derived during calibration is listed in Appendix F.

Since the catchment has a relatively quick response to rainfall, using 15 minute data between events to maintain a water balance had little effect on model performance. As a result, each event was automatically initialised starting from a low period of flow without recent rainfall and a 24 hour warm-up period discounted from the R^2 efficiency performance measure. Model performance was improved by invoking a small soil tension capacity, S_t .

The largest catchment, to Blue Bridge, was calibrated first. Note that the level record at Blue Bridge, converted to flow via a stage-discharge relation, was used for calibration in preference to the ultrasonic flow record as discussed in Section 5.3.2. Initially parameters were manually adjusted and then refined by automatic optimisation over the calibration events. The calibration results obtained for Blue Bridge were very good with R^2 values of 0.974 and 0.938: see Figure 7.15. This calibration was used as a basis for the PDM model for the sub-catchment to Ewood. The model transference was reasonable, although some adjustment was required to capture the flashier response of the smaller sub-catchment which is reflected in the smaller surface routing and baseflow storage parameters. The calibration results at Ewood were also very good with R^2 statistics in excess of 0.9: see Figure 7.15. The sets of calibration parameters obtained are listed in Appendix F for both catchments. The simulated flow from the calibrated PDM is compared to the observed flow for both catchments over the first calibration event in Figure 7.16 where the raingauge rainfall surface is used as the rainfall estimator (allowing a like-for-like comparison with the Grid- to-Grid model performance). These simulations

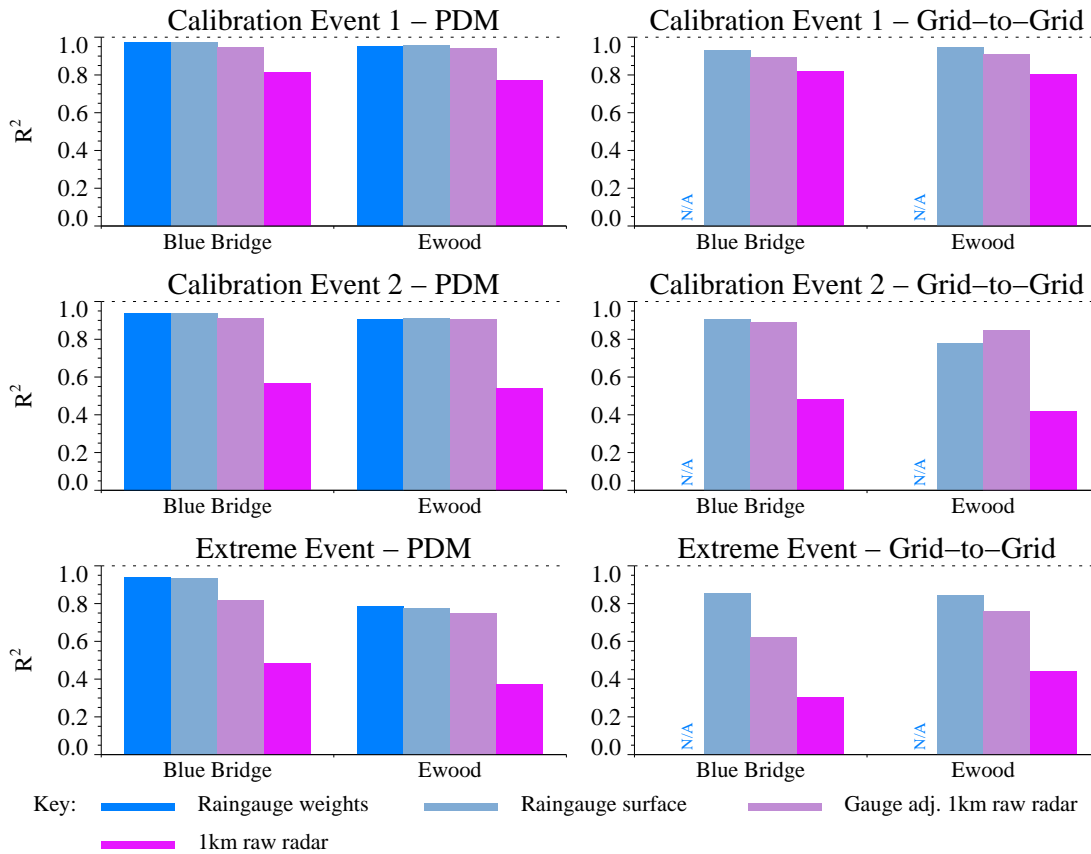


Figure 7.15 River Darwen catchments: R^2 statistics for PDM and Grid-to-Grid models using different rainfall estimators.

are very similar to those using weighted raingauge data and confirm the good model performance.

7.5.2 PDM model calibration – other rainfall estimators

Three other rainfall estimators were investigated for the River Darwen case study: using a fitted raingauge rainfall surface, 1km raw radar and gauge-adjusted 1km raw radar. This is the only case study that was able to use 1km radar data. For each different rainfall estimator only the rainfall factor was reassessed: these are listed in Appendix F.

The rainfall factors for the raingauge rainfall surface and gauge-adjusted 1km raw radar rainfall estimators are all very similar to the rainfall factor calibrated using the raingauge weights as input. The rainfall factor for the 1km raw radar data tended to be slightly higher than that used for the weighted raingauge data.

The R^2 statistics over the calibration events are presented for all rainfall estimators and catchments in Figure 7.15. The statistics show that the raingauge weights or ‘raingauge rainfall surface’ rainfall estimators give the best model performance for both calibration events and all catchments.

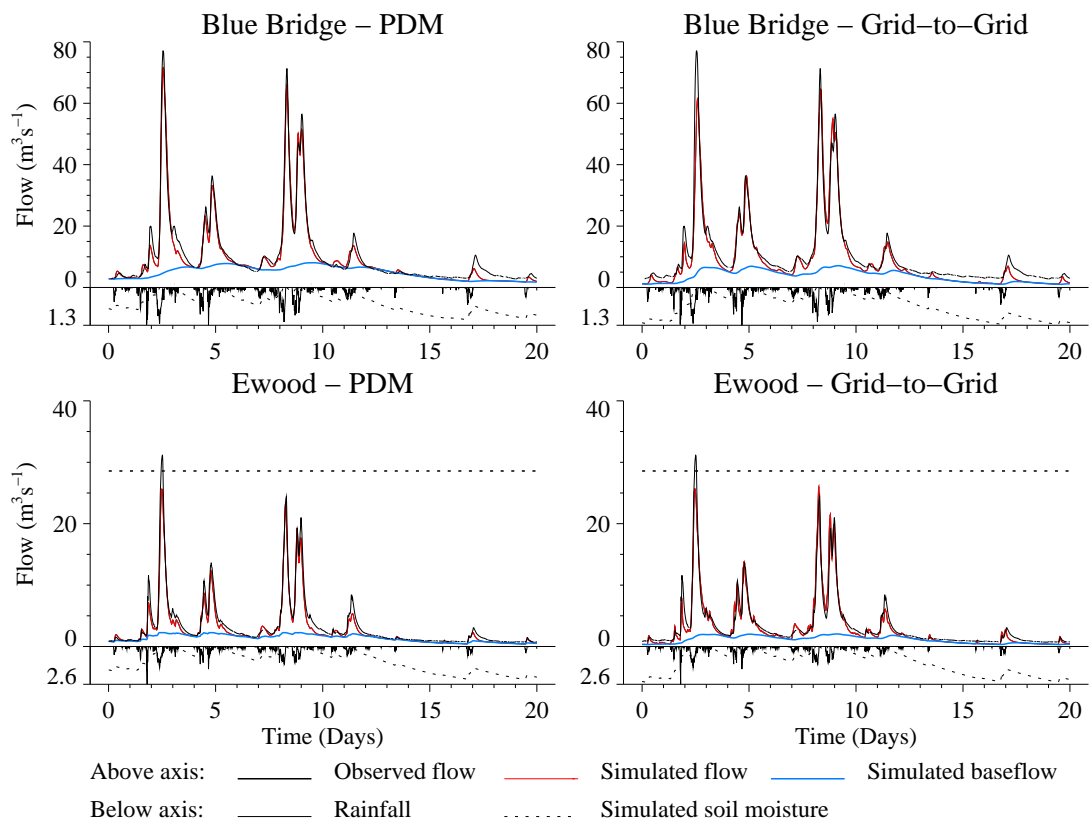


Figure 7.16 River Darwen catchment hydrographs for the PDM and Grid-to-Grid models over the calibration event 17 February to 9 March 2002. The rainfall estimator used is the raingauge rainfall surface. The figure below the axis is the maximum 15 minute catchment average rainfall for that event.

The R^2 statistics also show the significant benefit afforded to model performance by applying the gauge-adjustment to radar data, giving performance statistics comparable with the raingauge-only estimators. Over the 46944 5 minute intervals used for calibration only 767 (1.6%) of 1 km raw images were missing and therefore missing radar images had a negligible impact on model performance.

7.5.3 Grid-to-Grid model calibration – Raingauge data

For this case study the furthest downstream river gauge at Blue Bridge was primarily used to calibrate the distributed Grid-to-Grid model. The River Darwen is another quickly responding catchment that required a routing time-step of 5 minutes. Manual calibration gave good model performance at Blue Bridge over both calibration events.

The R^2 statistics for each catchment over both calibration events when using the raingauge rainfall surface as the rainfall estimator are presented in Figure 7.15. A long warm-up period of 1 month was discounted from the R^2 efficiency

performance measure. These statistics confirm the good model performance at Blue Bridge and show that the distributed model also performed well at Ewood, particularly over the first event. The simulated flow from the calibrated Grid-to-Grid model is compared to the observed flow for both catchments over the first calibration event in Figure 7.16.

The R^2 statistics presented in Figure 7.15 allow comparison between the PDM and the Grid-to-Grid model over the calibration events. Generally there is little difference between the two models but the PDM always performs slightly better when using the raingauge rainfall surface. Visual inspection of the simulated hydrographs over the first calibration event in Figure 7.16 reveals the similarity between the different model simulations.

The calibrated Grid-to-Grid model parameter values are listed in Appendix F. The responsive nature of the catchment is reflected in the relatively quick wave speeds and low regional grid-square maximum soil depth of 40 mm.

7.5.4 Grid-to-Grid model calibration –other rainfall estimators

The other rainfall estimators used in the River Darwen case study were the 1km raw radar data and the gauge-adjusted 1km raw radar data. The R^2 statistics for the Grid-to-Grid model over the calibration events are presented for all rainfall estimators and catchments in Figure 7.15. The statistics show a similar qualitative pattern to the PDM results discussed in Section 7.5.2. The raingauge rainfall surface gives the best model performance followed closely by the gauge-adjusted 1km raw radar data. Generally for a given catchment and rainfall estimator the PDM offers a marginal improvement in model performance but occasionally the Grid-to-Grid model performs best.

7.5.5 Model evaluation over the extreme event – Raingauge data

This section is concerned with the PDM and Grid-to-Grid model performance over the extreme convective event on 14 June 2002 affecting the River Darwen. Note that the raingauge rainfall surface is used as the rainfall estimator in this section.

The simulated model hydrographs are compared to the observed flows in Figure 7.17 for both catchments and both models. These should be used in conjunction with the corresponding R^2 statistics, presented in Figure 7.15, when assessing model performance. Warm-up periods of 24 hours and 1 month were used for the PDM and Grid-to-Grid models respectively.

Both model simulations for Ewood show reasonable agreement up to the limit of the rating equation but underestimate the 'observed' flood peak. The Grid-to-Grid model gives better agreement along the rising limb and a marginally higher peak, resulting in better R^2 statistics. The upper limit of the rating equation used for Blue Bridge is unknown but both models perform well, predicting peaks in excess of $100 \text{ m}^3\text{s}^{-1}$, although both models underestimate the flood peak. For

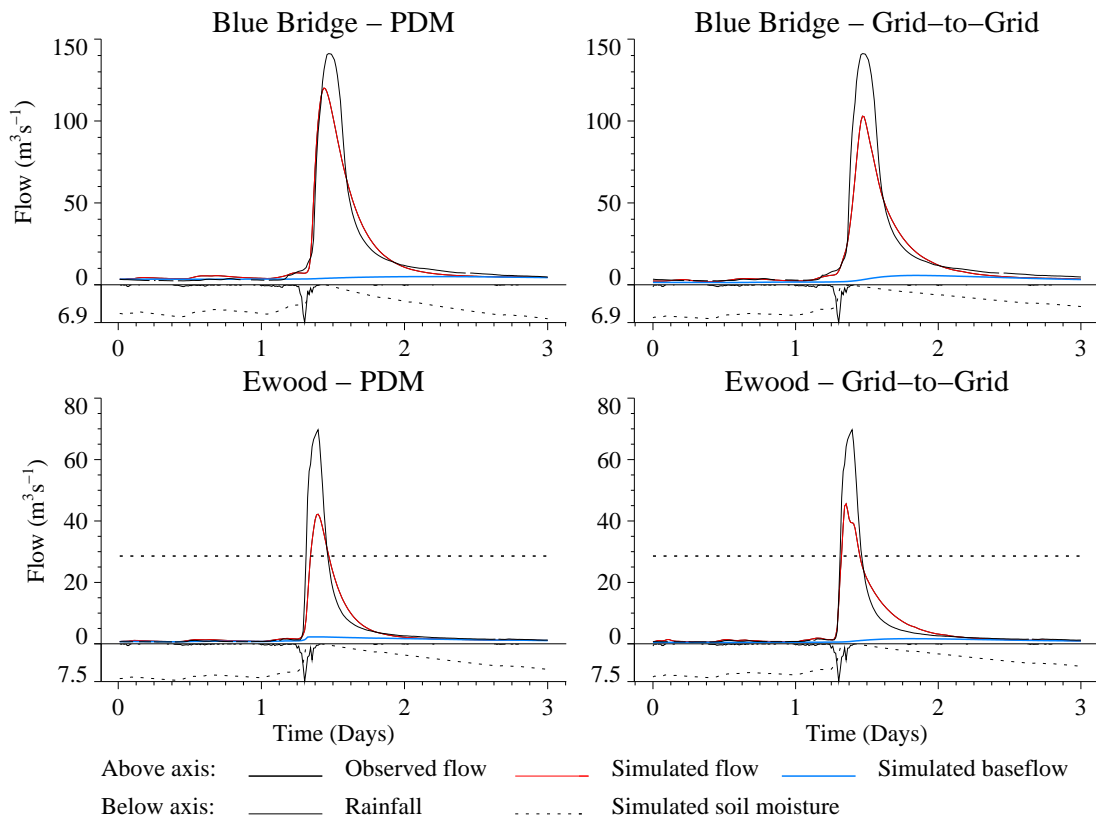


Figure 7.17 River Darwen catchment hydrographs for the PDM and Grid-to-Grid models over the case study extreme event: 13 to 16 June 2002. The rainfall estimator used is the raingauge rainfall surface. The figure below the axis is the maximum 15 minute catchment average rainfall for that catchment. The dashed line above the axis indicates the flow associated with the maximum stage used to derive the rating equation for that catchment.

Blue Bridge the PDM gives better agreement over the rising limb and predicts a higher flood peak than the Grid-to-Grid model and this is reflected in the R^2 statistics.

In summary, when using the raingauge rainfall surface, the PDM gives the best simulations at Blue Bridge and the Grid-to-Grid model performs best at Ewood. Both models simulate the flow peak at Blue Bridge better than at Ewood. This is partly due to the uncertainty in the Ewood rating equation beyond its upper limit of validity. Also, as this is a convective rainfall event there is a danger that the raingauge network may not fully 'experience' the storm but this is slightly mitigated by the relatively dense network in and around the Darwen catchment. Overall the models perform within expectations.

7.5.6 Model evaluation over the extreme event – other rainfall estimators

Model performance over the case study extreme event is assessed for all rainfall estimators. Simulated flows for the River Darwen at Blue Bridge using 1km raw radar data, gauge-adjusted 1km raw radar data and a raingauge rainfall surface are shown for the PDM and Grid-to-Grid models in Figure 7.18. The R^2 performance statistics over the extreme event are presented for both models over all catchments and rainfall estimators in Figure 7.15.

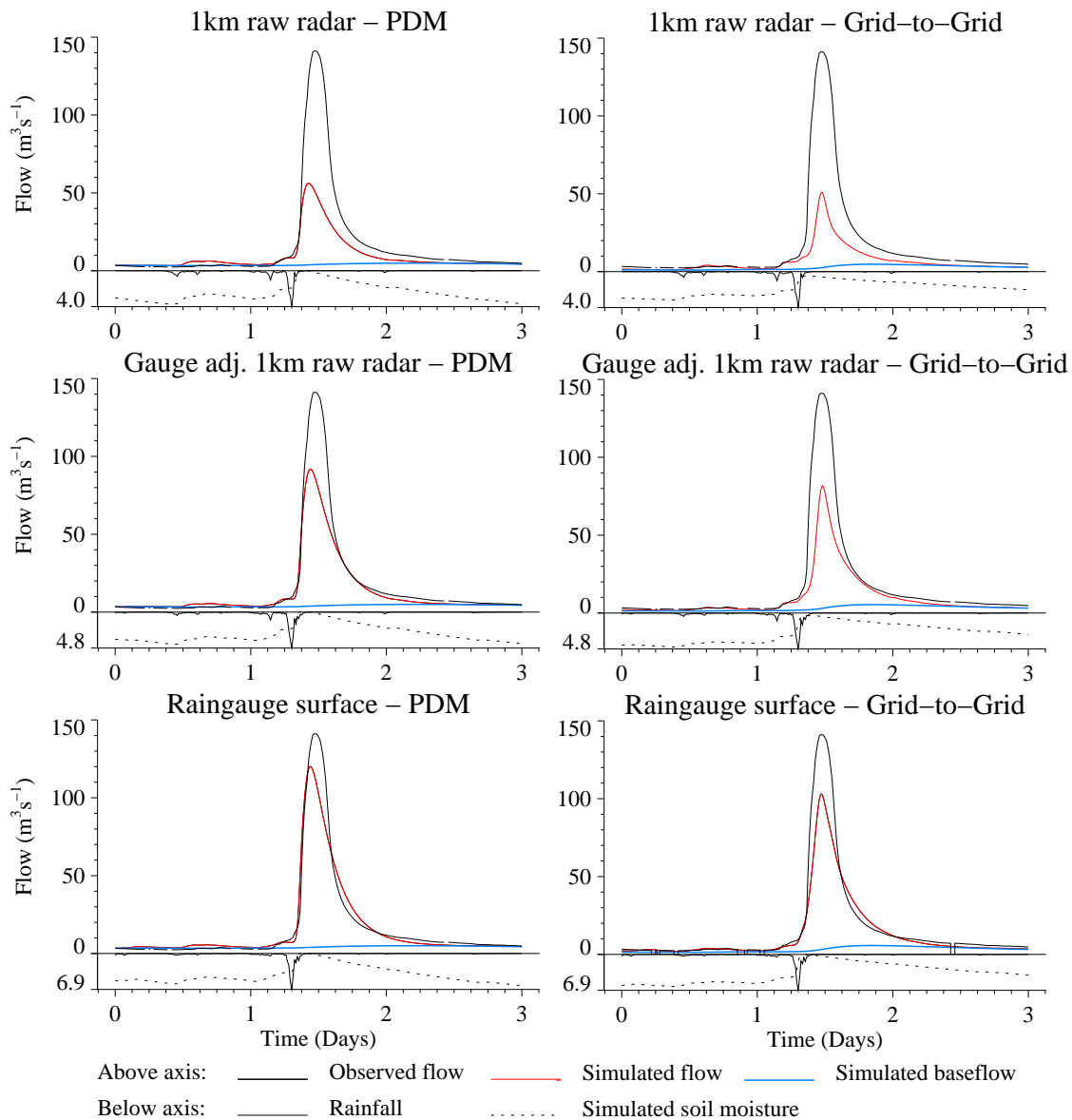


Figure 7.18 River Darwen at Blue Bridge hydrographs for the PDM and Grid-to-Grid models over the case study extreme event: 13 to 16 June 2002 for different rainfall estimators. The figure below the axis is the maximum 15 minute catchment average rainfall for that catchment. The dashed line above the axis indicates the flow associated with the maximum stage used to derive the rating equation.

Encouragingly only 3 radar images were missing over the case study so there was no impact from missing radar data on the model simulations over the extreme event.

The simulated hydrographs give an informative insight into the characteristics of the different rainfall estimators and their use for hydrological modelling. Analysing Figure 7.18 clearly shows both models seriously underestimating the observed peak when 1km raw data are used. The model performance is significantly improved when gauge-adjusted 1km raw radar data are used and provides more proof of the benefits gauge-adjustment can have. The R^2 performance statistics reveal that the 'raingauge rainfall surface' rainfall estimator gives best modelling results followed by the gauge-adjusted 1km radar data. The R^2 statistics also show that at Blue Bridge the PDM outperforms the Grid-to-Grid model for all rainfall estimators whereas at Ewood the Grid-to-Grid model performs best. This highlights that one model does not always perform 'best' for all catchments.

7.6 Prototype model development incorporating soil/geology information

Motivated by the shortcomings of the basic form of the Grid-to-Grid model to simulate the flood response across the Upper Thames and Stour catchments using a single set of regional parameters, this section considers the application of a new variant able to utilise both soil/geology and topographic information. A general approach to rainfall-runoff modelling based on a simple kinematic wave model foundation, as described in Section 3.3.2, is followed. The prototype model formulation allows the influence of soil/geology properties to be introduced into the model in a physically-based way using available digital datasets. Formulations are employed for lateral soil drainage, surface runoff and recharge that can make use of datasets on soil/geology properties and topography, instead of using site-calibrated parameters. The nature and limited availability of certain soil/geology properties has necessitated the use of various approximations in applying the prototype model formulation. Improvements to the nature and availability of spatial datasets for soil/geology/land-cover properties will strengthen the model's underpinning by properties, rather than calibrated model parameters, in the future.

The main motivation of this prototype model is to develop a region-wide model that encompasses the entire area affected by the extreme flood in order to help understand flood genesis and to improve hydrological modelling.

Digitised soil datasets

A derived quantity called the HOST (Hydrology of Soil Types) class is available with UK coverage. This classification has 29 classes and encompasses soil type, hydrological response and substrate hydrogeology (Boorman *et al.*, 1995). The database for England and Wales, which is available at a 1km resolution, is based on the soil-survey 1:250,000 maps produced by the Soil Survey and

Land Research Centre. A map of HOST classes covering the case study catchments in the Upper Thames and Stour is presented in Figure 7.7 (Section 7.4.1).

Although this classification only provides an integer identifier for 29 different soil types, a database of derived soil attributes supports the derivation of these classes and consists of properties such as air capacity, parent material, depth to gleying and depth to slowly permeable layer. These derived soil attributes are not made available as part of the standard HOST dataset. Here, highly derived soil properties have been extracted from the soil properties database, SEISMIC, available from the National Soil Resources Institute (NSRI). In SEISMIC, soil series are analysed down to a depth of 1.5 m. There are normally several horizons present in a given series. An upper and lower depth and some other soil properties are available for each horizon.

By comparing information from SEISMIC with the HOST dataset, Ragab *et al.* (pers. comm.) associated statistics for values of five soil properties with each of the 29 HOST classes. These properties are as follows:

- water content at field capacity, θ_{fc} : fractional volume at 5KPa
- residual water content, θ_r : half the fractional volume at 1500KPa
- porosity, ϕ : fractional volume
- hydraulic conductivity at saturation: k_s (cm d^{-1})
- depth to “C” and “R” horizons (cm).

Mean values for these soil properties for each HOST class are presented in Table 7.3. The depths to “C” and “R” horizons consist of two values. The SEISMIC User Manual defines the C-layer as “mineral substrate, relatively unweathered ‘soft’ unconsolidated material, gravel or rock rubble”, and the R-layer as “relatively unweathered, coherent rock”. The depth to the R-layer has been used here as a surrogate for soil depth. Where a value for depth to the R-layer is not available, the depth to the C-layer is used instead. In many cases (but not all), depth to the R-layer for each soil type is greater than the depth to the C-layer.

The residual soil water content, θ_r , and the saturated hydraulic conductivity, k_s , can be used directly in the runoff production scheme with lateral soil water drainage described in Section 7.6.1. The water content at field capacity, θ_{fc} , represents the water content below which drainage becomes negligible. As a rule of thumb, $\theta_{fc} = \theta_s / 2$, where θ_s is the water content at saturation (Or and Wraith, 2002). An estimate of θ_s is required for the runoff-production scheme and this might be seen to provide a convenient approximation. However, values for θ_{fc} in Table 7.3 range from 0.25 to 0.49 and seem rather large compared to

Table 7.3 Soil properties associated with each HOST class

| HOST class | Water content | | Porosity, ϕ (% volume) | Hydraulic conductivity, k_s (cm d ⁻¹) | Average depth to R-layer (cm) |
|------------|--|---|-----------------------------|---|-------------------------------|
| | at 5 kPa (field capacity, θ_{fc}) | at 1500 kPa (2 × residual, $2\theta_r$) | | | |
| 1 | 0.381 | 0.178 | 0.504 | 132. | 77. |
| 2 | 0.394 | 0.182 | 0.533 | 151. | 95. |
| 3 | 0.255 | 0.082 | 0.474 | 383. | 47. |
| 4 | 0.373 | 0.147 | 0.536 | 229. | 71. |
| 5 | 0.258 | 0.088 | 0.472 | 367. | 72. ^{*c} |
| 6 | 0.371 | 0.175 | 0.477 | 85. | 39. ^{*c} |
| 7 | 0.252 | 0.085 | 0.469 | 367. | 63. ^{*c} |
| 8 | 0.359 | 0.160 | 0.486 | 143. | 42. ^{*c} |
| 9 | 0.417 | 0.209 | 0.520 | 101. | 10. |
| 10 | 0.326 | 0.132 | 0.517 | 319. | 65. ^{*c} |
| 11 | 0.326* | 0.156* | 0.517* | 156.* | 100. ^{*c} |
| 12 | 0.346 | 0.156 | 0.477 | 156. | 100. ^{*c} |
| 13 | 0.330 | 0.142 | 0.459 | 138. | 62. |
| 14 | 0.344 | 0.158 | 0.436 | 58. | 14. |
| 15 | 0.346 | 0.121 | 0.540 | 322. | 65. |
| 16 | 0.352 | 0.162 | 0.469 | 108. | 52. |
| 17 | 0.396 | 0.175 | 0.531 | 138. | 35. |
| 18 | 0.353 | 0.174 | 0.442 | 64. | 59. |
| 19 | 0.361 | 0.126 | 0.547 | 302. | 66. |
| 20 | 0.420 | 0.230 | 0.467 | 29. | 50. |
| 21 | 0.391 | 0.207 | 0.459 | 29. | 78. |
| 22 | 0.405 | 0.158 | 0.602 | 333. | 106. |
| 23 | 0.447 | 0.260 | 0.495 | 18. | 48. |
| 24 | 0.376 | 0.198 | 0.452 | 51. | 39. |
| 25 | 0.429 | 0.248 | 0.469 | 24. | 27. ^{*c} |
| 26 | 0.408 | 0.201 | 0.490 | 57. | 80. |
| 27 | 0.488 | 0.229 | 0.688 | 329. | 132. |
| 28 | 0.488* | 0.229* | 0.688* | 329.* | 132.* |
| 29 | 0.488* | 0.229* | 0.688* | 329.* | 132.* |

* Indicates missing property values, now replaced by an estimated value for similar soil types.

^{*c} Indicates soils for which there is no value for depth to R-layer, so the value for depth to C-layer has been used instead.

literature values ranging from 0.1 for fine sand to 0.39 for clay (Dunne and Leopold, 1978). For the present purposes it will be assumed that $\theta_s = 1.25 \theta_{fc}$, which results in values of θ_s ranging from 0.31 to 0.61

The prototype distributed model and its use of these soil properties is detailed in the next section.

7.6.1 Enhanced Grid-to-Grid Model formulation

Runoff production scheme with lateral soil water drainage

Consider a sloping soil column of depth L and slope s_0 subject to precipitation falling at a rate p (ms^{-1}) as shown in Figure 7.19.

The actual and maximum water contents (m) in the column are given by

$$S = (\theta - \theta_r)L \quad (7.1)$$

$$S_{\max} = (\theta_s - \theta_r)L, \quad (7.2)$$

where θ_s is the content at saturation and θ_r is the residual content, estimated from HOST/SEISMIC data.

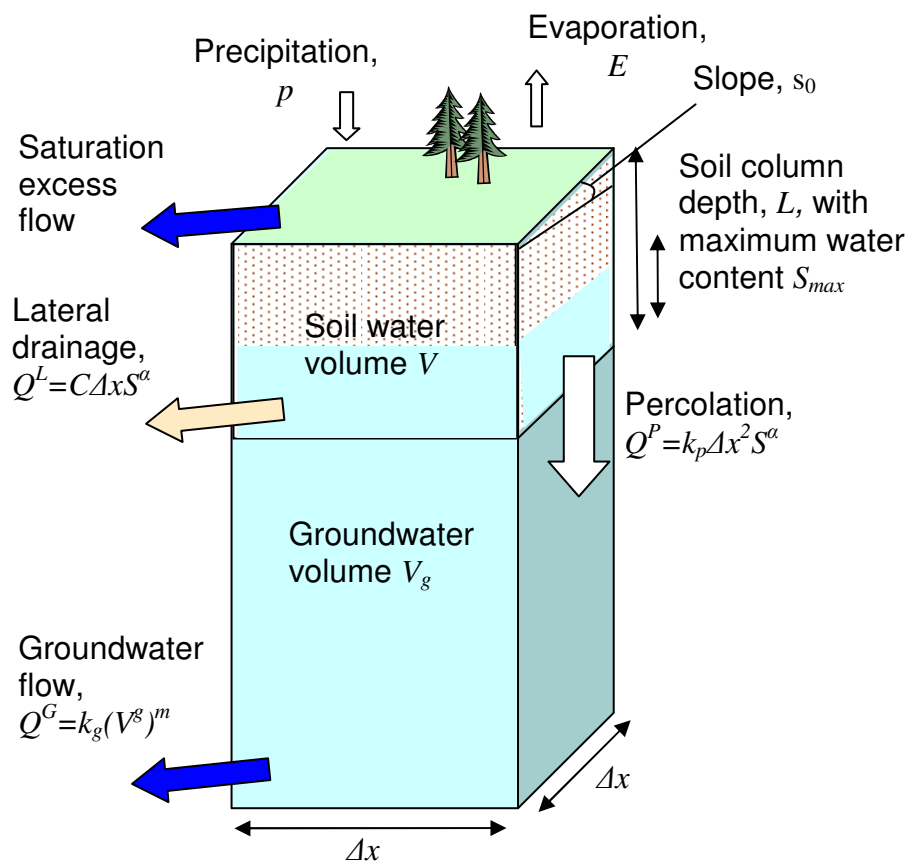


Figure 7.19 Conceptual diagram showing runoff production and lateral drainage in a sloping soil column.

Let $V = \Delta x^2 S$ denote the volume of water stored in the unsaturated layer of the i th soil column. From continuity, the rate of change in water volume is given by

$$\frac{\partial V}{\partial t} = p\Delta x^2 + Q^I - Q^L - Q^P, \quad (7.3)$$

where, Q^I is the inflow to cell i from contributing upstream cells, Q^L is the lateral drainage from the cell and Q^P is the downward percolation (drainage) to the saturated zone.

Lateral drainage, Q^L is given by

$$Q^L = \frac{C \Delta x}{\Delta x^{2\alpha}} V^\alpha = C \Delta x S^\alpha. \quad (7.4)$$

C is the conveyance term given by $C = Lk_s^L s_0 / S_{\max}^\alpha$, where s_0 is the local slope, derived from digital elevation data. The lateral saturated hydraulic conductivity, k_s^L is unknown but is assumed to be related to the vertical k_s taken from HOST/SEISMIC data via the relation $k_s^L = 1000k_s$. The parameter α is linked to the Brooks and Corey relation for hydraulic conductivity and typical values lie between 3 and 4, although a value of 1 has been used for the initial model formulation described here.

Percolation (a vertical downward flow, m^3s^{-1}), Q^P , is represented as a simple power law function of the soil water volume V , expressed as a fraction of the saturated water volume V_{\max} ,

$$Q^P = k_p \Delta x^2 \left(\frac{V}{V_{\max}} \right)^{\alpha_p} = k_p \Delta x^2 \left(\frac{S}{S_{\max}} \right)^{\alpha_p}, \quad (7.5)$$

where k_p is a vertical saturated hydraulic conductivity of the soil (ms^{-1}) and α_p is the exponent of the percolation function. Spatially varying estimates for k_p are not routinely available, so k_p is assumed to be linearly related to k_s , i.e. $k_p = \lambda k_s$, where λ is treated as a spatially invariant model parameter. Clapp and Hornberger (1978) indicate, on the basis of soil experiments, that α_p can vary from circa 11 for sand to 25 for clay. Here a constant value for α_p of 15 has been assumed.

A soil water balance for a time-step $(t_0, t_0 + \Delta t)$ gives the saturation excess flow volume as

$$q = \max\{[V'(t_0 + \Delta t) - \min(V'(t_0 + \Delta t), V_i^{\max})], 0\} \quad (7.6)$$

where V^{\max} is the saturated soil water storage.

The storage at the end of the interval is

$$V(t_0 + \Delta t) = \min(V'(t_0 + \Delta t), V^{\max}) - E_a \Delta x^2, \quad (7.7)$$

where E_a is the actual evaporation.

It is assumed that percolation freely drains as recharge to the groundwater saturated zone (for the cell), so that recharge $Q^R \equiv Q^P$. Let V^g denote the groundwater volume (m^3) stored in the cell and s_b the slope of the underlying bedrock in the flow direction.

Continuity for the groundwater volume is

$$\frac{dV^g}{dt} = Q^P - Q^G \quad (7.8)$$

where Q^G is the lateral groundwater flow from the cell.

Darcy's law gives the lateral groundwater flow out of the cell to a reasonable approximation by the linear relation

$$Q^G = \frac{k_g s_b}{\Delta x} V^g \quad (7.9)$$

where k_g is the horizontal hydraulic conductivity of the aquifer. However, suitable values for bedrock slope, s_b , and conductivity, k_g , are not straightforward to obtain. One approach is to assume that bedrock slope mirrors the surface topographic slope which can be estimated from digital terrain data. Conductivity information may be obtained from geology datasets but obtaining meaningful values for the present scale of application may present difficulties. For the present prototyping purposes geological datasets have not been used. Instead, a nonlinear storage function relating groundwater flow to volume has been invoked, such that

$$Q^G = k(V^g)^m, \quad k > 0, \quad m > 0, \quad (7.10)$$

where k is a rate constant with units of inverse time and m is the nonlinear power. For this application, a cubic storage function has been assumed ($m=3$), and k is treated as a spatially invariant parameter for estimation.

7.6.2 Estimation of river flows using the Grid-to-Grid routing model

Runoff from the soil column is considered to consist of the saturation excess flow volume, q , and groundwater flow, Q^G . These values of gridded runoff form the lateral inflows to the Grid-to-Grid routing model, which consists of a kinematic wave formulation for routing both surface and sub-surface gridded runoff to estimate river flow as outlined in Section 3.3.2. Figure 7.20 summarises the key features of the coupled runoff-production and routing scheme.

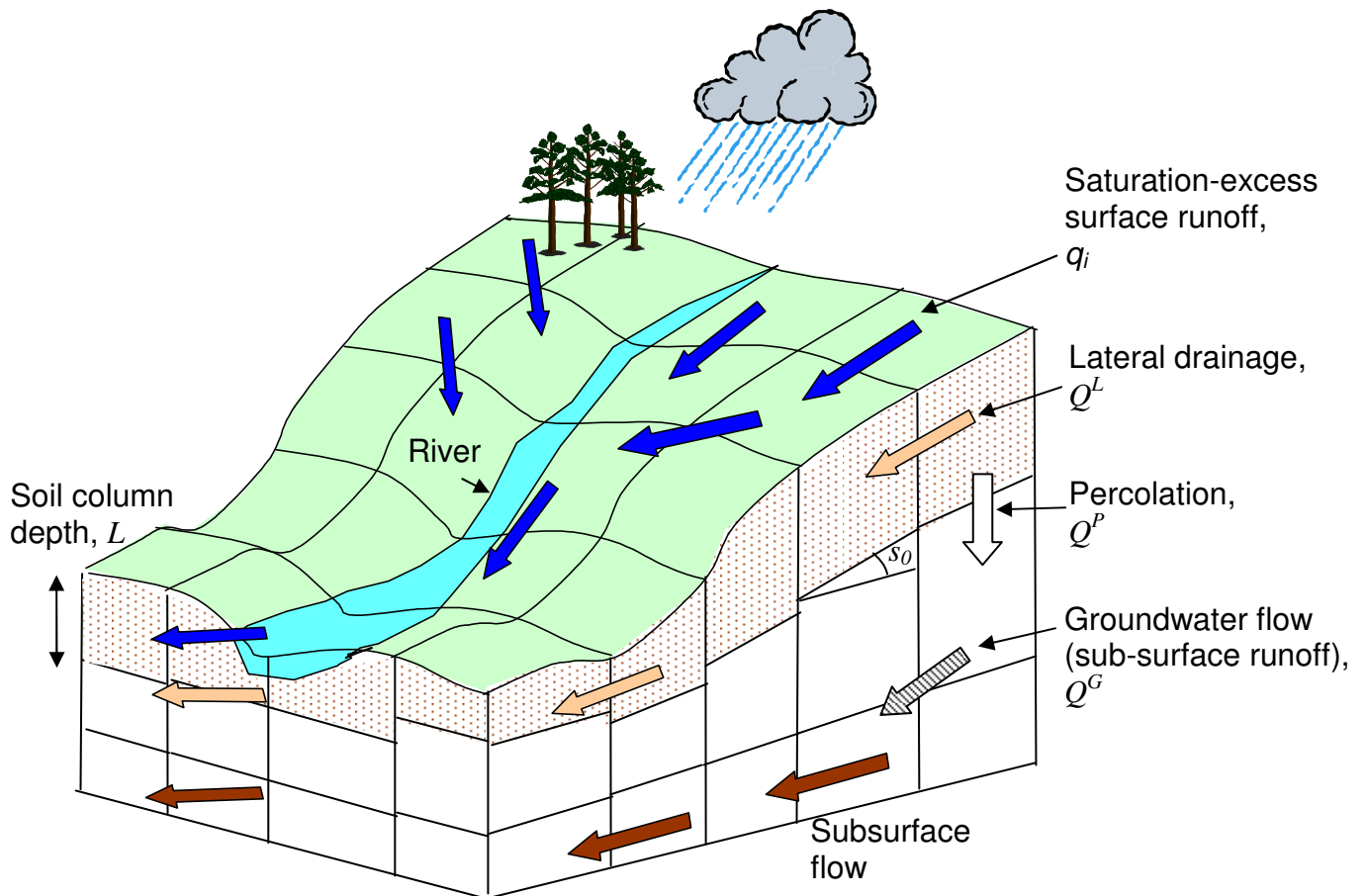


Figure 7.20 Key features of the coupled runoff-production and routing scheme.

7.6.3 Prototype model configuration

The Grid-to-Grid routing model requires the two DTM-derived datasets:

- (i) flow directions (each grid-cell can drain in only one of 8 directions),
- (ii) area draining to each 1 km grid-cell,

whilst the prototype runoff production scheme with lateral soil water drainage currently requires the following five digital datasets:

- average slope,
- residual soil water content, θ_r ,
- saturated soil water content, θ_s ,
- saturated hydraulic conductivity, k_s
- soil depth, L .

However, values for soil properties such as bedrock slope, s_b , horizontal hydraulic conductivity of the aquifer, k_g , vertical saturated hydraulic conductivity of the soil, k_p , lateral saturated hydraulic conductivity, k_s^L , and the exponents of the percolation function, α_p , and lateral drainage function, α , are currently not available as gridded datasets and have had to be estimated through parameterisation. Improved availability of datasets such as these should lead to a more physically-based formulation and less reliance on parameter adjustment.

Catchment average values of soil properties currently used by the model are presented in Table 7.4, together with values for the maximum soil water content, S_{max} , derived from soil depth and soil water content (residual and field capacity) properties using equation (7.2) and the modified rule-of-thumb between field capacity and saturated values.

Table 7.4 Catchment average values of soil properties for the Upper Thames and Stour catchments

| Catchment | Area (km ²) | Water content | | Depth (cm) | K_s (cm/day) | S_{max} (cm) range of values in brackets |
|---------------------|-------------------------|---|--|------------|----------------|--|
| | | at 5 kPa (field capacity, θ_{fc}) | at 1500 kPa (2 × residual, $2\theta_r$) | | | |
| Stour at Shipston | 185.2 | 0.418 | 0.229 | 46.9 | 55 | 24.0 (14.5-46.8) |
| Cherwell at Banbury | 199.4 | 0.416 | 0.229 | 43.4 | 53 | 22.2 (5.2-46.8) |
| Sor at Bodicote | 87.7 | 0.402 | 0.198 | 78.4 | 118 | 38.9 (14.5-46.8) |

7.6.4 Prototype model calibration and assessment

The prototype distributed model has been designed for area-wide application, providing estimates of flow for rivers throughout the Upper Thames and Stour region, irrespective of catchment boundaries. A small number of properties not set solely using digital datasets are set manually at a regional level and are treated as parameters for model calibration. These control the overall runoff response and flow translation of the model and are used, along with the gridded property datasets, to derive the grid-cell parameter values.

The model parameters have been manually adjusted for the period 1 September 2000 to 1 June 2001 using the raingauge-only rainfall surface data. In practice, the parameters have been manually calibrated to obtain the best match between modelled and observed flows at the two Upper Thames catchments only.

Table 7.5 presents a single set of routing and runoff-production model parameters for the whole Upper Thames and Stour region. Note that this is in contrast to Section 7.4 where the Grid-to-Grid model was calibrated on a catchment by catchment basis.

Table 7.5 Parameter values for the prototype distributed model

| Parameter name | Symbol | Units | Typical value | Description |
|----------------------------------|----------|------------------|--------------------|---|
| <i>Routing model parameters:</i> | | | | |
| Surface wave speeds: | | | | |
| Land: | c_l | ms^{-1} | 0.2 | Related to the flow velocity |
| River: | c_r | ms^{-1} | 0.25 | |
| Sub-surface wave speeds: | | | | |
| Land: | c_{lb} | ms^{-1} | 0.15 | Usually less than the surface wave speed |
| River: | c_{rb} | ms^{-1} | 0.15 | |
| Return flow factors: | | | | |
| Land: | r_l | - | 0.00 | Proportion of the sub-surface store that is routed to the surface/river |
| River: | r_r | - | 0.008 | |
| <i>Runoff model parameters:</i> | | | | |
| Drainage storage rate constant | k_p | s^{-1} | 0.00002 | Regulates drainage from the soil store into the saturated groundwater store |
| Baseflow storage rate constant | k_g | s^{-1} | 5×10^{-7} | Regulates drainage from the groundwater store into sub-surface runoff |

Model performance for the calibration and assessment periods is summarised in terms of the R^2 statistic in Table 7.6. Note that a single set of model parameters has been used to estimate flows for all catchments. Both calibration and evaluation periods were preceded by a two month “warm-up” period which has not been included in the performance evaluation. Modelled and observed flow hydrographs for the Upper Thames and Stour catchments are presented for the calibration and evaluation events in Figure 7.21.

The results over the calibration event show that the prototype distributed model is able to broadly reproduce a wide range of hydrological behaviour in catchments which have very different responses to rainfall. This is very encouraging for modelling flood response in regions, such as the Upper Thames, where heterogeneous soil/geology controls dominate over topographic controls. However, there can be a trade-off between using region-wide models and model performance for specific catchments. For the Upper Thames and Stour, the PDM and Grid-to-Grid models calibrated specifically for each catchment (see Section 7.4) perform better. This is accentuated over the extreme event where the prototype distributed model underestimates both the observed flood peaks and the simulated peaks from the catchment calibrated PDM and Grid-to-Grid models. The prototype distributed model simulations for the Sor at Bodicote, the slowest responding catchment, indicate that the hydrograph recession is too steep resulting in underestimation of the slow component of flow following a flow peak.

In summary, the prototype distributed model shows potential for modelling across regions where mixed soil and geology properties play a significant role in the flood response and can give insight into the flood formation process on a regional scale not possible using the topographically-controlled Grid-to-Grid model. This is particularly relevant for large-scale frontal rainfall events acting over lowland catchments. Unfortunately the trade-off between attempting to model an entire region and the model performance at specific locations means that region-wide models are nearly always outperformed by models calibrated at specific catchments. However, the prototype distributed model has shown enough potential to merit further research in narrowing the gap and addressing other model deficiencies highlighted earlier.

Table 7.6 Summary of model performance for the prototype distributed model using 15 minute raingauge rainfall surface data

| Catchment | R^2 | |
|---------------------|---|--------------------------------------|
| | Calibration period 1 Sep 2000 – 1 Jun 2001 | Evaluation period 6-19 April 1998 |
| Cherwell at Banbury | 0.592* | 0.506 |
| Sor at Bodicote | 0.676* | 0.438 |
| Stour at Shipston | 0.524 ¹ | 0.455 |

*In practice calibration has been undertaken on these catchments alone.

¹The calibration period used for the Stour to Shipston was 1 November 1991 to 1 May 1992

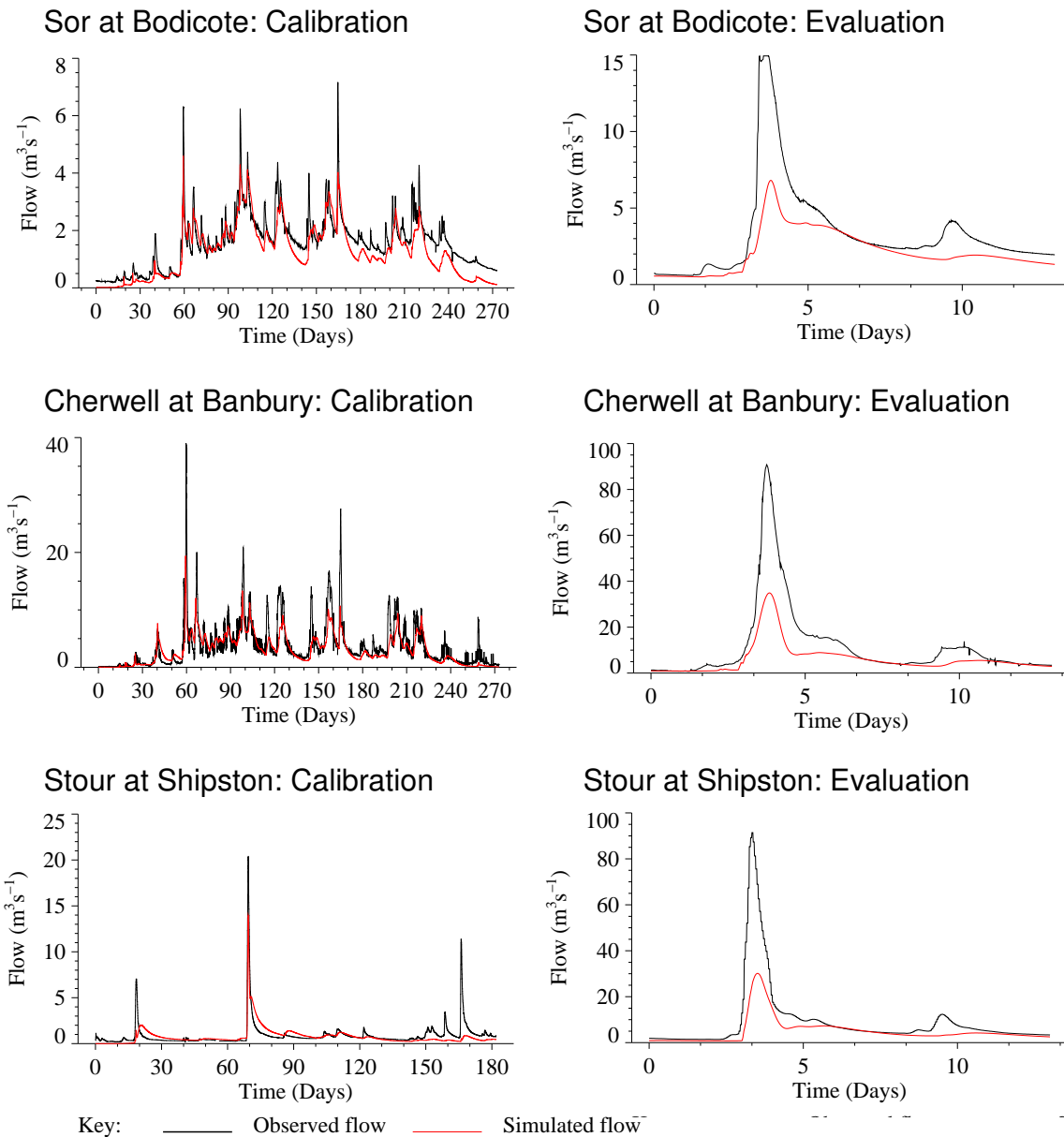


Figure 7.21 Upper Thames and Stour hydrographs for the prototype distributed model over the calibration event (1 September 2000 to 1 June 2000 for the Upper Thames, 1 November 1991 to 1 May 1992 for the Stour at Shipston) and evaluation event (6 to 19 April 1998). The rainfall estimator used is the raingauge rainfall surface.

7.7 Conclusions

Section 7 has investigated the flood response of case study catchments using both lumped and distributed rainfall-runoff models. The models have been calibrated using historical records for the catchments and independently assessed over the extreme events. The insights gained are summarised here as a set of conclusions split into three categories: (i) model calibration, (ii) model responses over the extreme events and (iii) areas for further investigation.

Model Calibration

- The responsive ‘flashy’ catchments of the River Kent (orographic case study) and the River Darwen (convective case study) were easiest to calibrate for both models. These are typical of upland catchments where topographic controls dominate flood hydrograph formation and soil/geology controls are homogeneous or weak. Very good model performance was achieved over the calibration events with R^2 performance statistics in excess of 0.9 for both models over all catchments.
- The Upper Thames and Stour catchments (frontal case study) proved more difficult to calibrate. These are lowland basins where complex flood responses are dominated by heterogeneous soils and geology controls rather than topographic controls. For the Sor catchment to Bodicote the deep soils covering the catchment give a significant slowly responding baseflow component to the historical hydrographs which proved challenging to model. For the Cherwell to Banbury the human influence on the historical hydrograph record is evident and hampered model calibration. These difficulties were partly overcome by using different model configurations available in the current models e.g. the cubic surface storage for the PDM at Bodicote. Also it has prompted model development e.g. looking at the digital datasets used by the Grid-to-Grid model and obtaining preliminary results from a prototype extended formulation which incorporates soil/geology controls via the HOST/Seismic dataset (see Section 7.6). The difficulties in calibrating the Grid-to-Grid model and PDM for the Upper Thames and Stour are reflected in the comparatively lower R^2 performance statistics.
- Which **rainfall estimator** gave the best hydrological model performance over the calibration events?
 - Generally the raingauge-based estimators (i.e. weighted raingauge data or a spatial surface fitted to raingauge rainfall data) performed best for both models.
 - When using radar-based rainfall estimators, without raingauge-adjustment, model hydrographs showed intermittent periods of over-/under-estimation of observed flows. The implication is that the radar data intermittently over-/under-estimates rainfall. This made model calibration from scratch virtually impossible so, for

the Grid-to-Grid model, the calibrated parameters obtained using the raingauge data were used whilst, for the PDM, only the rainfall factor was reassessed. The temporal fluctuations of the radar data impacted adversely on the model performance statistics. Also, as the calibration events covered long periods some (less than 8%) of the radar data were missing and this occasionally worsened the modelling performance.

- Adjusting radar data using raingauge data dramatically improved model performance and generally gave model R^2 performance statistics that were comparable to the raingauge-based estimators. This was encouraging as the model parameters derived using raingauge data were used apart from the rainfall factor for the PDM which was reassessed. This underlined the added value that combining raingauge and radar data can have for hydrological modelling whilst preserving the spatial information of the radar data.
- Which **hydrological model** performed best over the calibration events?
 - For raingauge-based rainfall estimators the PDM almost always offered a marginal improvement over the Grid-to-Grid model. This is not entirely surprising since, due to computation demands, automatic optimisation is not currently available for the Grid-to-Grid model whereas it is available for the PDM.
 - For other rainfall estimators neither model consistently outperformed the other.

Model responses over the extreme events

- None of the case studies revealed a serious 'model failure' but all models **underestimated** the 'observed' extreme flood peaks. Why?
 - **Flow observations:** All 'observed' flood peaks are beyond the upper limit of the rating curve. Therefore there is some uncertainty in the extrapolation of the rating curve used to derive the 'observed' flow values.
 - **Rainfall estimators:** The raingauge-based estimators generally gave the best model agreement over the extreme case studies. They were assumed to be reasonably accurate for the widespread frontal (Upper Thames and Stour) and orographic (River Kent) extreme events as the raingauge networks are relatively dense and the rain-rates experienced were well within measuring capabilities. For the convective (River Darwen) extreme event instantaneous rain-rates and the spatial variability were much higher. Therefore, despite a dense raingauge network, the raingauge-based estimators are less certain for the convective case study.
 - **Model parameter uncertainty.** There will always be model parameter uncertainty but it was mitigated by selecting calibration events which covered different seasons and a range of flows,

although none of the calibration events included a flow event as extreme as the case study events.

- **Model structure inadequacy.** For both the PDM and Grid-to-Grid models several configurations were considered when calibrating the models to give the best simulations. It could be that a key process in the genesis of extreme floods is not sufficiently represented in the current model configurations and that further model development is required. However, there is no clear evidence of this. Without further investigation of other model structures it is not possible to decide if model inadequacy has caused an underestimate by the modelled flows. As one example, it is common to assume that saturation excess runoff dominates over infiltration excess runoff when formulating models for application to catchments in humid temperate areas. It is possible that explicit modelling of the former may have benefit for extreme storms but this is far from being clear and adds to model complexity.
- Which **rainfall estimator** gave the best hydrological model performance over the extreme case study events?
 - The raingauge-based estimators (i.e. weighted raingauge data or a spatial rainfall surface fitted to raingauge data) performed consistently well over all case studies and provided the best model performance for most catchments.
 - When using radar-based rainfall estimators, without raingauge-adjustment, model hydrographs showed intermittent periods of over-/under-estimation of observed flows. In particular the model peaks seriously underestimated the flood peaks for the convective and frontal extreme case studies. Encouragingly the radar records over the extreme events were almost entirely complete and so missing radar data had little impact on model performance. The temporal fluctuations of the radar data impacted adversely on the model performance statistics and generally radar-based rainfall estimators gave the worst hydrological model performance statistics over the extreme events.
 - Adjusting radar data using raingauge data dramatically improved model performance and generally gave model R^2 performance statistics that were comparable to the raingauge-based estimators. In some instances, such as the orographic extreme case study, the gauge-adjusted radar gave the best hydrological model performance. This further underlined the added value that combining raingauge and radar data can have for hydrological modelling whilst preserving the spatial information of the radar data.
- Which **hydrological model** performed best over the extreme events?
 - Neither model consistently outperformed the other. Visual inspection of the simulated hydrographs used in conjunction with the R^2 performance statistics reveals that both models were, generally, in good agreement with one another (but not always

with the observed flows). The agreement between different models is, on the one hand, partly due to the calibration process but, on the other hand, can be seen as a source of model validation adding confidence to the simulated flows.

Areas for further investigation

- Conceptual-physical distributed models should be improved to capitalise on spatial soil/geology/land-cover datasets e.g. further development and operational trials of the prototype distributed model presented in Section 7.6. This is fundamental for modelling the area-wide flood response of complex catchments that are not dominated by topographical controls (e.g. lowland catchments with strong heterogeneous soil/geology controls) and for understanding extreme flood genesis at a regional scale.
- The application of distributed area-wide models for operational flood warning could be improved by addressing the following challenges: model initialisation, forecast updating, uncertainty estimation and utilisation of future advances in ensemble rainfall forecasting.
- The extreme event case studies should be used to explore the feasibility of rating curve extension via physically-based methods, such as those outlined in the Agency's Best Practice Guidance Manual W6-061/M.

8 Flood response experiments using amplified storms

8.1 Introduction

This section presents a set of flood response experiments for the case study catchments using the extreme storms in amplified and/or transposed form. The aim is to investigate the mechanisms controlling extreme flood genesis and to assess and ‘destruction test’ models. Understanding the controlling mechanisms of extreme floods within a modelling framework should provide a basis for early recognition of flood prone locations and support the planning of flood mitigation measures and improved flood warning. The framework for model testing under extreme storm conditions will help in model selection and improvement as well as demonstrating whether a given model behaves in a plausible manner in unusual circumstances.

The flood response experiments use historical storms and amplified forms of them following Approach 1 of Section 4.6. For a given catchment, the historical storms are amplified to attain FEH catchment average amounts for a given duration and return period (e.g. 100, 200, 500 or 1000 years). The Rainfall Transformation Tool, outlined in Section 4.3, requires certain characteristics of the historical storm to be estimated (e.g. speed and direction of travel) before the storm modification and transposition options can be applied. A methodology for identifying these from historical radar data, and the resulting estimated characteristics for each storm, are given in Section 8.2. Guidelines for applying the storm modification and transposition options are given for each storm type in Section 8.3 and Section 8.4 gives a summary of the information listed for each amplified storm in Appendix H.

The flood response experiments are grouped by hydrological case study in Section 8.5. Typically several convective storms are applied to each case study and either a frontal or orographic storm is used depending on location. The motivation for each experiment is given along with the amplified storms used, the time of year used and a summary of the main findings. Where models give unacceptable simulations, or the PDM and Grid-to-Grid model disagree significantly, understanding has been sought. On these occasions calculating the model water balance has provided added insight. Conclusions drawn from the experiments are given in Section 8.6.

8.2 Historical storm characteristics

A general methodology for estimating the historical storm characteristics needed to modify the storms has been derived. The methodology takes into account the storm type (orographic, frontal or convective) and is summarised in Table 8.1. It is intended to be a quick procedure that can be applied through visual inspection of the storm radar data, rather than a more complicated computational approach, as the main purpose is to obtain reasonable estimates that can be utilised by the Rainfall Transformation Tool (see Section 4.3). Hyrad has been used for visualisation of the radar data.

Table 8.1 Summary of the methodology used in identifying historical storm characteristics

| Storm characteristic | Orographic | Frontal | Convective |
|--|---|---|---|
| <i>Spatial Position</i> | Centre storm over orography | Select a suitable location, e.g. location of highest accumulation | Centre storm on highest intensity observed |
| <i>Temporal origin</i> | Use mid time point of event | Use mid time point of event | When the highest intensity was observed |
| <i>Movement</i> | Orographically enhanced storms are generally long duration events involving several bands of rain. Therefore estimate the speed and direction of the storm from time-frames near the temporal origin. | Frontal storms are generally long duration events involving several bands of rain. Therefore estimate the speed and direction of the storm from time-frames near the temporal origin. | Convective storms are generally short duration events. Therefore estimate speed and direction of the storm from a time-frame near the start of the convective cell with highest intensity and one near the end. |
| <i>Orientation of major bands of rainfall, distinct from direction of travel</i> | Estimate the orientation, if possible, from time-frames near the temporal origin. | Estimate the orientation, if possible, from time-frames near the temporal origin. | Generally not appropriate. |

The historical storm characteristics derived using this methodology are summarised in Table 8.2. It was not possible to identify the orientation of major bands of rainfall from the radar data for the frontal and orographic events. Since the Boscastle event comprised of several convective storms, initiated by a common orographic trigger, there is little benefit in assigning a storm velocity as modifying it would only emphasise one of the storms. Also the location of the greatest rainfall accumulation was used, rather than the highest instantaneous rain-rate, to spatially locate the event (this differs depending on the radar used) and the temporal location is simply the temporal mid-point of the event.

The start-time and duration of the storms are also given in Table 8.2. Note that the duration of the convective storms covers the duration of the storm as observed by radar (i.e. until the storm finishes or until the storm leaves the range of the radar) and is not solely focussed on the period of the greatest point raingauge recording. This allows the full duration of the storm to be included when modifying it (i.e. not just the period associated with the heaviest point

Table 8.2 Historical storm characteristics: (O) denotes orographic, (C) denotes convective and (F) denotes frontal.

| Event | Start time | Duration | Temporal Centre | Spatial Centre | Storm Velocity | | Storm Speed km hr ⁻¹ |
|--|-------------------|-------------------|-------------------|------------------|-----------------------------|------------------------------|------------------------------------|
| | | | | | East km hr ⁻¹ | North km hr ⁻¹ | |
| River Kent (O) 2km QC | 19:30 02/02/04 | 24 hours | 07:30 03/02/04 | 335000 511000 | 96 | 64 | 115 |
| Darwen (C) 1km raw | 15:30 14/06/02 | 2 hours | 16:20 14/06/02 | 371500 423500 | 54 | 42 | 68 |
| Darwen (C) 2km QC | 15:15 14/06/02 | 2 hours 45 min | 16:20 14/06/02 | 371000 424000 | 54 | 42 | 68 |
| Carlton-in- Cleveland (C) 2km QC | 06:45 10/08/03 | 3 hours | 09:20 10/08/03 | 433000 489000 | 40 | 40 | 56 |
| Halifax (C) 2km raw | 13:45 19/05/89 | 5 hours 15 min | 17:00 19/05/89 | 409000 425000 | 8 | -6 | 10 |
| Boscastle (C) 2km QC (Cobbacombe) | 11:30 16/08/04 | 5 hours 30 min | 14:15 16/08/04 | 215000 089000 | n/a | n/a | n/a |
| Boscastle (C) 2km QC (Predannack) | 11:30 16/08/04 | 5 hours 30 min | 14:15 16/08/04 | 217000 091000 | n/a | n/a | n/a |
| Upper Thames and Stour (F) 2/5km raw | 03:00 09/04/98 | 16 hours | 11:00 09/04/98 | 432500 247500 | -44 | 12 | 46 |

rainfall totals) and is particularly relevant when ‘slowing down’ storms such as the Carlton-in-Cleveland storm.

8.3 Guidelines for applying storm modification and transposition

Section 4.3 detailed the storm modification and transposition options available as part of the Rainfall Transformation Tool. Guidelines for the application of the different options are given in Table 8.3 for each type of extreme storm. For each hydrological case study, the historical extreme storms are firstly, if necessary, relocated to the case study catchments (without further modification) and the return period of the rainfall assessed. Secondly, the historical storms have been modified to attain given FEH estimated return periods for a particular catchment. The return periods of interest are 100, 200, 500 and 1000 years.

Guidelines for appropriate seasons in which to apply the modified storms have been derived using the analysis of 20th century historical extreme storms in the Phase I Study Report and are summarised in Table 8.3. This analysis indicates that the extreme frontal events only occurred between June and January with peak occurrence between July and September. However, the extreme frontal Easter 1998 event affecting the Upper Thames and Stour occurred during April and so April and May should also be considered.

Table 8.3 Guidelines for applying storm modification and transposition options by storm type

| Storm Modification | Orographic | Frontal | Convective |
|--|--|---|--|
| <i>Relative Temporal Position</i> | These storms should only be applied between November and mid-February. | These storms should only be applied between April and January, i.e. not in February or March. | These storms should only be applied between May and October with particular focus on June, July and August. |
| It is recommended that modified storms are applied at the same time of day as the historical storms. This is particularly relevant to convective events where insolation is an important forcing factor. | | | |
| <i>Relative Spatial Position</i> | These storms should only be 'relocated' to other catchments known to be affected by orographic enhancement. The target storm centre should correspond to the centre of the orography affecting the target catchment. | Storms can be freely moved to <i>lowland</i> parts of the country. Should not be moved to regions seriously affected by orographic enhancement. | Storms can be freely moved around the country. |
| <i>Relative Orientation</i> | Orientation of the storms can be altered but within meteorological limits i.e. orographic events on the west coast of the UK are generally caused only by a westerly or south-westerly flow. | Retain historical orientation. | Free to choose orientation of isolated convective events (not necessarily true for embedded convection; however only isolated events are considered here). |
| <i>Speed and Direction of travel</i> | Not suitable as storm must retain spatial location of orographic enhancement. | Retain historical speed and direction of travel. | Free to change speed and direction. |
| <i>Scaling of amounts</i> | Free to scale amounts within reason. The FEH provides point and area estimates of event rarity. | | |
| <i>Spatial squeezing (preserving rainfall amounts)</i> | Not suitable, rain generally widespread already. | Could be appropriate to alter in direction of bands. | Free to change. In particular to investigate what effect squeezing may have in creating a more localised and intense storm. |

Table 8.3 Continued

| Storm Modification | Orographic | Frontal | Convective |
|--|--|--|---|
| <i>Spatial expansion (not preserving rainfall amounts)</i> | Not suitable, rain generally widespread already. | Could be appropriate to alter in direction of bands. | Free to change. In particular to investigate what effect expansion may have in creating a larger convective cell of the same intensity. |
| <i>Time squeezing (preserving rainfall amounts)</i> | Free to use for all rain types. In particular to investigate what effect increasing rainfall rates, but not total rainfall amounts, and decreasing event duration will have. | | |
| <i>Time expansion (not preserving rainfall amounts)</i> | Free to use for all rain types. In particular to investigate what effect increasing event duration and total rainfall amounts, but not rainfall rates, will have. | | |

8.4 The amplified extreme storms

Details of each amplified extreme storm created are catalogued in Appendix H. The details listed are:

- **Year:** This is a fictitious year used to identify the storm within the dataset
- **Period:** This is the total period used for hydrological modelling. Over the period the modified spatial rainfall for each storm consists of three parts:
 1. **Warm-up.** Uses historical radar data to allow model warm-up. This usually ends with a period of low rainfall.
 2. **Modified storm.** Modified storm spatial data are used.
 3. **Cool down.** Zero rainfall.
- **Historical storm modified.** Identifies which historical storm was modified.
- **Storm modification and transposition settings.** Only settings that are altered are listed.
- **Comments.** This gives the catchment average rainfall amount, duration and estimated return period (using FEH) and any other points of interest.

Details of which rainfall estimator is used as the basis for the storm modifications are listed in Table 8.4. The modified storms created can be visualised through Hyrad.

Table 8.4 Summary of spatial rainfall data used as the basis for the modified storms

| Event | Spatial data used for modified storms | Radar used |
|--|--|-------------------|
| <i>Orographic rainfall</i> | | |
| 30 Jan –3 Feb 2004 River Kent | Raingauge-adjusted 2km Nimrod QC radar data | Hameldon Hill |
| <i>Frontal rainfall</i> | | |
| 8-9 Apr 1998 Upper Thames and Stour | Composite raingauge-adjusted 2 and 5km raw radar | Chenies |
| <i>Convective rainfall</i> | | |
| 14 Jun 2002 River Darwen | 1km raw radar | Hameldon Hill |
| 10 Aug 2003 Carlton-in-Cleveland | 2km Nimrod QC data | Hameldon Hill |
| 19 May 1989 Halifax | 2km raw data | Hameldon Hill |
| 16 Aug 2004 Boscastle | 2km Nimrod QC data | Cobbacombe Cross |

8.5 Flood response experiments

Flood response experiments have been performed using the amplified extreme storms to investigate the mechanisms controlling extreme flood genesis and to assess and ‘destruction test’ models. The experiments have been grouped by the catchment studied and the amplified storm used is identified by the fictitious year that it has been assigned. Full details of the amplified storms used are given in Appendix H.

Catchment average hyetographs and cumulative hyetographs are given for the amplified extreme storms to present both the overall storm total and the instantaneous rainfall intensities. Note that the instantaneous intensity hyetographs have a 15 minute interval and the average rainfall intensity for the preceding 15 minutes is used as the instantaneous value at that time.

8.5.1 Case study: River Kent

Return periods quoted relate to the River Kent at Victoria Bridge catchment unless otherwise stated.

Experiment 1

Target catchment: River Kent at Victoria Bridge

Historical storm used: River Kent (Orographic)

Amplified storms used (rainfall return period and duration):

3000 (69 year, 4 day), 3001 (100 year, 4 day), 3002 (200 year, 4 day),
3003 (500 year, 4 day), 3004 (1000 year, 4 day), 3005 (100 year, 5 day),
3007 (500 year, 5 day)

Time period presented in graphs: 09:00 30/01 – 09:00 06/02

The orographic storm which affected the River Kent catchment is used as the basis for this experiment. The final 24 hours of the historical 4 day storm, associated with the observed flood peak, has been amplified to make the storm more extreme. Firstly the amounts were simply scaled to attain given 4 day return periods. The simulated hydrographs are presented in the left hand column of Figure 8.1 and show the expected increase in flood peak with increase in rainfall return period.

Secondly, the last 24 hours have been stretched in time and amounts scaled to attain 100 and 500 year return period, 5 day duration rainfall amounts. The simulated hydrographs are presented in the right hand column of Figure 8.1 and are compared to the 4 day duration, 100 and 500 year return period rainfalls.

Key points

- Long duration orographic event used.
- Very responsive catchment.
- Good agreement between models over a range of storm magnitudes– no evidence of ‘model failure’.
- For a given duration, flood peak increases with rainfall return period as expected.
- For a given return period, the 5 day simulation peaks are significantly less than the 4 day peaks. Therefore, since the catchment responds quickly to rainfall, the short duration (less than 1 day, say) rainfall intensity profile is the main factor in determining flood peak rather than long duration rainfall amount/return period.

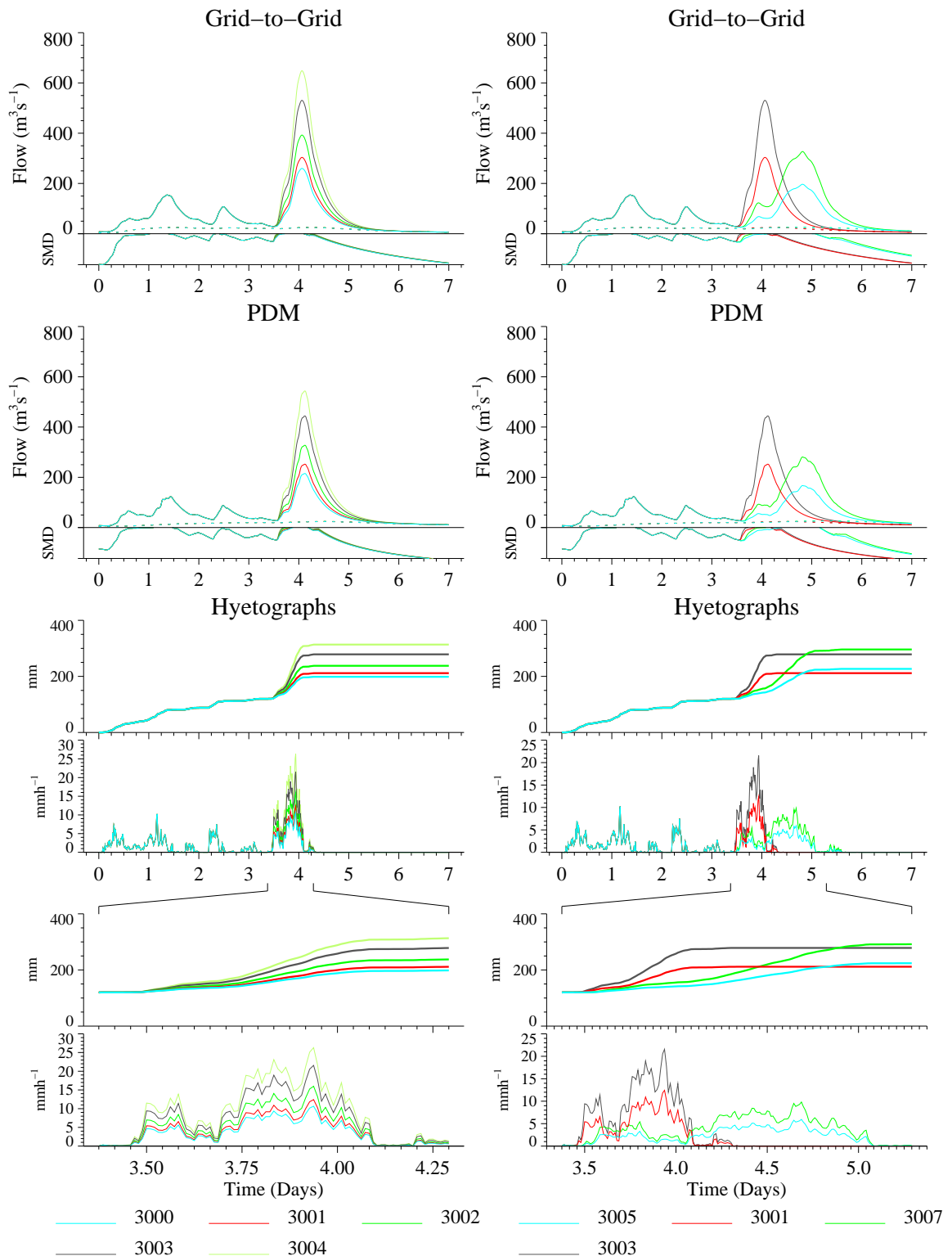


Figure 8.1 Amplified storms and hydrological model flood response for the River Kent at Victoria Bridge catchment. Experiment 1 using the River Kent orographic storm.

Experiment 2

Target catchment: River Kent at Victoria Bridge

Historical storm used: Carlton-in-Cleveland (convective)

Amplified storms used (rainfall return period and duration):

3018 (15 year, 1 hour), 3019 (100 year, 1 hour), 3020 (500 year, 1 hour),

3021 (15 year, 1 hour), 3022 (100 year, 1 hour), 3023 (500 year, 1 hour)

Time period presented in graphs: 00:00 16/08 – 00:00 18/02

The fast moving Carlton-in-Cleveland convective storm is relocated to the River Kent to explore how the relative alignment of storm direction and river channel orientation affects simulated flood response. Storms 3018, 3019 and 3020 have a South to North storm track which is up the river valley whilst storms 3021, 3022 and 3023 have a North to South storm track which is down the river valley. Storms 3018 and 3021 only involve changing the storm location, orientation and speed and their accumulations are depicted in Figure 8.2. The rainfall amounts for the other storms have been scaled to attain given return periods.

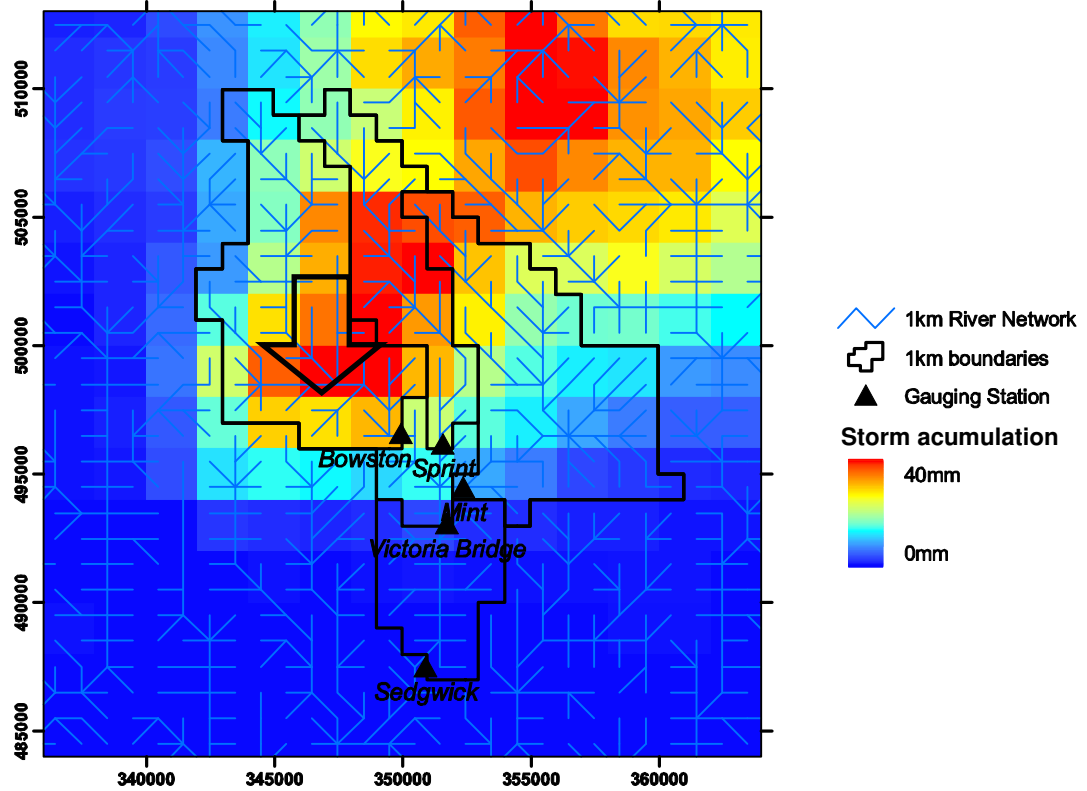
The left hand column of Figure 8.3 presents the simulated flood response at Victoria Bridge. For a given return period, the PDM response is identical for both storm directions, despite slight differences in the temporal distribution of the catchment average rainfall (see hyetographs). In contrast the Grid-to-Grid model responds differently to the two orientations of the storm. For a given return period, the storm aligned with the channel orientation produces a significantly larger peak at Victoria Bridge ($\approx 16\%$) and it is earlier (≈ 30 mins).

The right hand column presents the simulated responses at Bowston, upstream of Victoria Bridge. Here the sensitivity of the Grid-to-Grid model is even more noticeable. For a given return period, the storm aligned with the channel orientation produces a significantly larger peak at Bowston ($\approx 30\%$), despite having a smaller storm total over the catchment. In comparison, the PDM simulated peak is controlled by the storm total and therefore the aligned storms, which have a lower storm total for Bowston, produce a lower peak.

Key points

- Using a convective storm, explored how the relative alignment of storm direction and river channel orientation affects simulated flood response.
- The convective storm has a smaller spatial scale than the catchments.
- For quickly responding catchments and given a short duration storm total, lumped models do not differentiate between storms of differing direction. Their simulations are principally controlled by the storm total. This is a model limitation rather than a model failure.
- Distributed models can respond differently to storms of differing direction. The resulting model simulations can vary significantly in peak magnitude (up to 30% here). This underlines the potential advantage of using distributed modelling in extreme/unusual storm situations.
- For the typical situation where the storm direction and channel orientation are not aligned the PDM and Grid-to-Grid models agree well over a range of storm magnitudes.

(a) North to South storm track: Amplified storm 3021



(b) South to North storm track: Amplified storm 3018

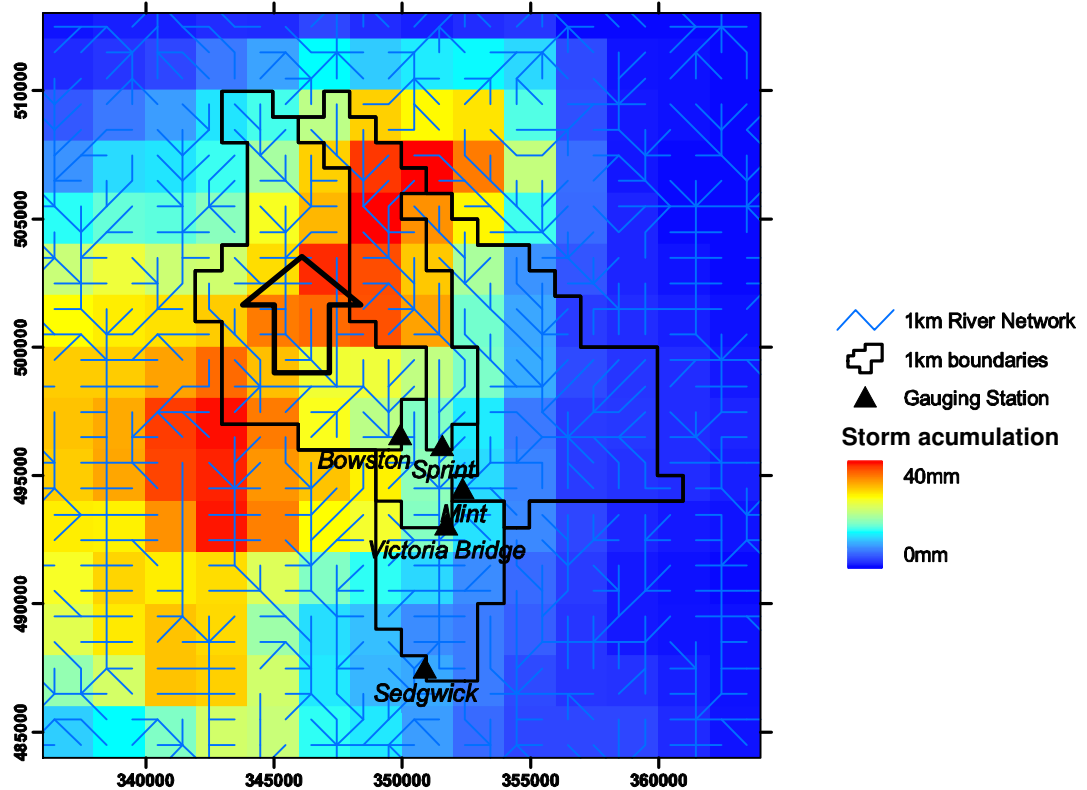


Figure 8.2 Amplified storm accumulations over the River Kent. Arrow indicates storm direction of travel. Experiment 2 using the Carlton-in-Cleveland convective storm.

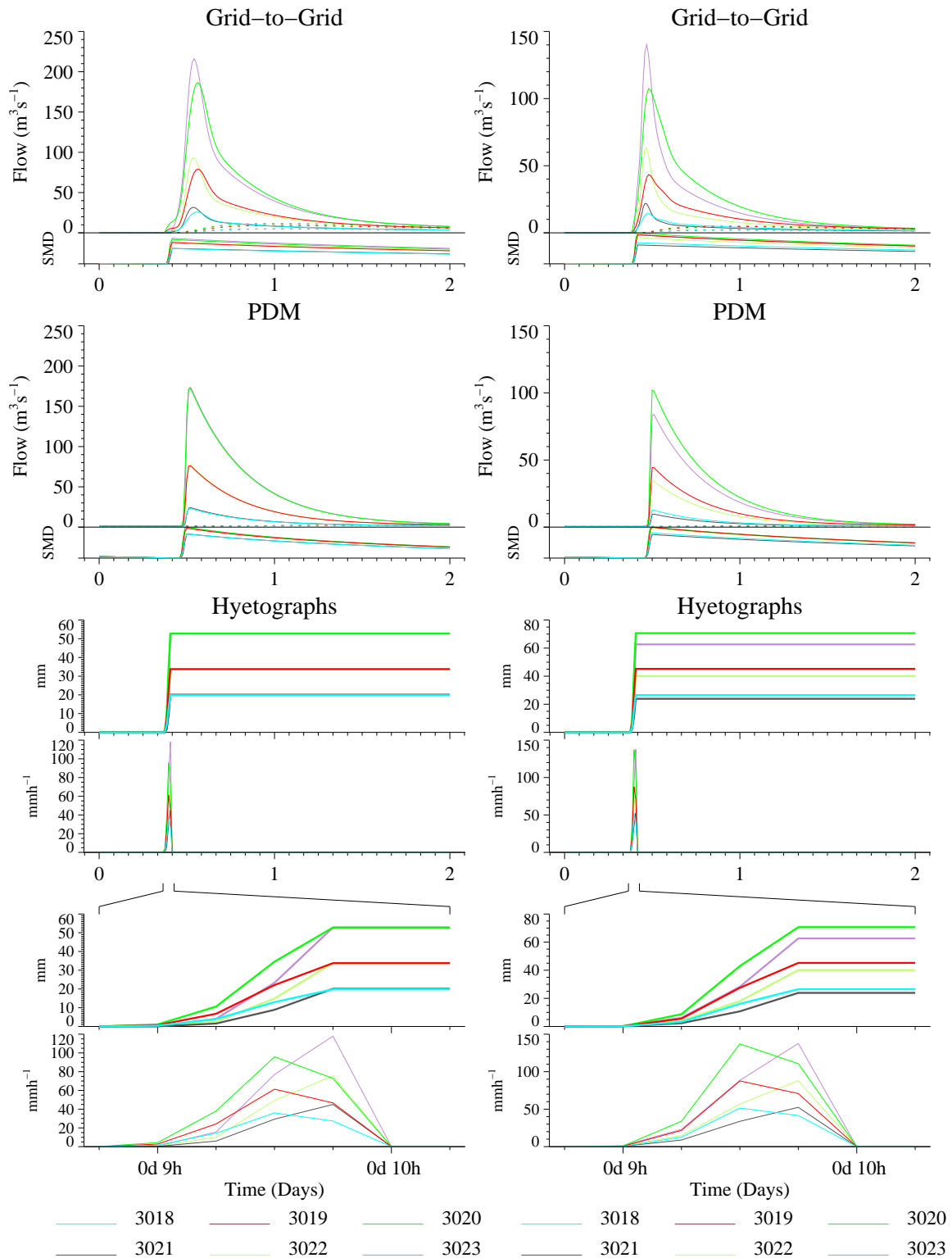


Figure 8.3 Amplified storms and hydrological model flood response for the River Kent at Victoria Bridge catchment (left hand column) and the River Kent at Bowston catchment (right hand column). Experiment 2 using the Carlton-in-Cleveland convective storm.

8.5.2 Case study: River Darwen

Return periods quoted relate to the River Darwen at Blue Bridge catchment.

Experiment 3

Target catchment: River Darwen at Blue Bridge

Historical storm used: River Darwen (convective)

Amplified storms used (rainfall return period and duration):

3005 (6.3 year, 2 hr), 3006 (100 year, 2 hr), 3008 (500 year, 2 hr),

3010 (6.7 year, 2 hr), 3011 (100 year, 2 hr), 3013 (500 year, 2 hr)

Time period presented in graphs: 09:00 14/06 – 21:00 15/02

The convective storm which affected the River Darwen catchment is used as the basis for this experiment. The storm direction and orientation has been altered so that storms 3005, 3006 and 3008 travel up the valley from West to East whilst the storms 3010, 3011 and 3013 travel down the valley from East to West. The rainfall amounts for storms 3005 and 3010 have not been scaled whilst the rest have been in order to attain given return periods.

The model simulations are presented in the left hand column of Figure 8.4. As expected, for a given return period, the PDM model simulations are virtually identical for both storm directions. In contrast to Experiment 2, the Grid-to-Grid model shows little sensitivity to the storm direction. Further investigation reveals that the spatial extent of the storm is generally as large as the catchment and therefore most of the catchment is covered at most points during the storm. This is reflected in the similar hyetographs for both storm directions at a given return period and explains why the Grid-to-Grid model is relatively insensitive to storm direction.

Key points

- Used a convective storm and explored how the relative alignment of storm direction and river channel orientation affects simulated flood response.
- Lumped models do not differentiate between storms of differing direction and, for quickly responding catchments, their simulations are principally controlled by the storm total.
- Convective storms must have a spatial extent smaller than the catchment or significant spatial variability on a subcatchment scale for the Grid-to-Grid model to be sensitive to the relative alignment of storm direction and channel orientation.
- The PDM and Grid-to-Grid model agree very well over a range of storm magnitudes.
- No evidence of model failure.

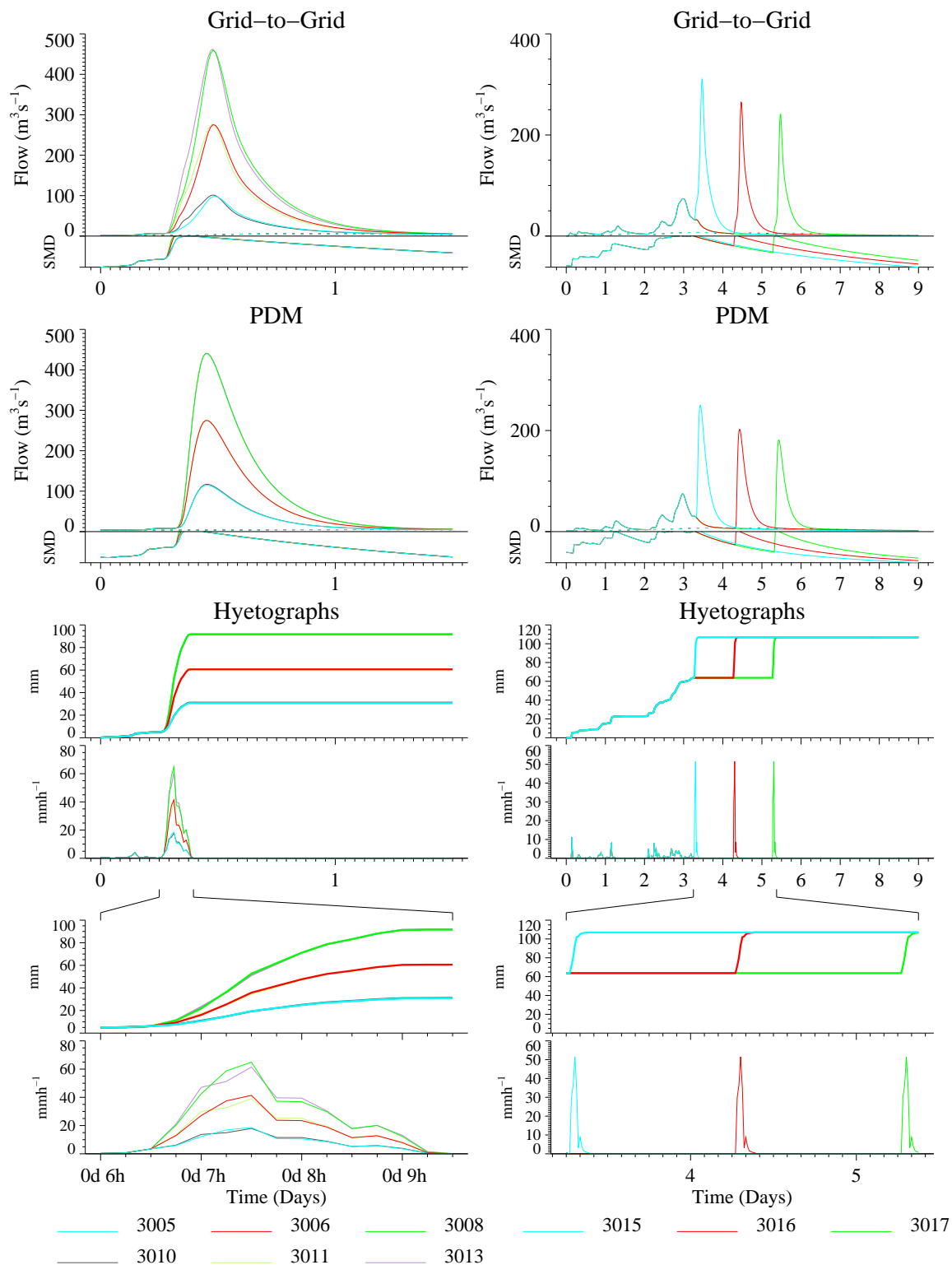


Figure 8.4 Amplified storms and hydrological model flood response for the River Darwen at Blue Bridge catchment. Left column: Experiment 3 on effect of storm direction and orientation. Right column: Experiment 4 on effect of soil moisture initial condition. The River Darwen convective storm is used.

Experiment 4

Target catchment: River Darwen at Blue Bridge

Historical storm used: River Darwen (convective)

Amplified storms used (rainfall return period and duration):

3015 (100 year, 1 hr), 3016 (100 year, 1 hr), 3017 (100 year, 1 hr)

Time period presented in graphs: 09:00 30/06 – 09:00 08/08

The objective of this experiment was to investigate the effect of soil moisture initial conditions on the model simulations. Due to difficulties in initialising distributed models, a historical warm up period (23/07/02 – 02/08/02) that ended with a reasonable flow peak was used as a proxy for initialising the model soil moisture. Then the convective Darwen storm with amounts scaled to a 1 hour, 100 year return period, was applied at different points during the flood peak recession. For storm 3015 the Darwen storm was applied immediately after the historical peak, for storm 3016 the Darwen storm was applied a day later and for storm 3017 the Darwen storm was applied a further day later.

The model simulations are presented in the right hand column of Figure 8.4. They agree qualitatively, with the difference in consecutive storm flood peaks rapidly tailing off.

Key points

- Investigated effect of model soil moisture initial conditions when applying a convective storm.
- Reasonable agreement between both models over all storms.
- No evidence of model failure.
- When applying an extreme short duration convective storm to a fast responding catchment, the effect of initial model soil moisture stores is limited since the soil stores soon become saturated. This is reflected in the modelled soil moisture deficits.

Experiment 5

Historical storm used: Upper Thames and Stour (frontal)

Amplified storms used (rainfall return period and duration):

3037 (100 year, 15 hr), 3041 (100 year, 24 hr),

3043 (100 year, 36 hr), 3045 (100 year, 48 hr)

Time period presented in graphs: 09:00 08/04 – 09:00 12/04

The Easter 1998 frontal storm has been relocated to the Darwen catchment. The storm has been stretched in time to create 24, 36 and 48 hour storms and the rainfall amounts scaled to attain a 100 year return period. The model simulations are presented in the left hand column of Figure 8.5. This is similar to Experiment 1.

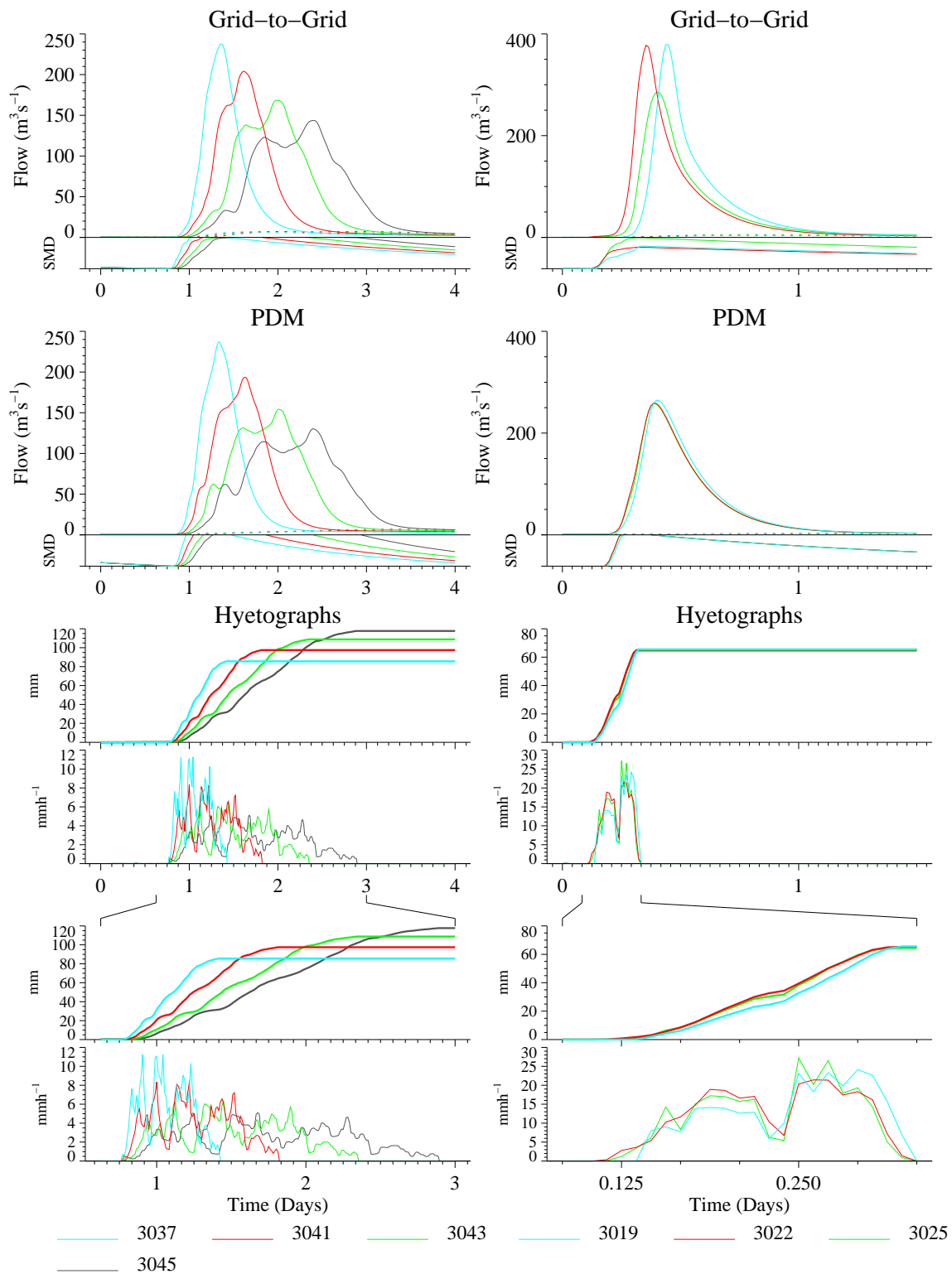


Figure 8.5 Amplified storms and hydrological model flood response for the River Darwen at Blue Bridge catchment. Left hand column: Experiment 5 using Upper Thames frontal storm. Right column: Experiment 6 using Boscastle convective storm.

Key points

- Medium to long duration frontal event.
- Responsive catchment.
- Very good agreement between models over a range of storm magnitudes– no evidence of ‘model failure’.
- For a given return period, the simulated peaks decrease with duration. Therefore, since the catchment responds quickly to rainfall, the short duration (less than 1 day, say) rainfall intensity profile is the main factor in determining the flood peak rather than the long duration rainfall amount/return period.

Experiment 6

Target catchment: River Darwen at Blue Bridge

Historical storm used: Boscastle (convective)

Amplified storms used (rainfall return period and duration):

3019 (100 year, 4 hr), 3022 (100 year, 4 hr), 3025 (100 year, 4 hr)

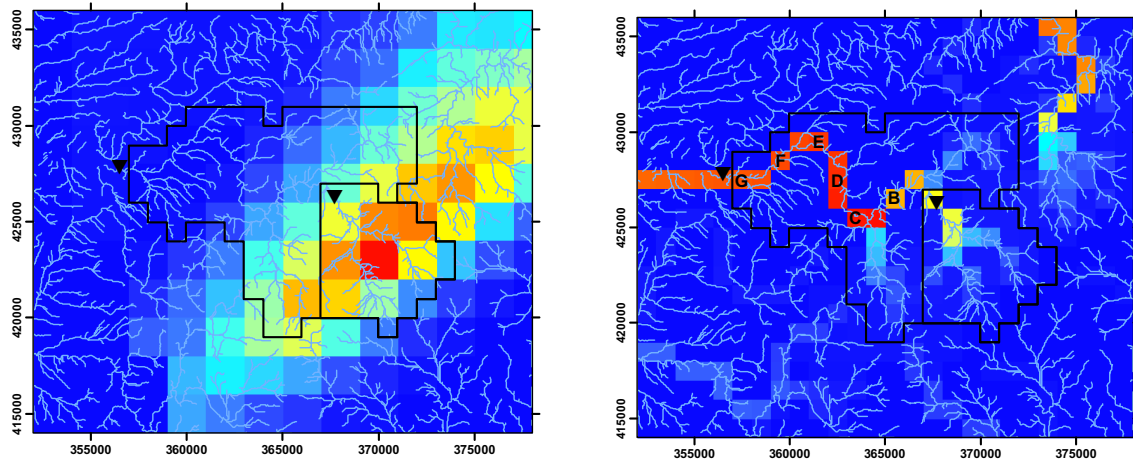
Time period presented in graphs: 09:00 19/08 – 21:00 19/08

The Boscastle convective storm has been relocated to the River Darwen at Blue Bridge catchment to explore how storm location and extent affect modelled flood response. The Boscastle has a relatively long duration for a convective event. For storm 3019 the Boscastle storm was relocated to the headwaters of the river Darwen, for storm 3022 it was relocated to the lower reaches, near the catchment outlet and for storm 3025 it was relocated centrally and stretched spatially to cover the majority of the catchment. All amplified storms had their amounts scaled to attain 4 hour, 100 year return periods (61.8 mm). The amplified storm accumulations, along with their spatial extent and location, are presented in Figure 8.6.

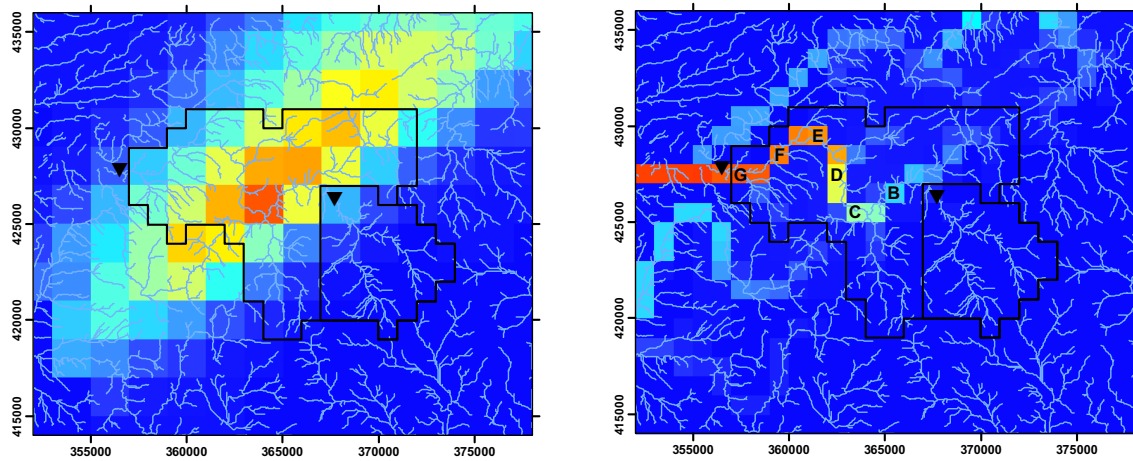
The model simulations for the River Darwen at Blue Bridge are given in the right hand column of Figure 8.5. As expected the PDM model simulations are almost identical for each storm because lumped models, over responsive catchments and short duration events, are primarily affected by the storm total rather than the spatio-temporal distribution of the storm.

In contrast the Grid-to-Grid model has a very different flood response to each storm. Firstly the timings of the modelled response vary. The localised storm near the catchment outlet (3022) gives the earliest response, then the centrally located catchment-wide storm (3025) followed finally by the localised storm in the headwaters (3019). Secondly the peak magnitude varies: the localised storms (3019 and 3022) produce peaks much larger ($\approx 33\%$) than the catchment-wide storm (3025). This is primarily due to the localised storms having a larger scaling factor and hence larger maximum grid-square accumulation (see Figure 8.6) creating increased localised runoff compared to the catchment-wide storm. Also the catchment-wide storm gives the closest agreement to the PDM. This is expected since the lumped model assumes a catchment-wide rainfall.

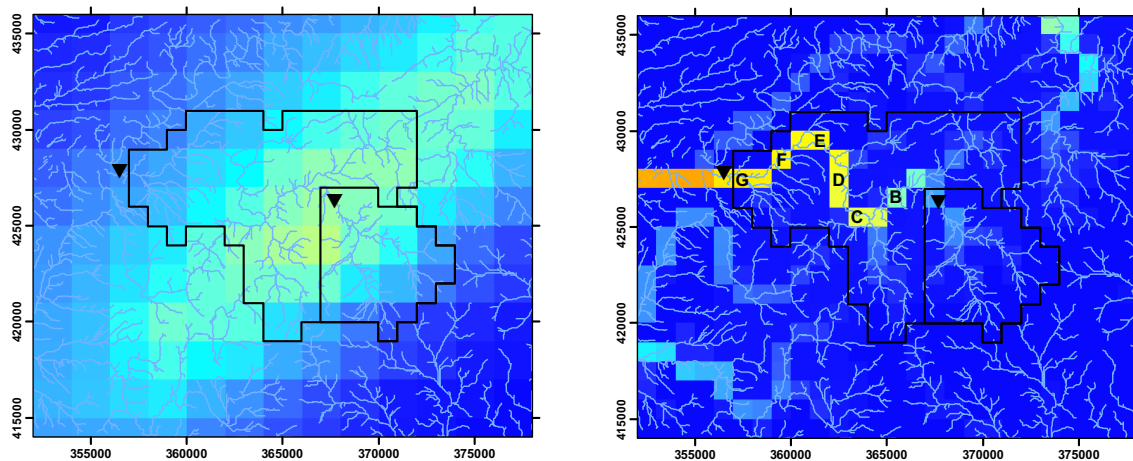
(a) Amplified storm 3019



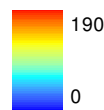
(b) Amplified storm 3022



(c) Amplified storm 3025



Storm total (mm)



- ▼ Gauging Station
- ⊕ 1km boundaries
- ⚡ 50m River Network

Max Flow (cumecs)

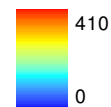


Figure 8.6 Amplified storm accumulations (left hand column) and maximum simulated river flow from the Grid-to-Grid model (right hand column) over the River Darwen catchment. Experiment 6 using the Boscastle convective storm.

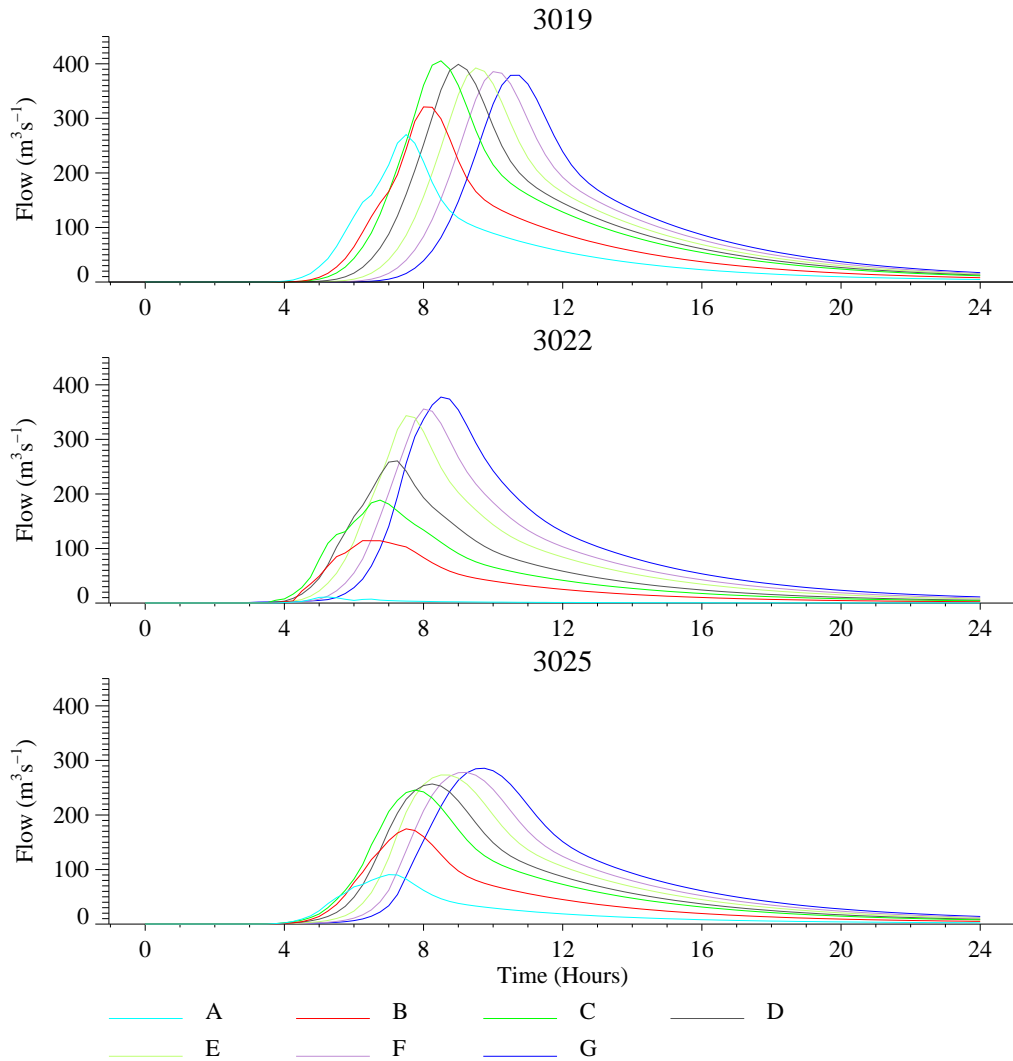


Figure 8.7 Grid-to-Grid model simulations at a sequence of grid squares between the modelling point for the River Darwen at Ewood (point A) to the modelling point for the River Darwen at Blue Bridge (point G). The points are marked in Figure 8.6. Experiment 6 using the Boscastle convective storm.

The distributed Grid-to-Grid model provides additional spatial information about the floods generated by these amplified storms. The maximum modelled flow over the storms is given for each grid-square of the modelling domain in Figure 8.6. These show that the headwater storm (3019) has a maximum flood peak upstream of Blue Bridge whereas the other storms peak downstream. The magnitudes of the flood peaks for the catchment-wide storm (3025) are significantly smaller.

A sequence of modelling locations between the upstream gauging stations at Ewood and the downstream station at Blue Bridge are labelled A to G in Figure 8.6. Simulated Grid-to-Grid hydrographs from each of these locations are given for each storm in Figure 8.7. These hydrographs emphasise the differences in

model flood response. In particular the headwater storm (3019) clearly shows the spatial flood peak occurring upstream of Blue Bridge and the catchment-wide storm (3025) has a comparatively less sharp peak. This highlights the useful additional spatial information and insight that distributed modelling can give into extreme flood genesis.

Key points

- Relocated a convective storm and explored how the spatial location and extent affects simulated flood response.
- For quickly responding catchments and given a short duration storm total, lumped models do not differentiate between storms of differing location or spatial extent. Their simulations are principally controlled by the storm total. This is a model limitation rather than a model failure.
- Distributed models can be very sensitive to storm location, spatial extent and spatial intensities. The resulting model simulations can vary significantly in magnitude (up to 33% here), spatial distribution and timing. This underlines the potential advantage of using distributed modelling in extreme/unusual storm situations.
- For the catchment-wide storm (3025) the PDM and Grid-to-Grid models agree well.

8.5.3 Case study: Stour at Shipston

Return periods quoted relate to the Stour at Shipston catchment.

Experiment 7

Target catchment: Stour at Shipston

Historical storm used: Upper Thames and Stour (frontal)

Amplified storms used (rainfall return period and duration):

3030 (100 year, 15 hr), 3034 (100 year, 24 hr),

3036 (100 year, 36 hr), 3036 (100 year, 48 hr)

Time period presented in graphs: 09:00 08/04 – 09:00 13/04

The Easter 1998 frontal storm which affected the Stour catchment is used as the basis for this experiment. The storm has been stretched in time to create 24, 36 and 48 hour storms and the rainfall amounts scaled to attain a 100 year return period. The model simulations are presented in Figure 8.8. The Stour is a relatively slower responding catchment than the Kent and Darwen catchments used in experiments 1 and 5 respectively.

Key points

- Medium to long duration frontal event.
- Slow responding catchment.
- Very good agreement between models over a range of storm magnitudes– no evidence of ‘model failure’.

- For a given return period, the largest simulated peaks occur for a 24 hour duration storm and then slowly decrease with duration. Therefore, since the catchment responds slowly to rainfall, the long duration rainfall total/return period is the main factor in determining flood peak rather than the short duration rainfall intensity profile.

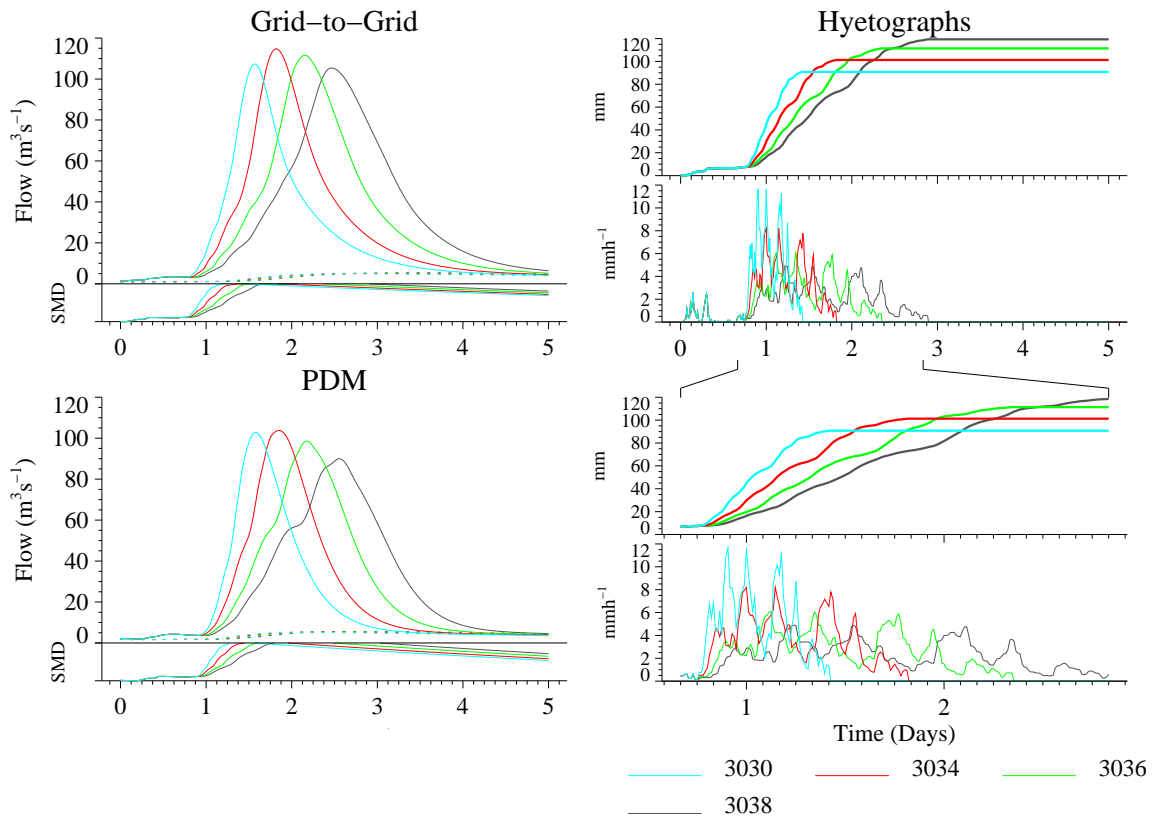


Figure 8.8 Amplified storms and hydrological model flood response for the Stour at Shipston catchment. Experiment 7 using the Upper Thames and Stour frontal storm.

Experiment 8

Target catchment: Stour at Shipston

Historical storm used: Boscastle (convective)

Amplified storms used (rainfall return period and duration):

3041 (100 year, 4 hr), 3044 (100 year, 4 hr), 3047 (100 year, 4 hr)

Time period presented in graphs: 09:00 21/04 – 09:00 25/04

The Boscastle convective storm has been relocated to the Stour at Shipston catchment to explore how storm location and extent affect modelled flood response. For storm 3041 the Boscastle storm was relocated to the western headwaters of the catchment, for storm 3044 it was relocated to the eastern headwaters and for storm 3025 it was relocated centrally and rotated to cover the majority of the catchment. All amplified storms had their rainfall amounts scaled to attain 4 hour, 100 year return periods (56.9 mm).

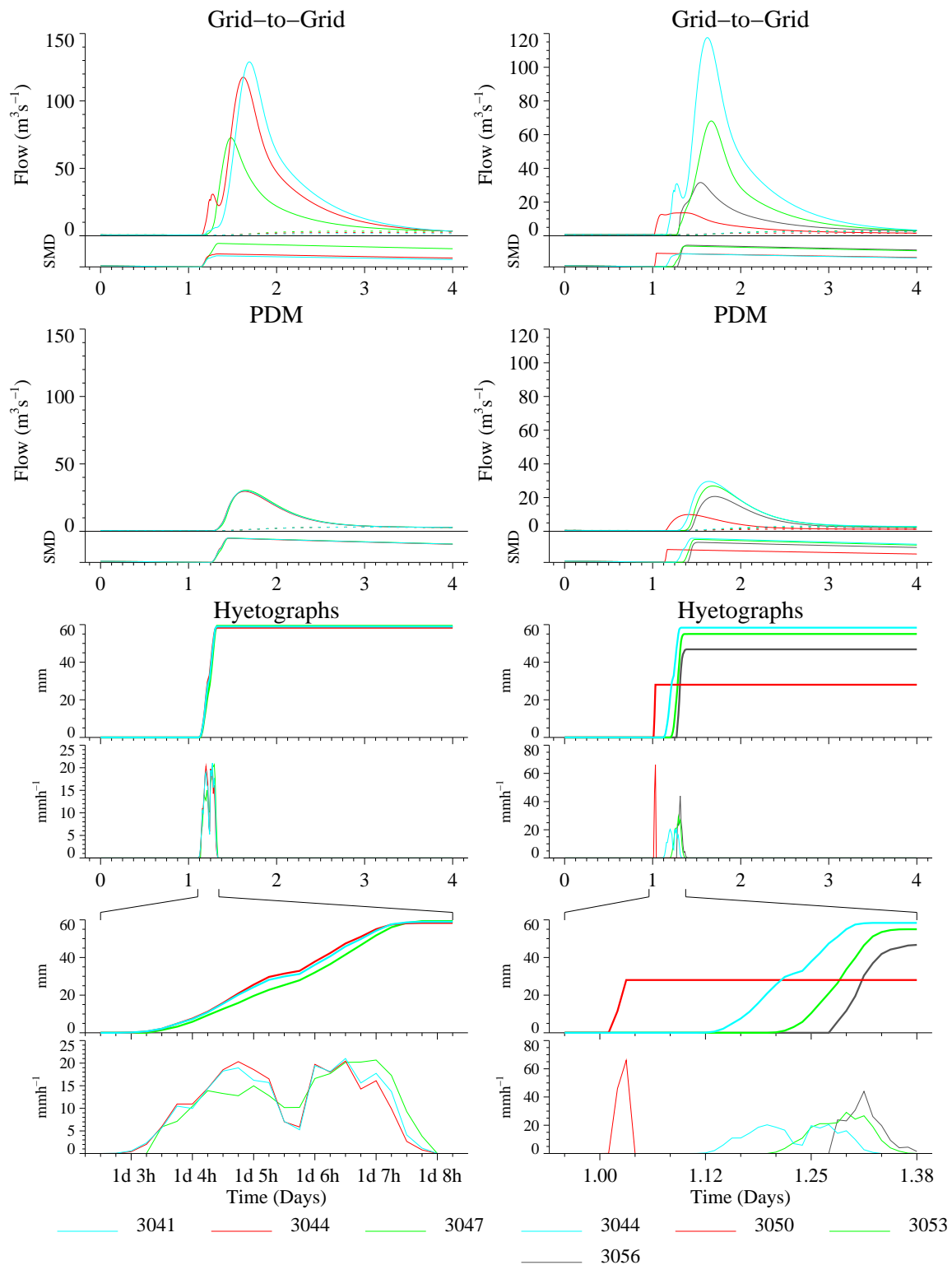


Figure 8.9 Amplified storms and hydrological model flood response for the Stour at Shipston catchment. Left column: Experiment 8 using the Boscastle convective storm. Right column: Experiment 9 using a variety of convective storms.

The model simulations for the Stour at Shipston are given in the left hand column of Figure 8.9. As expected the PDM model simulations are almost identical for each storm because lumped models, over responsive catchments and short duration events, are primarily affected by the storm total rather than the spatio-temporal distribution of the storm.

In contrast the Grid-to-Grid model has a very different flood response to each storm. Firstly the timings of the modelled response vary. The centrally located catchment-wide storm (3047) responded first followed by the two localised headwater storms (3041 and 3044) with a time lag of up to 5 hours. Secondly the peak magnitude varies: the localised storms (3041 and 3044) produce peaks much larger (up to 77%) than the catchment-wide storm (3025). This is primarily due to the localised storms having a larger scaling factor and hence larger maximum grid-square accumulation creating increased localised runoff compared to the catchment-wide storm.

For this experiment there is a considerable difference in magnitudes between the PDM and Grid-to-Grid model simulations that warrants further investigation, especially as calibration events and Experiment 7 suggested the models agreed well. The water balance terms for each model over a selection of events are given in Table 8.5 where all quantities are measured in mm across the catchment. The water balance equation 'Initial Storage + Net Rainfall = Final Storage + Outputted Flow' is seen to hold for all models and events and therefore neither of the models are 'gaining' or 'losing' water.

Only the outputs and the inputs of the two models should be directly compared as the initial and final storages are internal model quantities used to maintain mass balance. Examination of Table 8.5 reveals that, for a given storm, there is less net rainfall available to the PDM due to the calibrated rainfall factor of 0.76. This has the effect of dampening the PDM model response. For widespread, long duration events (e.g. storm 3030 or calibration events) this dampening is desirable as it reduces the amount of runoff created, bringing the simulation in line with observations and the Grid-to-Grid model. For short duration convective storms (3041 and 3047) the dampening effect prevents the PDM reaching saturation (see Figure 8.9) and dramatically reduces the volume of river flow generated. This is more noticeable for the Stour catchment compared to the Kent or Darwen catchments as it has a deeper soil moisture store. Knowing that the historical peak flood response to the Easter 1998 frontal event was circa $90 \text{ m}^3\text{s}^{-1}$, it is judged that the Grid-to-Grid model simulation is more plausible than the PDM.

Key points

- Relocated a convective storm and explored how the spatial location and extent affects simulated flood response.
- For slowly responding catchments and given a short duration storm total, lumped models do not differentiate between storms of differing location or spatial extent. Their simulations are principally controlled by the storm total. This is a model limitation rather than a model failure.

- Distributed models can be very sensitive to storm location, spatial extent and spatial rainfall intensities. The resulting model simulations can vary significantly in magnitude (up to 77% here), spatial distribution and timing. This underlines the potential advantage of using distributed modelling in extreme/unusual storm situations.
- For the Stour there is considerable difference between PDM and Grid-to-Grid model simulations. The calibrated PDM rainfall factor of 0.76 is primarily responsible for the over-damped PDM simulations whilst the Grid-to-Grid model can produce increased runoff in response to high localised rainfall intensities/amounts.

Table 8.5 Water balance information for Experiment 8 for the Stour at Shipston catchment using storms 3030, 3041 and 3047

| PDM water balance | | | | Grid-to-Grid water balance | | | |
|------------------------------|-------------|-------------|-------------|-----------------------------------|-------------|-------------|-------------|
| Quantity | 3030 | 3041 | 3047 | Quantity | 3030 | 3041 | 3047 |
| Inputs | | | | | | | |
| Rainfall | 71.2 | 44.8 | 45.1 | Rainfall | 94.1 | 60.7 | 59.2 |
| Potential Evap. | 21.2 | 11.5 | 11.5 | Potential Evap. | 21.6 | 11.3 | 11.3 |
| Actual Evap. | 20.0 | 10.1 | 10.1 | Actual Evap. | 20.2 | 8.9 | 10.1 |
| Net Rainfall | 51.2 | 34.7 | 35.0 | | 73.9 | 51.7 | 49.1 |
| Outputs | | | | | | | |
| Computed River Flow | 55.0 | 15.2 | 15.4 | Computed River Flow | 61.6 | 44.7 | 25.3 |
| | | | | Computed Subsurface Flow | 0.03 | 0.005 | 0.009 |
| Total output | 55.0 | 15.2 | 15.4 | | 61.6 | 44.7 | 25.3 |
| Initial Storage | | | | | | | |
| Soil Moisture | 38.6 | 20.4 | 20.4 | Grid Stores | 56.0 | 47.3 | 47.3 |
| Baseflow Store | 1.7 | 1.1 | 1.1 | Subsurface Stores | 0.08 | 0.05 | 0.05 |
| Surface Store | 0.0 | 0.0 | 0.0 | Surface Stores | 0.42 | 0.20 | 0.20 |
| Total Initial Storage | 40.3 | 21.5 | 21.5 | | 56.5 | 47.5 | 47.5 |
| Final Storage | | | | | | | |
| Soil Moisture | 34.9 | 39.2 | 39.3 | Grid Stores | 68.0 | 54.1 | 70.4 |
| Baseflow Store | 1.6 | 1.7 | 1.7 | Subsurface Stores | 0.15 | 0.09 | 0.18 |
| | | | | Surface Stores | 0.60 | 0.40 | 0.70 |
| Total Final Storage | 36.5 | 40.9 | 41.1 | | 68.8 | 54.6 | 71.3 |

Experiment 9

Target catchment: Stour at Shipston

Historical storms used: all convective, Boscastle (3044), Carlton-in-Cleveland (3050), Halifax (3053) and Darwen (3056)

Amplified storms used (rainfall return period and duration):

3044 (100 year, 4 hr), 3050 (100 year, 30 mins),

3053 (100 year, 3.5 hr), 3056 (100 year, 1.5 hr)

Time period presented in graphs: 09:00 21/04 – 09:00 25/04

The purpose of this experiment is to explore how convective events of differing durations, spatial extent and intensity can affect flood genesis. The historical convective storms have simply been relocated to the Stour catchment and their rainfall amounts scaled to attain 100 year return periods. The model simulations for the Stour at Shipston are given in the right hand column of Figure 8.9. The hyetographs show that, for a given return period, the longer duration convective storms are generally associated with lower peak intensities.

The model simulations show reasonable agreement between the PDM and Grid-to-Grid model for the shorter duration and lower rainfall total storms (3050 and 3056). For the longer duration and higher rainfall total storms (3044 and 3053) there is again significant difference between the simulations. As discussed in Experiment 8 the difference is mainly due to the calibrated PDM rainfall factor of 0.76 and that the localised nature of the storms saturates some grid-squares in the distributed model causing increased localised runoff whereas the PDM does not reach saturation (see Figure 8.9). The simulations also show that the Grid-to-Grid model can, due to its distributed nature and topographic routing controls, produce a variety of unusual flood responses when exposed to unusual convective storm/catchment configurations whereas the PDM, due to its lumped conceptual formulation, produces a similarly shaped hydrograph for each storm.

Key points

- Relocated a variety of convective storms to investigate model response to storms of differing durations, spatial extent and intensity.
- PDM simulations show that lumped conceptual models produce similarly shaped hydrographs regardless of the storm and catchment configuration.
- The Grid-to-Grid model can produce a range of flood responses when exposed to unusual convective storm to catchment configurations.
- For the longer duration, larger rainfall total storms (3044 and 3053) there is a noticeable difference between the model simulations. This is caused by the calibrated PDM rainfall factor of 0.76 whilst the Grid-to-Grid model can produce increased runoff in response to high localised rainfall intensities/amounts.

8.5.4 Case study: Sor at Bodicote, Upper Thames

Return periods quoted relate to the Sor at Bodicote catchment.

Experiment 10

Target catchment: Sor at Bodicote

Historical storms used: Upper Thames and Stour

Amplified storms used (rainfall return period and duration):

3000 (11 year, 15 hr), 3001 (100 year, 15 hr), 3002 (200 year, 15 hr),
3003 (500 year, 15 hr), 3004 (1000 year, 15 hr), 3005 (100 year, 24 hr),
3007 (100 year, 36 hr), 3009 (100 year, 48 hr)

Time period presented in graphs: 09:00 08/04 – 09:00 12/04

The Easter 1998 frontal storm which affected the Sor at Bodicote catchment is used as the basis for this experiment. The storm rainfall amounts have been scaled to attain 100, 200, 500 and 1000 year, 15 hour duration storms (see Figure 8.10, right column) and the storm has been stretched in time and scaled to create 24, 36 and 48 hour storms, with a 100 year return period (see Figure 8.10, left column). The Sor at Bodicote is the slowest responding catchment studied.

Comparison of the PDM and Grid-to-Grid model simulations show some significant differences in model flood response. The simulated hydrographs have different shape characteristics. Use of a cubic surface routing store in the PDM (a cascade of two linear reservoirs is used normally) produces a sharp response to the rainfall after the model time delay of 9 hours. In contrast the delay between the rainfall and simulated flow peak for the Grid-to-Grid model is controlled by the model wave speed parameters and creates a more rounded response.

The simulations also reveal a lower flood peak predicted by the Grid-to-Grid model, particularly for the high return periods (see Figure 8.10, right column) where the PDM reaches saturation. To investigate the cause of the low peaks the water balance terms have been calculated for a selection of storms in Table 8.6. These quantities reveal that for the lower rainfall amounts (3000 and 3013) the computed model flows compare well but when exposed to 15 hour, 1000 year return period rainfall (3004) the Grid-to-Grid model stores an unrealistic amount in the surface stores at the end of the event. This is because calibration of the Grid-to-Grid model proved very difficult for this catchment and resulted in a very slow land surface wave speed. Therefore the surface stores are taking too long to drain. Although this wasn't a problem for the calibration events, as the Grid-to-Grid model agreed well with observations (see Section 7.4), the recommendation would be to revisit the calibration periods taking the findings of Experiment 10 into account.

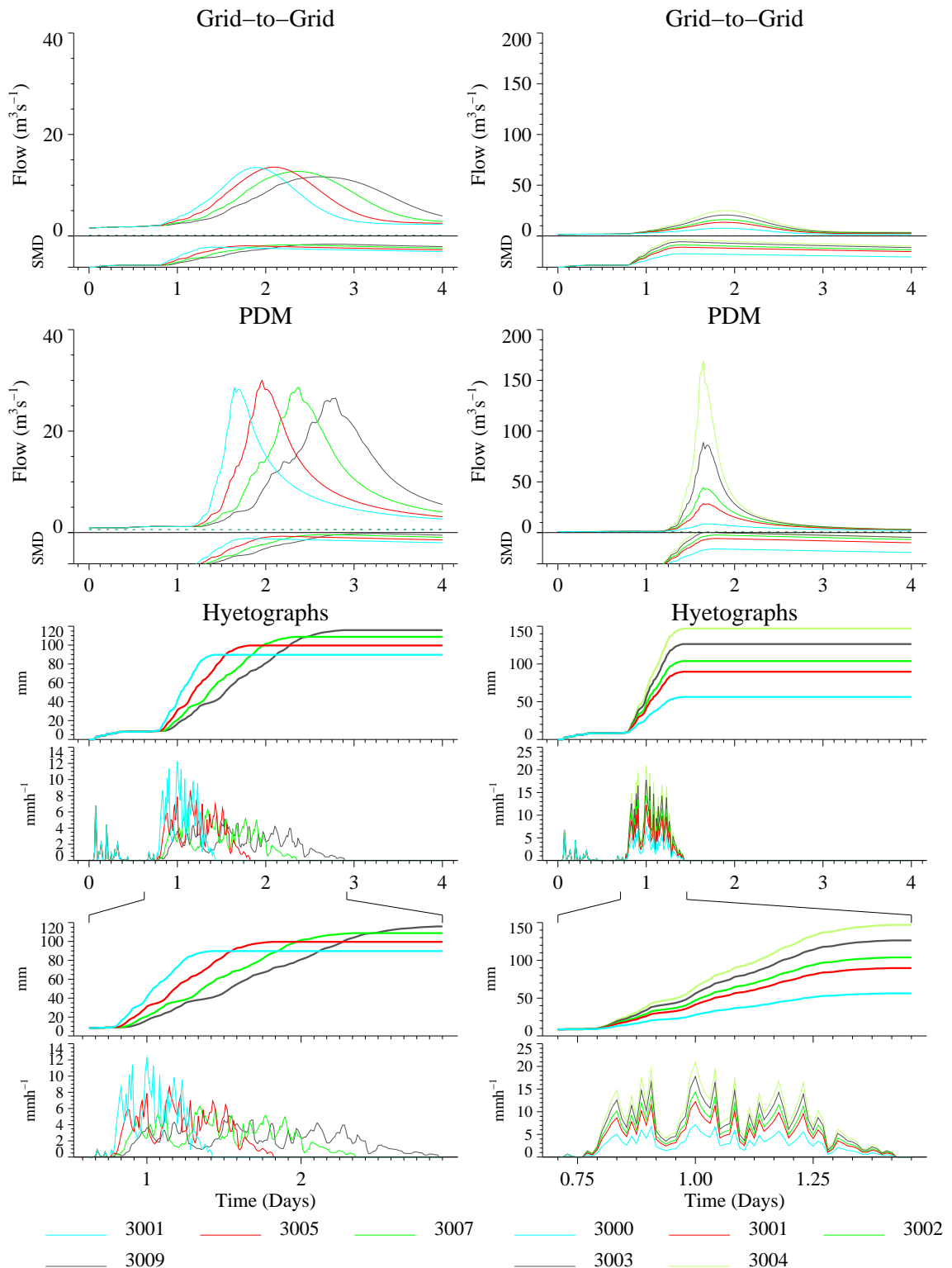


Figure 8.10 Amplified storms and hydrological model flood response for the Sor at Bodicote catchment. Experiment 10 using the Upper Thames frontal storm.

Table 8.6 Water balance information for Experiment 10 for the Sor at Bodicote using storms 3000, 3004 and 3013

| PDM water balance | | | | Grid-to-Grid water balance | | | |
|------------------------------|--------------|--------------|--------------|-----------------------------------|--------------|--------------|--------------|
| Quantity | 3000 | 3004 | 3013 | Quantity | 3000 | 3004 | 3013 |
| Inputs | | | | | | | |
| Rainfall | 54.1 | 141.1 | 91.5 | Rainfall | 56.5 | 147.5 | 97.4 |
| Potential Evap. | 6.5 | 6.5 | 13.0 | Potential Evap. | 6.7 | 6.7 | 12.8 |
| Actual Evap. | 6.3 | 6.4 | 11.9 | Actual Evap. | 6.4 | 6.6 | 11.1 |
| Net Rainfall | 47.8 | 134.7 | 79.7 | | 50.1 | 141.0 | 86.3 |
| Outputs | | | | | | | |
| Computed River Flow | 12.5 | 68.6 | 17.9 | Computed River Flow | 13.2 | 35.2 | 19.4 |
| | | | | Computed Subsurface Flow | 0.07 | 0.08 | 0.03 |
| Total output | 12.5 | 68.6 | 17.9 | | 13.3 | 35.3 | 19.5 |
| Initial Storage | | | | | | | |
| Soil Moisture | 106.6 | 106.6 | 77.4 | Grid Stores | 142.1 | 142.1 | 102.6 |
| Baseflow Store | 86.6 | 86.6 | 82.2 | Subsurface Stores | 1.9 | 1.9 | 0.9 |
| Surface Store | 6.4 | 6.4 | 4.4 | Surface Stores | 10.7 | 10.7 | 6.3 |
| Total Initial Storage | 197.7 | 197.7 | 164.0 | | 154.7 | 154.7 | 109.8 |
| Final Storage | | | | | | | |
| Soil Moisture | 136.8 | 163.4 | 132.7 | Grid Stores | 161.6 | 182.3 | 143.5 |
| Baseflow Store | 86.4 | 88.9 | 83.9 | Subsurface Stores | 4.1 | 11.1 | 4.6 |
| | 9.9 | 11.6 | 9.1 | Surface Stores | 25.8 | 66.8 | 28.4 |
| Total Final Storage | 233.0 | 263.9 | 225.7 | | 191.4 | 260.1 | 176.5 |

Key points

- Medium to long duration frontal event.
- Very slow responding catchment, difficult to calibrate.
- Reasonable agreement between models with 100 year return periods.
- For very extreme rainfalls in excess of 100 year return periods, the agreement between the models rapidly worsens. This identified the land surface wave speed of the Grid-to-Grid model as being too low and recalibration is recommended. This was not clearly evident during calibration and highlights the usefulness of using amplified extreme storms to test models.
- For a given return period, the largest simulated peaks for both models occur for 24 hour duration storms and then slowly decrease with duration. Therefore, since the catchment responds slowly to rainfall, the long duration rainfall total/return period is the main factor in determining flood peak rather than the short duration rainfall intensity profile.

Experiment 11

Target catchment: Sor at Bodicote

Historical storm used: River Darwen (convective)

Amplified storms used (rainfall return period and duration):

3024 (100 year, 1 hr), 3025 (100 year, 1 hr), 3026 (100 year, 1 hr),

3027 (100 year, 1 hr), 3028 (100 year, 1 hr)

Time period presented in graphs: 09:00 10/02 – 09:00 01/09

The objective of this experiment was to investigate the effect of soil moisture initial conditions on the model simulations. Due to difficulties in initialising lumped and distributed models for slowly responding catchments, a long historical warm-up period (01/07/00 – 10/02/01) that ended with a reasonable flow peak was used as a proxy for initialising the model soil moisture. Then the convective Darwen storm with rainfall amounts scaled to a 1 hour, 100 year return period, was applied at different points during the flood peak recession. For storm 3024 the Darwen storm was applied immediately after the historical peak; subsequent storms were applied at delays of 1 month. To avoid confusion, the potential evaporation at the end of the warm-up period was maintained for all storms.

The model simulations are presented in the left hand column of Figure 8.11. They agree qualitatively, with the difference in consecutive storm flood peaks rapidly tailing off. Quantitatively the Grid-to-Grid model produces larger flood peaks: this is because the localised nature of the storms saturates some grid-squares in the distributed model causing increased localised runoff whereas the PDM has a large catchment soil moisture capacity which does not reach saturation (see Figure 8.11) thus limiting the surface response of the PDM as the soil moisture deficit (SMD) increases.

Key points

- Investigated effect of model soil moisture initial conditions when applying a convective storm.
- Very slow catchment, difficult to calibrate
- Reasonable quantitative agreement between both models over all storms.
- Evidence of model disagreement. The PDM has a large catchment soil moisture capacity so the amount of runoff generated by a storm which does not cause catchment saturation is very sensitive to the initial SMD. The Grid-to-Grid model appears to be more sensitive to the spatial distribution of the rain than the initial SMD conditions so still produces large flood peaks for all storms.

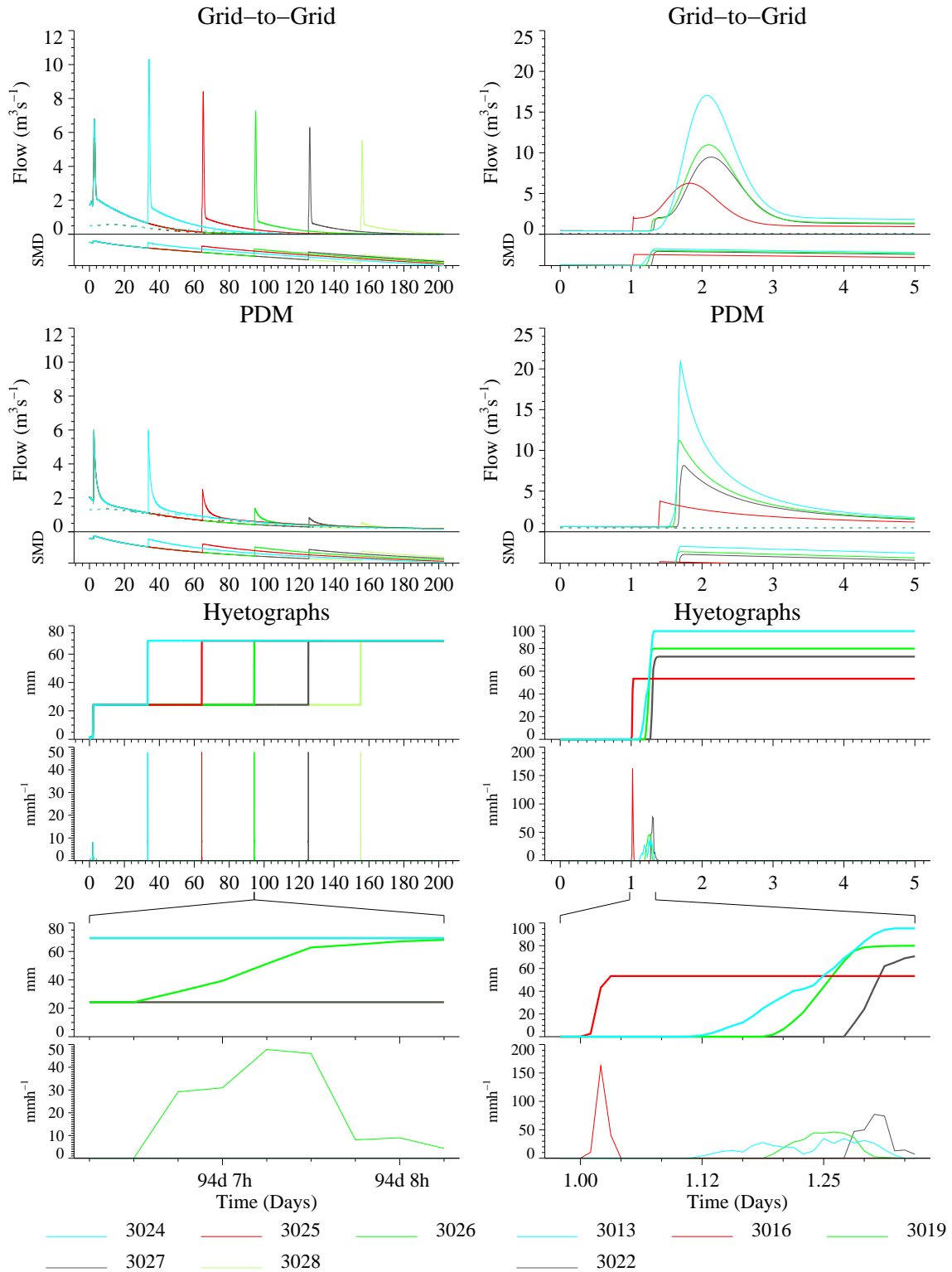


Figure 8.11 Amplified storms and hydrological model flood response for the Sor at Bodicote catchment. Left column: Experiment 11 using Darwen convective storm. Right column: Experiment 12 using a variety of convective storms.

Experiment 12

Target catchment: Sor at Bodicote

Historical storms used: all convective, Boscastle (3013), Carlton-in-Cleveland (3016), Halifax (3019) and Darwen (3022)

Amplified storms used (rainfall return period and duration):

3013 (500 year, 4 hr), 3016 (500 year, 30 mins),

3019 (500 year, 2.5 hr), 3022 (500 year, 1 hr)

Time period presented in graphs: 09:00 14/06 – 09:00 19/06

The purpose of this experiment is to explore how convective events of differing duration, spatial extent and intensity can affect flood genesis. The historical convective storms have simply been relocated to the Sor at Bodicote catchment and the rainfall amounts scaled to attain 500 year return periods. The model simulations for Bodicote are given in the right hand column of Figure 8.11. The hyetographs show that, for a given return period, the longer duration convective storms are generally associated with lower peak intensities.

The simulations show good agreement between the two models in terms of peaks but the Grid-to-Grid model simulations are always slightly later. The good agreement in volumes is confirmed from the water balance quantities given in Table 8.6 for storm 3013. The Grid-to-Grid model simulations show an initial jump in response followed by a slowly evolving peak. Although at first this behaviour seems odd it is not a sign of model failure. Closer examination reveals that the Grid-to-Grid model responds to the heavy rainfall by generating significant runoff in the grid squares affected: this causes the initial jump. Then the slow wave speeds route this runoff creating the slowly evolving flood peaks.

Key points

- Relocated a variety of convective storms to investigate model response to storms of differing duration, spatial extent and intensity.
- PDM simulations show that lumped conceptual models produce similarly shaped hydrographs regardless of the storm and catchment configuration.
- Since the catchment responds very slowly to rainfall the Grid-to-Grid model also produces similarly shaped hydrographs for each storm but can have an immediate jump in response caused by large rainfall and hence surface runoffs at the grid-square used for the model output.

8.6 Conclusions

The flood response experiments using amplified extreme storms have allowed investigation of the key mechanisms of extreme flood genesis. A summary of the main findings are given below with reference to the appropriate experiments. The following comments principally apply to small and medium catchments: the maximum catchment size used in this study is 209 km².

Long duration (>15 hours) frontal and orographic storms

- These storms are generally widespread and affect most of the catchment.
- Sensitivity of case study catchments to duration and magnitude of frontal and orographic storms was investigated by stretching the storm in time and scaling rainfall amounts to attain given return periods – see experiments 1, 5, 7 and 9.
- Good agreement between PDM (a lumped conceptual model) and the Grid-to-Grid model (a distributed model) for a range of storm magnitudes and durations over all case study catchments **except** the Sor at Bodicote.
- Evidence of poor agreement between model simulations for the Sor at Bodicote when using very extreme storms in excess of 100 year return period. This is not necessarily surprising as the Sor was the most challenging catchment to calibrate. Experiment 10 highlights the differences and recommends that the Grid-to-Grid model wave speed parameters be increased to avoid unrealistic land surface storage of water. A good example of where models that perform well over calibration events can show shortcomings when exposed to extreme rainfalls.
- For quickly responding case study catchments (e.g. the River Kent and the River Darwen) it is the rainfall intensity profile over a short duration (less than a day) that determines flood magnitude – see experiments 1 and 5.
- For slowly responding case study catchments (e.g. the Stour and Upper Thames) the long duration rainfall amount is the key factor in determining flood magnitude – see experiments 7 and 9.

Convective events

- Due to the multitude of factors that combine to cause an extreme convective event, no two storms are the same. The purpose of the flood response experiments using amplified extreme convective storms is to investigate the effect of storm to catchment configurations on flood genesis (e.g. storm location, storm direction or spatial extent) and to test and assess calibrated hydrological models.
- Lumped models, for a given short duration storm total and catchment, do not differentiate between storms with differing location, spatial extent or temporal distribution. The resulting simulations are virtually identical. This

is true for quick and slow response case study catchments – see experiments 2, 3, 6 and 8.

- For a given catchment, short duration convective storms cause lumped models to produce similarly shaped hydrographs regardless of the storm and catchment configuration – see experiments 9 and 12. This is true for quick and slow response case study catchments.
- In contrast the Grid-to-Grid model simulations showed sensitivity to storm location, direction, spatial extent and spatial intensities. The resulting simulations can vary dramatically in appearance due to the topographic routing and runoff controls used by the Grid-to-Grid model – see experiment 9. This emphasises the potential benefit of using distributed modelling for extreme convective storms. The main sensitivities found are summarised below.
 1. For a given storm duration and total, convective storms whose direction of travel is aligned with the river channel (i.e. from headwaters to outlet) can produce larger simulated peaks than storms that are not aligned. Experiment 2 shows a 30% difference.
 2. Convective storms that are simply relocated to another part of the catchment, whilst maintaining the same catchment rainfall, produced similar size simulated peaks but shifted in time to reflect the proximity of the storm centre to the catchment outlet. Experiment 6 showed that a storm confined to the headwaters of the catchment (3019) produced a peak response 2 hours 15 minutes later than a storm confined to the lower reaches. However the distribution of peak flows throughout the catchment is dependent on storm location: see Figure 8.7
 3. For a given storm total, a localised extreme convective storm covering only part of the catchment has greater grid-square intensities than a storm which covers the entire catchment. As a result the Grid-to-Grid model generally produces more runoff for the localised storm as there is less soil storage available over the storm domain compared to that available for the catchment-wide storm. Therefore the ratio of the storm spatial scale to the catchment scale can be very important. Experiments 6 and 8 show that, for a given storm total, the localised storms can produce simulated peaks up to 77% larger than catchment-wide storms.
- The lumped model and Grid-to-Grid models generally agreed well (except for the Stour at Shipston) when:
 1. the spatial extent of the storm covers the majority of the catchment – see experiment 3 and storm 3025 of experiment 4;
 2. the storm accumulation covers a majority of the catchment and the storm direction is not aligned down the main river valley – see experiment 2, storms 3018, 3019 and 3020; and
 3. the catchment responds very slowly – see experiment 12.
- Poor agreement between the PDM and Grid-to-Grid model was found for the Stour at Shipston catchment when using extreme convective storms, despite good agreement over calibration events. After analysing the historical record at Shipston the Grid-to-Grid simulations appeared more reasonable. The PDM predicted lower flows and this has been attributed to the low rainfall factor of 0.76. This highlighted how models that agree

well over a calibration period can diverge under extreme rainfall conditions.

- For quickly responding case study catchments (e.g. the River Darwen) the initial model soil moisture condition used when applying the extreme convective storms has a limited impact on simulated flood magnitudes. Only significant rainfall in the few days before the extreme convective storm increased the simulated flood peak. An example is given in Experiment 4 showing good agreement between both models.
- For slowly responding catchments (e.g. the Upper Thames) the initial model soil moisture condition used when applying extreme convective storms can have a significant impact on simulated flood magnitudes. Experiment 11 shows that both models are affected by significant rainfall events up to 6 months before the extreme convective storm. However the distributed Grid-to-Grid model gives more plausible and noticeably larger responses than the lumped PDM model.

9 Summary, conclusions and recommendations

9.1 Summary

A brief summary of the work carried out under this study is given below.

1. Case study selection and description (Sections 2 and 5). One orographic, one frontal and four convective rainfall events with radar coverage have been selected. Further discussion with Environment Agency hydrologists identified three extreme flood case studies, one for each type of rainfall. Hydrometric data have been obtained from the Agency for each case study and radar data, at the finest resolution available, have been obtained. These data are included in the Extremes Dataset that forms an important output of this study: see Cole and Moore (2006). Detailed descriptions of case study rainfall events and catchments are given in Section 5.

2. Rainfall-runoff model selection (Section 3). The PDM (Probability Distributed Model) is chosen as representative of a lumped rainfall-runoff model and is in use operationally by the Agency. The Grid-to-Grid model, developed by CEH to exploit spatial information in gridded rainfall data and topographic datasets, is used as the distributed model.

3. Rainfall estimation (Sections 4 and 6). Typically lumped rainfall-runoff models are used by the Agency with catchment average rainfall estimated by applying a set of linear weights to the point raingauge values. However, the focus in this study is on spatial rainfall estimators. Therefore, in addition to considering only *radar rainfall data*, a multiquadric surface fitting technique has been developed that creates a *raingauge-only rainfall surface* by forming gridded estimates of rainfall from the point raingauge values. This technique can also be used to combine raingauge and radar data to create a *raingauge-adjusted radar* estimate of rainfall. Optimum forms of these surfaces have been derived for each case study and are included in the extreme dataset. The gridded rainfall estimators were suitable for use as input to the distributed model. They could also be viewed through Hyrad allowing catchment average rainfall, needed for lumped modelling, to be calculated. Obtaining future rainfall estimates from extrapolating rainfall surfaces forward in time, sometimes referred to as nowcasting, has not been investigated.

4. Rainfall amplification (Section 4). A credible and practical approach to transforming historical spatial rainfall fields to more extreme ones has been developed. A Rainfall Transformation Tool has been created that can change the position, movement, orientation, size and shape of a spatio-temporal rainfall dataset. The methodology underpinning this tool is set down in Appendix A and B. A 4D visualisation tool has also been developed to obtain animated displays of the transformed rainfall fields to support work on catchment flood response studies.

5. *Generation and application of extreme rainfall datasets for flood response experiments (Section 4.6)*. Methods based upon the Flood Estimation Handbook (FEH) have been developed which utilise catchment specific return period estimates of both rainfall (amount and duration) and river flow. An illustrative example is given using simple synthetic rainfall profiles.

6. *Model flood response over historical events (Section 7)*. For each extreme flood case study both rainfall-runoff models (PDM and Grid-to-Grid) have been calibrated using each of the three rainfall estimators (radar, raingauge-only and raingauge-adjusted radar). The calibrated models have then been tested over the extreme flood event of interest. Model performance has been assessed and any failings noted. This prompted development of a prototype distributed model that utilises soil/geology datasets in addition to topography. The calibrated PDM input files have been included in the extreme dataset (see 9. below).

7. *Flood response experiments using amplified storms (Section 8)*. Over 100 amplified storms have been constructed using the above methodology and are contained in the extreme spatio-temporal rainfall dataset. This allowed the flood response experiments to investigate complex storm-to-catchment interactions and to give improved understanding of extreme flood genesis. The simulations using both models (lumped and distributed) have given insights into their individual merits and limitations.

8. *Use of rainfall datasets for model destruction testing*. During the historical event analysis and flood response experiments, obvious model failure has been noted as and when it occurred and where possible, a cause attributed. Possible causes of model failure include: poor coding of the model, inappropriate selection of model parameter values, model configuration, missing physical processes in the model and/or model limitations. In addition Appendix D demonstrated how a poorly formulated model solution can lead to chaotic disturbances in flow values at fixed time-points when using fixed-duration rainfall profiles of changing magnitude.

9. *Extreme spatio-temporal rainfall dataset*. A major output of the study is the 'Extremes Dataset' and its accompanying documentation (Cole and Moore, 2006). The collated raingauge, radar, river flow/level and MORECS potential evaporation data and created spatial rainfall estimators (raingauge-only rainfall surfaces and raingauge-adjusted radar rainfall fields) has generated a unique extreme storm dataset. For the flood response experiments the amplified spatio-temporal rainfalls are also provided. All the spatio-temporal rainfall data can be viewed through Hyrad. Software has been developed to allow users of the dataset to relocate and scale (in magnitude) any of the historical or amplified storms.

9.2 Conclusions

1. Rainfall estimation

Incidental parameters used to generate spatial rainfall estimators (e.g. raingauge-only rainfall surface or gauge-adjusted radar rainfall) were optimised by minimising an objective function, e.g. the *rmse* statistic. However, visualisation of the optimised estimator over different rainfall types revealed that the raingauge-only estimator had unwanted characteristics, e.g. convective storms being smoothed out across a larger area. Therefore a ‘zero parameter’ raingauge-only rainfall surface was proposed that had a small effect on the objective function but remedied the unwanted characteristic.

From a hydrological perspective, a more appropriate test of a rainfall estimator is its ability to predict simulated river flow through a rainfall-runoff model. Conclusions about the rainfall estimators from a hydrological perspective are given below.

Generally raingauge-based estimators (i.e. weighted raingauge data or raingauge-only rainfall surface) gave the best rainfall-runoff model performance for both models over the extreme events of interest and the periods used for calibration.

Radar rainfall estimators, without raingauge-adjustment, produced model hydrographs that intermittently over-/under-estimated observed flows. In particular the extreme convective (River Darwen) and frontal (Upper Thames and Stour) case studies were underestimated. The Nimrod QC product gave better model performance than the raw radar product but was still not as good as the raingauge-based simulations. Missing radar data had a minimal effect on model performance.

Adjusting radar data using raingauge data (at 15 minute time intervals) dramatically improved model performance to a level comparable with raingauge-only rainfall estimators. This highlighted the added value that combining raingauge and radar data can have for hydrological modelling whilst preserving the spatial information contained in the radar data.

However, radar data, unadjusted by raingauge, can still be used as a complementary source of rainfall estimation. They have particular advantages in areas with relatively few raingauges, for observing convective storms that are not always sampled by the raingauge network and as the basis of nowcasting.

2. Model performance over historical case study events

Whilst model performance over the calibration events was not of primary interest, it was still important to consider as it put the performance for the extreme events into context. Best model results were for the simply responding upland catchments (River Kent and River Darwen) where topographic controls dominate hydrograph formation and soil/geology/land-cover controls are

homogeneous or weak. In contrast the responses of lowland basins (Upper Thames and Stour) have strong heterogeneous soil/geology controls and were more challenging to model. For the calibration events the PDM almost always offered a marginal improvement over the Grid-to-Grid model. This is in keeping with results from the recent DMIP (Distributed Model Intercomparison Project) in the USA (Smith *et al.*, 2004) where lumped conceptual models often provide as reliable, if not better, flood forecast performance as distributed models, at least at the gauged sites used in model calibration.

Over the case study extreme events, neither model consistently outperformed the other. In general the lumped and distributed models agreed well with each other but tended to underestimate the observed flood peak. Again, best performance was achieved for the upland catchments. The performance of the area-wide Grid-to-Grid model for the extreme orographic event affecting the River Kent was particularly noteworthy as it successfully predicted the flow across five gauged sites. This has obvious implications for providing flood warning of extreme events at any location within the region, whether gauged or ungauged.

The relatively poor model performance for the extreme frontal event affecting the Upper Thames and Stour lowland catchments reflects the difficulties encountered during model calibration. This has been attributed to strong heterogeneous soil/geology controls on flood response and prompted development of a prototype distributed model able to make use of spatial soil/geology property datasets (see point 4 below).

It is difficult to attribute the general model underestimation of the observed flow peaks to any one cause. The flow observations, derived from extrapolated rating curves, provide a major source of uncertainty as the flood peaks were the largest on record at all gauging stations and were generally out of bank. The Environment Agency's Best Practice Guidance Manual on extension of rating curves at gauging stations (Ramsbottom and Whitlow, 2003) provides guidance on how this issue may be investigated further.

3. Model destruction testing

Appendix D illustrates how poorly-coded models can fail when subjected to unrealistically high values of rainfall input in excess of 15 metres in 12 hours. Therefore it is better to destruction test models by subjecting them to realistic extreme rainfall amounts, e.g. use FEH derived return periods as a guide, rather than increasing rainfalls to unrealistic amounts to force models to fail.

4. Model development

Understanding the flood genesis over a wide area for the Easter 1998 widespread frontal storm over the Upper Thames and Stour is important for identifying possible flood-prone areas. The inability of the topographically-driven Grid-to-Grid model to achieve satisfactory performance over all three of the Upper Thames and Stour gauging stations was attributed to strong heterogeneous soil/geology controls on flood response that were not

represented in the model formulation. This motivated the development of a prototype distributed model that encompassed the entire area affected by the extreme flood and utilised soil/geology information through the HOST/SEISMIC datasets. Not surprisingly, the catchment specific calibrations of the simple Grid-to-Grid and PDM models perform better at the gauged locations, especially over the extreme event, but fail to be robust in inferring flows at other sites, internal or external to the calibrated catchment. In contrast, the prototype model shows encouraging partial success in achieving a consistent area-wide simulation using a single parameter set (Section 7.6), particularly over the calibration event. This property of the prototype model is invaluable for identifying flood-prone locations and makes the model deserving of further investigation.

5. Flood response experiments

Long duration (>15 hours) frontal and orographic events

For amplified widespread frontal or orographic rainfall events the lumped and distributed models were expected to agree well. There was good agreement between models for all case studies **except** the Sor at Bodicote. The Sor at Bodicote illustrated how models that agree well during historical events can diverge when using amplified storms. This type of model failure is usually due to one model being inadequate in some way (e.g. a missing process or a breakdown of a process under extreme conditions) or the inappropriate selection of one or more model parameters. For the Sor at Bodicote the Grid-to-Grid model wave speed parameters need to be increased to avoid unrealistic land surface storage of water and therefore it was the model calibration that failed rather than the model. Identifying why models diverge under amplified extreme storms is vital for understanding extreme flood genesis and improving the physical-conceptual development of models and their robustness under extreme rainfall.

The experiments revealed that for quickly responding catchments (e.g. River Kent and River Darwen) the rainfall intensity profile over short durations (less than a day) is the principal factor determining flood magnitude and that for slowly responding catchments (e.g. the Upper Thames and Stour) the long duration rainfall total is the principle factor.

Convective events

For a given case study catchment, the flood response of lumped models for short duration events is dominated by the storm total and not the spatio-temporal storm pattern. A consequence is that all short duration storms cause lumped models to produce similarly shaped hydrographs.

In contrast the Grid-to-Grid model proved to be very sensitive to the spatio-temporal pattern of the amplified extreme storms due to the topographic routing and runoff controls used. In particular storm location, spatial extent, spatial intensities and direction and speed of travel significantly affected the distributed model simulation resulting in more plausible flood responses. This emphasises the potential benefit of using distributed models when exposed to extreme and/or unusual convective storms. This has obvious repercussions when

interfacing hydrological models to ensemble rainfall forecasts, particularly if convective storms are predicted.

Extreme event recognition

The flood response experiments have shown that exposing distributed hydrological models to storm conditions greater than those in the historical record can identify locations within a catchment that may be particularly vulnerable to flooding. This provides support to extreme flood recognition in advance of one occurring. Flood mitigation measures can be planned and flood warning schemes instigated. An awareness of the context within which extreme floods may develop will help in flood preparedness.

6. Extreme spatio-temporal rainfall dataset

The 'Extremes Dataset' provides an excellent platform for hydrological model testing and development and should be used to its full potential. The inclusion of data used for calibration purposes increases the value of the dataset, allowing others to recreate the entire process of model calibration through to model evaluation over the extreme storm events.

It also provides a valuable test-bed for developing distributed model initialisation and state-updating procedures (for use in real-time flood forecasting) using observational data at several spatial locations. Of particular relevance are the River Kent and River Darwen case studies which have multiple nested gauging locations.

The software developed for users to transpose and scale storms, along with the 'Extremes Dataset' documentation (Cole and Moore, 2006), makes the dataset even more flexible and useful. For example, flood warning practitioners within the EA can run 'what if?' scenarios using realistic extreme storms over any target catchment and study the hydrological model responses.

9.3 Recommendations

1. Rainfall estimators

- The 'zero parameter' raingauge-only rainfall surface, calculated on a 1km grid, has provided a good spatial rainfall estimator for rainfall-runoff modelling over the case study catchments for a range of storm types and magnitudes. As there are no incidental parameters to optimise, this spatial rainfall estimator could be implemented nationwide or on a catchment/regional basis. It could be made operational using existing functionality within Hyrad. A raingauge-based spatial rainfall estimator is seen as essential if distributed grid-to-grid modelling is to be used by the Agency. Further investigation might focus on the performance for sparse raingauge networks and what implications the 'flatness at large distance' constraint may have at locations far from dense parts of the network.
- Raingauge-adjustment of radar, at a 15 minute interval, provided much improved rainfall-runoff model performance relative to unadjusted radar

data. In this study, the incidental parameters of the surface fitting involved in the adjustment have been optimised for each case study catchment. The adjustment could be implemented operationally through existing Hyrad functionality. Further work might investigate its implementation on a nationwide scale.

- In the context of flood forecasting, the raingauge-adjusted radar rainfall (adjusted at intervals of 15 minutes) might be considered for use in nowcasting of rainfall, including use within Nimrod and Hyrad.

2. Model development

- The simple Grid-to-Grid formulation performed well for catchments dominated by topographic controls and is recommended for operational trials in upland catchments. The model may need to be calibrated over regions of interest to get the best performance. The model should add value when forecasting the area-wide flood response, at gauged and ungauged locations, from extreme and/or unusual storms.
- Hydrological distributed models of a conceptual-physical type should be developed further to capitalise on spatial soil/geology/land-cover datasets. Such approaches are key to forecasting the area-wide flood response of complex catchments with strong heterogeneous soil/geology controls and for identifying particularly flood-prone locations. Further development and operational trials of the prototype distributed model presented in Section 7.6 are recommended.
- The application of distributed area-wide models for operational flood warning could be improved by addressing the following challenges: model initialisation, forecast updating, uncertainty estimation and utilisation of future advances in ensemble rainfall forecasting.

3. Extreme spatio-temporal rainfall dataset

The Extremes Dataset and the software developed to allow users to transpose and scale storms (in magnitude) should be used:

- to destruction-test models and model calibrations within realistic rainfall ranges (e.g. use FEH for guidance)
- to serve as a catalyst for model improvement (see point 2 above)
- to run flood forecast ‘what if?’ scenarios using realistic extreme storms over any target catchment(s) of interest
- to train flood forecasters and flood warning officers by gaining the experience of extreme storms and the associated flood responses
- to gain a greater understanding of flood genesis
- to identify locations vulnerable to extreme floods, even in advance of them occurring – methods for implementation need to be developed.

4. Rating curve extension

- The extreme event case studies should be used to explore the feasibility of rating curve extension via physically-based methods, such as those outlined in the Agency’s Best Practice Guidance Manual W6-061/M.

References

- Balascio, C.C., 2001. Multiquadric equations and optimal areal rainfall estimation. *J. Hydrologic Engrg.*, **6**(6), 498-505.
- Bell, V.A. and Moore, R.J., 1998a. A grid-based distributed flood forecasting model for use with weather radar data: Part 1. Formulation. *Hydrol. Earth System Sci.*, **2**(2-3), 265-281.
- Bell, V.A. and Moore, R.J., 1998b. A grid-based distributed flood forecasting model for use with weather radar data: Part 2. Case Studies. *Hydrol. Earth System Sci.*, **2**(2-3), 283-298.
- Bell, V.A. and Moore, R.J., 2004. *Development of a flow routing and flood inundation facility for Nimrod/CMetS*. Report to the Met Office, CEH Wallingford, 56 pp.
- Boorman, D.B., Hollis, J.M. and Lilly, A., 1995. Hydrology of soil types: a hydrologically based classification of the soils of the United Kingdom. *IH Report No. 126*, Institute of Hydrology, Wallingford, 137pp.
- Box, G.E.P. and Jenkins, G.M., 1970. *Time series analysis forecasting and control*, Holden-Day.
- Bye, P., 1998. *Easter 1998 Floods, Report by the independent Review Team to the Board of the Environment Agency: Volume 2*, September 1998, Environment Agency, 341pp.
- CEH Wallingford, 2005. *PDM Rainfall-Runoff Model*. Version 2.2, Centre for Ecology & Hydrology, Wallingford. (Includes Guide, Practical User Guides, User Manual and Training Exercises).
- Cinderey M., 2005. The North Yorkshire-Teeside storm of 10 August 2003, *Weather*, **60**(3), 60-65.
- Cole, S.J. and Moore, R.J., 2006. *Spatio-temporal rainfall datasets and their use in evaluating the extreme event performance of hydrological models: The Extremes Dataset*. R&D Technical Report FD2208, Report to Defra and the Environment Agency, CEH Wallingford, 60pp.
- Collier, C.G., Fox, N.I. and Hand W.H., 2002. *Extreme Rainfall and Flood Event Recognition*. Contract Report FD2201 to Defra/Environment Agency, 57pp.
- Dooge, J.C.I., 1973. Linear theory of hydrologic systems. *Technical Bulletin No. 1468*, Agriculture Research Service, United States Department of Agriculture, U.S. Government Printing Office, Washington, DC20402, USA, 327 pp.
- Dunne, T. and Leopold, L.B., 1978. *Water in Environmental planning*. W.H. Freeman, San Francisco, 818pp.

- Environment Agency, 2004a. *The Kent Catchment Abstraction Management Strategy*. Environment Agency, 41pp.
- Environment Agency, 2004b. *The Swale, Ure, Nidd and Upper Ouse (SUNO) Catchment Abstraction Management Strategy*. Environment Agency, 34pp.
- Environment Agency, 2005. *The Cherwell Catchment Abstraction Management Strategy*. Environment Agency, 25pp.
- Faulkner, D., 1999. *Flood Estimation Handbook. Volume 2 Rainfall frequency estimation*. Institute of Hydrology, 110pp.
- Fekete, B.M., Vörösmarty, C.J. and Lammers, R.B., 2001. Scaling gridded river networks for macroscale hydrology: Development, analysis, and control of error. *Water Resour. Res.*, **37**(7), 1955-1967.
- Golding, B. (ed.), 2005. Boscastle and North Cornwall Post Flood Event Study – Meteorological analysis of the conditions leading to flooding on 16th August 2004, *Met Office Forecasting Research Technical Report No. 459*, Met. Office, UK, 85pp.
- Golding, B., Clark, P. and May, B., 2005. The Boscastle Flood: Meteorological analysis of the conditions leading to flooding on 16 August 2004, *Weather*, **60**(8), 230-235.
- Hand, W.H., Fox, N.I. and Collier, C.G., 2004. A study of twentieth-century extreme rainfall events in the United Kingdom with implications for forecasting. *Meteor. Apps.*, **11**, 15-31
- HR Wallingford, 2005. *Flooding in Boscastle and North Cornwall, August 2004 – Phase 2 Studies Report*, Contract Report EX5160 to the Environment Agency, HR Wallingford, 170pp.
- Moore, R.J., 1985. The probability-distributed principle and runoff production at point and basin scales, *Hydrol. Sci. J.*, **30**(2), 273-297.
- Moore, R.J., 1986. Advances in real-time flood forecasting practice. *Symposium on Flood Warning Systems*, Winter meeting of the River Engineering Section, Inst. Water Engineers and Scientists, 23 pp.
- Moore, R.J., 1999. Real-time flood forecasting systems: Perspectives and prospects. In: R. Casale and C. Margottini (eds.), *Floods and landslides: Integrated Risk Assessment*, Chapter 11, 147-189, Springer.
- Moore, R.J. and Bell, V.A., 2001. Comparison of rainfall-runoff models for flood forecasting. Part 1: Literature review of models. *Environment Agency R&D Technical Report W241*, Research Contractor: Institute of Hydrology, September 2001, Environment Agency, 94pp.

Moore, R.J. and Bell, V.A., 2002. Incorporation of groundwater losses and well level data in rainfall-runoff models illustrated using the PDM. *Hydrol. Earth System Sci.*, **6**(1), 25-38.

Moore, R.J., Bell, V.A. and Carrington, D.S., 2000. Intercomparison of rainfall-runoff models for flood forecasting. In: M. Lees and P. Walsh (eds.), *Flood forecasting: what does current research offer the practitioner?* Occasional Paper No. 12, British Hydrological Society, 69-76.

Moore, R.J., Watson, B.C., Jones, D.A. and Black, K.B., 1989. London weather radar local calibration study: final report. Contract report prepared for the National Rivers Authority Thames Region, September 1989, Institute of Hydrology, 85pp.

Morris D.G., 2003. *Appraisal of flood frequency estimates based on FEH statistical procedure*. Contract Report FD1603 to Defra, October 2003, Centre for Ecology & Hydrology, 207pp.

Morris, D.G. and Flavin, R.W., 1990. A digital terrain model for hydrology. *Proc. 4th Internat. Symp. on Spatial Data Handling*, 23-27 July, Zürich, Vol. 1, 250-262.

NERC 1975. *Flood Studies Report. Volume 2 Meteorological Studies*. Natural Environment Research Council, 81pp.

O'Connor, K.M., 1982. Derivation of discretely coincident forms of continuous linear time-invariant models using the transfer function approach. *J. Hydrol.*, **59**, 1-48.

Or, D. and Wraith, J.M. 2002. Soil water content and water potential relationships. In: Warrick, A.W. (ed.), *Soil physics companion*, CRC Press, Boca Rouge, 49-84.

Pegram, G.C. and Pegram, G.G.S., 1993. Integration of rainfall via multiquadric surfaces over polygons. *J. Hydr. Engrg.*, **119**(2), 151-163.

Ramsbottom, D.M. and Whitlow, C.D., 2003. *Extension of rating curves at gauging stations. Best Practice Guidance Manual*. R&D Manual W6-061/M, Research Contractor: HR Wallingford in association with Eden Vale Modelling Services, Environment Agency, 254pp.

Thiessen, A.H., 1911. Precipitation for large areas. *Mon. Wea. Rev.*, **39**, 1082-1084

Wood, S.J., Jones, D.A. and Moore, R.J., 2000. Static and dynamic calibration of radar data for hydrological use. *Hydrol. Earth System Sci.*, **4**, 545-554.

Appendix A Amplification of extreme spatio-temporal rainfall datasets

A.1 Context

The flood response of a rainfall-runoff model will depend on the spatio-temporal evolution of the storm causing it. Radar and raingauge data from extreme storms in the past can be collated to provide spatio-temporal datasets for studies of flood response using rainfall-runoff models. These datasets can be used to assess and improve model performance at times of extreme rainfall and for the purposes of model destruction testing.

To test model performance and resilience beyond the range of historical records, there is a need for even more extreme rainfall datasets. The approach to be taken in this study to this problem is to start with the historical datasets and to transform them to more extreme forms. This can be done by first identifying a small number of characteristics of the storm that, through manipulation of these characteristics, can be used to generate extreme rainfall fields exhibiting more extreme behaviour. The relevant storm characteristics to be considered are position, orientation, movement, size and shape. Formal specification of these characteristics will allow a Rainfall Transformation Tool to be developed. This specification is developed below.

The aim is to develop formulae for creating spatial rainfall datasets as modified forms of existing ones. The approach is to provide values with which to “fill-in” pixels within the set of time-frames to be created. This will work on a “come-from” basis (i.e. working out where a spatial point comes from in the original dataset) rather than on a “go-to” basis (i.e. starting from some point in the original dataset and working out where it moves to).

The implemented scheme will work out values for 4, 9, 16 or 25 points within each target grid-cell as the basis of an average value for the grid cell. It will be assumed that the original dataset of time-frames provides “all” the rainfall. Points in the target time-frames which “come from” points outside the range of the original dataset will be set to zero (rather than “missing” as in advection forecasting).

A.2 Specification of storm characteristics

A.2.1 Position

We need to be able to move a storm from one part of the country to another. This is the classical task of storm transposition. There may need to be some restrictions on position based on orography and storm-type, since certain types of storm may “never” occur in some locations. A specific definition of “position”

may be the location of the highest intensity (averaged over a moderately sized region) within the storm.

Let the “centre” of the storm be at location (x_0^0, y_0^0) in NGR units, and at time τ_0^0 .

Here, the superscript 0 indicated the original set of time-frames. Later, a superscript T indicates the target set of time-frames. The subscript 0 indicates that these coordinates refer to the “centre” of the storm.

A.2.2 Orientation

Specifically, here we are concerned with the orientation of major bands of rainfall within a storm as distinct from direction of travel. As with position, spatial transposition of storms may be restricted to particular orientations. A specific definition for each storm will be determined visually and will no doubt involve compromises. For some types of storm, “orientation” may not be defined.

Let the orientation of the bands be defined by θ_{band}^0 , an angular measure. The specific definition will be as shown in the diagram of Figure A.1, where orientation is defined as the angle of the perpendicular to the band relative to the West-East axis.

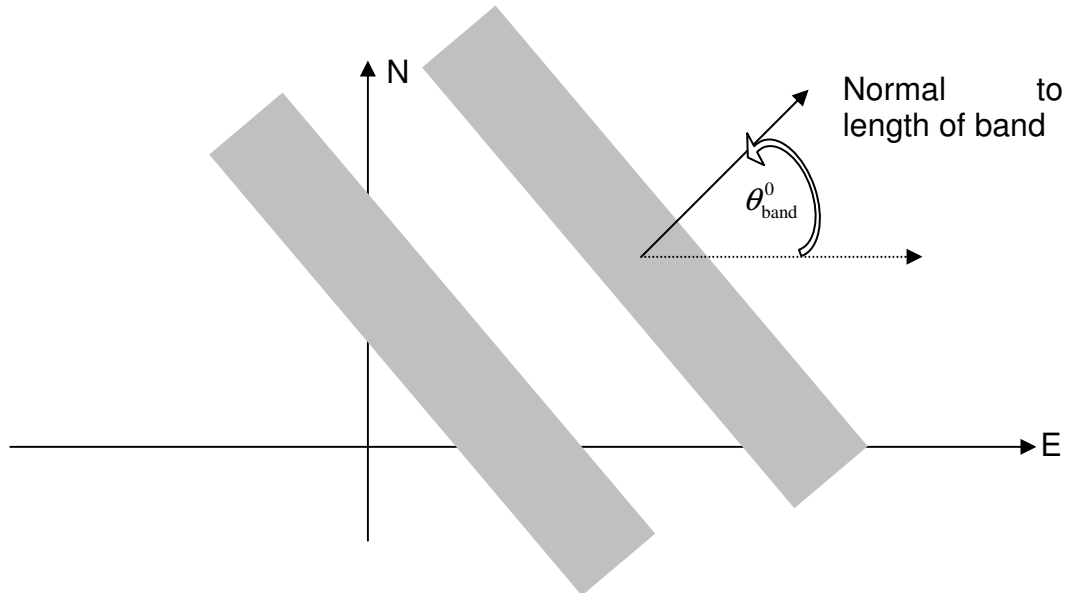


Figure A.1 Definition of “orientation” of rainfall bands

A.2.3 Movement

Specifically, movement will be characterised by the “advection velocity” defining the speed and direction of movement of the storm. A specific definition for each storm will be determined visually and will no doubt involve compromises.

Let the speed and direction associated with the original storm be determined by the pair (u_0^0, v_0^0) in units of NGR unit per time-step, where “time-step” is the fixed time-step between time-frames in the original dataset and in the target dataset.

A.2.4 Storm transposition and modification

Transposition and modification of storms will involve changing a number of aspects of the storm when creating the fictitious datasets. The following are some possibilities.

(i) *Relative position*: This concerns the location of the “centre” relative to catchment boundaries, where the centre would be the overall “location” identified in A.2.1. There is a need to allow the “centre” to lie over the upper, middle or lower part of a catchment.

Let the required “centre” of the storm be at location (x_0^T, y_0^T) in NGR units.

Here the superscript T indicates the target set of time-frames. The subscript 0 indicates that these coordinates refer to the “centre” of the storm. The centre-time for the target time-frames will be τ_0^T , which is derived from τ_0^0 by applying any time-contraction or expansion factors: the time-location is adjusted relative to the initial time-point of the dataset.

(ii) *Relative orientation*: This concerns the orientation of rainfall bands relative to catchment boundaries and involves turning all rainfall fields about a common centre (normally the overall “location” for the storm). This turning has an implied effect on the direction of travel of the storm which will be accounted for.

If the turning effect is defined via the identified orientation of bands of rainfall, the following approach is possible. Let the orientation of the bands in the dataset to be created be defined by θ_{band}^T , an angular measure. The specific definition is to be the same as that for the original dataset. Then θ_{band}^T , together with θ_{band}^0 , defines an angle, through which the original dataset needs to be turned,

$$\theta_{\text{turn}} = \theta_{\text{band}}^T - \theta_{\text{band}}^0.$$

However, θ_{turn} is the primary quantity in the computations and it may be defined in several ways:

- (i) directly as the angle to be turned through
- (ii) starting from a known θ_{band}^T , as the target angle for the bands

(iii) starting from a relative angle of the bands with respect to a catchment direction, which then goes on to define the target angle θ_{band}^T .

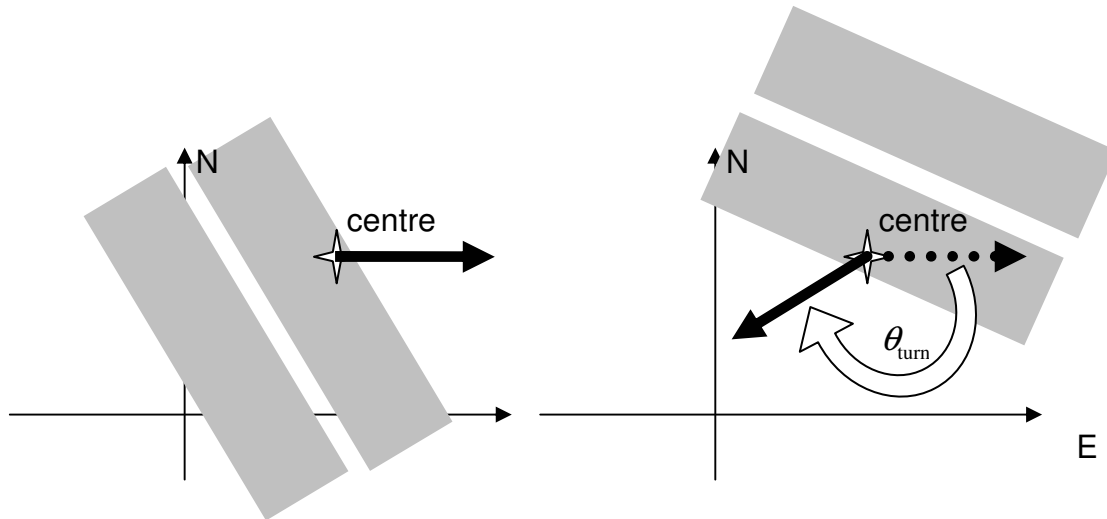


Figure A.2 Illustration of turning (turning through a negative angle)

(iii) *Relative Direction of Travel.* This concerns the need to create storms moving in given directions, where these directions may be measured relative to (a) the shape of the catchment, (b) the original direction of travel, or (c) the pattern of river-channels within the catchment.

(iv) *Speed of travel.* This concerns the need to create storms from the original that move across the catchment at different speeds. It involves an advection-type transposition of the individual time-frames, taking into account the original speed and direction of the storm, so that a zero speed results in a storm which remains centred at the central location for the storm.

Let the speed and direction associated with the target storm be determined by the pair (u_0^T, v_0^T) in units of NGR unit per time-step, where “time-step” is the fixed time-step between time-frames in the original dataset and in the target dataset.

There are several possibilities for defining (u_0^T, v_0^T) , either directly as a speed and required direction, or indirectly as a speed and direction relative to the originals or relative to a “direction” attributed to a catchment.

(v) *Scaling of amounts.* Here, the rainfall rates for the original storm would be multiplied by a common factor.

Let the required overall scaling factor be f .

(vi) *Spatial squeezing/relaxation.* Three types of squeezing can be considered: in two directions (along and perpendicular to the orientation of rainfall bands),

and as a uniform factor. Here the spatial “squeezing” will be calculated so that rainfall amounts are preserved (i.e. rainfall rates would be adjusted). The main use for “more extreme” storms will be squeezing to lead to increased rates, rather than the opposite with reduced rates.

Let the required squeeze factors be s_{a_band} , s_{n_band} , s_{space} . Here values $s_{xxxx} = 1$ imply no squeeze effect. These squeeze factors will lead to rainfall intensities being multiplied by $s_{a_band}^{-1}$, $s_{n_band}^{-1}$, s_{space}^{-2} respectively.

(vii) Spatial contraction/expansion. The aim here is to adjust the spatial extent of the storm, without affecting rainfall rates. For “more extreme” storms the main use will be expansion to lead to more spatially extensive storms, rather than the opposite with less area being affected.

Let the required expansion factors be e_{space} , e_{a_band} , e_{n_band} . Here values $e_{xxxx} = 1$ imply no expansion effect.

(viii) Time-squeezing. Here the time “squeezing” will be calculated so that rainfall amounts are preserved (i.e. rainfall rates would be adjusted). The main use for “more extreme” storms would be squeezing to lead to increased rates of rainfall, rather than the opposite with reduced rates.

Let the required time-squeeze factor be s_{time} . Here values $s_{time} = 1$ imply no squeeze effect. This squeeze factor will lead to rainfall intensities being multiplied by s_{time}^{-1} .

(ix) Time-contraction/expansion. The aim here is to adjust the temporal extent of the storm, without affecting rainfall rates. For “more extreme” storms the main use will be expansion to lead to longer duration storms, rather than the opposite with less time for flows to be built-up.

Let the required expansion factor be e_{time} . Here values $e_{time} = 1$ imply no expansion effect.

Transformations for the time dimension are illustrated in Figure A.3.

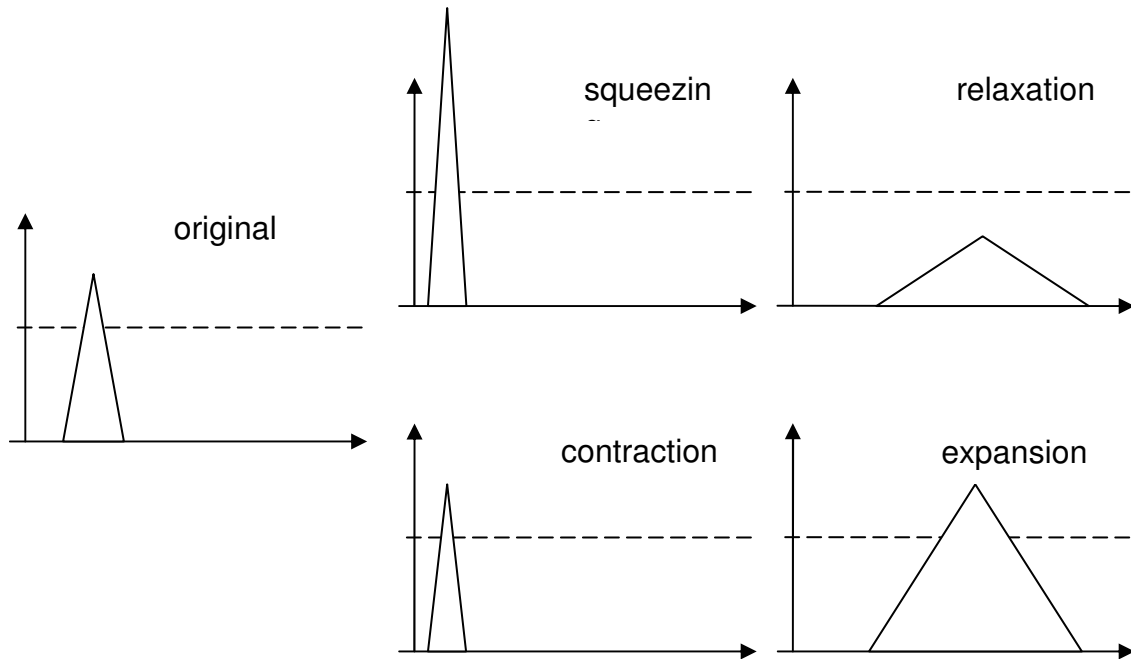


Figure A.3 Illustration of the squeezing/relaxation and contraction/expansion transformations for the time-dimension

Notionally, the order of modifications is as follows:

- (i) a “zero-velocity” storm is constructed by removal of the original velocity and transposition, creating a stationary storm centred on the target location;
- (ii) this storm is then modified by spatial and temporal squeezing and expansion effects;
- (iii) the storm is turned in space around the target location;
- (iv) the storm is given the required target velocity, remaining centred in time at the equivalent of the original central time-point.

A.3 Summary

This specification proposes various ways in which the radar datasets for historical events can be modified to create alternative versions. The new datasets are intended to be applied to rainfall-runoff models in order that the response to “more extreme” rainfall events can be explored. Basing the artificial data on historical events is a means of ensuring that the temporal and spatial patterns of rainfall are reasonably realistic, at least compared to the alternative of using patterns based on geometric shapes. Appendix B outlines some of the formulae required to implement these data-construction procedures.

Appendix B Formulae for rainfall modification

B.1 Introduction

For the purposes here, it is assumed that the new radar rainfall dataset will be constructed within an arbitrary time-frame. The first radar rainfall field in the new dataset will correspond directly to the first radar rainfall field in the original dataset. In the formulation here, the “time” attributed to the first field will be zero for both the original and new datasets: time-expansion/squeezing is relative to this time. Let the time of the final radar rainfall field in the original dataset be T and let there be $N+1$ time-frames in the dataset (N intervals) so that the common time-step is $\delta T = T/N$ (hours)

Let rainfall intensity in the original dataset be $R^{(0)}(x, y, t)$.

B.2 Removal of initial velocity

Consider as a first stage, a version of the rainfall field from which the initial speed and direction of travel have been removed. Let this field be $R^{(1)}$. According to the advection model, a point at $(x^{(0)}, y^{(0)})$ moves to $(x^{(1)}, y^{(1)})$ after a time $\tau = t^{(1)} - \tau_c$ after the centring time τ_c , where

$$x^{(1)} = x^{(0)} + u_0^0 \tau, \quad y^{(1)} = y^{(0)} + v_0^0 \tau.$$

To remove the original velocity, the required transformation is

$$x^{(1)} = x^{(0)} - u_0^0 \tau, \quad y^{(1)} = y^{(0)} - v_0^0 \tau.$$

Therefore $R^{(1)}$ can be constructed as

$$R^{(1)}(x^{(1)}, y^{(1)}, t^{(1)}) = R^{(0)}(x^{(1)} + u_0^0 \tau^{(1)}, y^{(1)} + v_0^0 \tau^{(1)}, t^{(1)}) = R^{(0)}(x^{(0)}, y^{(0)}, t^{(1)}).$$

where

$$x^{(0)} = x^{(1)} + u_0^0 \tau^{(1)},$$

$$y^{(0)} = y^{(1)} + v_0^0 \tau^{(1)},$$

$$\tau^{(1)} = t^{(1)} - \tau_0^0.$$

B.3 Expansion and scaling

At the next stage $R^{(1)}$ is used to define $R^{(2)}$ which is a revised version including the scaling and the spatial and temporal expansions and squeezes.

(i) *Scaling.* Rainfall intensity changes by a multiplicative factor

$$f s_{\text{space}}^{-2} s_{\text{a_band}}^{-1} s_{\text{n_band}}^{-1} s_{\text{time}}^{-1}$$

(ii) *Spatial expansion/squeezing.* This involves band-wise spatial expansion, including uniform expansion, plus translation to new location :

a point at $(x_0^0 + \delta x, y_0^0 + \delta y)$ moves to $(x_0^T + \delta x^*, y_0^T + \delta y^*)$, where

$$\delta x^* = \delta x (r_1 \cos^2 \theta_{\text{band}} + r_2 \sin^2 \theta_{\text{band}}) + \delta y (r_2 - r_1) \sin \theta_{\text{band}} \cos \theta_{\text{band}}$$

$$\delta y^* = \delta x (r_2 - r_1) \sin \theta_{\text{band}} \cos \theta_{\text{band}} + \delta y (r_2 \cos^2 \theta_{\text{band}} + r_1 \sin^2 \theta_{\text{band}})$$

$$r_1 = s_{\text{n_band}} e_{\text{n_band}} s_{\text{space}} e_{\text{space}}$$

$$r_2 = s_{\text{a_band}} e_{\text{a_band}} s_{\text{space}} e_{\text{space}}$$

Hence a point at $(x^{(2)}, y^{(2)})$ comes from a point $(x^{(1)}, y^{(1)})$ where

$$(x_0^T + \delta x^*, y_0^T + \delta y^*) = (x^{(2)}, y^{(2)})$$

$$(x_0^0 + \delta x, y_0^0 + \delta y) = (x^{(1)}, y^{(1)})$$

This gives, for example (see Appendix A.2),

$$\delta x = \left\{ \delta x^* (r_1^{-1} \cos^2 \theta_{\text{band}} + r_2^{-1} \sin^2 \theta_{\text{band}}) + \delta y^* (r_2^{-1} - r_1^{-1}) \sin \theta_{\text{band}} \cos \theta_{\text{band}} \right\}$$

$$\delta y = \left\{ \delta x^* (r_2^{-1} - r_1^{-1}) \sin \theta_{\text{band}} \cos \theta_{\text{band}} + \delta y^* (r_2^{-1} \cos^2 \theta_{\text{band}} + r_1^{-1} \sin^2 \theta_{\text{band}}) \right\}$$

Define

$$A_{\text{band}} = (r_1^{-1} \cos^2 \theta_{\text{band}} + r_2^{-1} \sin^2 \theta_{\text{band}})$$

$$B_{\text{band}} = (r_2^{-1} \cos^2 \theta_{\text{band}} + r_1^{-1} \sin^2 \theta_{\text{band}})$$

$$C_{\text{band}} = (r_2^{-1} - r_1^{-1}) \sin \theta_{\text{band}} \cos \theta_{\text{band}}$$

$$x^{(1)} = x_0^0 + A_{\text{band}} \{x^{(2)} - x_0^T\} + C_{\text{band}} \{y^{(2)} - y_0^T\}$$

$$y^{(1)} = y_0^0 + C_{\text{band}} \{x^{(2)} - x_0^T\} + B_{\text{band}} \{y^{(2)} - y_0^T\}$$

$$R^{(2)}(x^{(2)}, y^{(2)}, t^{(2)}) = R^{(1)}(x^{(1)}, y^{(1)}, t^{(2)}).$$

(iii) *Time expansion/squeezing.* Here a point at τ^0 moves to $s_{\text{time}} e_{\text{time}} \tau^0$.

Hence a point at $\tau^{(3)}$ comes from a point $\tau^{(2)}$ where

$$\tau^{(3)} = s_{\text{time}} e_{\text{time}} \tau^{(2)}$$

$$\tau^{(2)} = (s_{\text{time}} e_{\text{time}})^{-1} \tau^{(3)}$$

The temporal expansion defines time-frames over an extended range of times: from time-zero to $T^{(3)} = (s_{\text{time}} e_{\text{time}})T$. Similarly, the time-centre of the storm moves to τ_0^T , which is derived from τ_0^0 , by

$$\tau_0^T = (s_{\text{time}} e_{\text{time}}) \tau_0^0.$$

The “come-from” time $(s_{\text{time}} e_{\text{time}})^{-1} \tau^{(3)}$ will usually be located between two original time-frames, suggesting use of simple interpolation in time here. Let

$$j(\tau^{(3)}) = \lfloor (s_{\text{time}} e_{\text{time}})^{-1} \tau^{(3)} / \delta T \rfloor \quad (\text{highest integer not greater than})$$

and $p(\tau^{(3)}) = (s_{\text{time}} e_{\text{time}})^{-1} \tau^{(3)} - j(\tau^{(3)}) \delta T$.

Then the interpolation is according to

$$R^{(3)}(x, y, \tau^{(3)}) = R^{(2)}(x, y, (s_{\text{time}} e_{\text{time}})^{-1} \tau^{(3)})$$

where the between-frame time-point is dealt with by the interpolation:

$$R^{(2)}(x, y, (s_{\text{time}} e_{\text{time}})^{-1} \tau^{(3)}) = \{1 - p(\tau^{(3)})\} R^{(2)}(x, y, j(\tau^{(3)}) \delta T) + p(\tau^{(3)}) R^{(2)}(x, y, (j(\tau^{(3)}) + 1) \delta T)$$

In general $R^{(2)}$ is required for two different time-points:

$$R^{(3)}(x^{(3)}, y^{(3)}, t^{(3)}) = p_a^{(3)} R^{(2)}(x^{(3)}, y^{(3)}, t_a^{(2)}) + p_b^{(3)} R^{(2)}(x^{(3)}, y^{(3)}, t_b^{(2)}),$$

where

$$t_a^{(2)} = \lfloor (s_{\text{time}} e_{\text{time}})^{-1} t^{(3)} / \delta T \rfloor \delta T$$

$$t_b^{(2)} = t_a^{(2)} + 1$$

$$p_b^{(3)} = (s_{\text{time}} e_{\text{time}})^{-1} t^{(3)} - t_a^{(2)}$$

$$p_a^{(3)} = 1 - p_b^{(3)}$$

B.4 Turning

A point at $(x_0^T + \delta x, y_0^T + \delta y)$ moves to

$$(x_0^T + \cos(\theta_{\text{turn}}) \delta x - \sin(\theta_{\text{turn}}) \delta y, y_0^T + \sin(\theta_{\text{turn}}) \delta x + \cos(\theta_{\text{turn}}) \delta y)$$

A point at $(x_0^T + \tilde{\delta} x, y_0^T + \tilde{\delta} y)$ comes from

$$(x_0^T + \cos(\theta_{\text{turn}}) \tilde{\delta} x + \sin(\theta_{\text{turn}}) \tilde{\delta} y, y_0^T - \sin(\theta_{\text{turn}}) \tilde{\delta} x + \cos(\theta_{\text{turn}}) \tilde{\delta} y)$$

Hence a point $(x^{(4)}, y^{(4)})$ comes from a point $(x^{(3)}, y^{(3)})$, where

$$x^{(3)} = x_0^T + \cos(\theta_{\text{turn}})(x^{(4)} - x_0^T) + \sin(\theta_{\text{turn}})(y^{(4)} - y_0^T)$$

$$y^{(3)} = y_0^T - \sin(\theta_{\text{turn}})(x^{(4)} - x_0^T) + \cos(\theta_{\text{turn}})(y^{(4)} - y_0^T),$$

and, with this definition,

$$R^{(4)}(x^{(4)}, y^{(4)}, t^{(4)}) = R^{(3)}(x^{(3)}, y^{(3)}, t^{(4)}).$$

B.5 Addition of target velocity

At the final stage, a version of the rainfall field is created by adding the required speed and direction of travel. Let this field be $R^{(5)}$. According to the advection model, a point at $(x^{(4)}, y^{(4)})$ moves to $(x^{(5)}, y^{(5)})$ after a time $\tau = t^{(5)} - \tau_c$ after a centring time τ_c , where

$$x^{(5)} = x^{(4)} + u_0^T \tau,$$

$$y^{(5)} = y^{(4)} + v_0^T \tau.$$

Hence,

$$x^{(4)} = x^{(5)} - u_0^T \tau,$$

$$y^{(4)} = y^{(5)} - v_0^T \tau.$$

Therefore $R^{(5)}$ can be constructed as

$$R^{(5)}(x^{(5)}, y^{(5)}, t^{(5)}) = R^{(4)}(x^{(5)} - u_0^T \tau^{(5)}, y^{(5)} - v_0^T \tau^{(5)}, t^{(5)}) = R^{(4)}(x^{(4)}, y^{(4)}, t^{(5)}),$$

where

$$x^{(4)} = x^{(5)} - u_0^T \tau^{(5)},$$

$$y^{(4)} = y^{(5)} - v_0^T \tau^{(5)}.$$

$$\tau^{(5)} = t^{(5)} - \tau_0^T.$$

B.6 Construction of values: extended form

The above formulae can be summarised into the following set of formulae which lead to the eventual calculation of the target values $R^{(5)}$:

$$\tau_0^T = (s_{\text{time}} e_{\text{time}}) \tau_0^0$$

$$R^{(5)}(x^{(5)}, y^{(5)}, t^{(5)}) = R^{(4)}(x^{(4)}, y^{(4)}, t^{(5)}),$$

$$x^{(4)} = x^{(5)} - u_0^T \tau^{(5)},$$

$$y^{(4)} = y^{(5)} - v_0^T \tau^{(5)}.$$

$$\tau^{(5)} = t^{(5)} - \tau_0^T.$$

$$R^{(4)}(x^{(4)}, y^{(4)}, t^{(4)}) = R^{(3)}(x^{(3)}, y^{(3)}, t^{(4)}).$$

$$x^{(3)} = x_0^T + \cos(\theta_{\text{turn}})(x^{(4)} - x_0^T) + \sin(\theta_{\text{turn}})(y^{(4)} - y_0^T)$$

$$y^{(3)} = y_0^T - \sin(\theta_{\text{turn}})(x^{(4)} - x_0^T) + \cos(\theta_{\text{turn}})(y^{(4)} - y_0^T),$$

$$R^{(3)}(x^{(3)}, y^{(3)}, t^{(3)}) = p_a^{(3)} R^{(2)}(x^{(3)}, y^{(3)}, t_a^{(2)}) + p_b^{(3)} R^{(2)}(x^{(3)}, y^{(3)}, t_b^{(2)}),$$

$$t_a^{(2)} = \left[(s_{\text{time}} e_{\text{time}})^{-1} t^{(3)} / \delta T \right] \delta T$$

$$t_b^{(2)} = t_a^{(2)} + 1$$

$$p_b^{(3)} = (s_{\text{time}} e_{\text{time}})^{-1} t^{(3)} - t_a^{(2)}$$

$$p_a^{(3)} = 1 - p_b^{(3)}$$

$$R^{(2)}(x^{(2)}, y^{(2)}, t_a^{(2)}) = R^{(1)}(x^{(1)}, y^{(1)}, t_a^{(2)}).$$

$$R^{(2)}(x^{(2)}, y^{(2)}, t_b^{(2)}) = R^{(1)}(x^{(1)}, y^{(1)}, t_b^{(2)}).$$

$$x^{(1)} = x_0^0 + A_{\text{band}} \{x^{(2)} - x_0^T\} + C_{\text{band}} \{y^{(2)} - y_0^T\}$$

$$y^{(1)} = y_0^0 + C_{\text{band}} \{x^{(2)} - x_0^T\} + B_{\text{band}} \{y^{(2)} - y_0^T\}$$

$$R^{(1)}(x^{(1)}, y^{(1)}, t_a^{(1)}) = R^{(0)}(x_a^{(0)}, y_a^{(0)}, t_a^{(1)}).$$

$$x_a^{(0)} = x^{(1)} + u_0^0 \tau_a^{(1)},$$

$$y_a^{(0)} = y^{(1)} + v_0^0 \tau_a^{(1)},$$

$$\begin{aligned}
\tau_a^{(1)} &= t_a^{(1)} - \tau_0^0, \\
R^{(1)}(x^{(1)}, y^{(1)}, t_b^{(1)}) &= R^{(0)}(x_b^{(0)}, y_b^{(0)}, t_b^{(1)}), \\
x_b^{(0)} &= x^{(1)} + u_0^0 \tau_b^{(1)}, \\
y_b^{(0)} &= y^{(1)} + v_0^0 \tau_b^{(1)}, \\
\tau_b^{(1)} &= t_b^{(1)} - \tau_0^0.
\end{aligned}$$

B.7 Construction of values: reduced form

The above set of equations can be reduced to

$$\tau_0^T = (s_{\text{time}} e_{\text{time}}) \tau_0^0$$

$$R^{(5)}(x^{(5)}, y^{(5)}, t^{(5)}) = p_a^{(3)} R^{(0)}(x_a^{(0)}, y_a^{(0)}, t_a^{(2)}) + p_b^{(3)} R^{(0)}(x_b^{(0)}, y_b^{(0)}, t_b^{(2)}),$$

$$\begin{aligned}
\tau^{(5)} &= t^{(5)} - \tau_0^T, \\
t_a^{(2)} &= \left[(s_{\text{time}} e_{\text{time}})^{-1} t^{(5)} / \delta T \right] \delta T \\
t_b^{(2)} &= t_a^{(2)} + 1 \\
p_b^{(3)} &= (s_{\text{time}} e_{\text{time}})^{-1} t^{(5)} - t_a^{(2)} \\
p_a^{(3)} &= 1 - p_b^{(3)}
\end{aligned}$$

$$\begin{aligned}
x^{(3)} - x_0^T &= \cos(\theta_{\text{turn}})(x^{(5)} - u_0^T \tau^{(5)} - x_0^T) + \sin(\theta_{\text{turn}})(y^{(5)} - v_0^T \tau^{(5)} - y_0^T) \\
y^{(3)} - y_0^T &= \sin(\theta_{\text{turn}})(x^{(5)} - u_0^T \tau^{(5)} - x_0^T) + \cos(\theta_{\text{turn}})(y^{(5)} - v_0^T \tau^{(5)} - y_0^T),
\end{aligned}$$

$$\begin{aligned}
x^{(1)} &= x_0^0 + A_{\text{band}} \{x^{(3)} - x_0^T\} + C_{\text{band}} \{y^{(3)} - y_0^T\} \\
y^{(1)} &= y_0^0 + C_{\text{band}} \{x^{(3)} - x_0^T\} + B_{\text{band}} \{y^{(3)} - y_0^T\}
\end{aligned}$$

$$\begin{aligned}
x_a^{(0)} &= x^{(1)} + u_0^0 \tau_a^{(1)}, \\
y_a^{(0)} &= y^{(1)} + v_0^0 \tau_a^{(1)}, \\
\tau_a^{(1)} &= t_a^{(1)} - \tau_0^0, \\
x_b^{(0)} &= x^{(1)} + u_0^0 \tau_b^{(1)}, \\
y_b^{(0)} &= y^{(1)} + v_0^0 \tau_b^{(1)}, \\
\tau_b^{(1)} &= t_b^{(1)} - \tau_0^0.
\end{aligned}$$

Appendix C Multiquadric surface fitting and areal rainfall estimation

C.1 Introduction

Multiquadric surface fitting can be applied to raingauge totals (over 15 minute time intervals) to infer the spatial distribution of rainfall across a region under consideration (for example, see Moore *et al.*, 1989). A brief summary of the multiquadric surface fitting technique is given in Section C.2 . Having derived the fitted surface, it is possible to integrate the inferred rainfall totals over a catchment to calculate the catchment average rainfall total. Indeed, any area of interest can be considered. For example, an area may be assigned a grid and areal estimates for each grid-square obtained. The assigned grid may be defined as the 1 km radar grid so as to mirror radar datasets.

It will be shown, following Balascio (2001), that the catchment (or grid) average rainfall total is in fact equivalent to applying a set of (constant) linear weights to the set of raingauge totals. A formula and method for calculating these linear weights are presented in Sections C.3 and C.4 respectively. The original motivation for deriving these sets of linear weights is their use in lumped, catchment-based, conceptual rainfall-runoff models such as the PDM. However, Section 6 presents a new application for these weights in constructing spatio-temporal rainfall datasets for use as input to distributed rainfall-runoff models configured on a grid. This includes both raingauge-only based datasets and the recalibration (adjustment) of radar data using raingauge data.

C.2 Multiquadric surface fitting techniques

C.2.1 Introduction

The classical problem of surface fitting is to find a surface $s(\underline{x})$ which passes exactly through N data values, z_i , specified at the N points, $\underline{x}_i = (x_i, y_i)$. The multiquadric calibration surface is defined as the weighted sum of N distance, or basis functions centred on each of the N data locations; that is

$$s(\underline{x}) = \sum_{j=1}^N a_j g(\underline{x} - \underline{x}_j) + a_0 \quad (\text{C.1})$$

where $\{a_j, j=0,1,2,\dots,N\}$ are parameters of the surface. There are many choices for the form of the distance function. The three examples presented here are all based on the simple Euclidean distance

$$d = \|\underline{x}\| = \sqrt{(x^2 + y^2)}. \quad (\text{C.2})$$

The example distance functions are defined as:

$$\text{Cone: } g(\underline{x}) = d, \quad (\text{C.3a})$$

$$\text{Exponential: } g(\underline{x}) = \exp(-d/l), \quad (\text{C.3b})$$

$$\text{Reciprocal: } g(\underline{x}) = 1/(1+d/l). \quad (\text{C.3c})$$

For the exponential and reciprocal distance functions, equations (C.3b-c), l is an additional constant parameter, referred to as the scaling length, which is prescribed prior to the surface fitting procedure. When using just the Euclidean distance, equation (C.3a), the surface defined by (C.1) is constructed from a set of N right-sided cones, each centred on one of the N data locations \underline{x}_i .

Evaluation of the surface parameters $\{a_j, j=0,1,2,\dots,N\}$ is achieved by imposing the condition that the fitted surface should take the values z_i at the points \underline{x}_i for $i=1,\dots,N$. Formally the N equations are

$$s(\underline{x}_i) = \sum_{j=1}^N a_j g(\underline{x}_i - \underline{x}_j) + a_0 = z_i \quad (i = 1, 2, \dots, N) \quad (\text{C.4})$$

which when expressed in matrix form results in

$$\underline{\underline{G}}\underline{a} + a_0\underline{1} = \underline{z} \quad (\text{C.5})$$

where $\underline{\underline{G}}$ is an N by N matrix with the (i,j) 'th element given by $G_{ij} = g(\underline{x}_i - \underline{x}_j)$, $\underline{1}$ is a unit vector of order N , \underline{z} is the vector containing the N data values z_i , $i=1,\dots,N$ and \underline{a} is the vector containing the N surface parameters $\{a_j, j=1,2,\dots,N\}$. The distance functions used here mean that the matrix $\underline{\underline{G}}$ is symmetric and this assumption is used later. Equation (C.5) provides N constraints towards evaluating the $N+1$ surface parameters $\{a_j, j=0,1,2,\dots,N\}$. The remaining constraint can be applied in two forms, both of which are detailed below.

C.2.2 Flatness at large distance

One approach to fully define the surface fitting procedure is to include the additional constraint that the slope of the surface should be zero for large distances from the surface fitting points. This ensures that the surface neither continually increases nor decreases at large distances (note that the limiting surface value may well be different in different directions). When the Euclidean distance function (C.3a) is used, the zero-slope constraint is

$$\underline{a}^T \underline{1} = 0. \quad (\text{C.6})$$

This additional constraint can be used to complete the specification of the surface fitting problem for other distance functions as well. However, the application of condition (C.6) to other distance functions usually leads to either the quickest approach to a constant value at large distances or to the least rapid increase or decrease. More importantly, constraint (C.6) arises in a different way when a surface-fitting procedure is required to be strictly additive. That is, if a constant value is added to all observations the fitted surface is obtained by adding the same constant to the original surface. This is known as additive invariance.

Solution of equation (C.5) subject to constraint (C.6) for the surface parameters $\{a_j, j=0,1,2,\dots,N\}$ gives

$$a_0 = (\underline{\mathbf{1}}^T \underline{\underline{G}}^{-1} \underline{\underline{z}}) / (\underline{\mathbf{1}}^T \underline{\underline{G}}^{-1} \underline{\mathbf{1}}), \quad (\text{C.7a})$$

$$\underline{\underline{a}} = \underline{\underline{G}}^{-1} (\underline{\underline{z}} - a_0 \underline{\mathbf{1}}). \quad (\text{C.7b})$$

C.2.3 Fixed value at large distance

An alternative way of fully defining the surface fitting problem is to force the fitting surface to approach a given fixed value at large distances from the surface fitting points. This constraint is only suitable for distance functions which approach a finite limit for large distances. For the examples encountered so far, this approach is appropriate for the exponential and reciprocal distance functions, where the finite limit is zero, but is not suitable for the Euclidean distance since $d \rightarrow \infty$ for large distances.

Suppose that the limiting value of the distance function for large distances is zero, as is the case for the exponential and reciprocal distance functions. Then, if b is the required limiting value for the surface, this additional parameter constraint leads to $a_0=b$ and then the surface fitting parameters $\{a_j, j=1,2,\dots,N\}$ are given by

$$\underline{\underline{a}} = \underline{\underline{G}}^{-1} (\underline{\underline{z}} - b \underline{\mathbf{1}}). \quad (\text{C.8})$$

Equation (C.8) is analogous to equation (C.7b) and completes the specification of the surface.

C.2.4 Offset parameter, K

For some scenarios it can be desirable to relax condition (C.4) by not forcing the fitted surface to pass exactly through the surface fitting data. Instead the fitted surface is only required to pass *near* to the surface fitting data. This is achieved by introducing an offset parameter, K . The distance functions (C.3) are then modified to take the following zero distance values:

$$\text{Cone: } \tilde{g}(\underline{0}) = -K, \quad (\text{C.9a})$$

$$\text{Exponential: } \tilde{g}(\underline{0}) = 1 + K, \quad (\text{C.9b})$$

$$\text{Reciprocal: } \tilde{g}(\underline{0}) = 1 + K, \quad (\text{C.9c})$$

where \tilde{g} is the modified distance function. Note that when this modification is used, the fitted surface formally has point discontinuities at each of the fitting points; however this problem is avoided by using the unmodified form of the basis function for surface evaluation.

These modified distance functions can be used with either the 'Flatness at large distance' condition (Section C.2.2), or the 'Fixed value at large distance', (Section C.2.3). The former condition has the following interpretation when using an offset parameter. The modified distance function satisfies the constraint

$$z_i = \sum_{j=1}^N a_j \tilde{g}(\underline{x}_i - \underline{x}_j) + a_0 \quad (i = 1, 2, \dots, N). \quad (\text{C.10})$$

However the surface value (evaluated using the unmodified distance function g) at the point \underline{x}_i will be

$$z_i^* = \sum_{j=1}^N a_j g(\underline{x}_i - \underline{x}_j) + a_0 = \sum_{j=1}^N a_j \tilde{g}(\underline{x}_i - \underline{x}_j) + a_0 \pm Ka_i \quad (\text{C.11})$$

where the sign depends on the distance measure used. Therefore

$$z_i - z_i^* = \mp Ka_i \quad (\text{C.12})$$

and the flatness constraint $\underline{a}^T \underline{1} = 0$ will ensure that these 'errors' or 'discrepancies' add up to zero.

C.3 Estimation of areal average rainfall totals

C.3.1 Introduction

A method of calculating time-series of catchment average rainfall totals is required for use as input to lumped conceptual rainfall-runoff models such as the PDM. The following method of areal average estimation is a development of the work of Balascio (2001). Formally the catchment average rainfall P is defined as follows. Let the function $f(x,y)$ be the rainfall total at every point (x,y) within the catchment under consideration. Let R denote the catchment region with associated (horizontal) surface area A . Then the catchment average rainfall total is defined as

$$P = \frac{1}{A} \iint_R f(x, y) dx dy \quad \text{where} \quad A = \iint_R dx dy. \quad (\text{C.13})$$

Of course the function $f(x, y)$ is unknown. However, we may estimate the function $f(x, y)$, and in turn the catchment average rainfall total, by fitting a multiquadric surface $s(\underline{x})$ to a given network of N raingauge totals. In this context $\underline{x}_i = (x_i, y_i)$ represents the location of the i^{th} raingauge and z_i represents the rainfall total (over 15 minute intervals) at the i^{th} raingauge.

Therefore the estimated catchment average rainfall total \hat{P} obtained using the multiquadric surface is

$$\begin{aligned} \hat{P} &= \frac{1}{A} \iint_R s(\underline{x}) dx dy &= \frac{1}{A} \iint_R \left\{ \sum_{j=1}^N a_j g(\underline{x} - \underline{x}_j) + a_0 \right\} dx dy \\ & &= \frac{1}{A} \iint_R \sum_{j=1}^N a_j g(\underline{x} - \underline{x}_j) dx dy + a_0. \end{aligned} \quad (\text{C.14})$$

Since $s(\underline{x})$ is a linear combination of the distance functions $g(\underline{x} - \underline{x}_j)$, the summation in equation (C.14) may be integrated term by term. Let \underline{v} be a vector of order N comprising of the distance functions $g(\underline{x} - \underline{x}_j)$ such that

$$\underline{v} = \begin{pmatrix} g(\underline{x} - \underline{x}_1) \\ \vdots \\ g(\underline{x} - \underline{x}_N) \end{pmatrix}. \quad (\text{C.15})$$

This definition allows equation (C.14) to be rewritten as

$$\hat{P} = \frac{1}{A} \iint_R \underline{v}^T \underline{a} dx dy + a_0. \quad (\text{C.16})$$

Recalling that the vector \underline{a} is a constant, the only dependence on x and y in equation (C.16) enters through the distance functions contained in \underline{v} which can be separated out. Integrating \underline{v} term by term yields the volume vector \underline{V} :

$$\underline{V} = \iint_R \underline{v} dx dy. \quad (\text{C.17})$$

Separating the x and y dependence out of equation (C.16) and using the definition (C.17), the estimated catchment average rainfall total becomes:

$$\hat{P} = \frac{1}{A} \underline{V}^T \underline{a} + a_0. \quad (\text{C.18})$$

Depending on the form of the distance function and catchment boundary, \underline{V} can be calculated explicitly. For example, Pegram and Pegram (1993) derive a

solution for the conic distance function over a polygon boundary. Their method could be applied to the DTM-derived catchment boundaries. Alternatively, Balascio (2001) describes a method for the conic distance function using 3-D CAD software. However, within the present study, a general numerical scheme has been developed which can be applied to a range of basis functions over polygon boundaries. This generalised scheme is detailed in Section C.4 .

C.3.2 Flatness at large distance

Recall from Section C.2.2 that the condition of flatness at large distances is achieved by adding the constraint $\underline{a}^T \underline{1} = 0$. Substituting the resulting solutions for \underline{a} and a_0 (see equation (C.7)) into equation (C.18) yields:

$$\hat{P} = \frac{1}{A} \left[\underline{V}^T \underline{G}^{-1} + \frac{(A - \underline{V}^T \underline{G}^{-1} \underline{1})}{\underline{1}^T \underline{G}^{-1} \underline{1}} \underline{1}^T \underline{G}^{-1} \right] \underline{z}. \quad (\text{C.19})$$

Equation (C.19) implies that the catchment average rainfall total, derived by integrating the multiquadric surface over the region, is equivalent to applying a set of constant linear weights to the raingauge totals *regardless* of the actual value of \underline{z} . To see this explicitly, let w_i be the constant linear weighting coefficient for the i^{th} raingauge. Then equation (C.19) can be rewritten as

$$\hat{P} = \underline{w}^T \underline{z} \quad (\text{C.20a})$$

where

$$\underline{w} = \frac{\underline{G}^{-1}}{A} \left[\underline{V} + \frac{(A - \underline{V}^T \underline{G}^{-1} \underline{1})}{\underline{1}^T \underline{G}^{-1} \underline{1}} \underline{1} \right]. \quad (\text{C.20b})$$

This is equivalent to equation (17) of Balascio (2001) (except for a typographical error). Clearly \underline{w} is a constant vector and it is trivial to show that the sum of the weights equals one, i.e. $\underline{1}^T \underline{w} = 1$. Since the sum of the weights is equal to one, multiquadric surfaces give an *unbiased* estimate of the catchment average rainfall total when the constraint of flatness at large distance (or of additive invariance) is applied. Note that in deriving (C.20), use has been made of the matrix rules that $(\underline{D}\underline{E})^T = \underline{E}^T \underline{D}^T$ and that if \underline{F} is symmetric then $\underline{F}^T = \underline{F}$.

C.3.3 Fixed value at large distance

As discussed in Section C.2.2 , the constraint of fixed value at large distance is only appropriate if the distance function tends to a finite value at large distances from the raingauge network. Without loss of generality, consider the case when the fixed value is zero (i.e. $a_0 = b = 0$) since any other choice can be recast in

this form by replacing z_i with $z_i - b$. For the case $a_0 = b = 0$ the vector \underline{a} is given by:

$$\underline{a} = \underline{G}^{-1} \underline{z}. \quad (\text{C.21})$$

Substituting (C.21) and $a_0 = b = 0$ into equation (C.18) yields:

$$\hat{P} = \frac{1}{A} \underline{V}^T \underline{G}^{-1} \underline{z}. \quad (\text{C.22})$$

This implies, as in Section C.3.2, that the catchment average rainfall total is equivalent to applying a set of constant linear weights to the raingauge totals, z_i , regardless of their values. Let w_i be the constant linear weighting coefficient for the i^{th} raingauge. Then equation (C.19) can be rewritten as

$$\hat{P} = \underline{w}^T \underline{z} \quad (\text{C.23a})$$

where

$$\underline{w} = \frac{1}{A} \underline{G}^{-1} \underline{V}. \quad (\text{C.23b})$$

Once again \underline{w} is clearly constant. However, for the constraint of a fixed value at large distances, the sum of the weights is not necessarily equal to one and therefore the weights give a *biased* estimate of the catchment average rainfall. The estimators are unbiased in the special case that the “fixed value at large distance” is specified to be equal to the long-term mean rainfall.

C.3.4 Offset parameter, K

When an offset parameter, K , is used (see Section C.2.4) the weighting definitions derived above are still valid. However, care must be taken over which distance measure is used for defining \underline{V} and \underline{G} . The correct method is to use the unmodified distance function g when calculating \underline{V} whilst using the modified distance function \tilde{g} when defining \underline{G} .

C.4 Outline of method for calculating the volume vector \underline{V}

The aim of this section is to outline the method used to calculate the volume vector \underline{V} (see equation (C.17)) which is required to derive the linear weighting coefficients \underline{w} .

To illustrate the method, consider integrating a function $h(x,y)$ over a polygon boundary. Let R denote the catchment region. Let \underline{x}_0 be a fixed point (e.g. a raingauge location) that can lie inside or outside the polygon boundary and let the vertices of the polygon boundary be numbered in a clockwise sense from \underline{x}_1

to \underline{x}_M , where M is the total number of vertices. This configuration is presented in Figure C.1 for a simple catchment boundary.

Step 1: Starting at the first edge of the polygon boundary between \underline{x}_1 and \underline{x}_2 construct a triangle with the fixed point \underline{x}_0 . This has area T_1 and is illustrated in Figure C.2.

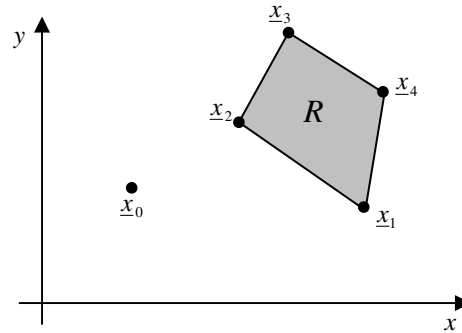


Figure C.1 Configuration of a simple catchment region R within a polygon boundary with vertices \underline{x}_1 to \underline{x}_4 and with a raingauge located at \underline{x}_0

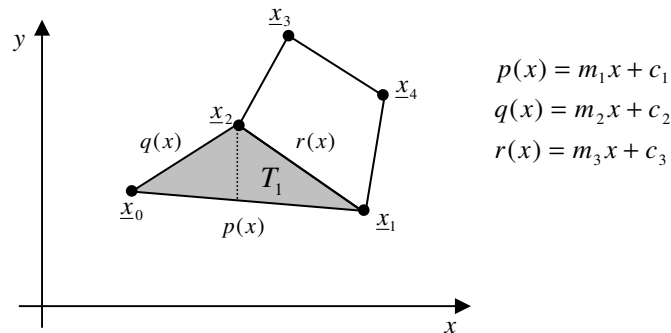


Figure C.2 Construction of triangle T_1

Step 2: T_1 is then split into two smaller triangles by a vertical line emanating from the vertex of T_1 whose x position lies between the others: in the current example it is \underline{x}_2 . Simple geometry gives the equations of the lines that form the triangle T_1 , namely $p(x)$, $q(x)$ and $r(x)$. Let I_1 be the integration of $h(x, y)$ over T_1 which is equivalent to integrating over the two smaller triangles. For the current example,

$$I_1 = \iint_{T_1} h(x, y) dx dy = \int_{x=x_0}^{x=x_2} \int_{y=p(x)}^{y=q(x)} h(x, y) dy dx + \int_{x=x_2}^{x=x_1} \int_{y=p(x)}^{y=r(x)} h(x, y) dy dx. \quad (\text{C.24})$$

The integration over the smaller triangles can be estimated by a numerical scheme. Here, Gaussian quadrature has been used.

Step 3: The integral I_1 is then multiplied by a rotation factor r_1 where

$$\begin{aligned} r_1 &= 1 \quad \text{if moving from } \underline{x}_1 \text{ to } \underline{x}_2 \text{ results in a clockwise rotation about } \underline{x}_0, \\ r_1 &= -1 \quad \text{if moving from } \underline{x}_1 \text{ to } \underline{x}_2 \text{ results in an anti-clockwise rotation about } \underline{x}_0. \end{aligned} \quad (\text{C.25})$$

This rotation can easily be determined from basic geometry. For example, let θ_1 be the rotation of \underline{x}_1 about \underline{x}_0 with respect to the y direction and let θ_2 be the rotation of \underline{x}_2 about \underline{x}_0 . Then

$$\begin{aligned} r_1 &= 1 && \text{if } \theta_2 - \theta_1 > 0, \\ r_1 &= -1 && \text{if } \theta_2 - \theta_1 < 0. \end{aligned} \quad (\text{C.26})$$

For the current example $\theta_2 - \theta_1 < 0$, see Figure C.3, and so $r_1 = -1$.

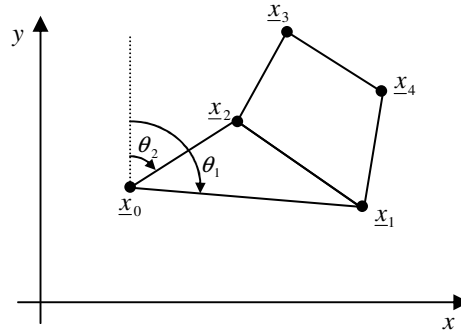


Figure C.3 Evaluation of rotation factor r_1

Step 4: Repeat steps 1 to 3 for the next edge of the boundary, e.g. edge \underline{x}_2 to \underline{x}_3 with associated triangle T_2 , integration I_2 and rotation factor r_2 . Repeat until the final edge of the boundary, edge \underline{x}_M to \underline{x}_1 , is reached. Then the integration of $h(x, y)$ over the region R , bounded by the polygon boundary is given by

$$\begin{aligned} I &= \iint_R h(x, y) dx dy && = r_1 \iint_{T_1} h(x, y) dx dy + \dots + r_M \iint_{T_M} h(x, y) dx dy \\ &&& = r_1 I_1 + \dots + r_M I_M \\ &&& = \sum_{j=1}^M r_j I_j \end{aligned} \quad (\text{C.27})$$

Note that $R = \sum_{j=1}^M r_j T_j$. The triangles and rotation factors derived using this method for the example are illustrated in Figure C.4.

Once the volume vector \underline{V} has been calculated by this method, it is simple to calculate the constant weighting coefficient vector \underline{w} from either (C.20b) or (C.23b) depending on the additional constraint used.

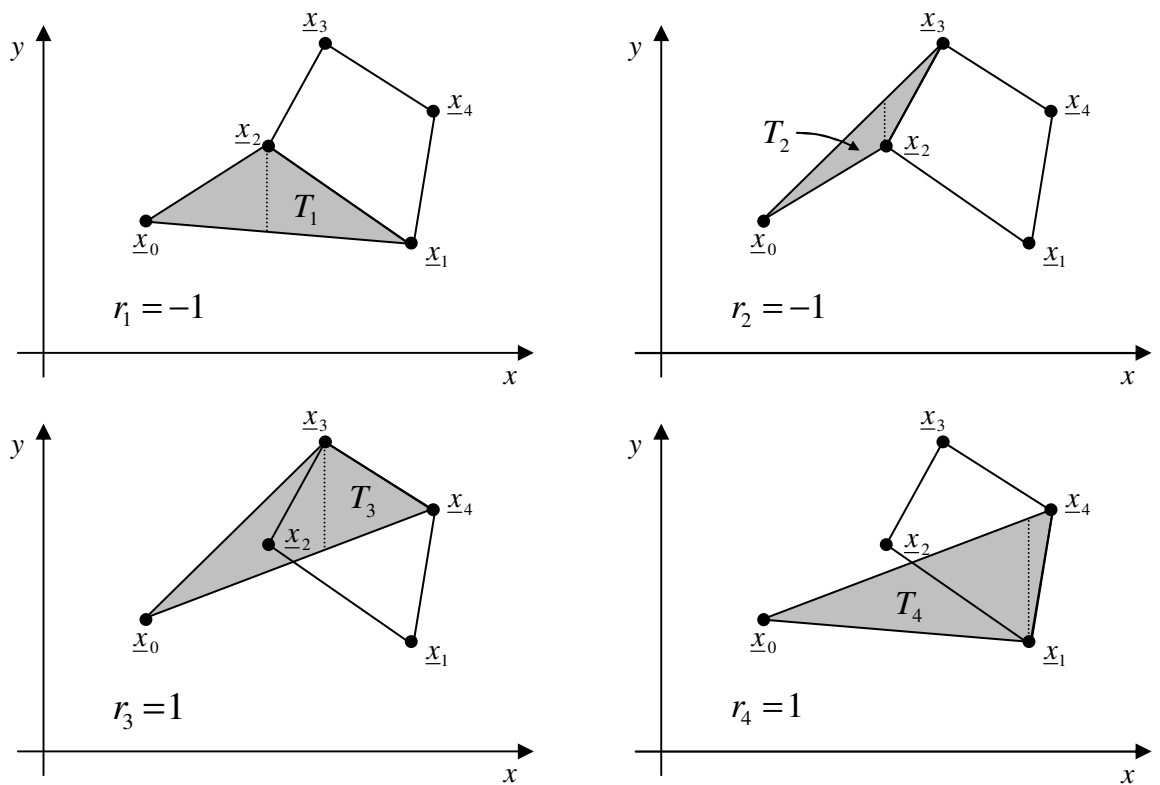


Figure C.4 Illustration of method for calculating the volume vector \underline{V}

However, it is important to stress that this method does not guarantee that the raingauge weights are all positive. If negative weights do occur, the recommendation is to remove the raingauge in question from the network and repeat the method – note that this only involves eliminating the appropriate elements from \underline{V} , \underline{G} and \underline{z} and then recalculating \underline{w} .

Appendix D Destruction testing of rainfall-runoff models

D.1 Introduction

A special and important use of rainfall datasets and profiles for the present study is for destruction testing of rainfall-runoff models. This special use is dealt with in detail in this section. To help consider how rainfall-runoff models can be subject to destruction testing using extreme rainfall datasets, a simple model has been set-up and deliberately coded so as to exhibit poor behaviour when subject to large rainfalls. This model illustrates some of the problems that can arise when converting conceptual hydrological models into computer code. It is useful in gaining experience of alternative approaches to destruction testing.

D.2 Destruction testing

The approach taken here to model destruction testing is that the models should be run in the same way as usual, except that unusually large rainfall values are supplied as input. Model failure is said to occur if either the model execution fails to complete or if the model results fail to display a physically realistic response to the rainfall input. The concern is NOT that the model produces “accurate” computations for some mathematical model of hydrological processes. Only a very approximate representation of these processes in the real-world will constitute the model under test. The chief concern of hydrological modelling is that the models should provide a reasonably good representation of the real-world hydrological responses over a range of conditions.

The destruction testing applied here runs the rainfall-runoff model over a relatively short time-period, but subject to a number of different versions of rainfall input. Each version is obtained from a basic source rainfall dataset by applying a multiplying factor to it. The destruction test considers the value of the modelled flow at a fixed time point as a function of this multiplying factor. A rainfall-runoff model is said to fail to produce a realistic response if the modelled flow (at a fixed time-point) ever decreases as the multiplying factor increases. This type of criterion is appropriate for a range of modelling contexts, but not to models where catastrophic changes occur (for example dam and embankment failures in hydrodynamic models and snowpack break-up in snowmelt models).

Other relevant destruction-testing criteria include:

- (a) Failure occurs if execution does not complete or if the computational results are non-numeric (such as INF or NAN, where computer systems allow these).
- (b) Failure occurs if the modelled flow at a fixed time-point ever decreases, or if there is a sharp increase, as the multiplying factor applied to the rainfall increases.

For destruction testing, it is important that models are implemented exactly as they would be for routine use. Problems can be expected to arise in relation to the time-step length used within numerical calculations, and thus must be left as for routine use. Rainfall-runoff models usually employ a fixed time-step for internal calculations; only in unusual cases will a model implementation include automatic adjustment of the lengths for sub-steps within the basic time-step. Rainfall-runoff models will have usually been calibrated against observational records. Settings for time-step lengths within the calibration procedures should be the same as used for operational versions of the models. Given calibrated model parameters, the model should produce a realistic response for rainfall-inputs within the range experienced in the record used for calibration.

The demonstration of destruction testing considered here is based on a special model, described in the next section, implemented using a calculation time-step of 15-minutes. This is the time-step commonly used for real-time forecasting in the UK. The special model is first calibrated using data for the Mole at Kinnersley Manor. Then the model, with the calibrated parameters, is subject to destruction testing using a simple rainfall profile as input. This profile is such that rainfall is constant over a 12 hour period and then zero thereafter. The total rainfall for the 12 hour period is used to characterise the profile for input to the model. To complete the input specification, the potential evaporation is set at 1 mm day^{-1} and the model is initialised to have an initial model output of $1 \text{ m}^3\text{s}^{-1}$.

D.3 Overview of the special models

The structure of the special model (Figure D.1) bears some similarity to one of the basic forms of the PDM model, except that the probability-distributed moisture store is replaced by a single soil moisture store. This makes the model easier to understand and avoids any fear that any bad behaviour arises from this relatively complex part of the PDM. Thus the model being used to develop destruction-testing procedures is NOT a PDM model.

The soil storage in the simple model is such that the water in store is added to by rainfall less evaporation and overflows when the storage capacity is exceeded. The overflow is split proportionately between:

- (i) “direct runoff”, which enters the Surface Storage part of the model;
- (ii) “groundwater recharge”, which enters the Subsurface Storage part of the model.

Actual evaporation is proportional to the amount of water in the soil storage, and equal to the potential evaporation when the store is full. The Surface Storage routing component consists of two linear storages in series, as usually invoked for the PDM.

The Subsurface Storage routing component is represented by a non-linear storage, with an outflow proportional to the cube of the water in storage. This is similar to the cubic storage option in the PDM normally invoked for this component, but differs in the way it is implemented. The form of implementation has deliberately been chosen to exhibit poor behaviour, but is one that might well be chosen in practice. The choice of implementation of storage components in rainfall-runoff models can be influenced by computation time

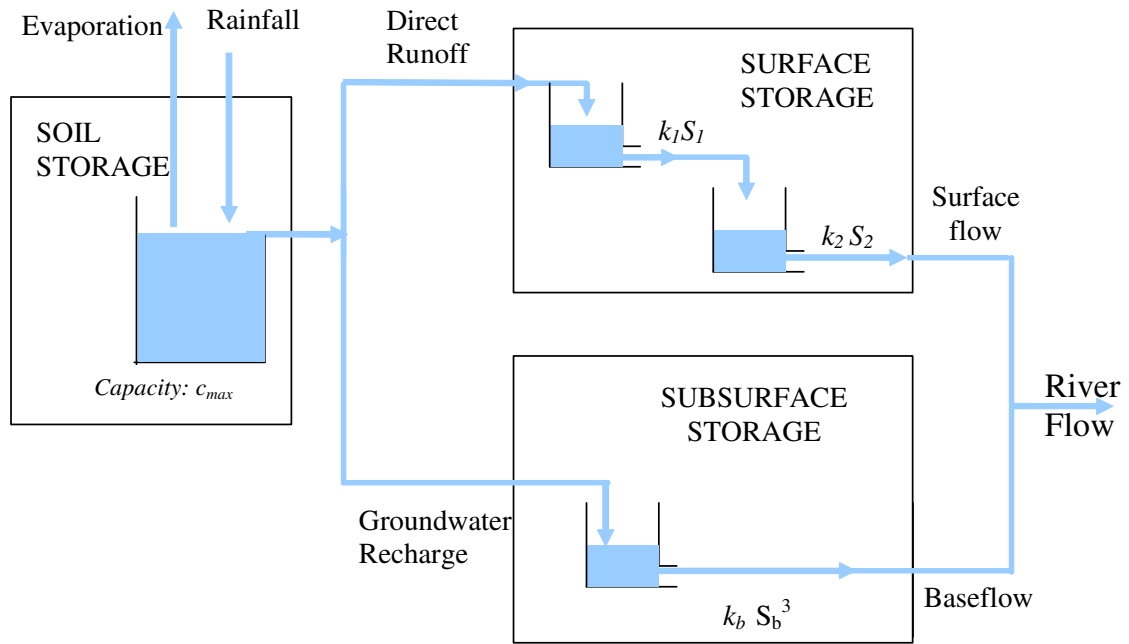


Figure D.1 Structure of the simple rainfall-runoff model

considerations. Simpler computational schemes may be selected in preference to adopting highly accurate solutions of the underlying differential equations.

The Subsurface Storage component of the special model is based on the usual basic conceptualisation that the water storage S , outflow rate q and inflow rate u (each expressed per unit area) are linked by the differential equation for water-balance,

$$\frac{dS}{dt} = u - q, \quad (D.1)$$

and the “momentum equation”

$$q = kS^3, \quad (D.2)$$

where k is a model parameter. The implementation of this storage model considered here is based directly on the differential equation for the water storage S :

$$\frac{dS}{dt} = u - kS^3. \quad (D.3)$$

Note that different solutions would be obtained by applying similar numerical techniques to the equivalent model representation as a differential equation for the flow q :

$$\frac{dq}{dt} = 3k^{1/3}q^{2/3}(u - q) . \quad (D.4)$$

The quantity required from the cubic storage model is the rate of flow from the store at the end of a fixed time interval of length T , given conditions at the start of the interval (time $t = 0$). (Other models might compute the total outflow from the store over the interval). Input to the store is assumed to be at a constant rate u within any given computational interval. The approach taken is to assume that S_0 (storage at $t = 0$) is known, to then use the differential equation to approximate S_T (storage at $t = T$), and finally to compute q_T (outflow rate at $t = T$) via equation (D.2). The quantity S_T is then available for carry-over to the start of the next computation interval, where it becomes the new S_0 . However, the approach taken is to carry-over q_T to the next step, where it becomes the new q_0 , and the required value for S_0 is compute by inversion of equation (D.2). This may be schematised as follows:

$$q_0 \rightarrow S_0 \xrightarrow{\text{approx}} S_T \rightarrow q_T \\ \xrightarrow{\text{carryover}} q_T \rightarrow S_T \xrightarrow{\text{approx}} S_{T+T} \rightarrow q_{T+T}$$

Three versions of solutions derived from the above are outlined here. They are all based on using the usual simple finite difference approximation to the derivative in equation (D.3), and using the known initial condition in the right hand side. Thus

$$\frac{S_T - S_0}{T} = u - kS_0^3, \quad (D.5)$$

giving

$$S_T = S_0 + T(u - kS_0^3), \quad (D.6)$$

or, since q_0 is available,

$$S_T = S_0 + T(u - q_0). \quad (D.7)$$

The three versions are shown in Table D.1.

Version 0 in Table D.1 is a direct implementation of the above. This version failed the destruction testing by failing to complete the execution. In fact an infinite loop occurred within an auxiliary function for computing the cube-root at step (i). However, the cause of this was the occurrence of computed values of INF or -INF for the water storage S_T , so that the first criterion for destruction testing would have failed had a more carefully programmed cube-root function been available. Version 1 is a simple adaptation of Version 0 which derives from the conceptual idea that the water in store, S , cannot be negative, and hence

negative values are reset to zero within the computations. It will be seen later that the direct implementation (Version 0) has a tendency to create time-series of water in store which oscillate through positive and negative values: the truncation at zero introduced in Version 1 has the effect of trimming or stopping such oscillations. The truncation also has the effect of preventing negative flows from being generated.

Table D.1 Versions of numerical scheme for the special cubic model

| |
|---|
| <p>Version 0:</p> <p>(i): $S_0 = \left(\frac{q_0}{k}\right)^{1/3}$</p> <p>(ii): $S_T = S_0 + T(u - q_0)$</p> <p>(iii): $q_T = kS_T^3$</p> <p>Version 1:</p> <p>(i): $S_0 = \left(\frac{q_0}{k}\right)^{1/3}$</p> <p>(ii): $S_T = \max(S_0 + T(u - q_0), 0)$</p> <p>(iii): $q_T = kS_T^3$</p> <p>Version 2:</p> <p>(i): $S_0 = \left(\frac{q_0}{k}\right)^{1/3}$</p> <p>(ii)a: $S_{\text{lim}} = \left(\frac{u}{k}\right)^{1/3}$</p> <p>(ii)b: if $u > q_0$ then $S_T = \min(S_0 + T(u - q_0), S_{\text{lim}})$ if $u \leq q_0$ then $S_T = \max(S_0 + T(u - q_0), S_{\text{lim}})$</p> <p>(iii): $q_T = kS_T^3$</p> |
|---|

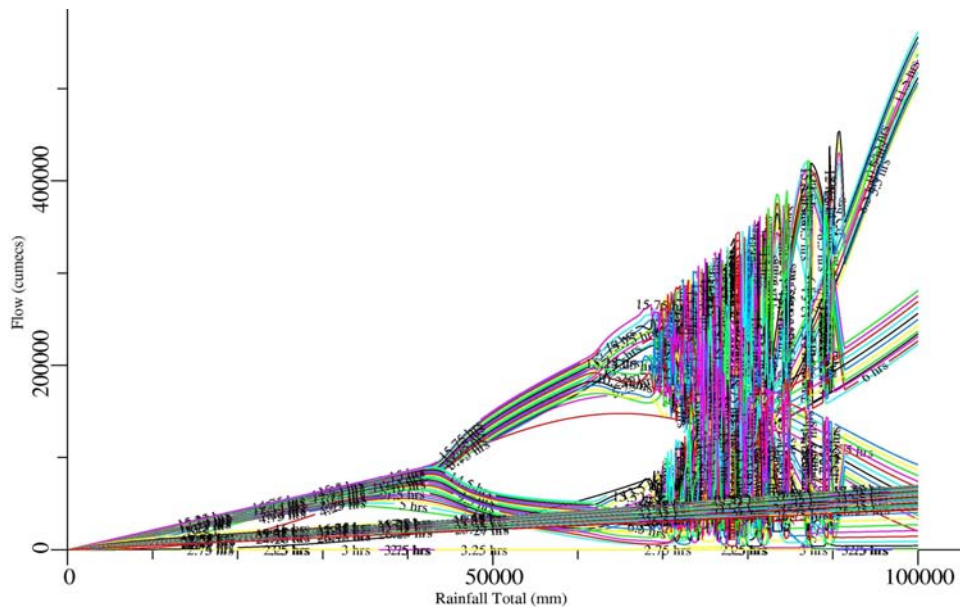
Version 2 in Table D.1 is a further simple adaptation of the direct implementation which encompasses the change made for Version 1. This adaptation again derives from the conceptual nature of the storage model. The quantity S_{lim} , calculated at step (ii)a, represents the equilibrium storage level for the store subject to an input rate of u . If the initial conditions are such that the water storage should rise (input greater than output, $u > q_0$) then the water storage should continue to rise but will never exceed the equilibrium level. In contrast, if the initial conditions are such that the storage should fall (input less than output, $u \leq q_0$) then the water storage will continue to decrease but will never fall below the equilibrium level.

It should be noted that the version of the cubic groundwater-storage model implemented within the PDM model is different from all of the versions discussed here.

D.4 Results of model destruction testing

Destruction testing results for two versions of the special cubic model are shown in Figures D.2 and D.3. These show the value of the modelled flow at a fixed time point as the total amount of rainfall (constant over a 12 hour period) changes. The 100 time-points selected start at 2 hours 15 minutes and extend to 27 hours in increments of 15 minutes. Plots are shown for the total model output and for the output from the groundwater storage component only. Results are not shown for Version 0 of the implementation because of the failure to complete the execution. It is clear from Figure D.2 that Version 1 of the model fails the destruction test. The plot for the groundwater flow shows characteristics commonly seen in chaotic systems. It should be noted that the range of rainfall events being considered here go up to 100m in 12 hours, and that “bad” behaviour apparently sets-in at about 30m in 12 hours. These are clearly highly unrealistic amounts of rainfall and a full consideration of destruction testing will need to consider a reasonable limit to the range used for testing. Figure D.3 shows that Version 2 of the implementation does not have the extremely poor behaviour of Version 1, with all of the curves apparently showing an increasing response to rainfall. Figure D.4, which shows the results over a more limited range of rainfall totals, shows that Version 2 does still fail the destruction testing, at least if the criterion is applied to the outflow from the groundwater model: failure is apparent when the rainfall total reaches 15m in 12 hours.

(a) Total flow response



(b) Baseflow response

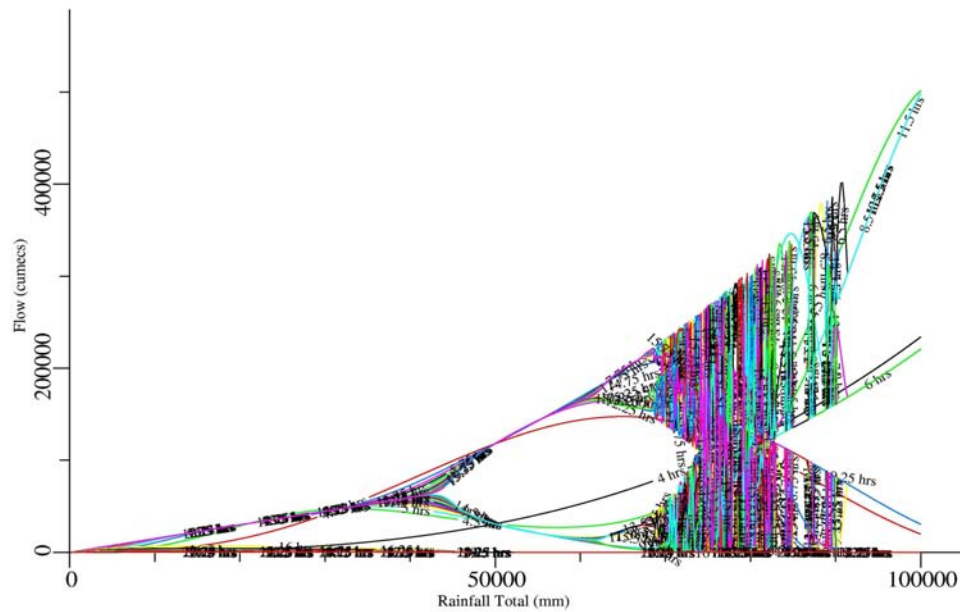
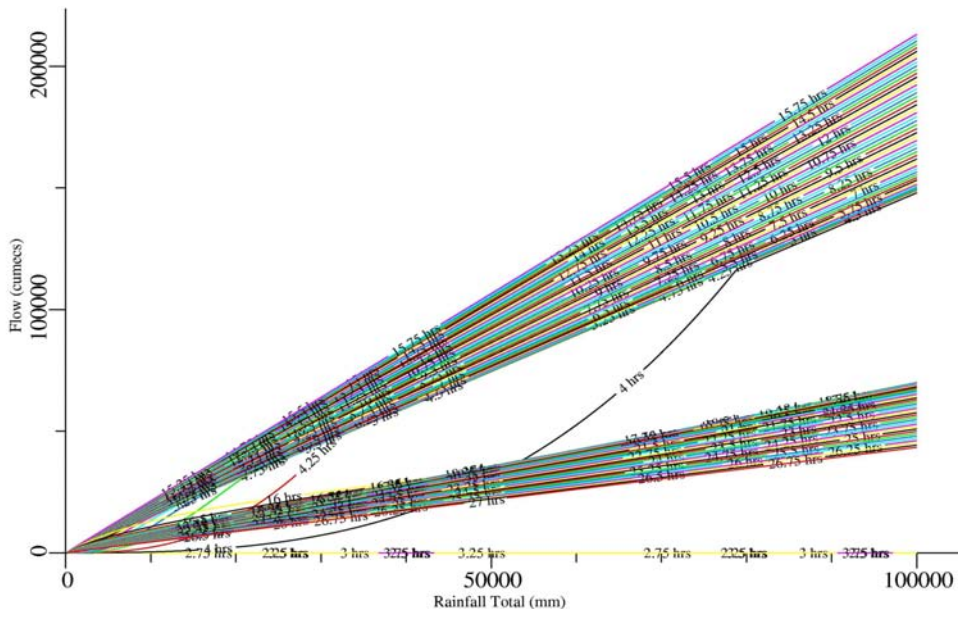


Figure D.2 Destruction testing of Version 1 implementation. Flow response at fixed times to different rainfalls in 12 hours.

(a) Total flow response



(b) Baseflow response

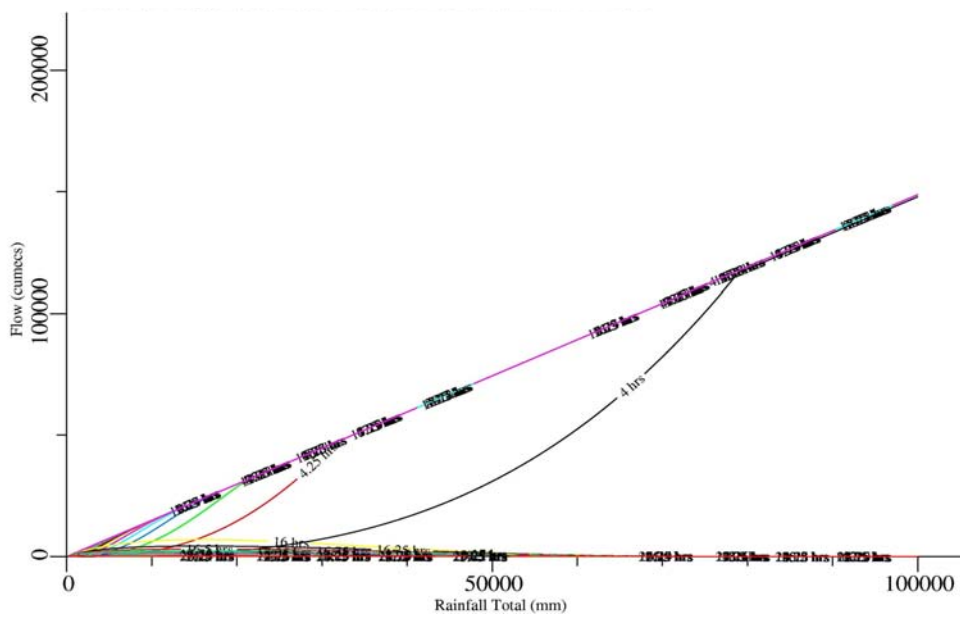
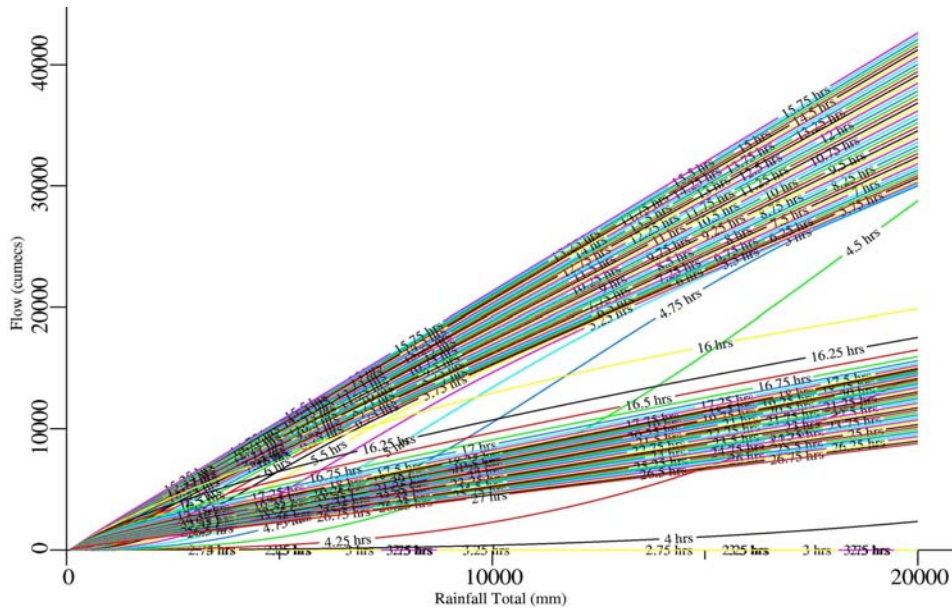


Figure D.3 Destruction testing of Version 2 implementation. Flow response at fixed times to different rainfalls in 12 hours.

(a) Total flow response



(b) Baseflow response

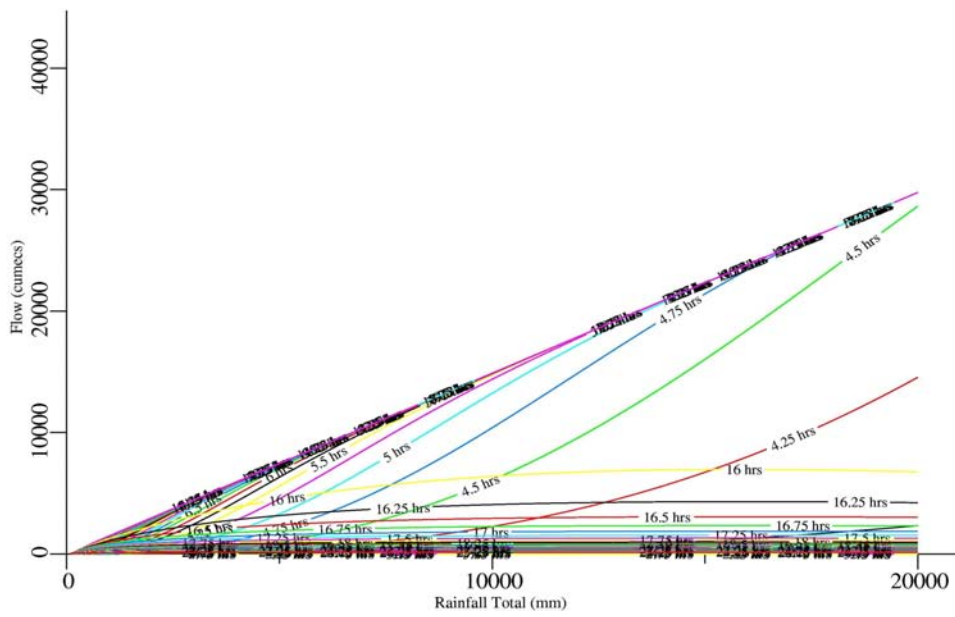
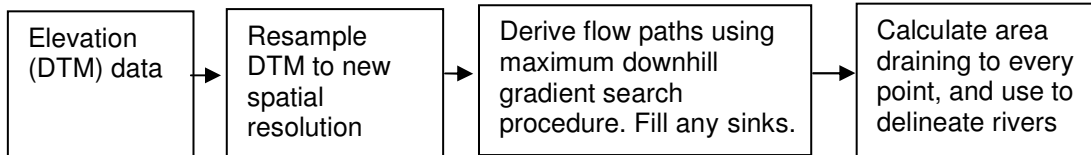


Figure D.4 Destruction testing of Version 2 implementation. Flow response at fixed times to different rainfalls in 12 hours. Lower range of rainfall.

Appendix E Deriving flow path directions and drainage areas for the Grid-to-Grid model

The process of deriving routing pathways from a DTM is summarised in the diagram below.



The process of creating a network of routing pathways involves automated search procedures that iteratively calculate flow paths, correcting them by artificially raising or lowering elevations to remove sinks. This process will usually lead to a network of flow paths that has no sinks and bears some resemblance to the actual river network which, if required, can be further refined by hand correction. Occasionally automated procedures produce unrealistic river networks and, although techniques exist to correct them in a semi-automated way, it can often be straightforward to manually “burn” more realistic river flow paths into the terrain.

With the aim of combining the accuracy of high resolution flow paths and the computational efficiency of lower resolution grid cells, a scheme to automatically identify flow directions and catchment areas on a low resolution grid (1km) using flow directions on a finer grid (e.g. 50m) has been investigated by Fekete *et al.* (2001). This method divides a larger grid cell into a block of $n \times n$ smaller grid cells for which flow directions and accumulated areas are known. The flow directions of the larger cells are determined from the magnitude (and sometimes the position) of the maximum value of the accumulated areas of the smaller cells in the $n \times n$ block.

Here the automated procedure of Fekete has been implemented to derive an initial set of flow directions. The method determines flow directions of the 1km cells from the magnitude of the maximum value of the accumulated areas of the 50m cells, taken from the IHDTM (Integrated Hydrological Digital Terrain Model, Morris and Flavin, 1990), in the 1×1km block. Once a set of flow directions has been identified, the catchment area draining to any point can be determined. Table E.1 shows the catchment areas derived from the Fekete flow paths compared to the 50m resolution catchment areas. Values of percentage error are given in brackets. Use of the Fekete method to derive flow networks generally results in reasonable agreement between derived and observed catchment areas, though there are significant errors for some catchments.

Although good agreement in terms of catchment area was achieved by the automated Fekete method for a majority of the catchments studied, closer examination and comparison with 50m flow directions revealed that the 1km flow directions for all catchments might benefit from a degree of hand correction

in order to achieve a satisfactory water-balance for the catchment. By way of illustration, Fekete-derived and hand corrected 1km flow directions and boundaries for the catchments draining to the River Kent are presented in Figure E.1, together with the detailed 50m elevation, flow directions and catchment boundaries. The map highlights the deficiencies of the automated method for the smaller River Kent catchments. Figure E.2 shows the improvement provided by hand correction.

Table E.1 Comparison of observed and DTM-derived catchment areas

| Catchment | Derived Area (km ²) and percentage error | | |
|---------------------------|--|-------------------|----------------------------------|
| | 50m DTM | 1km Fekete Method | Hand corrected 1km Fekete Method |
| River Kent | | | |
| Sedgwick | 212.3 | 212 (0%) | 212 (0%) |
| Victoria | 184.7 | 188 (2%) | 185 (0%) |
| Bowston | 69.8 | 69 (-1%) | 70 (0%) |
| Mint | 65.5 | 49 (-26%) | 67 (+2%) |
| Sprint | 34.5 | 45 (+29%) | 36 (+3%) |
| River Stour | | | |
| Shipston | 185.2 | 185 (0%) | 185 (0%) |
| Upper Thames | | | |
| River Cherwell at Banbury | 201.9 | 205 (+2%) | 202 (0%) |
| Sor Brook at Bodicote | 88.8 | 98 (+10%) | 88 (-1%) |
| River Darwen | | | |
| Blue Bridge | 135.7 | N/A | 137 (+1%) |
| Ewood | 39.0 | 36 (-8%) | 40 (+3%) |

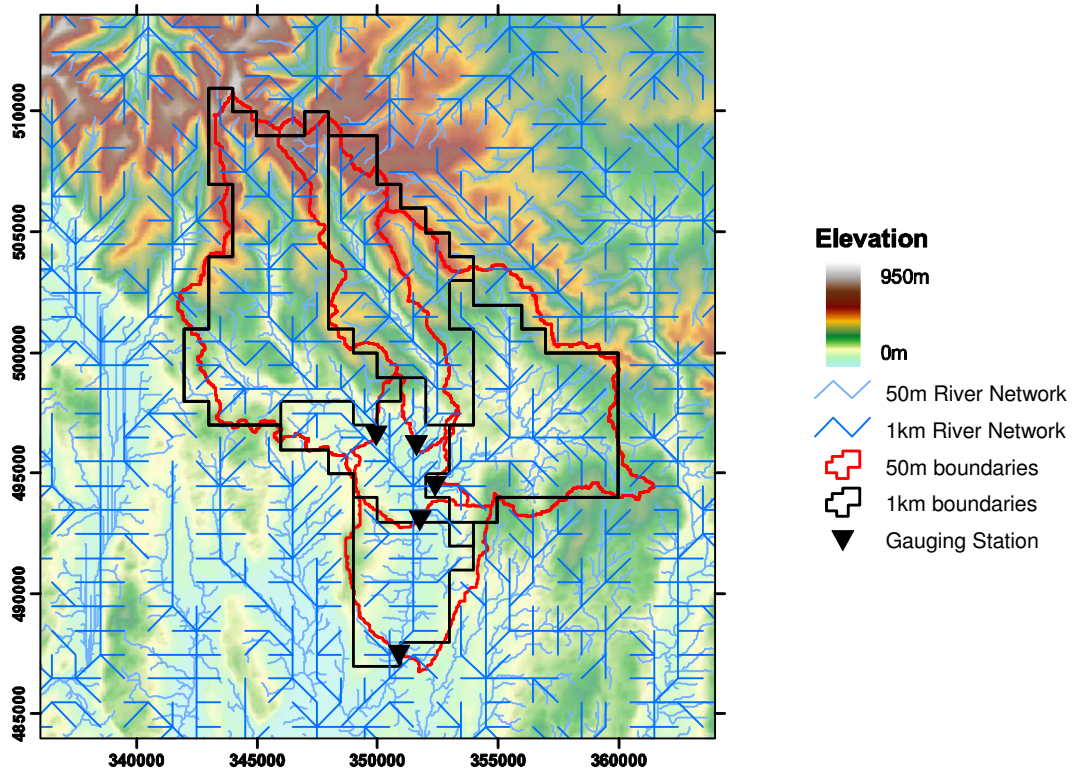


Figure E.1 Fekete derived 1km and IHDTM 50m resolution flow directions and catchment boundaries: River Kent catchment.

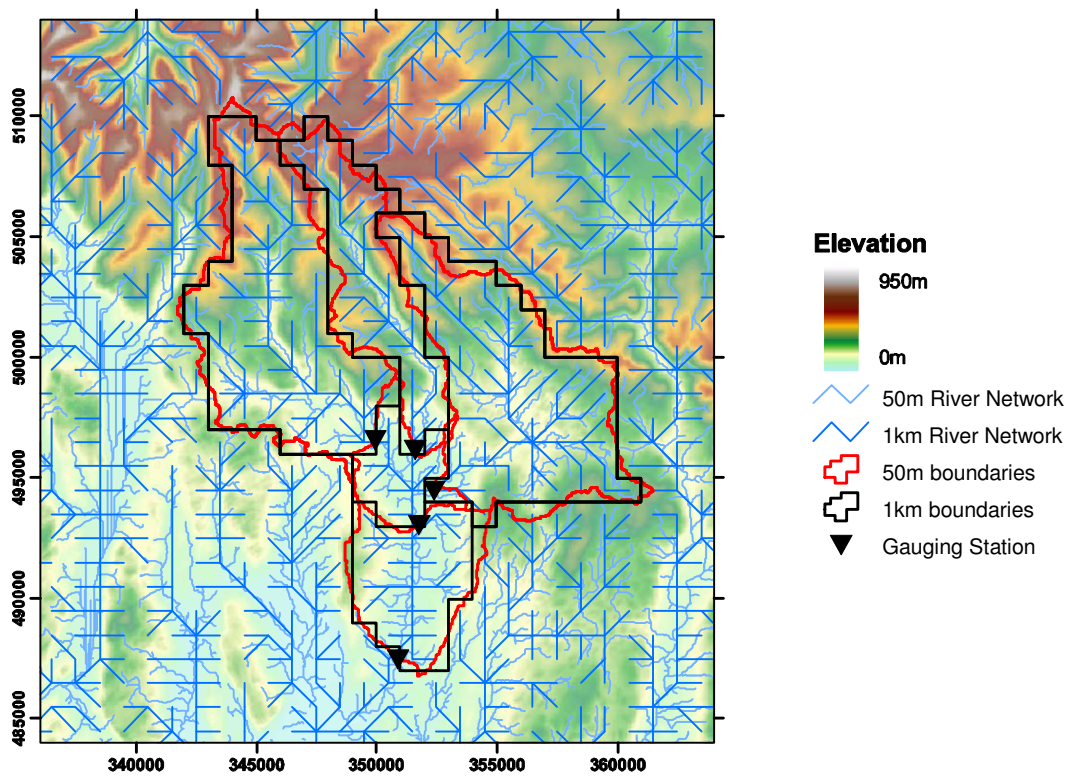


Figure E.2 Hand corrected 1km and IHDTM 50m resolution flow directions and catchment boundaries: River Kent catchment.

Appendix F Calibrated model parameters

This appendix lists the calibrated model parameters for each study catchment. The PDM model is presented first followed by the Grid-to-Grid model.

F.1 PDM models

This section lists the model form and PDM model parameters for each of the study catchments. The revised rainfall factors and time delay parameters used for the different types of rainfall estimators are also listed. For completeness the linear sets of raingauge weights used are listed and compared to the weights derived from multiquadric surface fitting (using the Euclidean distance measure with a zero offset parameter) and Thiessen methods.

Table F.1 River Kent catchments. Calibrated PDM model parameters. The different rainfall factors used for each rainfall estimator are given (other parameters remain the same).

| Parameter name | Catchment | | | | |
|--------------------------|-----------|--------|-------|----------|----------|
| | Bowston | Sprint | Mint | Victoria | Sedgwick |
| Rainfall factor | | | | | |
| f_c raingauge weights | 1.010 | 0.963 | 0.950 | 0.903 | 0.913 |
| f_c raingauge surface | 1.010 | 0.963 | 0.980 | 0.930 | 0.940 |
| f_c 2km raw radar | 0.850 | 0.750 | 0.780 | 0.800 | 0.800 |
| f_c 2km raw gauge adj. | 0.950 | 0.850 | 0.900 | 0.800 | 0.840 |
| f_c 2km QC radar | 1.010 | 0.963 | 0.950 | 0.903 | 0.913 |
| f_c 2km QC gauge adj. | 1.010 | 0.963 | 0.950 | 0.903 | 0.913 |
| Time Delay | | | | | |
| τ_d | 2.151 | 1.890 | 1.301 | 2.192 | 2.156 |
| Soil Moisture | | | | | |
| c_{min} | 35.9 | 27.1 | 31.3 | 25.0 | 26.9 |
| c_{max} | 80.2 | 70.3 | 69.46 | 65.41 | 64.06 |
| b | 1.342 | 1.995 | 1.918 | 2.085 | 1.743 |
| Evaporation function | | | | | |
| b_e | 2.5 | 2.5 | 2.5 | 2.5 | 2.5 |
| Recharge function | | | | | |
| k_g | 2140 | 1203 | 1483 | 1007 | 1495 |
| b_g | 2.093 | 2.183 | 2.015 | 2.205 | 2.156 |
| S_t | 26.55 | 22.65 | 20.61 | 19.87 | 18.43 |
| Surface routing | | | | | |
| k_1 | 7.568 | 5.699 | 6.791 | 7.816 | 6.417 |
| k_2 | 0.017 | 0.008 | 0.005 | 0.137 | 1.236 |
| Baseflow storage (cubic) | | | | | |
| k_b | 53.53 | 31.99 | 50.87 | 55.00 | 54.38 |
| Returns/abstractions | | | | | |
| q_c | 0.276 | 0.276 | 0.179 | 0.814 | 0.946 |

Table F.2 River Kent catchments. Sets of linear weights derived using Thiessen and multiquadric surface fitting methods and revised final sets used within the PDM

| Catchment | Raingauge | | | | | | | |
|---------------------|--------------|--------------|----------------|--------------|--------------|--------------|--------------|-------|
| | Brathay Hall | Tower Wood | Brothers Water | Kentmere | Levens | Watchgate | Wet Sleddale | Orton |
| Bowston | | | | | | | | |
| <i>Thiessen</i> | 0.007 | 0.009 | - | 0.730 | - | 0.255 | - | - |
| <i>Multiquadric</i> | 0.130 | 0.098 | - | 0.510 | 0.033 | 0.229 | - | - |
| PDM | 0.075 | 0.075 | - | 0.55 | - | 0.30 | - | - |
| Sprint Mill | | | | | | | | |
| <i>Thiessen</i> | - | - | - | 0.634 | - | 0.366 | - | - |
| <i>Multiquadric</i> | 0.004 | 0.012 | 0.017 | 0.496 | - | 0.360 | 0.106 | 0.005 |
| PDM | - | - | - | 0.575 | - | 0.375 | 0.05 | - |
| Mint Bridge | | | | | | | | |
| <i>Thiessen</i> | - | - | - | 0.067 | - | 0.933 | - | - |
| <i>Multiquadric</i> | - | - | - | 0.038 | 0.073 | 0.681 | 0.033 | 0.175 |
| PDM | - | - | - | 0.075 | 0.05 | 0.875 | - | - |
| Victoria Br. | | | | | | | | |
| <i>Thiessen</i> | 0.002 | 0.003 | - | 0.409 | - | 0.585 | - | - |
| <i>Multiquadric</i> | 0.040 | 0.036 | - | 0.314 | 0.061 | 0.462 | 0.031 | 0.057 |
| PDM | 0.025 | - | - | 0.35 | 0.075 | 0.50 | 0.05 | - |
| Sedgwick | | | | | | | | |
| <i>Thiessen</i> | 0.002 | 0.003 | - | 0.355 | 0.075 | 0.566 | - | - |
| <i>Multiquadric</i> | 0.033 | 0.035 | - | 0.272 | 0.120 | 0.462 | 0.023 | 0.055 |
| PDM | 0.04 | - | - | 0.35 | 0.10 | 0.51 | - | - |

Table F.3 Upper Thames and Stour catchments. Calibrated PDM model parameters. The different rainfall factors used for each rainfall estimator are given (other parameters remain the same).

| Parameter name | Catchment | | |
|---------------------------------------|-----------|----------|---------|
| | Stour | Bodicote | Banbury |
| Rainfall factor | | | |
| f_c raingauge weights | 0.760 | 1.000 | 0.900 |
| f_c raingauge surface | 0.840 | 1.000 | 0.900 |
| f_c 2/5km raw radar | 0.760 | 0.960 | 0.900 |
| f_c 2/5km raw gauge adj. | 0.700 | 0.960 | 0.940 |
| Time Delay | | | |
| τ_d | 3.120 | 9.000 | 3.000 |
| Soil Moisture | | | |
| c_{min} | 0.0 | 20.0 | 20.0 |
| c_{max} | 84.8 | 225.0 | 90.0 |
| b | 0.340 | 0.350 | 0.300 |
| Evaporation function | | | |
| b_e | 2.5 | 2.5 | 2.5 |
| Recharge function | | | |
| k_g | 97596 | 80000 | 10000 |
| b_g | 2.240 | 1.900 | 1.500 |
| S_t | 0.00 | 60.0 | 40.0 |
| Surface routing | | | |
| <i>Cascade of 2 linear reservoirs</i> | | | |
| k_1 | 6.080 | N/A | 5.000 |
| k_2 | 6.080 | N/A | 25.000 |
| <i>A single cubic store</i> | | | |
| k_1 | N/A | 25.000 | N/A |
| Baseflow storage (cubic) | | | |
| k_b | 5.0 | 300.0 | 25.0 |
| Returns/abstractions | | | |
| q_c | 0.000 | 0.000 | 0.000 |

Table F.4 Upper Thames catchments. Sets of linear weights derived using Thiessen and multiquadric surface fitting methods and revised final sets used within the PDM (only Thames Region raingauges are considered).

| Catchment | Raingauge | | | |
|-------------------------|-------------|-------------|----------|-----------------|
| | Grimsbury | Byfield | Bicester | Chipping Norton |
| <i>Weighting method</i> | | | | |
| Bodicote | | | | |
| <i>Thiessen</i> | 1 | - | - | - |
| <i>Multiquadric</i> | 0.664 | 0.089 | - | 0.247 |
| PDM | 0.67 | 0.08 | - | 0.25 |
| Banbury | | | | |
| <i>Thiessen</i> | 0.328 | 0.672 | - | - |
| <i>Multiquadric</i> | 0.237 | 0.733 | - | - |
| PDM | 0.25 | 0.75 | - | - |

Table F.5 Stour catchment. Sets of linear weights derived using Thiessen and multiquadric surface fitting methods and revised final sets used within the PDM (only Midlands Region raingauges are considered).

| Catchment | Raingauge | | |
|-------------------------|------------------|--------------|---------|
| | Chipping Campden | Shipston | Langley |
| <i>Weighting method</i> | | | |
| Stour | | | |
| <i>Thiessen</i> | 0.377 | 0.623 | - |
| <i>Multiquadric</i> | 0.348 | 0.580 | 0.072 |
| PDM | 0.878 | 0.122 | - |

**Table F.6 River Darwen catchments. Calibrated PDM model parameters.
The different rainfall factors used for each rainfall estimator are given (other parameters remain the same).**

| Parameter name | Catchment | |
|--------------------------|-------------|-------|
| | Blue Bridge | Ewood |
| Rainfall factor | | |
| f_c raingauge weights | 1.100 | 1.088 |
| f_c raingauge surface | 1.110 | 1.100 |
| f_c 1km raw radar | 1.100 | 1.088 |
| f_c 1km raw gauge adj. | 1.150 | 1.190 |
| Time Delay | | |
| τ_d | 1.211 | 0.280 |
| Soil Moisture | | |
| c_{min} | 0 | 0 |
| c_{max} | 27.595 | 41.06 |
| b | 0.335 | 0.306 |
| Evaporation function | | |
| b_e | 2.5 | 2.5 |
| Recharge function | | |
| k_g | 302.9 | 628.0 |
| b_g | 1.650 | 1.571 |
| S_t | 5.0 | 5.0 |
| Surface routing | | |
| k_1 | 4.103 | 3.039 |
| k_2 | 0.937 | 0.524 |
| Baseflow storage (cubic) | | |
| k_b | 32.70 | 0.004 |
| Returns/abstractions | | |
| q_c | 5 | 5 |

Table F.7 River Darwen catchments. Sets of linear weights derived using Thiessen and multiquadric surface fitting methods and revised final sets used within the PDM

| Catchment | Raingauge | | | | | | | |
|---------------------|-------------|---------------|-------------------|-------------|--------------------|-------------|--------------|--------------|
| | Common Bank | Great Harwood | Darwen Sunnyhurst | Pickup Bank | Haighton Reservoir | Moor Park | Holden Wood | Springs |
| Blue Bridge | | | | | | | | |
| <i>Thiessen</i> | 0.014 | 0.147 | 0.496 | 0.149 | 0.068 | 0.126 | - | - |
| <i>Multiquadric</i> | 0.088 | 0.151 | 0.402 | 0.175 | 0.096 | 0.088 | - | - |
| PDM | 0.05 | 0.16 | 0.45 | 0.16 | 0.08 | 0.10 | - | - |
| Ewood | | | | | | | | |
| <i>Thiessen</i> | - | - | 0.639 | 0.361 | - | - | - | - |
| <i>Multiquadric</i> | - | - | 0.477 | 0.416 | - | - | 0.053 | 0.054 |
| PDM | - | - | 0.55 | 0.40 | - | - | 0.025 | 0.025 |

F.2 Grid-to-Grid models

The calibrated Grid-to-Grid model parameters for each catchment are listed in Table F.8. Note that the same parameters are used regardless of the type of rainfall estimator used.

Table F.8 All case studies: Calibrated Grid-to-Grid model parameters

| Parameter name | Case study | | | | |
|-----------------------------------|----------------------|----------------------|----------------------|----------------------|----------------------|
| | Kent | Darwen | Stour | Banbury | Bodicote |
| Wave Speeds | | | | | |
| Surface land, c_l | 0.05 | 0.07 | 0.025 | 0.04 | 0.04 |
| Surface river, c_r | 1.1 | 1.5 | 0.4 | 0.2 | 0.2 |
| Sub-surface land, c_{lb} | 0.05 | 0.05 | 0.01 | 0.005 | 0.005 |
| Sub-surface river, c_{rb} | 0.55 | 0.5 | 0.05 | 0.005 | 0.005 |
| Return Flows | | | | | |
| Land, r_l | 0.07 | 0.05 | 0.02 | 0.0005 | 0.0005 |
| River, r_r | 0.07 | 0.05 | 0.02 | 0.0005 | 0.0005 |
| Runoff generation | | | | | |
| c_{max} Regional maximum | 55 | 40 | 120 | 100 | 380 |
| \bar{c}_{min} Regional minimum | 10 | 20 | 10 | 10 | 10 |
| S_r | 0 | 0 | 0 | 15 | 150 |
| k_d | 1.5×10^{-4} | 1.5×10^{-4} | 2.5×10^{-6} | 1.5×10^{-5} | 9.0×10^{-6} |
| Land/River designation | | | | | |
| Accumulated area threshold, a_0 | 2 | 1 | 1 | 4 | 5 |
| Routing time-step (mins) | 5 | 5 | 5 | 15 | 15 |

Appendix G R^2 model performance statistics for case studies

This appendix lists the R^2 performance statistics for all case study catchments over calibration and extreme events, for all rainfall estimators and for both the PDM and Grid-to-Grid models.

Table G.1 River Kent catchments. R^2 performance statistics for the PDM (Grid-to-Grid results are in brackets) over calibration events listed by type of rainfall estimator used

| Rainfall estimator | Catchment | | | | |
|---|-------------------|-------------------|-------------------|--------------------|--------------------|
| | Bowston | Sprint | Mint | Victoria | Sedgwick |
| Calibration Event 1: 25 October – 30 December 2003 | | | | | |
| Raingauge weights | 0.965 (-) | 0.964 (-) | 0.963 (-) | 0.965 (-) | 0.967 (-) |
| Raingauge surface | 0.968 (0.912) | 0.962 (0.937) | 0.964 (0.930) | 0.967 (0.901) | 0.968 (0.942) |
| 2km raw radar | 0.399 (-0.687) | 0.168 (-1.361) | 0.063 (-1.431) | -0.174 (-2.239) | 0.115 (-1.323) |
| Gauge-adjusted 2km raw radar | 0.851 (0.728) | 0.689 (0.271) | 0.717 (0.490) | 0.788 (0.358) | 0.838 (0.608) |
| 2km QC radar | 0.606 (0.365) | 0.406 (0.306) | 0.465 (0.313) | 0.395 (-0.181) | 0.578 (0.260) |
| Gauge-adjusted 2km QC radar | 0.942 (0.868) | 0.869 (0.817) | 0.918 (0.859) | 0.904 (0.721) | 0.947 (0.857) |
| Calibration Event 2: 15 June – 30 August 2004 | | | | | |
| Raingauge weights | 0.945 (-) | 0.934 (-) | 0.903 (-) | 0.957 (-) | 0.952 (-) |
| Raingauge surface | 0.952 (0.726) | 0.938 (0.876) | 0.936 (0.846) | 0.960 (0.756) | 0.954 (0.755) |
| 2km raw radar | 0.115 (-2.170) | 0.195 (-1.729) | 0.472 (-1.220) | 0.026 (-2.527) | -0.036 (-2.612) |
| Gauge-adjusted 2km raw radar | 0.877 (0.272) | 0.826 (0.308) | 0.881 (0.544) | 0.940 (0.224) | 0.926 (0.243) |
| 2km QC radar | 0.559 (0.400) | 0.496 (0.297) | 0.794 (0.675) | 0.663 (0.416) | 0.657 (0.411) |
| Gauge-adjusted 2km QC radar | 0.876 (0.755) | 0.803 (0.633) | 0.867 (0.781) | 0.882 (0.688) | 0.886 (0.695) |

Table G.2 River Kent catchments. R^2 performance statistics for the PDM over the case study extreme event 09:00 29 January to 09:00 8 February 2004, listed by type of rainfall estimator used (Grid-to-Grid model results are in brackets).

| Rainfall estimator | Catchment | | | | |
|------------------------------|------------------|------------------|------------------|------------------|------------------|
| | Bowston | Sprint | Mint | Victoria | Sedgwick |
| Raingauge weights | 0.908 (-) | 0.891 (-) | 0.904 (-) | 0.952 (-) | 0.865 (-) |
| Raingauge surface | 0.912 (0.921) | 0.891 (0.894) | 0.927 (0.918) | 0.952 (0.887) | 0.879 (0.900) |
| 2km raw radar | 0.605 (0.587) | 0.592 (0.628) | 0.635 (0.613) | 0.715 (0.420) | 0.589 (0.594) |
| Gauge-adjusted 2km raw radar | 0.914 (0.917) | 0.902 (0.906) | 0.926 (0.885) | 0.955 (0.684) | 0.880 (0.899) |
| 2km QC radar | 0.817 (0.813) | 0.751 (0.786) | 0.763 (0.737) | 0.761 (0.551) | 0.781 (0.767) |
| Gauge-adjusted 2km QC radar | 0.931 (0.925) | 0.915 (0.915) | 0.930 (0.907) | 0.933 (0.759) | 0.905 (0.908) |

Table G.3 Upper Thames and Stour catchments. R^2 performance statistics for the PDM (Grid-to-Grid results are in brackets) over calibration events, listed by type of rainfall estimator used

| Rainfall estimator | 1 Sep 2000 – 1 Jun 2001 | | Stour at Shipston | |
|--------------------------------|-------------------------|------------------|----------------------------|----------------------------|
| | Banbury | Bodicote | 8 Jan 1990 - 8 Apr 1990 | 1 Nov 1991 - 1 May 1992 |
| Raingauge weights | 0.748 (-) | 0.906 (-) | 0.929 (-) | 0.758 (-) |
| Raingauge surface | 0.752 (0.666) | 0.907 (0.890) | 0.913 (0.927) | 0.723 (0.503) |
| 2/5km raw radar | 0.459 (0.408) | 0.771 (0.707) | - (-) | 0.087 (-0.705) |
| Gauge-adjusted 2/5km raw radar | 0.730 (0.655) | 0.890 (0.883) | - (-) | 0.641 (-0.067) |

Table G.4 Upper Thames and Stour catchments. R^2 performance statistics for the PDM over the case study extreme event 09:00 6 April to 09:00 19 April 1998, listed by type of rainfall estimator used (Grid-to-Grid model results are in brackets).

| Rainfall estimator | Banbury | Bodicote | Shipston |
|--------------------------------|------------------|------------------|------------------|
| Raingauge weights | 0.868 (-) | 0.759 (-) | 0.590 (-) |
| Raingauge surface | 0.848 (0.811) | 0.715 (0.662) | 0.676 (0.717) |
| 2/5km raw radar | 0.082 (0.279) | 0.045 (0.240) | 0.069 (0.023) |
| Gauge-adjusted 2/5km raw radar | 0.647 (0.726) | 0.524 (0.576) | 0.438 (0.496) |

Table G.5 River Darwen catchments. R^2 performance statistics for the PDM (Grid-to-Grid results are in brackets) over calibration events listed by type of rainfall estimator used.

| Rainfall estimator | Calibration Event 1 17 Feb – 9 Mar 2002 | | Calibration Event 2 26 Jul – 16 Nov 2002 | |
|------------------------------|--|------------------|---|------------------|
| | Blue Bridge | Ewood | Blue Bridge | Ewood |
| Raingauge weights | 0.974 (-) | 0.952 (-) | 0.938 (-) | 0.907 (-) |
| Raingauge surface | 0.972 (0.929) | 0.954 (0.944) | 0.937 (0.908) | 0.911 (0.777) |
| 1km raw radar | 0.811 (0.817) | 0.769 (0.802) | 0.566 (0.482) | 0.541 (0.417) |
| Gauge-adjusted 1km raw radar | 0.944 (0.894) | 0.943 (0.909) | 0.911 (0.889) | 0.904 (0.848) |

Table G.6 River Darwen catchments. R^2 performance statistics for the PDM over the case study extreme event 09:00 13 June to 09:00 16 June 2002, listed by type of rainfall estimator used (Grid-to-Grid model results are in brackets).

| Rainfall estimator | Blue Bridge | Ewood |
|------------------------------|------------------|------------------|
| Raingauge weights | 0.940 (-) | 0.788 (-) |
| Raingauge surface | 0.934 (0.853) | 0.778 (0.843) |
| 1km raw radar | 0.487 (0.307) | 0.375 (0.440) |
| Gauge-adjusted 1km raw radar | 0.819 (0.624) | 0.752 (0.759) |

Appendix H Catalogue of amplified storms

This appendix catalogues details of the amplified storms that have been created. The details given for each storm are set down below.

- **Year.** This is a fictitious year used to identify the storm within the dataset.
- **Period.** This is the total period used for hydrological modelling. Over the period the modified spatial rainfall for each storm consists of three parts:
 1. **Warm-up.** Uses historical radar data to allow model warm-up. This usually ends with a period of low rainfall.
 2. **Amplified storm.** Amplified storm data are used
 3. **Cool-down.** Zero rainfall
- **Historical storm modified.** Identifies which historical storm was modified.
- **Storm modification and transposition settings.** Only settings that are altered are listed.
- **Comments.** This gives the catchment average rainfall amount, duration and estimated return period (using FEH) and any other points of interest.

The modified storms created for each hydrological case study are listed below.

H.1 River Kent case study

The details of the amplified storms are listed in Table H.1. Note that the rainfall amount, duration and FEH-estimated return period quoted relate to the River Kent at Victoria Bridge catchment.

Table H.1 Details of the amplified storms created for the River Kent case study. Note that the rainfall amount, duration and FEH-estimated return period quoted relate to the River Kent at Victoria Bridge catchment.

| Year | Period | Historical storm modified | Storm modification and transposition settings | Comments |
|------|---------------|---------------------------|---|---|
| 3000 | 22/01 – 08/02 | Kent (Orographic) | None, used original 2 km QC gauge-adjusted radar. | 195.9 mm in 4 days to 11:00 02/02. Estimated return period of 69 years |
| 3001 | 22/01 – 08/02 | Kent (Orographic) | $f=1.165$ | 208.5 mm in 4 days to 11:15 02/02. Estimated return period of 100 years |
| 3002 | 22/01 – 08/02 | Kent (Orographic) | $f=1.50$ | 234 mm in 4 days to 11:15 02/02. Estimated return period of 200 years |

| | | | | |
|------|------------------|--|---|---|
| 3003 | 22/01 – 08/02 | Kent (Orographic) | $f=2.022$ | 273.8 mm in 4 days to 11:15 02/02. Estimated return period of 500 years |
| 3004 | 22/01 – 08/02 | Kent (Orographic) | $f=2.467$ | 307.7 mm in 4 days to 11:15 02/02. Estimated return period of 1000 years |
| 3005 | 22/01 – 08/02 | Kent (Orographic) | $f=1.36$ $s_{time}=2.5$ | 223.8 mm in 5 days to 10:45 03/02. Estimated return period of 100 years |
| 3006 | 22/01 – 08/02 | Kent (Orographic) | $f=1.71$ $s_{time}=2.5$ | 250.4 mm in 5 days to 10:45 03/02. Estimated return period of 200 years |
| 3007 | 22/01 – 08/02 | Kent (Orographic) | $f=2.244$ $s_{time}=2.5$ | 291.1 mm in 5 days to 10:45 03/02. Estimated return period of 500 years |
| 3008 | 22/01 – 08/02 | Kent (Orographic) | $f=2.702$ $s_{time}=2.5$ | 326.0 mm in 5 days to 10:45 03/02. Estimated return period of 1000 years |
| 3009 | 04/08 – 18/08 | Carlton-in- Cleveland (Convective) | $(x_0^T, y_0^T)=(347000, 489000)$ $(u_0^T, v_0^T)=(3333, 3333)$ | Historical storm orientation, velocity and direction have been preserved. 14.4 mm in 30mins to 09:45 16/08. Estimated return period of 19 years |
| 3010 | 04/08 – 18/08 | Carlton-in- Cleveland (Convective) | $(x_0^T, y_0^T)=(347000, 489000)$ $(u_0^T, v_0^T)=(3333, 3333)$ $f=1.642$ | Historical storm orientation, velocity and direction have been preserved. 23.7 mm in 30mins to 09:45 16/08. Estimated return period of 100 years |
| 3011 | 04/08 – 18/08 | Carlton-in- Cleveland (Convective) | $(x_0^T, y_0^T)=(347000, 489000)$ $(u_0^T, v_0^T)=(3333, 3333)$ $f=2.015$ | Historical storm orientation, velocity and direction have been preserved. 29.1 mm in 30mins to 09:45 16/08. Estimated return period of 200 years |

| | | | | |
|------|------------------|--|---|--|
| 3012 | 04/08 – 18/08 | Carlton-in- Cleveland (Convective) | $(x_0^T, y_0^T) = (347000, 489000)$ $(u_0^T, v_0^T) = (3333, 3333)$ $f = 2.642$ | Historical storm orientation, velocity and direction have been preserved. 38.1 mm in 30mins to 09:45 16/08. Estimated return period of 500 years |
| 3013 | 04/08 – 18/08 | Carlton-in- Cleveland (Convective) | $(x_0^T, y_0^T) = (347000, 489000)$ $(u_0^T, v_0^T) = (3333, 3333)$ $f = 3.242$ | Historical storm orientation, velocity and direction have been preserved. 46.8 mm in 30mins to 09:45 16/08. Estimated return period of 1000 years |
| 3014 | 04/08 – 18/08 | Carlton-in- Cleveland (Convective) | $(x_0^T, y_0^T) = (347000, 489000)$ $(u_0^T, v_0^T) = (1190, 1190)$ $f = 0.855$ $e_{time} = 2.8$ | Historical storm orientation and direction have been preserved. Storm velocity and time altered to make 1 hr storm. Amounts downscaled. 33.8 mm in 1 hour to 12:00 16/08. Estimated return period of 100 years |
| 3015 | 04/08 – 18/08 | Carlton-in- Cleveland (Convective) | $(x_0^T, y_0^T) = (347000, 489000)$ $(u_0^T, v_0^T) = (1190, 1190)$ $f = 1.338$ $e_{time} = 2.8$ | As per 3014 except amounts scaled. 52.8 mm in 1 hour to 12:00 16/08. Estimated return period of 500 years |
| 3016 | 04/08 – 18/08 | Carlton-in- Cleveland (Convective) | $(x_0^T, y_0^T) = (347000, 489000)$ $(u_0^T, v_0^T) = (606, 606)$ $f = 0.606$ $e_{time} = 5.5$ | Historical storm orientation and direction have been preserved. Storm velocity and time altered to make 2 hr storm. Amounts downscaled. 46.6 mm in 2 hours to 12:00 16/08. Estimated return period of 100 years |
| 3017 | 04/08 – 18/08 | Carlton-in- Cleveland (Convective) | $(x_0^T, y_0^T) = (347000, 489000)$ $(u_0^T, v_0^T) = (606, 606)$ $f = 0.924$ $e_{time} = 5.5$ | As per 3016 except amounts scaled. 71.1 mm in 2 hours to 12:00 16/08. Estimated return period of 500 years |

| | | | | |
|------|------------------|--|---|--|
| 3018 | 04/08 – 18/08 | Carlton-in- Cleveland (Convective) | $(x_0^T, y_0^T) = (351000, 501000)$ $(u_0^T, v_0^T) = (0, 2000)$ $\theta_{\text{turn}} = 45^\circ$ | Storm velocity and orientation changed to give a south to north storm track. 19.8 mm in 1 hour to 9:45 16/08. Estimated return period of 15 years |
| 3019 | 04/08 – 18/08 | Carlton-in- Cleveland (Convective) | $(x_0^T, y_0^T) = (351000, 501000)$ $(u_0^T, v_0^T) = (0, 2000)$ $\theta_{\text{turn}} = 45^\circ$ $f = 1.703$ | As per 3018 except amounts scaled. 33.8 mm in 1 hour to 9:45 16/08. Estimated return period of 100 years |
| 3020 | 04/08 – 18/08 | Carlton-in- Cleveland (Convective) | $(x_0^T, y_0^T) = (351000, 501000)$ $(u_0^T, v_0^T) = (0, 2000)$ $\theta_{\text{turn}} = 45^\circ$ $f = 2.661$ | As per 3018 except amounts scaled. 52.8 mm in 1 hour to 9:45 16/08. Estimated return period of 500 years |
| 3021 | 04/08 – 18/08 | Carlton-in- Cleveland (Convective) | $(x_0^T, y_0^T) = (347000, 505000)$ $(u_0^T, v_0^T) = (0, -2000)$ $\theta_{\text{turn}} = 225^\circ$ | Storm velocity and orientation changed to give a north to south storm track. 20.1 mm in 1 hour to 9:45 16/08. Estimated return period of 15 years |
| 3022 | 04/08 – 18/08 | Carlton-in- Cleveland (Convective) | $(x_0^T, y_0^T) = (347000, 505000)$ $(u_0^T, v_0^T) = (0, -2000)$ $\theta_{\text{turn}} = 225^\circ$ $f = 1.678$ | As per 3021 except amounts scaled. 33.8 mm in 1 hour to 9:45 16/08. Estimated return period of 100 years |
| 3023 | 04/08 – 18/08 | Carlton-in- Cleveland (Convective) | $(x_0^T, y_0^T) = (347000, 505000)$ $(u_0^T, v_0^T) = (0, -2000)$ $\theta_{\text{turn}} = 225^\circ$ $f = 2.621$ | As per 3021 except amounts scaled. 52.8 mm in 1 hour to 9:45 16/08. Estimated return period of 500 years |
| 3024 | 17/05 – 29/05 | Halifax Storm (Convective) | $(x_0^T, y_0^T) = (351000, 500000)$ $(u_0^T, v_0^T) = (667, -500)$ | Historical storm orientation, velocity and direction have been preserved. 37.8 mm in 4 hours to 16:30 16/08. Estimated return period of 13 years |

| | | | | |
|------|------------------|------------------------------------|--|---|
| 3025 | 17/05 – 29/05 | Halifax Storm (Convective) | $(x_0^T, y_0^T) = (351000, 500000)$ $(u_0^T, v_0^T) = (667, -500)$ $f = 1.669$ | As per 3024 except amounts scaled. 63.1 mm in 4 hours to 16:30 16/08. Estimated return period of 100 years |
| 3026 | 17/05 – 29/05 | Halifax Storm (Convective) | $(x_0^T, y_0^T) = (351000, 500000)$ $(u_0^T, v_0^T) = (667, -500)$ $f = 2.476$ | As per 3024 except amounts scaled. 93.6 mm in 4 hours to 16:30 16/08. Estimated return period of 500 years |
| 3027 | 17/05 – 29/05 | Boscastle Storm (Convective) | $(x_0^T, y_0^T) = (351000, 500000)$ | Historical storm orientation, velocity and direction have been preserved. 37.8 mm in 4 hours to 16:30 16/08. Estimated return period of 13 years |
| 3028 | 17/05 – 29/05 | Boscastle Storm (Convective) | $(x_0^T, y_0^T) = (351000, 500000)$ $f = 1.669$ | As per 3027 except amounts scaled. 63.1 mm in 4 hours to 16:30 16/08. Estimated return period of 100 years |
| 3029 | 17/05 – 29/05 | Boscastle Storm (Convective) | $(x_0^T, y_0^T) = (351000, 500000)$ $f = 2.746$ | As per 3027 except amounts scaled. 93.6 mm in 4 hours to 16:30 16/08. Estimated return period of 500 years |

H.2 River Darwin case study

The details of the amplified storms are listed in Table H.2. Note that the rainfall amount, duration and FEH-estimated return period quoted relate to the River Darwin at Blue Bridge catchment.

Table H.2 Details of the amplified storms created for the River Darwin case study. Note that the rainfall amount, duration and FEH-estimated return period quoted relate to the River Darwin at Blue Bridge catchment.

| Year | Period | Historical storm modified | Storm modification and transposition settings | Comments |
|------|---------------|---------------------------|---|---|
| 3000 | 06/06 – 16/06 | River Darwin (Convective) | None, used original 1km raw radar. | 11.9 mm in 1 hour to 16:30 14/06. Estimated return period of 2.5 years |
| 3001 | 06/06 – 16/06 | River Darwin (Convective) | $f=3.21$ | 38.2 mm in 1 hour to 16:30 14/06. Estimated return period of 100 years |
| 3002 | 06/06 – 16/06 | River Darwin (Convective) | $f=3.95$ | 47.0 mm in 1 hour to 16:30 14/06. Estimated return period of 200 years |
| 3003 | 06/06 – 16/06 | River Darwin (Convective) | $f=5.19$ | 61.8 mm in 1 hour to 16:30 14/06. Estimated return period of 500 years |
| 3004 | 06/06 – 16/06 | River Darwin (Convective) | $f=6.39$ | 76.0 mm in 1 hour to 16:30 14/06. Estimated return period of 1000 years |
| 3005 | 06/06 – 16/06 | River Darwin (Convective) | $(x_0^T, y_0^T) = (366500, 428500)$ $(u_0^T, v_0^T) = (5667, 0)$ $\theta_{\text{turn}} = 308^\circ$ | Storm velocity and orientation changed to give a west to east storm track. 22.1 mm in 2 hours to 17:30 14/06. Estimated return period of 6.3 years |
| 3006 | 06/06 – 16/06 | River Darwin (Convective) | $(x_0^T, y_0^T) = (366500, 428500)$ $(u_0^T, v_0^T) = (5667, 0)$ $\theta_{\text{turn}} = 308^\circ$ $f = 2.22$ | As per 3005 except amounts scaled. 49.1 mm in 2 hours to 17:30 14/06. Estimated return period of 100 years |

| | | | | |
|------|------------------|---------------------------------|---|--|
| 3007 | 06/06 – 16/06 | River Darwen (Convective) | $(x_0^T, y_0^T) = (366500, 428500)$ $(u_0^T, v_0^T) = (5667, 0)$ $\theta_{\text{turn}} = 308^\circ$ $f = 2.70$ | As per 3005 except amounts scaled. 59.8 mm in 2 hours to 17:30 14/06. Estimated return period of 200 years |
| 3008 | 06/06 – 16/06 | River Darwen (Convective) | $(x_0^T, y_0^T) = (366500, 428500)$ $(u_0^T, v_0^T) = (5667, 0)$ $\theta_{\text{turn}} = 308^\circ$ $f = 3.48$ | As per 3005 except amounts scaled. 77.1 mm in 2 hours to 17:30 14/06. Estimated return period of 500 years |
| 3009 | 06/06 – 16/06 | River Darwen (Convective) | $(x_0^T, y_0^T) = (366500, 428500)$ $(u_0^T, v_0^T) = (5667, 0)$ $\theta_{\text{turn}} = 308^\circ$ $f = 4.24$ | As per 3005 except amounts scaled. 93.8 mm in 2 hours to 17:30 14/06. Estimated return period of 1000 years |
| 3010 | 06/06 – 16/06 | River Darwen (Convective) | $(x_0^T, y_0^T) = (366500, 428500)$ $(u_0^T, v_0^T) = (5667, 0)$ $\theta_{\text{turn}} = 128^\circ$ | Storm velocity and orientation changed to give an east to west storm track. 22.5 mm in 2 hours to 17:30 14/06. Estimated return period of 6.7 years |
| 3011 | 06/06 – 16/06 | River Darwen (Convective) | $(x_0^T, y_0^T) = (366500, 428500)$ $(u_0^T, v_0^T) = (5667, 0)$ $\theta_{\text{turn}} = 128^\circ$ $f = 2.18$ | As per 3010 except amounts scaled. 49.0 mm in 2 hours to 17:30 14/06. Estimated return period of 100 years |
| 3012 | 06/06 – 16/06 | River Darwen (Convective) | $(x_0^T, y_0^T) = (366500, 428500)$ $(u_0^T, v_0^T) = (5667, 0)$ $\theta_{\text{turn}} = 128^\circ$ $f = 2.66$ | As per 3010 except amounts scaled. 59.7 mm in 2 hours to 17:30 14/06. Estimated return period of 200 years |
| 3013 | 06/06 – 16/06 | River Darwen (Convective) | $(x_0^T, y_0^T) = (366500, 428500)$ $(u_0^T, v_0^T) = (5667, 0)$ $\theta_{\text{turn}} = 128^\circ$ $f = 3.43$ | As per 3010 except amounts scaled. 77.0 mm in 2 hours to 17:30 14/06. Estimated return period of 500 years |
| 3014 | 06/06 – 16/06 | River Darwen (Convective) | $(x_0^T, y_0^T) = (366500, 428500)$ $(u_0^T, v_0^T) = (5667, 0)$ $\theta_{\text{turn}} = 128^\circ$ $f = 4.17$ | As per 3010 except amounts scaled. 93.7 mm in 2 hours to 17:30 14/06. Estimated return period of 1000 years |

| | | | | |
|------|------------------|---------------------------------|--|--|
| 3015 | 23/07 – 12/08 | River Darwen (Convective) | $f=3.21$ | As per 3001 except relocated in time to occur immediately after a hydrograph peak. 38.2 mm in 1 hour to 16:30 02/08. Estimated return period of 100 years |
| 3016 | 23/07 – 12/08 | River Darwen (Convective) | $f=3.21$ | As per 3015 except relocated in time to occur 1 day after a hydrograph peak. 38.2 mm in 1 hour to 16:30 03/08. Estimated return period of 100 years |
| 3017 | 23/07 – 12/08 | River Darwen (Convective) | $f=3.21$ | As per 3015 except relocated in time to occur 2 days after a hydrograph peak. 38.2 mm in 1 hour to 16:30 04/08. Estimated return period of 100 years |
| 3018 | 12/08 – 24/08 | Boscastle (Convective) | $(x_0^T, y_0^T)=(370000, 423000)$ | Relocated to headwaters of Darwen catchment. 43.3 mm in 4 hours to 16:30 18/08. Estimated return period of 26 years |
| 3019 | 12/08 – 24/08 | Boscastle (Convective) | $(x_0^T, y_0^T)=(370000, 423000)$ $f=1.427$ | As 3018 but scaled amounts. 61.8 mm in 4 hours to 16:30 18/08. Estimated return period of 100 years |
| 3020 | 12/08 – 24/08 | Boscastle (Convective) | $(x_0^T, y_0^T)=(370000, 423000)$ $f=2.182$ | As 3018 but scaled amounts. 94.4 mm in 4 hours to 16:30 18/08. Estimated return period of 500 years |
| 3021 | 12/08 – 24/08 | Boscastle (Convective) | $(x_0^T, y_0^T)=(364000, 426000)$ | Relocated to outlet of Darwen catchment. 46.9 mm in 4 hours to 16:30 18/08. Estimated return period of 42 years |

| | | | | |
|------|------------------|--------------------------------------|--|--|
| 3022 | 12/08 – 24/08 | Boscastle (Convective) | $(x_0^T, y_0^T) = (364000, 426000)$ $f = 1.318$ | As 3021 but scaled amounts. 61.8 mm in 4 hours to 16:30 18/08. Estimated return period of 100 years |
| 3023 | 12/08 – 24/08 | Boscastle (Convective) | $(x_0^T, y_0^T) = (364000, 426000)$ $f = 2.013$ | As 3021 but scaled amounts. 94.4 mm in 4 hours to 16:30 18/08. Estimated return period of 500 years |
| 3024 | 12/08 – 24/08 | Boscastle (Convective) | $(x_0^T, y_0^T) = (367000, 424000)$ $S_n = 2.0$ $S_a = 2.0$ | Relocated to Darwen catchment and stretched spatially to cover entire catchment. 21.3 mm in 4 hours to 16:30 18/08. Estimated return period of 2.3 years |
| 3025 | 12/08 – 24/08 | Boscastle (Convective) | $(x_0^T, y_0^T) = (367000, 424000)$ $S_n = 2.0$ $S_a = 2.0$ $f = 2.907$ | As per 3024 except amounts scaled. 61.8 mm in 4 hours to 16:30 18/08. Estimated return period of 100 years |
| 3026 | 12/08 – 24/08 | Boscastle (Convective) | $(x_0^T, y_0^T) = (367000, 424000)$ $S_n = 2.0$ $S_a = 2.0$ $f = 4.44$ | As per 3024 except amounts scaled. 94.4 mm in 4 hours to 16:30 18/08. Estimated return period of 500 years |
| 3027 | 12/08 – 24/08 | Carlton-in-Cleveland (Convective) | $(x_0^T, y_0^T) = (363000, 424000)$ $(u_0^T, v_0^T) = (3333, -3333)$ $\theta_{\text{turn}} = 270^\circ$ | Relocated storm to Darwen catchment, velocity modified to give NW to SE storm track. 14.2 mm in 30 mins to 09:45 18/08. Estimated return period of 11 years |
| 3028 | 12/08 – 24/08 | Carlton-in-Cleveland (Convective) | $(x_0^T, y_0^T) = (363000, 424000)$ $(u_0^T, v_0^T) = (3333, -3333)$ $\theta_{\text{turn}} = 270^\circ$ $f = 2.03$ | As per 3027 except amounts scaled. 28.9 mm in 30 mins to 09:45 18/08. Estimated return period of 100 years |
| 3029 | 12/08 – 24/08 | Carlton-in-Cleveland (Convective) | $(x_0^T, y_0^T) = (363000, 424000)$ $(u_0^T, v_0^T) = (3333, -3333)$ $\theta_{\text{turn}} = 270^\circ$ $f = 3.379$ | As per 3027 except amounts scaled. 48.1 mm in 30 mins to 09:45 18/08. Estimated return period of 500 years |

| | | | | |
|------|------------------|---|---|---|
| 3030 | 12/08 – 24/08 | Carlton-in- Cleveland (Convective) | $(x_0^T, y_0^T) = (370000, 430000)$ $(u_0^T, v_0^T) = (-3333, 3333)$ $\theta_{\text{turn}} = 90^\circ$ | Relocated storm to Darwen catchment, velocity modified to give SE to NW storm track. 16.1 mm in 30 mins to 09:45 18/08. Estimated return period of 16 years |
| 3031 | 12/08 – 24/08 | Carlton-in- Cleveland (Convective) | $(x_0^T, y_0^T) = (370000, 430000)$ $(u_0^T, v_0^T) = (-3333, 3333)$ $\theta_{\text{turn}} = 90^\circ$ $f = 1.794$ | As per 3027 except amounts scaled. 28.9 mm in 30 mins to 09:45 18/08. Estimated return period of 100 years |
| 3032 | 12/08 – 24/08 | Carlton-in- Cleveland (Convective) | $(x_0^T, y_0^T) = (370000, 430000)$ $(u_0^T, v_0^T) = (-3333, 3333)$ $\theta_{\text{turn}} = 90^\circ$ $f = 2.985$ | As per 3027 except amounts scaled. 48.1 mm in 30 mins to 09:45 18/08. Estimated return period of 500 years |
| 3033 | 02/05 – 12/05 | Halifax Strom (Convective) | $(x_0^T, y_0^T) = (370000, 430000)$ | Relocated to Darwen catchment. 23.1 mm in 3 hours to 17:15 08/05. Estimated return period of 4.2 years |
| 3034 | 02/05 – 12/05 | Halifax Strom (Convective) | $(x_0^T, y_0^T) = (370000, 430000)$ $f = 2.431$ | As per 3033 except scaled amounts. 56.2 mm in 3 hours to 17:15 08/05. Estimated return period of 100 years |
| 3035 | 02/05 – 12/05 | Halifax Strom (Convective) | $(x_0^T, y_0^T) = (370000, 430000)$ $f = 3.764$ | As per 3033 except scaled amounts. 87.0 mm in 3 hours to 17:15 08/05. Estimated return period of 500 years |
| 3036 | 02/04 – 15/04 | Upper Thames and Stour (Frontal) | $(x_0^T, y_0^T) = (370000, 430000)$ | Relocated to Darwen catchment. 59.0 mm in 15 hours to 19:00 09/04. Estimated return period of 15 years |
| 3037 | 02/04 – 15/04 | Upper Thames and Stour (Frontal) | $(x_0^T, y_0^T) = (370000, 430000)$ $f = 1.569$ | As per 3036 except scaled amounts. 92.6 mm in 15 hours to 19:00 09/04. Estimated return period of 100 years |

| | | | | |
|------|------------------|---|---|--|
| 3038 | 02/04 – 15/04 | Upper Thames and Stour (Frontal) | $(x_0^T, y_0^T) = (370000, 430000)$ $f = 1.842$ | As per 3036 except scaled amounts. 108.7 mm in 15 hours to 19:00 09/04. Estimated return period of 200 years |
| 3039 | 02/04 – 15/04 | Upper Thames and Stour (Frontal) | $(x_0^T, y_0^T) = (370000, 430000)$ $f = 2.276$ | As per 3036 except scaled amounts. 134.3 mm in 15 hours to 19:00 09/04. Estimated return period of 500 years |
| 3040 | 02/04 – 15/04 | Upper Thames and Stour (Frontal) | $(x_0^T, y_0^T) = (370000, 430000)$ $f = 2.669$ | As per 3036 except scaled amounts. 157.5 mm in 15 hours to 19:00 09/04. Estimated return period of 1000 years |
| 3041 | 02/04 – 15/04 | Upper Thames and Stour (Frontal) | $(x_0^T, y_0^T) = (370000, 430000)$ $e_{\text{time}} = 1.6$ $f = 1.118$ | Relocated to Darwen catchment, stretched time and scaled amounts. 105.5 mm in 24 hours to 04:30 10/04. Estimated return period of 100 years |
| 3042 | 02/04 – 15/04 | Upper Thames and Stour (Frontal) | $(x_0^T, y_0^T) = (370000, 430000)$ $e_{\text{time}} = 1.6$ $f = 1.591$ | Relocated to Darwen catchment, stretched time and scaled amounts. 150.1 mm in 24 hours to 04:30 10/04. Estimated return period of 500 years |
| 3043 | 02/04 – 15/04 | Upper Thames and Stour (Frontal) | $(x_0^T, y_0^T) = (370000, 430000)$ $e_{\text{time}} = 2.4$ $f = 0.832$ | Relocated to Darwen catchment, stretched time and scaled amounts. 117.8 mm in 36 hours to 17:15 10/04. Estimated return period of 100 years |
| 3044 | 02/04 – 15/04 | Upper Thames and Stour (Frontal) | $(x_0^T, y_0^T) = (370000, 430000)$ $e_{\text{time}} = 2.4$ $f = 1.164$ | Relocated to Darwen catchment, stretched time and scaled amounts. 164.8 mm in 36 hours to 17:15 10/04. Estimated return period of 500 years |

| | | | | |
|------|------------------|---|---|--|
| 3045 | 02/04 – 15/04 | Upper Thames and Stour (Frontal) | $(x_0^T, y_0^T) = (370000, 430000)$ $e_{\text{time}} = 3.2$ $f = 0.674$ | Relocated to Darwen catchment, stretched time and scaled amounts. 127.2 mm in 48 hours to 06:15 11/04. Estimated return period of 100 years |
| 3046 | 02/04 – 15/04 | Upper Thames and Stour (Frontal) | $(x_0^T, y_0^T) = (370000, 430000)$ $e_{\text{time}} = 3.2$ $f = 0.932$ | Relocated to Darwen catchment, stretched time and scaled amounts. 176.0 mm in 48 hours to 06:15 11/04. Estimated return period of 500 years |

H.3 Upper Thames and Stour case study

The details of the amplified storms for the Upper Thames case study are listed in Table H.3. Note that the rainfall amount, duration and FEH-estimated return period quoted relate to the Sor at Bodicote catchment.

The details of the amplified storms for the Stour at Shipston case study are listed in Table H.4. Note that the rainfall amount, duration and FEH-estimated return period quoted relate to the Stour at Shipston catchment.

Table H.3 Details of the amplified storms created for the Upper Thames case study. Note that the rainfall amount, duration and FEH-estimated return period quoted relate to the Sor at Bodicote catchment.

| Year | Period | Historical storm modified | Storm modification and transposition settings | Comments |
|------|-----------------|---|--|--|
| 3000 | 01/01- 20/04 | Upper Thames and Stour (Frontal) | None, used composite 2 and 5km raingauge- adjusted raw radar | 47.1 mm in 15 hours to 18:45 09/04. Estimated return period of 10.5 years |
| 3001 | 01/01- 20/04 | Upper Thames and Stour (Frontal) | $f = 1.706$ | 80.4 mm in 15 hours to 18:45 09/04. Estimated return period of 100 years |
| 3002 | 01/01- 20/04 | Upper Thames and Stour (Frontal) | $f = 2.003$ | 94.4 mm in 15 hours to 18:45 09/04. Estimated return period of 200 years |

| | | | | |
|------|---------------|----------------------------------|-----------------------------------|--|
| 3003 | 01/01-20/04 | Upper Thames and Stour (Frontal) | $f=2.478$ | 116.8 mm in 15 hours to 18:45 09/04. Estimated return period of 500 years |
| 3004 | 01/01-20/04 | Upper Thames and Stour (Frontal) | $f=2.911$ | 137.2 mm in 15 hours to 18:45 09/04. Estimated return period of 1000 years |
| 3005 | 01/01-20/04 | Upper Thames and Stour (Frontal) | $s_{time}=1.6$ $f=1.914$ | Stretched time and scaled amounts. 90.2 mm in 24 hours to 04:15 10/04. Estimated return period of 100 years |
| 3006 | 01/01-20/04 | Upper Thames and Stour (Frontal) | $s_{time}=1.6$ $f=2.730$ | Stretched time and scaled amounts. 128.7 mm in 24 hours to 04:15 10/04. Estimated return period of 100 years |
| 3007 | 01/01-20/04 | Upper Thames and Stour (Frontal) | $s_{time}=2.4$ $f=2.109$ | Stretched time and scaled amounts. 99.4 mm in 36 hours to 16:45 10/04. Estimated return period of 100 years |
| 3008 | 01/01-20/04 | Upper Thames and Stour (Frontal) | $s_{time}=2.4$ $f=2.964$ | Stretched time and scaled amounts. 139.7 mm in 36 hours to 16:45 10/04. Estimated return period of 500 years |
| 3009 | 01/01-20/04 | Upper Thames and Stour (Frontal) | $s_{time}=3.6$ $f=2.257$ | Stretched time and scaled amounts. 106.4 mm in 48 hours to 05:30 11/04. Estimated return period of 100 years |
| 3010 | 01/01-20/04 | Upper Thames and Stour (Frontal) | $s_{time}=3.6$ $f=3.138$ | Stretched time and scaled amounts. 147.9 mm in 48 hours to 05:30 11/04. Estimated return period of 500 years |
| 3011 | 01/04 – 25/06 | Boscastle (Convective) | $(x_0^T, y_0^T)=(441000, 241000)$ | Relocated storm. 59.2 mm in 4 hours to 16:30 15/06. Estimated return period of 113 years |

| | | | | |
|------|------------------|--------------------------------------|--|---|
| 3012 | 01/04 – 25/06 | Boscastle (Convective) | $(x_0^T, y_0^T) = (441000, 241000)$ $f = 0.968$ | As per 3011 except scaled amounts. 57.3 mm in 4 hours to 16:30 15/06. Estimated return period of 100 years |
| 3013 | 01/04 – 25/06 | Boscastle (Convective) | $(x_0^T, y_0^T) = (441000, 241000)$ $f = 1.481$ | As per 3011 except scaled amounts. 87.7 mm in 4 hours to 16:30 15/06. Estimated return period of 500 years |
| 3014 | 01/04 – 25/06 | Carlton-in-Cleveland (Convective) | $(x_0^T, y_0^T) = (445000, 237000)$ | Relocated storm. 15.0 mm in 30 mins to 09:45 15/06. Estimated return period of 11 years |
| 3015 | 01/04 – 25/06 | Carlton-in-Cleveland (Convective) | $(x_0^T, y_0^T) = (445000, 237000)$ $f = 2.040$ | As per 3014 except scaled amounts. 30.6 mm in 30 mins to 09:45 15/06. Estimated return period of 100 years |
| 3016 | 01/04 – 25/06 | Carlton-in-Cleveland (Convective) | $(x_0^T, y_0^T) = (445000, 237000)$ $f = 3.380$ | As per 3014 except scaled amounts. 50.7 mm in 30 mins to 09:45 15/06. Estimated return period of 500 years |
| 3017 | 01/04 – 25/06 | Halifax storm (Convective) | $(x_0^T, y_0^T) = (453000, 233000)$ | Relocated storm. 36.0 mm in 2.5 hours to 16:00 15/06. Estimated return period of 30 years |
| 3018 | 01/04 – 25/06 | Halifax storm (Convective) | $(x_0^T, y_0^T) = (453000, 233000)$ $f = 1.402$ | As per 3017 except scaled amounts. 50.4 mm in 2.5 hours to 16:00 15/06. Estimated return period of 100 years |
| 3019 | 01/04 – 25/06 | Halifax storm (Convective) | $(x_0^T, y_0^T) = (453000, 233000)$ $f = 2.186$ | As per 3017 except scaled amounts. 78.6 mm in 2.5 hours to 16:00 15/06. Estimated return period of 500 years |
| 3020 | 01/04 – 25/06 | Darwen (Convective) | $(x_0^T, y_0^T) = (441500, 241500)$ | Relocated storm. 14.4 mm in 1 hour to 16:30 15/06. Estimated return period of 4.2 years |

| | | | | |
|-----------|-----------------------|---------------------------------|--|--|
| 3021 | 01/04 – 25/06 | Darwen (Convective) | $(x_0^T, y_0^T) = (441500, 241500)$ $f = 2.666$ | Relocated storm. 38.5 mm in 1 hour to 16:30 15/06. Estimated return period of 100 years |
| 3022 | 01/04 – 25/06 | Darwen (Convective) | $(x_0^T, y_0^T) = (441500, 241500)$ $f = 4.301$ | Relocated storm. 62.1 mm in 1 hour to 16:30 15/06. Estimated return period of 500 years |
| 3023 | 1/7/22 – 1/9/23 | River Darwen (Convective) | $(x_0^T, y_0^T) = (441500, 241500)$ $f = 2.666$ | As per 3021 except relocated in time to occur immediately after a hydrograph peak. 38.5 mm in 1 hour to 16:30 15/02. Estimated return period of 100 years |
| 3024 * | 1/7/23 – 1/9/24 | River Darwen (Convective) | $(x_0^T, y_0^T) = (441500, 241500)$ $f = 2.666$ | As per 3021 except relocated in time to occur 1 month after a hydrograph peak. 38.5 mm in 1 hour to 16:30 15/03. Estimated return period of 100 years |
| 3025* | 1/7/24 – 1/9/25 | River Darwen (Convective) | $(x_0^T, y_0^T) = (441500, 241500)$ $f = 2.666$ | As per 3021 except relocated in time to occur 2 months after a hydrograph peak. 38.5 mm in 1 hour to 16:30 15/04. Estimated return period of 100 years |
| 3026* | 1/7/25 – 1/9/26 | River Darwen (Convective) | $(x_0^T, y_0^T) = (441500, 241500)$ $f = 2.666$ | As per 3021 except relocated in time to occur 2 months after a hydrograph peak. 38.5 mm in 1 hour to 16:30 15/05. Estimated return period of 100 years |
| 3027* | 1/7/26 – 1/9/27 | River Darwen (Convective) | $(x_0^T, y_0^T) = (441500, 241500)$ $f = 2.666$ | As per 3021 except relocated in time to occur 2 months after a hydrograph peak. 38.5 mm in 1 hour to 16:30 15/06. Estimated return period of 100 years |

| | | | | |
|-------|-----------------------|---------------------------------|--|---|
| 3028* | 1/7/27 – 1/9/28 | River Darwen (Convective) | $(x_0^T, y_0^T) = (441500, 241500)$ $f = 2.666$ | As per 3021 except relocated in time to occur 2 months after a hydrograph peak. 38.5 mm in 1 hour to 16:30 15/07. Estimated return period of 100 years |
|-------|-----------------------|---------------------------------|--|---|

* Note that for amplified storms 3024 to 3028 the same PE values taken from February (i.e. storm 3023) are used so that the different model responses are purely due to the initial condition at the start of the storm.

Table H.4 Details of the amplified storms created for the Stour at Shipston case study. Note that the rainfall amount, duration and FEH-estimated return period quoted relate to the Stour at Shipston catchment.

| Year | Period | Historical storm modified | Storm modification and transposition settings | Comments |
|------|-----------------|---|--|---|
| 3029 | 06/02- 20/04 | Upper Thames and Stour (Frontal) | None, used composite 2 and 5km raingauge- adjusted raw radar | 46.4 mm in 15 hours to 18:15 09/04. Estimated return period of 8.6 years |
| 3030 | 06/02- 20/04 | Upper Thames and Stour (Frontal) | $f = 1.774$ | 82.3 mm in 15 hours to 18:15 09/04. Estimated return period of 100 years |
| 3031 | 06/02- 20/04 | Upper Thames and Stour (Frontal) | $f = 2.078$ | 96.4 mm in 15 hours to 18:15 09/04. Estimated return period of 200 years |
| 3032 | 06/02- 20/04 | Upper Thames and Stour (Frontal) | $f = 2.563$ | 118.9 mm in 15 hours to 18:15 09/04. Estimated return period of 500 years |
| 3033 | 06/02- 20/04 | Upper Thames and Stour (Frontal) | $f = 3.002$ | 139.3 mm in 15 hours to 18:15 09/04. Estimated return period of 1000 years |
| 3034 | 06/02- 20/04 | Upper Thames and Stour (Frontal) | $s_{\text{time}} = 1.6$ $f = 2.000$ | 92.8 mm in 24 hours to 03:35 10/04. Estimated return period of 100 years |
| 3035 | 06/02- 20/04 | Upper Thames and Stour (Frontal) | $s_{\text{time}} = 1.6$ $f = 2.839$ | 131.7 mm in 24 hours to 03:35 10/04. Estimated return period of 500 years |

| | | | | |
|------|-------------|----------------------------------|--|--|
| 3036 | 06/02-20/04 | Upper Thames and Stour (Frontal) | $s_{\text{time}}=2.4$ $f=2.216$ | 102.8 mm in 36 hours to 15:45 10/04. Estimated return period of 100 years |
| 3037 | 06/02-20/04 | Upper Thames and Stour (Frontal) | $s_{\text{time}}=2.4$ $f=3.093$ | 143.5 mm in 36 hours to 15:45 10/04. Estimated return period of 500 years |
| 3038 | 06/02-20/04 | Upper Thames and Stour (Frontal) | $s_{\text{time}}=3.2$ $f=2.382$ | 110.5 mm in 48 hours to 04:00 11/04. Estimated return period of 100 years |
| 3039 | 06/02-20/04 | Upper Thames and Stour (Frontal) | $s_{\text{time}}=3.2$ $f=3.283$ | 152.3 mm in 48 hours to 04:00 11/04. Estimated return period of 500 years |
| 3040 | 14/03-01/05 | Boscastle (Convective) | $(x_0^T, y_0^T)=(417000, 237000)$ | Relocated storm to west of catchment. 29.9 mm in 4 hours to 16:15 22/04. Estimated return period of 9 years |
| 3041 | 14/03-01/05 | Boscastle (Convective) | $(x_0^T, y_0^T)=(417000, 237000)$ $f=1.902$ | As per 3040 but amounts scaled. 58.9 mm in 4 hours to 16:15 22/04. Estimated return period of 100 years |
| 3042 | 14/03-01/05 | Boscastle (Convective) | $(x_0^T, y_0^T)=(417000, 237000)$ $f=2.901$ | As per 3040 but amounts scaled. 89.9 mm in 4 hours to 16:15 22/04. Estimated return period of 500 years |
| 3043 | 14/03-01/05 | Boscastle (Convective) | $(x_0^T, y_0^T)=(433000, 237000)$ $\theta_{\text{band}}=0^\circ$ $e_n=-1.0$ | Relocated storm to east of catchment and reflected about the N-S axis. 26.5 mm in 4 hours to 16:15 22/04. Estimated return period of 6 years |
| 3044 | 14/03-01/05 | Boscastle (Convective) | $(x_0^T, y_0^T)=(433000, 237000)$ $\theta_{\text{band}}=0^\circ$ $e_n=-1.0$ $f=2.151$ | As per 3043 but amounts scaled. 58.9 mm in 4 hours to 16:15 22/04. Estimated return period of 100 years |
| 3045 | 14/03-01/05 | Boscastle (Convective) | $(x_0^T, y_0^T)=(433000, 237000)$ $\theta_{\text{band}}=0^\circ$ $e_n=-1.0$ $f=3.281$ | As per 3043 but amounts scaled. 89.9 mm in 4 hours to 16:15 22/04. Estimated return period of 500 years |

| | | | | |
|------|-------------|--------------------------------------|--|--|
| 3046 | 14/03-01/05 | Boscastle (Convective) | $(x_0^T, y_0^T) = (433000, 237000)$ $\theta_{\text{turn}} = 0^\circ$ | Rotated storm to cover majority of catchment. 55.8 mm in 4 hours to 16:30 22/04. Estimated return period of 93 years |
| 3047 | 14/03-01/05 | Boscastle (Convective) | $(x_0^T, y_0^T) = (433000, 237000)$ $\theta_{\text{turn}} = 0^\circ$ $f = 1.020$ | As per 3046 but amounts scaled. 58.9 mm in 4 hours to 16:30 22/04. Estimated return period of 100 years |
| 3048 | 14/03-01/05 | Boscastle (Convective) | $(x_0^T, y_0^T) = (433000, 237000)$ $\theta_{\text{turn}} = 0^\circ$ $f = 1.556$ | As per 3046 but amounts scaled. 89.9 mm in 4 hours to 16:30 22/04. Estimated return period of 500 years |
| 3049 | 14/03-01/05 | Carlton-in-Cleveland (Convective) | $(x_0^T, y_0^T) = (420000, 229000)$ | Relocated storm to Stour catchment. 13.2 mm in 30mins to 09:45 22/04. Estimated return period of 10 years |
| 3050 | 14/03-01/05 | Carlton-in-Cleveland (Convective) | $(x_0^T, y_0^T) = (420000, 229000)$ $f = 2.119$ | As per 3049 but amounts scaled. 28.0 mm in 30mins to 09:45 22/04. Estimated return period of 100 years |
| 3051 | 14/03-01/05 | Carlton-in-Cleveland (Convective) | $(x_0^T, y_0^T) = (420000, 229000)$ $f = 3.518$ | As per 3049 but amounts scaled. 46.5 mm in 30mins to 09:45 22/04. Estimated return period of 500 years |
| 3052 | 14/03-01/05 | Halifax Storm (Convective) | $(x_0^T, y_0^T) = (432000, 231000)$ | Relocated storm to Stour catchment. 23.7 mm in 3hours 30mins to 17:30 22/04. Estimated return period of 5 years |
| 3053 | 14/03-01/05 | Halifax Storm (Convective) | $(x_0^T, y_0^T) = (432000, 231000)$ $f = 2.310$ | As per 3052 but amounts scaled. 54.7 mm in 3hours 30mins to 17:30 22/04. Estimated return period of 100 years |
| 3054 | 14/03-01/05 | Halifax Storm (Convective) | $(x_0^T, y_0^T) = (432000, 231000)$ $f = 3.544$ | As per 3052 but amounts scaled. 83.9 mm in 3hours 30mins to 17:30 22/04. Estimated return period of 500 years |

| | | | | |
|------|-------------|------------------------------|--|--|
| 3055 | 14/03-01/05 | Darwen storm (Convective) | $(x_0^T, y_0^T) = (421000, 231000)$ | Relocated storm to Stour catchment. 12.1 mm in 1 hour 30mins to 17:00 22/04. Estimated return period of 2 years |
| 3056 | 14/03-01/05 | Darwen storm (Convective) | $(x_0^T, y_0^T) = (421000, 231000)$ $f = 3.444$ | As per 3055 but amounts scaled. 41.9 mm in 1 hour 30mins to 17:00 22/04. Estimated return period of 100 years |
| 3057 | 14/03-01/05 | Darwen storm (Convective) | $(x_0^T, y_0^T) = (421000, 231000)$ $f = 5.467$ | As per 3055 but amounts scaled. 66.5 mm in 1 hour 30mins to 17:00 22/04. Estimated return period of 500 years |

Ergon House
Horseferry Road
London SW1P 2AL
www.defra.gov.uk

